Synthesis and Implementation of Electronic Materials for Smart Sensor Module

A THESIS SUBMITTED TO

SOLAPUR UNIVERSITY, SOLAPUR

FOR THE DEGREE OF

DOCTOR OF PHILOSOPHY

IN

ELECTRONICS

UNDER THE FACULTY OF SCIENCE

BY

MR. PATIL SUHAS NAMADEV

M.Sc.

UNDER THE GUIDANCE OF

PROF. (DR.) B. P. LADGAONKAR

Head

POST GRADUATE DEPARTMENT OF ELECTRONICS

SHANKARRAO MOHITE MAHAVIDYALAYA

AKLUJ DIST. SOLAPUR

July, 2015

D E C L A R A T I O N

I hereby declare that, the thesis entitled **"Synthesis and Implementation of Electronic Materials for Smart Sensor Module"** completed and written by me has not previously formed the basis for the award of any Degree or Diploma or other similar title of any other University or Examining Body.

Research Student

Place: Akluj

Date: /07/2015

Mr. Suhas Namadev Patil
Post Graduate Department of Electronics
Shankarrao Mohite Mahavidyalaya
Akluj Dist. Solapur

CERTIFICATE

This is to certify that, the thesis, entitled **"Synthesis and Implementation of Electronic Materials for Smart Sensor Module",** which is being submitted herewith for the award of the degree of **DOCTOR OF PHILOSOPHY** in **ELECTRONICS** under the faculty of Science of **SOLAPUR UNIVERSITY, SOLAPUR** is the result of original research work completed by **Mr. Suhas Namadev Patil** under my supervision and guidance and to the best of my knowledge and belief the work embodied in this thesis has not formed earlier the basis for the award of any degree or similar title of this or any other University or Examining Body.

Research Guide

Place: Akluj

Date: /07/2015

Dr. B. P. Ladgaonkar
Professor and Head
Post Graduate Department of Electronics
Shankarrao Mohite Mahavidyalaya
Akluj Dist. Solapur

Acknowledgement

I got an immeasurable support from many people as the milestones and in diverse ways, that it could be an impossible task for me to enumerate them to express my gratitude. In the beginning, I would like to thank the almighty God for blessing me at every stage of my life.

I would like to express my deep sense of gratitude, honor and admiration to my guide **Dr. B. P. Ladgaonkar,** Professor and Head, Post Graduate Department of Electronics, Shankarrao Mohite Mahavidyalaya, Akluj. He is prime mentor for me. He has taught me, how good experimental physics is done. I appreciate his devotion and ideas to make my Ph.D. experience productive and stimulating. His observations and comments helped me to establish overall direction of the research and to move forward with investigation in depth. I thank him for providing me an opportunity to work with a talented team of researchers. His patience, flexibility, genuine caring, concern and faith on me during the research work that enabled me to attend to life. He is motivating, encouraging, and enlightening. He provided the right vision and direction, which led to the completion of this work. I feel without him, it could not be possible for me to reach up to this stage.

I express my sincere thanks to **Hon. Shri. Jaysinh Mohite-Patil**, President and **Hon. Shri. Abhijit Rananaware**, Secretory, Shikshan Prasark Mandal, Akluj for providing an infrastructural facilities to carry out this research work.

I am also grateful to **Dr. Abasaheb L. Deshmukh**, Principal, Shankarrao Mohite Mahavidyalaya, Akluj for providing infrastructural facilities for completion of my research work. His proactive and supportive thoughts inspired me to undertake the research work.

I express my most sincere thanks to the **University Grants Commission**, New Delhi for project Fellowship under Major Research Project. I express my thanks to **Shri. R. H. Kumbhar,** Associate Professor, Department of Electronics, Shankarrao Mohite Mahavidyalaya, Akluj for his encouragement.

It is my duty to express my thanks to **Shri. S. K. Tilekar,** Associate Professor, Department of Electronics, Shankarrao Mohite Mahavidyalaya, Akluj for his key role as a researcher. He helped me for designing of hardware of the Smart Sensor Module (SSM). **Miss. Aparna M. Pawar,** Assistant Professor**,** Post Graduate Department of Electronics helped me allot during firmware design. The research work undertaken emphasizes the synthesis of electronic materials. **Shri. Abhijeet S. Powar,** project fellow and **Shri. Prashant V. Mane-Deshmukh** had extended valuable support during synthesis.

I express my thanks to **Prof. J.S. Kadadevarmath,** Head, Department of Electronics, Karnataka University, Dharwad, for his help to entend experimental facilities for FTIR spectroscopy. For synthesis of materials, the help from chemistry department is taken.

Therefore, I am thankful to **Dr. L. V. Nimbalkar**, Head, Department of Chemistry of this college. I also grateful to **Prof. S. I. Patil**, Head, Department of Physics, Savitribai Phule Pune University, Pune for his support during characterization of the .the composition. I also thankful **to Prof. Vijay Fulari,** Department of Physics, Shivaji University, Kolhapur for his help for SEM studies.

It is my duty to express my sincere thanks to my faculty members, Assistant Professors and research fellows **Mr. Sarfraj. S. Shaikh, Mr. Ajit B. Ladgaonkar, Miss Asha R. Raskar, Mr. Sachin V. Chavan, Miss. Sushma V. Nikam, Miss. Prajakta A. Pote, Mrs. Sumaiyya S. Shaikh, and Miss Gangdali G. Mokashi** of Post Graduate Department of Electronics, Shankarrao Mohite Mahavidyalaya, Akluj for their co-operation during experimental work. I would also like to express my thanks to **Mr. Satish Jadhav, Mr. Vishal Patil, Mr. Jakir Mulani, Mr. Aakash Badhe and Mr. Gurudev Arde,** who contributed to this work. Indeed, the Smart Sensor Module ensures the embedded design, wherein design of hardware precisely, plays vital role on its reliability. Therefore, they helped me to fabricate the PCB in the laboratory. I must thanks to **Mrs. Sunita Kate, Mr. N. S. Kadam**, Lab. Assistant and **Mr. D. R. Potdar, Mr. Uday J. Jadhav** and **Santosh Gaikwad** Lab Attendant of our college for their relentless technical assistance. I also thankful to the teaching as well as non-teaching staff of this college for their co-operation during this work.

I also express my thanks to **Mr. Prakash Chougule** and **Mr. Namadev Harale, Dept. of Physics, Shivaji University, Kolhapur** for extending the library and laboratory facilities.

I feel a great pleasure to express the thanks **Mrs. Sudha Ladgaonkar** wife of my guide for her encouragement. She acted as backbone for completion of this work.

If one assumes that, I have not gone insane, then it might be due to **my Parents** Tirth Swarup **Shri. Namdev Patil** and **Mrs. Rajshri Patil** and members of my **in-laws family** Tirth Swarup **Shri. Madhukar Pawar** and **Mrs. Padma Pawar,** who have provided endless encouragement, valuable support, continuous inspiration and moral support.

I also thanks to my family members brother **Sangram**, **Akshay, Ganesh, Mr. Subhash-Mrs. Vasudha** (brother-in-law & Sister), **Mr. Amol-Mrs. Vidhya** (brother-in-law & Sister), and **Mr. Vikram–Mrs. Pallavi** (brother-in-law & Sister), **Shruti, Harshvardhan** and **Arnav (**nephews**)** for the moral support received from them.

It is my duty to express my sense of gratitude to my Wife **Mrs. Aparna. S. Patil,** who had taken relentless efforts of diverse kind, during this research work. She helped me for implementation and interpretation of the results as well. Moreover, she had given me such strength and encouragement, that “thank" seems too cold and empty of a word. I also thanks to all well-wishers, who have directly or indirectly helped me during the course of this work.

Mr. Suhas N. Patil

Dedicated

to

My wife

and

My Parents

PREFACE

Recently, the great revolution is taking place in the field of electronic instrumentation for precise measurement of the physical as well as chemical parameters. It is found that, the embedded technology is an innovative and ubiquitous field of electronics instrumentation particularly the development of an embedded instrumentation for plethora of applications. Now days, a novel field of Smart Sensor Module is emerging. Smart Sensor Module is electronic system, wherein the intellectual devices are incorporated along with analog signal condition. It is standardized by IEEE 1451 standard. Therefore, present research work realizes the confluence of two novel technologies, an ubiquitous embedded technology for development of Smart Sensor Module (SSM) and synthesis of electronic materials for development of sensors required for SSM. The major objective of this research work is to synthesis of electronic materials for development of sensor to measure various environmental parameters as well as typical gases. The compositions of polycrystalline spinel ferrites are synthesized and employing these materials the sensors and sensor modules are developed. For present research work, the compositions of polycrystalline, $Mg_xZn_{1-x}Fe_2O_4$, $Ni_xZn_{1-x}Fe_2O_4$ and $Mn_xZn_{1-x}Fe_2O_4$ (x = 0.2, 0.4, 0.6 and 0.8) spinel ferrites have been synthesized by using co-precipitation method and formation of compositions is confirmed after characterization by X-ray diffraction, FTIR absorption and SEM technique. The results of characterization reveal the formation of single phase composition with nano particle size. These compositions are studied for suitability of the same for sensor based applications. Employing screen printing technique, the thick film sensors are fabricated, wherein different substrates such as epoxy resin, glass, ceramic are attempted. The sensors are developed for relative humidity, temperature, CO_2 gas, H_2S gas and NH_3 gas. Moreover, according to IEEE 1451 standards, the Smart sensor module is developed wherein the novel embedded philosophy is employed. Considering the features of the embedded technology, the hardware and firmware for the Smart Sensor module is designed. The hardware is designed about advanced microcontroller AVR ATmega 8L and firmware is developed in embedded C using CodeVision AVR an IDE to ensure synchronization of operation of hardware. Present SSM is facilitated with, RS232, Serial, SPI outputs. Thus, with design of hardware and

development of the firmware, the design of Smart Sensor Module is successfully carried out. The process of calibration is adopted for these parameters and the results of implementation are presented in this thesis through six topics.

The first topic is of introductory nature. Present research work comprises various fields, such as embedded technology, synthesis of the materials for sensing element, development of sensors, optimizations of properties of the sensors and utilization of the sensor to design smart sensor module. The fundamentals of these fields are explored and described in this topic. The properties of polycrystalline ferrite materials, due to which these materials are recognized as the sensing materials, are also discussed. The concept of Smart Sensor Module is elaborated and architecture of sensor module is proposed. At the end of first topic the origin of the problem is given, which is followed by significance of the research work. Methodology, Aims and objectives of the proposed research work are also discussed in detail.

The second topic is devoted for synthesis and characterization of sensing materials. As per proposal the spinel ferrite materials have been synthesized by employing co-precipitation method and characterized by using standard tools such as, X-ray diffraction, FTIR spectroscopy, SEM etc. The results regarding preparation and characterization of the sensing materials are spread over four sections, A, B, C and D respectively. The conclusion is given at the end of each section. The topic is concluded with the suitability of nanoferrites to ensure for sensing mechanism.

Emphasizing the fact that, ferrite materials reveal sensing abilities, the electrical properties of nano structured ferrites are investigated. The results of investigation are interpreted in topic 3. The temperature dependent electrical properties are studied and used for designing of temperature sensor. The humidity dependent electrical properties are investigated. The variation in the resistance, due to relative humidity is attributed to the process of chemisorption, wherein the protonic conduction mechanism is realized. From this investigation, it is concluded that, the ferrites can be suitably used for humidity sensor. Further, the gas sensing properties of the materials are studied and results are interpreted in topic 3. Topic 3 is concluded with the suitability of the compositions for development of the sensors for gas sensing applications.

Topic 4 is devoted to the designing of sensor module. This sensor module is the realization of embedded technology. Therefore, the details regarding designing issues of both hardware as well as software are discussed in this topic. The sensor module is

designed for five sensors. While designing sensor module, the features such as range, sensitivity, nature of output, power consumption etc. are considered.
Furthermore, implementation of sensor module is carried out and details regarding these are discussed in topic 5. Sensor module is calibrated for different parameters such as temperature, humidity, gas etc in scientific units.The process of calibration and data analysis is also discussed. Topic six is devoted for summary and conclusion.

The PCB design and layout, program listing and the list of the research publications are included in the appendix part. The references are given at the end of each topic. Author has tried to go through the original references as far as possible. The title, given for tables, figures and photographs, are also section-wise and captioned accordingly. Bibliography, depicting terminology employed is also given. Author has duly acknowledged the persons and authorities for their help in connection with work.

INDEX

Synthesis and Implementation of Electronic Materials for Smart Sensor Module

Abstract:

Present research work realizes the confluence of two innovative technologies, an ubiquitous embedded technology for development of Smart Sensor Module (SSM) and synthesis of electronic materials for development of sensors required for SSM. The major objective of this research work is to synthesis of electronic materials for development of sensor to measure various environmental parameters as well as typical gases. The compositions of polycrystalline spinel ferrites are synthesized and employing these materials the sensors and sensor modules are developed. For present research work, the compositions of polycrystalline, $Mg_xZn_{1-x}Fe_2O_4$, $Ni_xZn_{1-x}Fe_2O_4$ and $Mn_xZn_{1-x}Fe_2O_4$ (x = 0.2, 0.4, 0.6 and 0.8) spinel ferrites have been synthesized by using co-precipitation method and formation of compositions is confirmed after characterization by X-ray diffraction, FTIR absorption and SEM technique. The results of characterization reveal the formation of single phase composition with nano particle size. These compositions are studied for suitability of the same for sensor based applications. Employing screen printing technique, the thick film sensors are fabricated, wherein different substrates such as epoxy resin, glass, and ceramic are attempted. The sensors are developed for relative humidity, temperature, CO_2 gas, H_2S gas and NH_3 gas. Moreover, according to IEEE 1451 standards, the Smart sensor module is developed wherein the novel embedded philosophy is employed. Considering the features of the embedded technology, the hardware and firmware for the Smart Sensor module is designed. The hardware is designed about advanced microcontroller AVR ATmega 8L and firmware is developed in embedded C using CodeVision AVR an IDE to ensure synchronization of operation of hardware. Present SSM is facilitated with, RS232, Serial, SPI outputs. Thus, with design of hardware and development of the firmware, the design of Smart Sensor Module is successfully carried out. The process of calibration is adopted for these parameters and the results of implementation are presented in this thesis.

Keywords: Embedded Technology, Smart Sensor Module, polycrystalline ferrites, X-ray diffraction, FTIR absorption, SEM technique.

Topic 1

INTRODUCTION

1. A Introduction:

Present research work realizes the confluence of two technologies an electronic technology, wherein ubiquitous embedded philosophy is used to ensure the development of smart sensor module and second synthesis of electronic materials suitable for development of sensors of promising features required to develop the sensor module of great portability.

Recently, a great revolution is taking place in the field of electronic instrumentation for precise measurement of the physical as well as chemical parameters. Now days, it is found that, an embedded system is an innovative and ubiquitous field of electronics instrumentation. Particularly, the development of an embedded instrumentation required for industrial, agricultural, medical and R & D etc sectors is the need of the hour. An embedded technology is the results of the revolution in the integration technology and computer technology. It is known that, according to Moore's Law, the development in an integration technology doubles every eighteen months [1]. Hence, the advancements in the integration technology result into advanced microcontrollers of promising characteristics. Recently, the deployment of programmable devices, revealing the static as well as dynamic reconfigurable soft and hard cores, for development of embedded system is emerging [2,3]. Use of such sophisticated electronic technologies realizes the emergence of systems with great preciseness and reliability.

Recent trend is to employ smart electronic modules to develop the instrument of desired features. Therefore, the researchers are showing interest in the design of smart electronic module of dedicated features, wherein the technology such as embedded technology is employed. The development of smart sensor module is one of the areas of electronic system design. Therefore, in present research work, it is proposed to develop a sensor module for typical parameters. It is also proposed to design the sensors and then deploy it for above purpose. For design of sensor, the sensing material of required

features is essential, which can be synthesized by availing techniques of materials` research. Thus, the research work undertaken comprises, synthesis of electronic materials, exploring the properties of the sensing materials, designing of the sensor using various techniques, development of sensor module and implementation of the same. The details regarding various technologies, involved in the present research are studied and described in this topic through following major points.

- An Embedded System Design
- Sensing Materials
- The sensors
- The Sensor Module

1.B An Embedded System Design:

Recently, the field of embedded technology is becoming more and more ubiquitous. Therefore, considering the need of hour, it is essential to explore the details regarding this innovative technology. An embedded system is electronic system, comprising a hardware wired about computing device (Microprocessor, Microcontroller, DSP Processors, VLSI devices etc.) and software embedded into target device and designed for dedicated application.

In fact, the microcontrollers are becoming an integral part of the Engineering design known as Embedded System [4]. The designing of microcontroller based embedded system finds wide range of applications in various fields, such as instrumentation for agriculture, test & measurement instrumentation, instrumentation for process control, automobile, consumer electronics, entertainment, domestic applications, R & D, medical instrumentation, industrial automations, etc. Such extreme diversity of applications is resulting into evolution of wide range of embedded systems [5, 6] and related fields of hardware & software co-design [7]. In addition to the emphasis on interaction with the external world (sensors, actuators etc.) the embedded systems also provides functionality related to their dedicated applications. Many technologist and scientists are contributing to development of smart system to improve the quality of the instruments. Now days, the computing industry has passed through a rapid sequence of technological development giving rise to open the fields of industrial and domestic applications [8]. Hence, it is essential to use the sensor, which converts the change in the physical quantity into electrical energy. Prior to further

processing such signals are conditioned. The signals are always in analog form, which have to be digitized by using highly precise ADC. It is possible to use advanced microcontroller and On-chip facilities of microcontroller for data acquisition. The embedded system reduces the tedious job of data processing and calibration [9]. It also increases the flexibility and portability in the application of the devices.

Moreover, recently, the field of VLSI design and development of embedded system is revolutionary and many technologists are employing this ubiquitous technique for sophisticated instrumentation development for research and development purpose. It is need of the hour to develop most reliable and intelligent system for measurement of various physical parameters. Microcontroller based embedded system is found to be most reliable, because these are developed about high performance Microcontroller. On literature survey, it is found that many investigators have shown the interest in the use of microcontrollers for development of sophisticated instrumentation [10-12]. There are different high performances Microcontroller from different vendors. The investigators have reported the design of embedded systems, wherein the microcontroller from MCS51 family is employed for dedicated application. However, due to its limitations, such as the sinking and sourcing current level, on chip RAM and flash ROM, its use for sophisticated embedded system is constrained. Moreover, recently the Microcontrollers from AVR family, PIC family, ARM family, etc of promising characteristics are readily available. In addition to this, the required on chip resources such as ADC, DAC, etc are also available in these microcontrollers. Deploying the silent features of the microcontroller one can design highly reliable and more precise electronic system for measurement of physical parameters. The microcontrollers from AVR families are showing promising features such as on chip ADC, DAC etc [13]. Moreover, the on-chip ADC of 10 bit resolution really helps to enhance the preciseness in the data, which is rather expected. This not only causes to reduce complexity in hardware and software but also the cost. In addition to ADC these microcontrollers are having other on chip resources deploying which a sophisticated instrument can be designed [14]. In short a development of advanced microcontroller based embedded system is the novel field of development of instrumentation for R&D application.

1.B.(a) Definition of an Embedded System:

The various authors have their own views regarding the structure of embedded system. Therefore, there are various definitions of the embedded system. However, each definition focuses the words Hardware, Software and Dedicated application. That

means an embedded system consists of both hardware and software programmed into the target device. But the system should be designed for dedicated application only and not the general purpose.

According to Raj Kamal an embedded system is one that has computing hardware with software embedded in it as one of its most important component[15]. There are several definitions of embedded system, stated by various author [16-18] The word embedded implies that, it lies inside the overall system, hidden from view, forming an integral part of whole. Tim Wilmshourst [19] had given the wide definition as, "An embedded system is a microcontroller based system, software-driven, reliable, real-time control, autonomous, human as well as network interactive, operating on diverse physical variables and diverse environments". Wayne Wolf [20] loosely defined "Embedded Computing System is any device that includes a programmable processor but is not itself intended to be a general-purpose computer", whereas, according to T. D. Morton [21] the Embedded Systems are electronic systems that contain a microprocessor or microcontroller, but we do not think of them as computer" and D. E. Simon [22] stated that "People use the term Embedded System to mean any computing system hidden in any of these products". Moreover, by tracing many aspects, T. Wilmshurst [19], defined the embedded system as, "an Embedded System is a system whose principal function is not only computational function, but also controlling by a computer embedded within it. The computer is likely to be a microprocessor or microcontroller. The word embedded implies that it lies inside the overall system, hidden from view, forming an integral part of whole system.

1.B.(b) Salient Features of an Embedded System:

It is essential to enumerate the characteristics of the typical embedded system.

- Embedded systems are dedicated to specific tasks, whereas PCs are generic computing platforms.
- Embedded systems are supported by a wide array of processors and processing architectures.
- Embedded systems are usually cost sensitive.
- Embedded systems have real-time constraints.
- Embedded system comprises OS like RTOS rather than Windows NT, Windows 2000. However, the TinyOs is OS used for developing NOdes for WSN type architecture.

- Embedded systems often have power constraints.
- Embedded systems often must operate under extreme environmental conditions.
- Embedded systems have far fewer system resources than desktop systems.
- Embedded systems often store all their object code in ROM.
- Embedded systems require specialized tools and methods to be efficiently designed.
- Embedded microprocessors often have dedicated debugging circuitry.
- Once developed, the system operates stand alone.

1.B.(c) Basic Architecture of an Embedded System:

The general architecture of an embedded system is shown in Figure 1.1. This is realization of layered architecture, wherein application specific hardware is act as a core. It also contains the memory chip onto which the software is loaded. The software residing on the memory chip is also called as 'Firmware'. The operating system runs above the hardware and application software is the outermost layer. This architecture is similar to that of desktop computer. However, significant difference is that, the desktop computers compulsory need the operating system and the operating system is optional for embedded system [23]. As depicted in Figure 1.2, the hardware of an embedded system consists of various building blocks such as computing unit, ROM and RAM, I/O devices, sensors, analog to digital converter, small keypad, digital to analog converter, LED, LCD, communication interface, power supply units, etc. Moreover, communication interface helps to establish the communication between an embedded system and other system or desktop computers. To facilitate this, the communication interface such as RS232, RS422, USB, IEEE 802.11, I2C, SPI etc may be incorporated in embedded system.

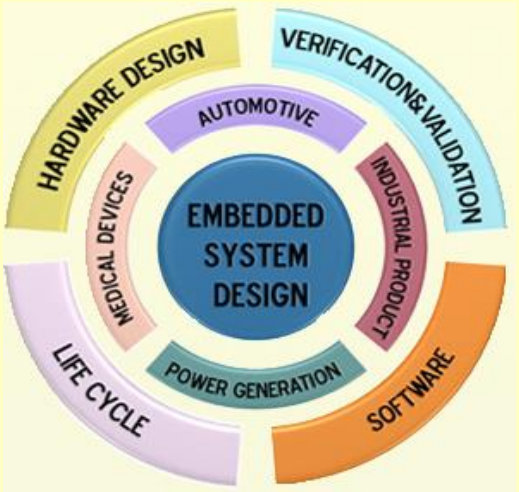

Figure 1.1: General Architecture of an embedded system

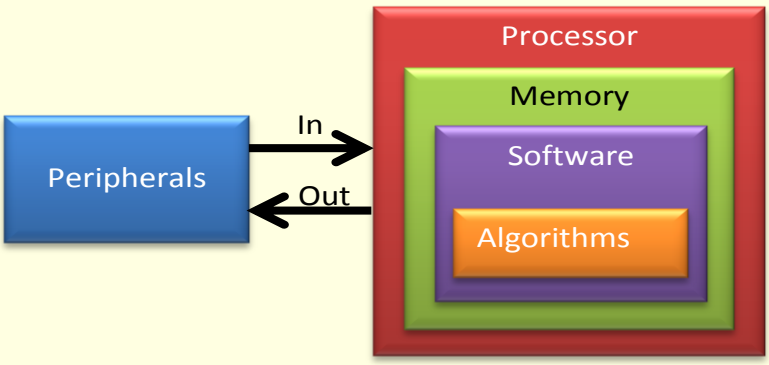

Figure 1.2: Overview of an embedded system architecture

1.B.(d) Classification of an Embedded System:

According to CPU used the embedded systems are two types.

1. General Purpose Processor (GPP)
2. Digital Signal Processor (DSP)

The GPP embedded systems normally employ general purpose microcontroller, whereas the DSP embedded system consists of DSP processor, which is a Application Specific Instruction set Processor (ASIP). The embedded systems are also broadly classified into three classes such as Small Scale Embedded System, Medium Scale Embedded System and Sophisticated Embedded System.

(i) Small Scale Embedded System:

These systems are designed with a single 8-bit or 16-bit microcontroller. They have small hardware & software complexities. While developing embedded software for these systems, the editor, assembler & cross-assembler, specific to the microcontroller, are the major programming tools, which further incorporated into the IDE[24]. Usually, 'Embedded C' is used as IDE to develop these systems. It uses on-chip memory for information processing. Moreover, it consists of application software only without the layers of operating system.

(ii) Medium Scale Embedded System:

These systems are designed with a single or few 16-bit or 32-bit Microcontrollers or DSPs of Reduced Instruction Set Computers (RISCs) types. They have both hardware and software complexities. The software programming tools are RTOS, source code engineering tool, simulator,

debugger & integrated development environment (IDE) [25]. These tools also provide the solution to hardware complexities.

(iii) Sophisticated Embedded System:

These systems have enormous hardware & software complexities and may need scalable processors or configurable processors & FPGA[26]. They are used for cutting edge applications that need hardware & software co-design and integration in target system. However, these systems are constrained by the processing speed available in their hardware units. The Transmission Control Protocol/Internet Protocol (TCP/IP) stacking and network driver functions are incorporated in hardware to obtain additional speed by saving time. Moreover, the software also implements some functions of the hardware resources.

The embedded systems can also be categorized on the basis of functionality and performance requirements as,

(i) Stand-alone Embedded System:

As the name implies, stand-alone system works in stand-alone mode. They take inputs, process them and produce the desired output. Embedded systems used in process control instrumentation, automobiles, consumer electronic items etc are grouped in this category.

(ii) Real-time Embedded System:

Embedded system, in which some specific task has to be completed in a specific period are called real-time embedded system. Meeting the deadlines is the most important requirement of real-time embedded system. The real-time embedded system are further categorized as Hard Real-time Embedded System – a system missing the deadline may lead to a catastrophe and Soft Real-time Embedded System – meeting the deadline is important but missing the deadline will not lead to catastrophe. In addition to application software based on embedded C, it consists of Real-Time Operating System (RTOS).

(iii) Network Information Appliances:

The embedded systems, which is provided with network interfaces & accessed by networks such as LAN or the internet are called network information appliances. Such systems are connected to the internet or company's intranet network, typically a network running TCP/IP protocol suite. The IEEE 802.11 is the best example of network information appliances. The

embedded system developed for telemetry applications are involved in this category.

(iv) Mobile Devices:

Mobile devices such as mobile phones, Personal Digital Assistant (PDA), smart phones etc. are a special category of embedded system. The constraints such as small memory, small size, limited of I/O devices etc. provide impediment to the user.

1.B.(e) Embedded System Processors Architecture:

As discussed in previous article the CPU, i.e. microcontroller, performs major job of data processing and it plays vital role in establishing communication between I/O devices and internal as well as external memory through data buses, address buses and handshaking control signals. According to the nature of memory that, the microcontrollers can accesses, there are three architectures viz, Von Neumann architecture, Harvard architecture and Super Harvard architecture.

(i) Von Neumann Architecture:

This architecture has single memory device that handles both code and data. Figure 1.3 depicts the realization of Von Neumann architecture. The processor communicates with memory via address & data buses. To speed up the communication, this architecture makes the use of pre-fetching and pipelining during the execution of instruction. The part of fetch cycle is super imposed on the part of previous execution cycle. The biggest advantage of Von Neumann architecture is that, it simplifies the embedded chip design, because system accessed only one memory chip. This architecture allows greater flexibility to embedded system designer in designing software, primarily in the area of RTOS and hence, it is most widely used architecture.

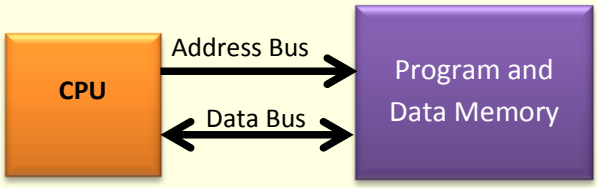

Figure 1.3: Von Neumann architecture

(ii) Harvard Architecture:

This architecture has two separate memory devices, one for program (instruction) memory and second for data memory. As shown in Figure 1.4. memory chip can also be partitioned as the code segment and data segment. As the program and data memories are separate blocks, their interfacing with

processor is also isolated, i.e. the code memory and data memory are mapped at different addresses.

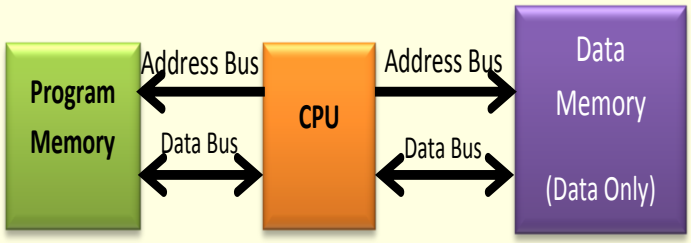

Figure 1.4: Harvard architecture

Moreover, this architecture provides accessing of instruction and data very fast, as parallelism operation is possible. Therefore, this architecture is very efficient. Nevertheless, in initial development phases of embedded system this architecture was strongly ignored by the designers until they realized the architecture had advantages for devices, which were currently designing.

(iii) Super Harvard Architecture:

The disadvantage of the Harvard Architecture is that the data memory is accessed more frequently than the program memory. Therefore, in Harvard architecture, provisions have been made to store some data as a secondary data in the program memory to access the both memories equally. This structure is called Super Harvard Architecture. That is, this architecture is nothing but the significant modification of the previous Harvard Architecture. It is as shown in Figure 1.5. This architecture is extensively used in Digital Signal Processors.

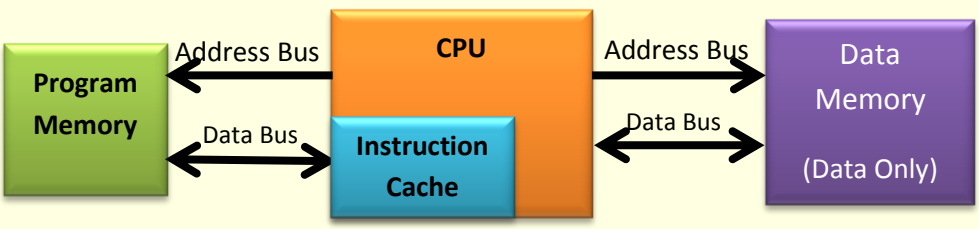

Figure 1.5: Super-Harvard architecture

(iv) CISC and RISC Architecture:

The Complex Instruction Set Computer (CISC) architecture has large number of instruction set with number of addressing modes. This provides small number of registers. Therefore, to do particular task the few instructions are needed and hence less memory is needed. The overall design of CISC processor is to reduce the software complexities by increasing hardware complexity of processor. The CISC has a micro-programmed unit with a control memory. The CISC features to provide easy compiler design and precise & intensive

calculations slower than RISC. The Intel x86 family and Motorola 68000 series processors are examples of CISC processors.

The Reduced Instruction Set Computer (RISC) architecture has limited number of instruction in the instruction set architecture with very few addressing modes. This provides large number of registers and hence large memory is needed. The overall design of RISC architecture is reducing the hardware complexity of processor by increasing software complexity. The RISC features provide a complex compiler design and precise & intensive calculations faster than CISC. Another feature of the RISC processor is the pipelined instruction execution, which makes faster execution of the program. The RISC processor can provide processing power more than three times that of a CISC processor in particular field of application [27]. The ARM, ATMEL, PIC, AVR, MIPS, Microchip and Power PC are the best examples of RISC processor. Some processors may have combination of CISC and RISC features such as ARM7, ARM9 and Intel 80960. The combination features provide advantage of using CISC in terms of functionality and using RISC in terms of faster program implementation as well as reduce code length.

1.B.(f) Characteristics of Embedded Systems:

The microcontroller as well as VLSI device based embedded systems are characterized with following salient features.

1. Reliability:

Reliability is the important paramount of the embedded system. It should continue to work for thousands of hours without break. The results shown by the system are accurate and reliable. The facilities such as, watchdog timer, brown-out reset, power down reset etc. significantly help to improve the reliability of the designed system.

2. Flexibility:

Embedded system comprises microcontroller or VLSI devices as the central computing unit. These devices are featured with the configurability. Deploying static as well as dynamic configurability of these devices, the flexibility in the design can be ensured. The flexibility in the designing of

hardware and software for the embedded system indeed widens the application areas.

3. Performance:

The embedded systems are developed about microcontroller and highly sophisticated logic devices. This leads to increase the performance of the system, particularly in industrial process control applications. The FPGA based embedded systems also exhibit promising performance.

4. Power Consumption:

Mostly, all embedded system operates on rechargeable battery. The microcontroller used to develop the system is primarily low power device. Moreover, it uses good quality and low power consuming hardware components like LCD. Therefore, the embedded system usually exhibits low power consumption. Moreover, the use of power down mode and sleep mode help in reduction of power consumption.

5. Cost:

For designing embedded system for industrial, Biomedical etc. applications, the cost is not limiting factor. But embedded system used in consumer electronics, office automation, domestic instrumentation, etc., the cost is of utmost important factor. The microcontroller based embedded systems exhibit rather less cost.

6. Limited User Interface:

Unlike desktop, which has sophisticated I/O interface, the embedded system has very less I/O interface. Moreover, many embedded system, which only takes electrical signal as input and produces electrical signal as output, do not have much user interface. While in many embedded system, the input is through a limited function keypad or a set of buttons and output is a displayed either on a small LCD or a set of LED's, for example, mobile phones, iPod etc.

7. Software Up gradation Capabilities:

For specific task, it is not necessary to upgrade the software once ported into the target memory. However, the software upgradation is the prominent feature of embedded system. The on-chip memory or external memory can be reprogrammed easily. The software of Public Call Office (PCO) and Automatic Teller Machine (ATM) frequently needs to upgrade, which could be done by reprogramming the chips.

8. Size & Weight:

The size and weight are the important parameters for many embedded system used in mobile, defense etc applications. Moreover, to reduce the size and weight, hardware designer has to design the embedded system within the minimum possible components. The day-by-day revolutionary development in microelectronics reduces the size and weight of embedded system, increases the reliability and performance.

1.B.(g) General Applications of Embedded System:

Embedded system finds diversified applications in various fields such as industrial sectors, consumer electronics, automobile & transportation, biomedical engineering, manufacturing process control & industrial automation, data communication, telecommunication, defense missiles & satellite, security, wireless communication, finance, computer networking & so on.

i) Consumer appliances:

It is found that the number of embedded system, such as digital cameras, digital diary, DVD player, electronic toys, microwave oven, remote control for TV and air-conditioner, VCD player, video game consoles, video recorders etc. are available for common people. Today's high-tech cars have about 20 embedded systems for transmission control, engine spark control, air-conditioning, navigation etc. The palmtops are powerful embedded systems using which number of general-purpose tasks is carried out such as word processing and playing games.

ii) **Office Automation:**

For office automation, the devices using embedded system, are copying machine, fax machine, key telephone, modem, printer, scanner etc.

iii) Industrial Automation:

Now a day a lot of industries, pharmaceutical, sugar, cement, nuclear energy, electricity generation and transmission, use embedded systems for process control. Recently, the embedded are also designed to control the PLC operation in industrial automation. The embedded systems for industrial use are designed to carry out specific tasks such as monitoring the temperature, pressure, humidity, voltage, current etc. and then take appropriate action based on the monitored levels to other devices or to send the information to a

centralized monitoring station [27]. The robots, which are programmed to do the specific tasks, are now becoming very powerful and carry out many interesting and complicated tasks such as hardware assembly, hazardous industrial environment.

iv) Medical Electronics:

Presently, almost every equipments in the hospital is an embedded system. These equipments include diagnostic aids such as ECG, EEG, blood pressure monitoring devices, X-ray scanners; equipment used in blood analysis, radiation, colonoscopy, endoscopies, etc. The best examples are pulse oximeter and ECG Monitor [28, 34,35].

v) Computer Networking:

Computer networking products such as bridges, routers, Integrated Services Digital Networks (ISDN), Asynchronous Transfer Mode (ATM), X.25 and frame relay switches are embedded systems which implement necessary data communication protocols. Most networking equipments, other than the end-systems (desktop computers) required to access the networks are embedded systems.

vi) Telecommunications:

In this field embedded systems are categorized as subscriber terminals and network equipments. The subscriber terminals such as key telephones, ISDN phones, terminal adapters, web camera are the embedded systems. The network equipments includes multiplexers, multiple access systems, Packet Assemblers Disassemblers (PADs), satellite modems etc. IP phone, IP gateway, IP gatekeeper etc. are the latest embedded systems that provide very low-cost voice communication over the Internet.

vii) Wireless Technologies:

Advances in mobile communication are mainly due to the application of embedded systems. The mobile phone is very powerful embedded system that provides voice, data and video communication. Mobile communication infrastructure such as base station controllers, mobile switching centers are the powerful embedded systems. Wireless sensor network is good example wherein embedded philosophy is deployed in the sensor nodes [29]. Moreover, today

PDAs and palmtops can be used to access multimedia services over Internet. The Zigbee also reveals the use of an embedded technology [30]

viii) Test and Measurement Instrumentation:

Testing and measurement of physical and chemical parameters are the fundamental requirement in all scientific and engineering activities. For measuring instruments used in laboratories to measure parameters such as weight, temperature, pressure, humidity, voltage, magnetic parameter, current etc. the embedded systems can be used. The test instruments such as oscilloscope, spectrum analyzer, logic analyzer, protocol analyzer, radio communication test set etc. are embedded systems built around powerful DSP. Recently, due to miniaturization, the test and measurement instruments becoming portable facilitating ease of measurement in the remote area.

ix) Security:

Security of persons and of information has always become a major issue. Security devices that developed for security applications at homes, offices, airports etc. for authentication and verification are the embedded systems.

x) Finance:

The smart card and ATM machines, which are used for financial transactions in place of cash and cheques, are the examples of embedded systems.

xi) Environmental Monitoring

During recent days, the monitoring of environmental parameters such as temperature, humidity, light intensity, concentration of typical environmental gases etc is need of the hour [31]. An embedded system design is most suitable solution for monitoring of the environmental parameters [32].

xii) Food Security and Cold Storage:

It is known that the, fruits are seasonal and one has to preserve the same to make it available in off season as well. For this purpose, recently, the cold storage houses are emerging. Various parameters of the cold storage environment must be precisely monitored for which design and implementation of embedded system is the essential solution [33].

1. C: Sensing Materials and Sensors:

Recent trend is to develop smart systems, based on an embedded philosophy, to measure and control of physical parameters. A sensor is the key portion of measurement system that, responds directly to the physical variables to be measured. Therefore, one should opt for proper sensor of better characteristics. The reliable detection of environmental parameters, toxic or harmful gases, is becoming a major issue of environment and safety regulations. Therefore, many researchers and scientists focused on the activities of development of sensing devices, especially for humidity and gas sensors. In spite of considerable effort, the development of good sensors is not possible. The monitoring of environmental gases plays significant role in industry as well as general public sectors. Detectors or sensors can be used for different applications, such as continuous monitoring of the humidity, temperature, the concentration of gases in the environment and premises, detection of toxic gases, drugs, smoke, fire, health, control of automotives, industrial emissions etc [36]. The detection of combustible gases like coal gas and liquefied petroleum gas (LPG) has become very important because explosion accidents might be caused when they leak out accidentally. Moreover, for the manufacturing highly sophisticated integrated circuits in semiconductor industry, humidity and temperature is constantly measured and monitored for wafer processing. There are many domestic applications, such as cooking control for microwave ovens, intelligent control of the living environment in building and foundry etc. In automobile vehicles, such as smart cars, the temperature and humidity control should be ensured by the use of electronically controlled foggers and ventilators. In industry humidity, temperature and gas sensors are deployed for purifications, dryers, film desiccation, paper and textile production and food processing etc. In medical field, these sensors are used in blood storage, pharmaceutical processing, incubators, respiratory equipments and biological products. In agricultural field the monitoring of environmental parameters plays significant role on the crop growth and yield as well, particularly in case of polyhouse where the plants are cultivated in controlled environment [37]. Therefore, humidity, temperature, gas concentration and soil parameters should be measured with highly sophisticated sensor systems. As discussed earlier, the sensor plays vital role in the design and implementation of precise measurement system.

Therefore, developments of smart sensors have gained increasing applications in industrial processing and environmental control. Promisingly featured sensors help to

enhance the features of sensor module, which would be further deployed for device fabrication [38]. Significant achievements in the technology have encouraged the development of a large variety of very small sensors for miscellaneous applications such as measurement of the humidity, temperature and gas etc. Therefore, one should opt for proper sensor of better characteristics. The characteristics of sensor depend upon material used and the fabrication technology adopted [39]. The wide spectrum of sensing materials is reported by many researchers. During early days, the metal oxides, such as zinc oxide, tin oxide, cadmium oxide, tungsten oxide etc, are deployed for fabrication of the sensors [40]. These metal oxides reveal the properties of adsorption and absorption, availing which the sensors have been fabricated either in bulk or thick or thin film form. These sensors are more expensive. Therefore, on deployment of such readily available sensors, of desired features, to develop smart sensor module is not affordable. This may causes to increase the system cost as well. Therefore, it is proposed to synthesize the sensing material to cater the needs of present design. Characterization and implementation of these sensing materials, to fabricate the sensor of required features, is carried out.

On extensive study of physical properties of ferrites, it is found that the polycrystalline ferrite exhibits its suitability for development of such sensor. Therefore, many investigators are showing interest in ferrite materials for sensor development [41,42]. It is well-known that, many porous metal oxides can be used as humidity-sensing materials. The adsorption of water vapor can enhance the surface electrical conductivity and dielectric constant of the metal oxides. It is found that, the ceramic materials, ferrimagnetic oxides, called ferrites exhibit more interesting electrical as well as magnetic properties [41]. These intrinsic properties are found to be sensitive to the substituted cations and also distribution of cations among the tetrahedral (A) and octahedral (B) sites. It is found that these properties are mostly sensitive to the microstructure of the compositions, which depends on the preparation methods and sintering temperature as well [42]. The electrical resistivity shows negative temperature coefficient with temperature and hence the materials could be used to design temperature sensors [43].

During recent days, it is proved that, the ferrite compositions are mostly suitable candidates for gas sensing and humidity sensing as well. Therefore, new area of deployment of ferrites for sensor based application is emerging. On literature survey, it is observed that, generally, there are two types of gases called reducing gases and

oxidizing gases. The gases such as NO_2, NO, N_2O, CO_2 etc are oxidizing gases. However, the gases such as NH_3, H_2S, CH_4, ethanol, acetone etc are come under the group of reducing gases [44]. On study, it is found that, the ferrites are suitable for detection as well as measurement of these gases. The ferrite materials also depict humidity sensitive electrical properties. To keep pace with the objectives of the present research work, the synthesis of sensing materials is carried out and the fundamentals of ferrite materials are explored and discussed in brief.

1.C.1 The Polycrystalline Ferrite as a Sensing Material :

The word ferrite was first time used at the beginning of 20^{th} century, which is derived from Latin word ferrum means iron [45]. Ferrites, the ferrimagnetic oxides, are a new class of magnetic materials, having partially compensated antiparallel spins resulting into non-zero magnetic moment [46]. Along with magnetic properties, these materials also have remarkable electrical properties such as high resistance with negative temperature coefficient of resistance, low dielectric loss, thermoelectric power etc. Therefore, these materials are also called as "Magnetic Semiconductor". Along with the milestones, many investigators were contributed to the development of ferrite materials [46-48]. Near about room temperature the ferrite compositions exhibit abnormal behavior in variation of log ρ against 1/T. This metalic conductivity behaviour may be attributed to the environmental humidity [49]. This behavior of the ferrite compositions leads to develop humidity sensors. In shorts ferrites plays vital role in the development of sensors for various physical parameter measurements. The ferrite finds the applications as device and sensor [50]. Kyoshiro Seki et al have reported the use of ferrites as humidity sensor [51], which is further developed by Vaingankar et al in the laboratory [52]. Rezlescu et al have reported the gas sensing properties of porous Cu-, Cd- and Zn- ferrites [53]. Singh et al also reported gas sensor properties of ferrite material [54]. Sláma et al have reported ferrites for passive sensors applications [55]. Brito et al have reported Ni-Zn Ferrite used for Temperature Sensors [56]. Moreover, many researchers are reported the use of ferrite sensor for Wireless Sensor Network based smart home automation, mine gas sensor, Precision Agriculture etc [57]. Recently, ferrites of nanocrystallite size are synthesized by many researchers, by using different methods of preparation. Due to existence of nano particles the effective

surface area in significantly increased [58], which favours the process of chemisorption required for sensing environmental gases.

Now days, ferrite in liquid form called "Ferrofluid" is becoming popular [59-61]. This ferrofluid find tremendous applications in medical, industrial etc fields. It can also be used for sensor developments. The magnetic ceiling is the best application of ferrofluids.

Ferrimagnetic oxides, ferrites, a major constituent of magnetic ceramic materials, have attracted considerable attention, because of their wide applications in electronic and magnetic devices [62]. These ferrites have interesting intrinsic properties. These properties are found to be sensitive to the method of preparation and preparation conditions. Also, the properties are sensitive to the substitution of foreign ions into parent compositions. The ferrites exhibit magnetic properties such as saturation magnetization, magnetic moments, retaintivity, coercivity, magnetic loss, susceptibility, permeability etc. The temperature as well as frequency dependent data of these parameters reveal structural details about the materials under investigation [63]. These data also help to check the materials suitability for different fields of applications. The magnetic properties are mainly due to magnetic interactions between the magnetic ions distributed among two crystallographic sites; A sites and B sites [64]. On the basis of spin interaction, Neel had [65] developed the theory showing resultant magnetization is $M = |M_B| - |M_A|$. This relation is used by Upadhyaya et al to predict cation distribution [66], which is further modified by Vasambekar et al considering the fact that Curie temperature is function of strength of magnetic interaction.[62] .

Electrical properties such as high resistivity and low mobility make the ferrites suitable for development of electronic sensors. Electrical conduction process can be explained with the help of the principle based on hopping of charge carriers from Fe^{2+} to Fe^{3+} ions located at B site [67,68]. The ferrites also show thermo emf. The sign of Seebeck coefficient gives information regarding type of majority charge carriers either holes or electrons [69]. Due to the dielectric behaviour, the ferrites also find applications in microwave region [70]. Moreover, the existence of protonic conduction is also suggested, which may lead to use these ferrites for development of humidity sensors. The most important technical properties, considered from application point of view, such as saturation magnetization, coercivity, permeability, magnetic loss etc, changes drastically as the size of particle changes to nanometric length [71,72]. The

composites of ferrites and ferroelectric materials also show very interesting magneto electric properties [73].

Properties of ferrites, which decide the field of applications, depend on method of preparation. Most commonly used method is standard ceramic method. However, this method has its own limitations regarding homogeneity, density, porosity etc. However, wet chemical method, wherein principle of co-precipitation is used, involves reaction at atomic level. Hence, it can produce the ferrites of high density and nano particle size [74]. On reduction of particle size to few nm, the electrical resistivity can be enhanced, due to which the materials can be used for sensor based applications. This low grain size can be obtained by wet chemical method. The details regarding preparation of ferrites compositions under investigation are explained in next topic. Therefore, it is proposed to use co-precipitation method for preparation of the compositions under investigation. The electrical characteristics play vital role in deciding the area of application. These are useful for development of sensor, not only based on resistivity measurement but also on the capacitive properties.

The spinel structure, in brief is discussed followed by the types of spinel ferrites.

1.C.1(a)The Spinel Structure:

Polycrystalline ferrites, having general formula MFe_2O_4 (M is the divalent cation such as Cd^{2+}, Zn^{2+}, Ni^{2+}, Co^{2+}, Cu^{2+} , Fe^{2+}, Mn^{2+}etc), is iso-structural with mineral spinel $MgAl_2O_4$ having space group Fd3m No. 227 [75]. The unit cell is cubic and comprizes 8 formula units. That means the unit cell has 8 divalent metal ions, 16

TABLE 1.1: The Spinel structure

Sr. No.	Sites and space group symmetry	Tetrahedral (A) site	Octahedral (B)site
1	No of sites available	64	32
2	No. of Sites occupied	8	16
3	Positional co-ordinates of Fd3m space group	8a or 8b	16c or 16d

trivalent metal ions and 32 oxygen ions. The metals ions are accommodated in the lattice of 32 oxygen ions. Such unit cell of spinel structure consists of two crystallographic equivalent sites; the tetrahedral (A) site and octahedral (B) site [76]. Total 96 sites are available. Both A and B sites are partially filled. According to

Wyckoff`s notations, the positional co-ordinates for A and B sites are 8a or 8b and 16c or 16d respectively. However, oxygen ions have 32e coordinates. The oxygen ion parameter (u) is important parameter and ideally, it is 3/8. This varies with the cation distribution in the spinel structure [77]. This could be summarized in the table 1.1.

1.C.1(b) Classification of the Spinel ferrites :

According to crystal structure the ferrites are classified into four groups, as Spinel ferrites, Garnet, Hexa ferrites and pervoskite. Moreover, a new class of ferrites i.e. ferrofuild is also recently progressing. According to cation distribution the ferrites can be classified as,

- **Normal spinel**

Cation distribution : $(M^{2+} \uparrow)^{A}$ $[Fe^{3+} \downarrow Fe^{3+} \uparrow]^{B}O_4$

- **Inverse spinel**

Cation distribution : $(Fe^{3+} \uparrow)^{A}$ $[M^{2+} \downarrow Fe^{3+} \uparrow]^{B}O_4$

- **Random spinel**

Cation distribution : $(M_{\delta} Fe_{1-\delta})^{A}$ $[M_{1-\delta} Fe_{1+\delta}]^{B}O_4$

Based on chemical compositions they have following classes.

- **Simple ferrites**

Fe^{2+} ion is substituted by one metal ion.

- **Mixed ferrites**

Fe^{2+} ion is substituted by more than one metal ions.

- **Substitutional ferrites.**

  Fe^{2+} ion is substituted by one or more than one metal ions and also Fe^{3+} ion is partially substituted by another trivalent cation such as Cr^{3+}, Nd^{3+}, Gd^{3+} etc.

1.C.1(c) Properties of spinel ferrite:

The polycrystalline ferrites have interesting electrical and magnetic properties. These properties are found to be sensitive to the method of preparation, sintering temperature chemical compositions and also to the substitution of the foreign ions. Due

to this they find wide applications in various fields. On controlling above conditions, the material of required properties can be synthesized. These properties are discussed in brief.

i) Magnetic Properties:

Magnetic properties of spinel ferrite can be discussed based on the magnetic parameters such as saturation magnetization, magnetic moments, retaintivity, coercivity, magnetic loss, susceptibility, permeability etc. These magnetic parameters depend upon chemical compositions, cation distribution and microstructure of the spinel ferrite. However, it depends on the substitution of divalent or trivalent ions. Magnetization in ferrite is the results of super exchange interaction between magnetic ions located at tetrahedral site and octahedral site of the spinel structure. The magnetic nature of the ferrites can be explained by Weiss Law and then by Neel theory of ferrimagnetization. The compositional dependence of magnetic moments are described by existence Yafet-Kittle angle. The susceptibility and permeability of composition reveals the microstructural features of the compositions. The temperature dependent behaviour of susceptibility demonstrates the existence of single domain or multi-domain nature of the particles. The superparamagnetic behaviour can be detected from susceptibility data. From magnetization, the distribution of cations can be predicted. The information regarding distribution of cations may help to support the electrical characteristics of the compositions. Therefore, it is also suggested to use the sensor at operating temperature, typically above the Curie point. The magnetic nature of the ferrite materials, reveal very low eddy current loss. Therefore, these are suitable for high frequency applications.

ii) Electrical Properties:

Due to intrinsic electrical Properties such as a high resistivity and low mobility etc the ferrite materials exhibit its suitability as sensing materials. These properties are sensitive to the temperature and applied frequency also they show their dependence on chemical composition. The study of electrical properties provides information regarding transparent phenomenon for both bulk as well as at surface [78]

- Polycrystalline nanoferrites reveal semiconducting behaviour with negative temperature coefficient of resistivity. The temperature dependence of resistivity can

be described by using Wilson relation, $\rho=\rho_0 \exp(\Delta E/KT)$. Where, ΔE is the activation energy and K is the Boltzman constant. On investigation of electrical properties, it is also found that, the electrical properties are influenced by magnetic interaction as well. These properties can be used to obtain the Curie temperature, which is prime characteristic of magnetic material [79]. The ferrite materials, either in the bulk or film form, depict thermistor nature. Hence, it could be used as a sensing material for development of temperature sensor. However, the exponential nature of the ferrite sensor should be linearized by employing electronic means.

- The ferrites are magnetic oxide materials, which favour the mechanism of chemisorption at the surface of the gains. The chemisorption of water molecules, in vapour form, causes the dissociation of H_2O to for H^+ ions and OH^- ions. As described in topic 3, it favours the protonation and reveals humidity sensitive nature of the compositions [80]. The resistance of the sensing element decreases with increase in the relative humidity. Therefore, the ferrite can be used as humidity sensing material.
- Similarly, at typical operating temperature, the species of oxygen ions adsorb at the crystallographic sites of the sensing material. This emerges the gas sensing properties of the ferrite compositions [81,82]. Therefore, the ferrite materials can be suitably used for gas sensing applications.

1.C.2 The Sensors:

Development of the sensors for different application is an innovative area of the research. Therefore, deploying the sensing materials of the sensors, desired features can be designed. As discussed earlier, the polycrystalline nanoferrite materials are mostly suitable for development of the sensors. The sensor required for measurement of the humidity, temperature, concentration of various environmental gases etc are need of the present day measurement instrumentation. The sensors would be designed by employing various techniques. Depending upon the techniques used the sensor could be classified into the types such as, Bulk, Thick film, Thin Film,

Figure 1.6: The sensor of bulk type

Interdigitated sensor etc. The sensors of above types are characterized with their own merit and limitations. Therefore, depending upon the requirement, sensor may be designed by employing one of the above techniques.

- The sensor, of the bulk form, is either in tablet or rod form of the specific dimensions. The electrical contacts are developed by pasting silver electrodes or employing techniques such as ion implantation. This sensor is based on bulk properties of the sensing materials. Therefore, features of such sensors and application areas depend upon bulk properties. The bulk sensor is typically depicted in figure 1. 6.
- Various methods, such as spin coating, vapor deposition, Spray pyrolysis, photolithography, screen printing etc, of developing film of sensing materials are evolved. By employing these methods the thin film sensor, as presented in figure 1.7 can be designed. Due to nanotechnology and its merits, the sensors of promising features may be designed. Thin film sensors, due to salient features find wide spectrum of applications in various fields. However, development of thin film of desired sensing materials, maintaining crystallography, is difficult. Therefore, the researchers are attracted towards the preparation of thick film sensors.

Figure 1.7: The Thin film sensor.

Figure 1.8: The Thick film sensors.

- Employing the well suited screen printing technology, the thick film of the sensing elements can be deposited on typically designed substrate. The substrate may be either ceramic or glass. The substrate should also satisfy the need of the sensor. Many times the sensors are operating at high temperature. Therefore, the substrate and hence the thick film should withstand to these condition. The thick film sensors developed on cylindrical and rectangular substrate are shown in figure 1.8.

- Now days, an ubiquitous technology is pervasively progressing, wherein inter-digitated electrodes are ensured. Figure 1.9 depicts the interdigitated sensors. The inter-digitated electrodes are developed by depositing gold, silver or copper on the typical substrate. These sensors show promising features for both humidity as well as gas sensing.

Figure 1.9: The Interdigitated sensors.

In present investigation, the thick film sensors are prepared by using screen printing technology. The substrates such as glass tube, epoxy resin, ceramic etc are used. The fabricated sensors are availed to develop the sensor modules, wherein embedded technology is realized.

1.D. The Sensor Module:

An embedded technology is the revolutionary field of electronics, which find wide range of applications in diverse areas. Modern instrumentation is based on an embedded technology. To design measurement and control instrumentation with great preciseness, a sophisticated sensor module is necessary. On interfacing of sensor module to the system, the design cost and time is drastically reduced. Moreover, the reliability of the system significantly increases. Therefore, instead of interfacing directly sensors to the measurement instrumentation, a smart sensor module of promising features is procured and then employed to the instrumentation design.

"***Sensor module is the realization of electronic system, wherein the sensor of desired salient features is hardwired to get output either in analog voltage or current form or in digital form with either serial or parallel communication facilities".***

The sensor modules are basically calibrated and can provide output voltage (in mV) or current (in mA). While designing sensor module the analog part of the data acquisition system is carefully designed to enhance its features. While design of the sensor module range, accuracy, resolution, operating conditions, linearity, sensitivity, response timings, power consumed etc parameters are optimized [83]. Such sensors

modules for typical parameters are available. Figure 1.10 depicts the sensor module used for humidity sensing. As shown in the figure 1.10, the photograph of humidity sensor module SY-HS-220 consists of humidity sensor along with signal conditioning stages. This humidity sensor is of capacitive type [84]. It is fabricated by using interdigitated technology. The sensing material is of ceramic (Al_2O_3) oxides. It comprises on board signal conditioner and other required stages, which make sensor rather smarter. In addition to the humidity sensing unit the module consists of oscillator, wherein the sensor plays the role of timing capacitor. The frequency of this oscillator varies with the humidity. Moreover, it also consists of AC amplifier, frequency to voltage converter and precision rectifier etc stages. Incorporation of such stages on the board significantly helps to enhance the performance of the sensor module. Moreover, it helps to provide impediment to the noise. The module also has provision for temperature compensation. This smart sensor module provides DC voltage proportional to humidity of the surrounding in RH%. This operates with +5 Volt power supply and typically the current consumption is less than 3 mA. The sensor module exhibits better linearity over the range of 30% RH to 90% RH. The standard DC output voltage provided at 25^0C and for 60 % RH humidity is 1980 mV [85]. The accuracy is ± 5% RH at 25^0C. For the interfacing purpose, the three pins named as B, W and R are provided [Figure 1.10]. The assignment to these three pins is as, pin W DC output voltage, pin B ground and pin R- power supply (+5V). This is mounted in such a way that, it can be probe in to desired environment.

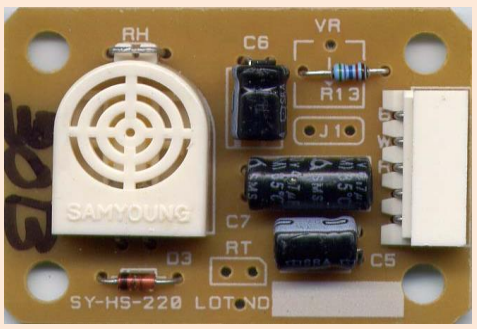

Figure 1.10: Humidity Sensor module SY-HS-220

Such sensor modules for other parameters are also available. The sensor module for Liquefied Petroleum Gas (LPG) is demonstrated in the figure 1.11. This sensor module is based on LPG sensor MQ5. Along with MQ5 as

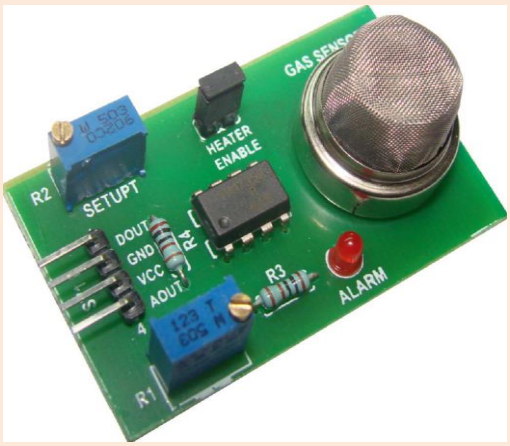

Figure 1.11: Sensor module for LPG

sensor, the module depicts signal conditioning circuitry. However, it does not any digital configurability. For further computing, the designer has to include microcontroller based hardware [86]. However, the cost of such sensor module is very high. Therefore, entire cost of the system becomes unaffordable. Such smart sensor module was reported by Bhattacharjee et al [87] for different gases. They deployed sensor from TGS series for Carbon dioxide gas, LPG etc to ensure sensor module. They used PIC 18F877 microcontroller to make the module programmable. The wireless sensor node of the WSN is also the realization of smart sensor module. Based of microcontroller of promising features the sensor module is designed be Hema et al [88] and reported is requirements to enhance the reliability of the WSN. As shown in figure, 1.12, a smart sensor module is designed to measure environmental temperature, humidity and gas and reported by opera et al [89]. They employed ΔΣ ADC for analog to digital converter, which helps to increase the preciseness in the digital data. They concluded that, such module can be suitably deployed for development of the instrumentation for environmental parameter monitoring. Deploying TGS 2620 sensor, a sensor module for carbon dioxide gas is also available. [Figure 1.13]. This is chemical sensor, wherein resistive type thick film of sensing material is deposited on ceramic substrate. The sensor module comprises analog signal processing parts to produce the output in mV range proportional to the concentration of the carbon dioxide gas. However, this module does

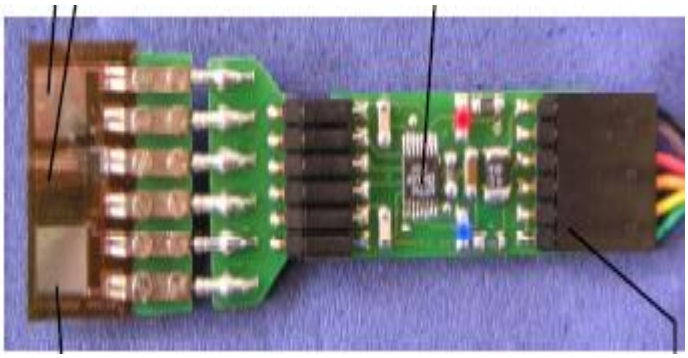

Figure 1.12: A sensor module for Humidity, Temperature gas designed on epoxy substrate.

Figure 1.13: Sensor module for Carbon Dioxide gas.

not have any computing unit. Hence it is not smart sensor module Moreover, most of the sensor modules comprise only analog part the electronic system. Therefore, such sensor modules are not smart sensor modules. Therefore, they are featured with limited applicability.

1.D.(a) General Architecture of Proposed Sensor Module :

The smart sensor module with promising features is designed. An architecture proposed to the sensor module is schematically depicted in figure 1.14. As shown in the figure 1.14, the proposed architecture is the realization of an embedded technology. It

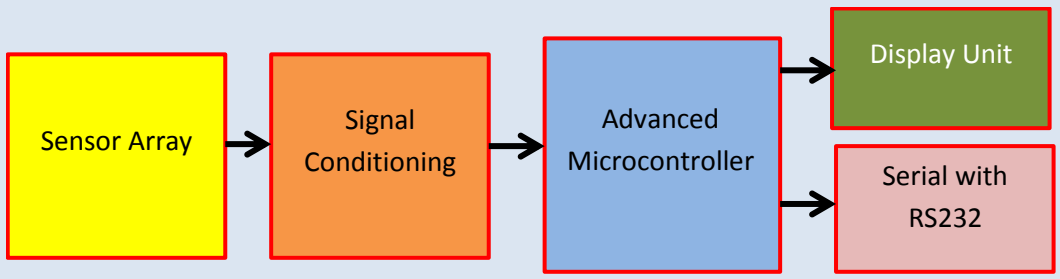

Figure 1.14: Proposed architecture of the smart sensor module to be designed by using sensors developed about ferrite based sensing element.

consists of an array of the sensors. Each sensor of an array is dedicated designed for specific parameters. The sensor module, as depicted in figure 1.14, has signal conditioning blocks. This analog part of the module decides the preciseness and reliability of the module itself. Generally, it is designed to get output in the form of mV. The proposed sensor module is a smart module, because it is the realization of embedded technology and would be wired about advanced microcontroller. The firmware designed for this dedicated application, synchronization the operation of the module to produce desired output. As per requirement, sensor module provides the parameter values directly on the LCD in real units. Also, there is provision of output in the serial format as well. The RS232 port would be made available, so that present sensor module may be deployed in smart instrumentation. The necessary power supply, +5V, may be obtained from source of main board or can be dedicatedly designed. Deploying present electronic technologies, such as an embedded technology, the salient feature of advanced microcontrollers can be added into the fundamental features of the

sensors. This results into sensor module with programming facilities. Therefore, the smart sensor module may be realized.

In present research work, deploying promising features of AVR microcontroller and interfacing nanoferrite based sensor, a sensor module is developed for temperature, humidity and industrial gases etc. The details regarding design issues of the sensor module are interpreted in topic 4.

1.E. Origin of the problem:

On survey, it is found that, the technologists are attempting to make the instrument more versatile and smart with bright features. Particularly, in measurement instrumentation, they used to deploy promising featured sensor modules. In fact, the characteristics of the sensor decide the reliability of the measurement and control instrument. Recently, an embedded technology is evolving to provide suitable solution to many electronic problems. The sensor modules for various parameters are available. However, these modules consist of only analog part of the required electronic circuit. Therefore, these modules provide analog output only, which should be processed for precise instrumentation. Such present day sensor modules rarely consist of any computing unit. Therefore, these modules are not configurable and do not provide the outputs of different domains. This provide impediment to the modern instrumentation. Therefore, deploying embedded technology a sensor module could be designed, which may cater the needs of present day instrumentation. The smart sensor module, if wired using embedded technology, may be more advantageous and show rather more portability. Therefore, it is proposed to design the embedded technology based smart sensor module for measurement of physical parameters,

On literature survey, it is found that, the Ferrimagnetic materials, polycrystalline spinel nanoferrites exhibit interesting electrical properties. The semiconducting behaviour with temperature leads to deploy these materials as a sensing element for temperature sensor. As per the conductivity mechanism, it shows the ionic conductivity as well as protonic conductivity, due to the water molecules absorbed at the surface as well as trapped into the pores. Employing such property one can develop humidity sensor. It is also found that, the electrical properties of the ferrites are sensitive to the adsorption and absorption phenomenon ensuring surface transportation. At typical operating temperature, the oxygen ion species are chemisorbed at the sites of the grains. This property of the ferrite materials demonstrates its use as a sensing material for

detection of various gases. It is also found that, the electrical resistance of the ferrite is sensitive to the oxidizing as well as reducing gases. The sensitivity of the material depends upon chemical composition and operating temperature. Therefore, wide variety of the sensing material could be synthesized. Moreover, deploying thick film technology, the sensor of desired features can be designed. On implementation of such sensors, the sensor module of promising features may be designed. Such sensor modules provide better solution for modern electronic instrumentation. Therefore, it is proposed to undertake the research work of designing of embedded technology based smart sensor module, wherein the sensor of ferrite sensing materials is deployed.

1.F Orientation of the Proposed Research Work:

The research work undertaken emphasizes the realization of an embedded technology to design smart sensor module to sense environmental parameters and typical gases. It is known that, in modern instrumentation, the recent trend is to deploy sensor module to sense desired parameters. To cater this need, it is proposed to design sensor module, wherein an embedded philosophy is ensured. Deployment of advanced microcontrollers to ensure the required features is the major objective of the research. On survey, it is found that, the spinel nanoferrite materials exhibit the electrical properties, which are sensitive various environmental parameters and gases as well. Therefore, these materials can be synthesized and used as sensing element. Employing thick film technology a sensors of desired characteristics can be prepared. Therefore, it is proposed to develop an embedded philosophy based highly portable sensor module which provides digital output. The research work of synthesis of sensing materials and development of sensor to design embedded based sensor module is of interdisciplinary relevance and reveal wide scope in modern instrumentation. Considering this fact into account, it is proposed to undertake the research work entitled **"Synthesis and Implementation of Electronic Materials for Smart Sensor Module"**. The major objective of proposed work is to develop smart sensor modules, which could support better portability.

The objectives of the proposed research work are as follows.

1. To synthesize polycrystalline mixed ferrites based sensing materials suitable for electronic sensors.
2. Characterization of the materials by standard tools.
3. Investigation of Electrical properties of sensing materials

4. Development of sensors for Humidity, temperature and typical gases.
5. Designing of smart sensor module, wherein embedded technology is realized
6. Interpretation of the result.

As per objectives, the research work is carried out. Ensuring embedded technology, the smart sensor modules are developed. The AVR ATmega 8L microcontroller is employed to design an embedded system.

1.G Research design and methodology :

The compositions of polycrystalline, $A_xB_{1-x}Fe_2O_4$ (where A & B are divalent metal ions such as Mg, Zn, Ni and Mn), for x = 0.20, 0.40, 0.60 and 0.80, spinel ferrites will be prepared by co-precipitation method, employing AR grade starting materials in stoichiometric weight proportion. The hydroxides of the constituents will be allowed to co-precipitate with controlled conditions. The precipitate will be washed, dried and sintered to obtained the desired ferrite compositions. Formation of compositions will be confirmed after characterization by X-ray diffraction, FTIR absorption and SEM tech. After confirmation of satisfactory preparation, the material will be used for further investigations. The electrical parameters such as DC resistivity, dielectric polarization etc. will be studied. The humidity sensitive electrical properties will be investigated and results will be used to decide the suitability of the sensing material for humidity sensor. Moreover, the materials will also be studied for gas sensing properties. It is proposed to study the sensing properties for CO_2, H_2S and NH_3 gas. Based on thick film technology, the screen printing technology, sensors will be developed. It proposed to avail epoxy resin, glass and ceramic materials as the substrates. Employing embedded technology a smart sensor module will be designed. Advanced microcontroller, AVRAtmega 8L will be used as computing unit of the proposed module. The hardware will be designed. Using Code Vision AVR an IDE a firmware will be designed to ensure the synchronization of operation of hardware. The sensor module will be calibrated to provide the parameter values in respective units. The results of implementation will be interpreted.

1.H. Organization of the thesis:

The research work emphasizing designing of embedded technology based smart sensor module, wherein the polycrystalline ferrite based sensors are employed, is

carried out and results obtained are interpreted in this report. The thesis comprises five topics.

The first topic is introduction. Present research work comprises various different fields, such as embedded technology, synthesis of the materials for sensing element, development of sensors, optimizations of properties of the sensors and utilization of the sensor to design smart sensor module. The fundamentals of these fields are explored and described in this topic. The properties of polycrystalline ferrite materials, due to which these materials are recognized as the sensing materials, are discussed. The concept of sensor module is elaborated and architecture of sensor module is proposed. At the end of first topic the origin of the problem is given, which is followed by significance of the research work. Aims and objectives of the proposed research work are also discussed in detail. The methodology adopted during this research work is also given in this topic.

The second topic is devoted for synthesis and characterization of sensing materials. As per proposal the spinel ferrite materials have been synthesized by employing co-precipitation method and characterized by using standard tools such as, X-ray diffraction, FTIR spectroscopy, SEM etc. The results regarding preparation and characterization of the sensing materials are spread over four sections, A, B, C and D respectively. The conclusion is given at the end of each section. The topic is concluded with the suitability of nanoferrites to ensure for sensing mechanism.

Emphasizing the fact that, ferrite materials reveal sensing abilities, the electrical properties of nano structured ferrites are investigated. The results of investigation are interpreted in topic 3. The temperature dependent electrical properties are studied and used for designing of temperature sensor. The humidity dependent electrical properties are investigated. The variation in the resistance, due to relative humidity is attributed to the process of chemisorption, wherein the protonic conduction mechanism is realized. From this investigation, it is concluded that, the ferrites can be suitably used for humidity sensor. Further, the gas sensing properties of the materials are studied and results are interpreted in topic 3. Topic 3 is concluded with the suitability of the compositions for development of the sensors for dedicated applications.

Topic 4 is devoted to the designing of sensor module. This sensor module is the realization of embedded technology. Therefore, the details regarding designing issues of both hardware as well as software are discussed in this topic. The sensor module is designed for four sensors. An analog part of the hardware is designed precisely. While

designing sensor module, the features such as range, sensitivity, nature of output, power consumption etc. are considered. The topic is concluded with the table of specification of the sensor module. Implementation of sensor module is carried out and details regarding the implementation are discussed in topic 5. Sensor module is calibrated for different parameters such as temperature, humidity, gas etc. The process of calibration and data analysis is also discussed. The summary and conclusion of entire research is discussed at the end of this topic.

The citations are given at the end of each topic and sequentially called in the text. The figures and tables are captioned sequentially in each topic. The content of figures and tables is also listed separately. The thesis includes different symbols and abbreviation, which are tabulated and given at the end of report. The thesis also includes the publications.

References:

1. G. E. Moore, “Cramming More Components Onto Integrated Circuits”, Electronics, 38 8 (1965) 114–117.
2. A.R. Wagh, M.V. Nimbalkar and B.P. Ladgaonkar, “AMS-VLSI Technology: An Innovative Field for Embedded Technology”, Proceed. National Conference on Recent Initiative towards Green Electronics (NCRIGE-2013), Published by SPEEDS (2013) 399.
3. A. Doboli, Currie and H. Edward, “Introduction to Mixed-Signal, Embedded Design”, Springer (2011).
4. P. Thimmaiah, K. R. Rao and E. R. Gopal, “External Device Control Using Ibm Pc’s Centronics Printer Port”, J. Instrum. Soc. India, 32 4 (2006) 239-247.
5. M. V. Laxmaiah, P. Thimmaiah and K. R. Rao, J. Instrum. Soc. India, 34 4 (2004) 208.
6. D. K. Fisher and H. Kebede, “A Low-Cost Microcontroller-Based System to Monitor Crop Temperature and Water Status”, Computers and Electronics in Agriculture, 74 1 (2010) 168-173.
7. A. H. G. Al-Dhaher, “Integrating Hardware and Software for the Development of Microcontroller based Systems”, Microprocessors and Microsystems, 25 (2001) 317-328.
8. R. Saleh, S. Senior, S. Mirabbasi, A. Hu, M. Greenstreet, G. Lemieux, P. P. Pande, C. Grecu, and A. Ivanov, “System-on-Chip: Reuse and Integration”, Proceedings of the IEEE, 94 6 (2006) 1050-1069.
9. S. K. Tilekar, S. N. Patil, S. S. Shaikh, A. M. Pawar and B. P. Ladgaonkar, “Development and Implementation of an Embedded System to Measure Initial Permeability of Magnetic Materials”, Intern. J. Electronic Engineering Research, 3 1 (2011) 21.
10. R. P. Suvarna, K. R. Rao and K. Subbarangaiah, “A Simple Technique for A.C. Conductivity Measurements”, Bull. Mater. Sci., 25 7 (2002) 647–651.
11. A. H. G. Al-Dhaher, “Integrating Hardware And Software For The Development Of Microcontroller-Based Systems”, Microprocessor and Microsystems, 25 7 (2001) 317-328.
12. S. M. Mohaiminul Islam and G. M. Sharif, “Microcontroller Based Sinusoidal PWM Inverter for Photovoltaic Application”, 1st International Conference on the

Developments in Renewable Energy Technology (ICDRET 2009), IEEE Conference Publications, (2009) 1-4.

13. Datasheet of AVR ATmega 8L Microcontroller.
14. S.N. Patil, S.K. Tilekar and B.P. Ladgaonkar, Development of LPC 2378 based an embedded system for precision measurement of displacement", International Journal of Industrial Engineering Practice", 4 2, (2012) 59-61.
15. R. Kamal, "Embedded systems architecture, programming and design", TMH, New Delhi (2003).
16. J. B. Peatman, "Design with Microcontrollers and Microcomputers", MGH, (1998)
17. J. G. Ganssle, "Art of Programming Embedded Systems", Academic Press, USA, (1992)
18. R. Grassnick, H. I. Trankler, C. Geissler and M. Heinze, "Development and Realization of the Microsystem for Energy-Saving Food Storage", J. Inst. Meas. Auto. Techn.(IMA) (2001)137.
19. T. Wilmshurst, "An Introduction to the Design of Small Scale Embedded System with Examples from PIC, 80C51 and 68HC05/08 Microcontrollers", Palgrave, Great Britain (2001).
20. W. Wolf, "Computer as Components – Principles of Embedded Computing System Design", Academic Press, A Harcourt Science and Technology Company, USA (2001).
21. T. D. Morton, "Embedded Microcontrollers", Pearson education, New Delhi (2005).
22. D. E. Simon, "An Embedded Software Primer", Pearson Education, New Delhi (2006).
23. M. J. Pont, "Embedded C", Addison Wesley; 1 edition (2002).
24. K. V. K Prasad, "Embedded Real Time Systems: Concepts, Design Programming Black Book", Dreamtech, (2013)
25. www.keil.com/uvision/
26. T. R. Parthasarathy, N. Venkatakrishnan and K. Balamurugan, "Analysis of Partitioning between ARM and FPGA on Performance Characteristics", IEEE International Conference on Advanced Communication Control and Computing Technologies (ICACCCT 2012), (2012) 78-82.
27. https://en.wikipedia.org/wiki/Complex_instruction_set_computing
28. A.B. Ladgaonkar, P. Balsundar, V. Konde and S. Purushothaman, "Analog And Mixed Signal Based System on Chip for ECG Monitoring", Proceeding of National

Conference on Advances in Wireless Sensor Network and Application (NCAWSNA-2014) A special Issue of SPEED the Journal of Research in Electronics (ISSN: 2349-8226) (2015) 8.

29. A.M. Pawar, S. N. Patil and B. P. Ladgaonkar, "Design and Implementation of Wireless Sensor Node for WSN for Automatic Meter Reading", Intern. J. Recent Research in Mathematics Computer Science and Information Technology, 1 1(2014) 28-31.
30. B. P. Ladgaonkar and A. M. Pawar, "Design and Implementation of Sensor Node For Wireless Sensors Network To Monitor Humidity of High-Tech Polyhouse Environment", Intern. J. Advances in Engineering and Technology, IJAET, 1 3 (2011) 1.
31. P. H. Baker, G. H. Golbraith, R. C. McLean and C. H. Sanders, "The Development Of Instrumentation For The Measurement Of Relative Humidity Within Building Microenvironments**",** Measurement, 39 6 (2006) 565-574.
32. F. Adamo, G. Andria, F. Attivissimo and N. Giaquinto, "An Acoustic Method For Soil Moisture Measurement", IEEE Trans. Instrum. & Meas., 53 4 (2004) 891-898.
33. S. D. Nelson, A. W. Kraszewski, S. Trabelsi and K. C. Lawrence, "Using Cereal Grain Permittivity For Sensing Moisture Content", IEEE Trans. Instrum. & Mears., 49 3 (2000) 470-475.
34. R. Gupta, J.N. Bera, M. Mitra, "Development of an Embedded System and MATLAB-Based GUI for Online Acquisition And Analysis of ECG Signal", Measurement, 43 (2010) 1119-1126.
35. A. Choudhary, M. Kumar, K. Kumar, R. Singh and S.Katiyar, "Design and Development of Low Cost Microconoller Based ECG System for Real-Time Analysis", Intern. J. Electron. Comm. & Instrum. Engg. Res. Develop., 2 3 (2012)121- 129.
36. O. Postolache, P. Girao, M. Pereira and H. Ramos, "An Internet and Microcontroller-Based Remote Operation Multi-Sensor System For Water Quality Monitoring", Proceedings of IEEE Sensors, 2 (2002) 1532-1536
37. N. Wang, N. Zhang and M. Wang, "Wireless Sensors In Agriculture And Food Industry—Recent Development And Future Perspective", Computers and Electronics in Agriculture, 50 1 (2006) 1–14

38. Y. C. Jo, K. N. Kim and T. Y. Nam, “Low Power Capacitive Humidity Sensor Readout IC With On-Chip Temperature Sensor And Full Digital Output For USN Applications”,IEEE Sensors (2009) 1354-1357.
39. M. Simić, “Design of Monitoring and Data Acquisition System for Environmental Sensors”, Proceed. International Symposium on Industrial Electronics INDEL 2014, Banja Luka, 6 8 (2014) 146-148.
40. R. L. Vander Wal, G. W. Hunter, J. C. Xu, M. J. Kulis, G. M. Berger and T. M. Ticich, “Metal Oxide Nanostructure And Gas Sensing Performance”, Sensors and Actuators B : Chemical, 138 (2009) 113-119.
41. S.A. Masti, A. K. Sharma and P. N. Vasambekar, “Liquefied Petroleum Gas Sensor Base On Cr^{3+} Substituted Mixed Mg. Cd. Spinel Ferrites”, Arch Phys. Res., 6 1 (2015) 1-6.
42. A. Jain, R. K. Baranwal, A. Bharti, Z. Vakil and C. S. Prajapati, “Study of Zn-Cu Ferrite Nano-Particales for LPG Sensing”, The Sci. World J., (2013) 1.
43. A. Munir, F. Ahmed, M. Saqib and M. Annis Ur Rehman, “Electrical Properties of Ni Zn Nanoparticles Prepared By Simplified Sol Gel Method”, J. Super Cond. Nov Magn., 28 (2015) 983-987.
44. K. Wetchakun, T. Samerjai, N. Tamaekong, C. Liewhiran, C. Siriwang, V. Kruefu, A. Wisitsoroat, A. Tuantranont and S. Phanichphant, “Semiconducting Metal Oxides As Sensors For Environmentally Hazardous Gases”, Sensors and Actuators B: Chemical, 160 (2011) 580-591.
45. M. A. Gilleo and S. Geller, ActaCryst., 10 (1957) 239.
46. B. P. Ladgaonkar, C. B. Kolekar and A. S.Vaingankar, “Magnetization and Initial Permeability Studies of Nd^{3+} Substituted Zn-Mg Ferrite Bull”, Mater. Sci., 22 5 (1999) 917.
47. C. B. Kolekar A.Y. Lipare, B. P. Ladgaonkar, P. N. Vasambekar and A.S. Vaingankar, “The Effect of Gd^{3+} and Cd^{2+} Substitution on Magnetization of Copper Ferrites”, J. Magn. and Magn Mater.247 (2002)142.
48. O. M. Hemeda, “Structural and Magnetic Properties of $Co_{0.6}Zn_{0.4}$ $Mn_xFe_{2-x}O_4$”, Turk. J. Phys., 28 (2004)121 – 132.
49. S.G Bachhav, R.S Patil, P.B Ahirrao, A.M Patil and D.R. Patil, “Microstructure And Magnetic Studies Of Mg–Ni–Zn–Cu Ferrites”, Mater. Chem. Phys. 129 (2011) 1104-1109.

50. V. D. Kapse, F. C. Raghuwanshi and V. S. Sangawar, “Preparing And Ethanol Sensing Behavior Of Spinel-Type Nano-Sized Mixed Ferrites Containing Zn”, Int. J. Chem. and Phys. Sci. 4 1 (2015) 121-127.
51. Kyoshio-Seki, Jun-Ichi, Shida Koichi and Murakani, IEEE Trans. on Instrum. & Measurement, 39 (1988) 3.
52. A. S. Vaingankar, S. K. Kulkarni and M. S. Sagare, Proceed., ICF-7 (1997) 155.
53. N. RezlescU, E. Rezlescu, F. Tudorache, P. D. Popa, Romanian Reports in Physics, 61 2, 223–234 (2009)
54. P. P. Singh, International Journal of Emerging trends in Engineering and Development, 2 5 (July 2012)
55. J. Sláma, A. Grusková, M. Ušáková, E. Ušák Ján Šubrt and J. Lukáč, J. Electrical Engineering, 57 8/S (2006) 159-162.
56. V. L. O. Brito, A. K. Hirata, A. C. C. Migliano and L. F. A. de Almeida , Progress In Electromagnetics Research Letters, 13 103 (2010) 112.
57. U. B. Desai, B. N. Jain and S. N. Merchant, “Wireless Sensor Networks: Technology Roadmap”, A Project Supported by Department of Information Technology, Ministry of Information and Communication Technology, India
58. I. A. Abdel-Latif, “Fabrication of Nano - Size Nickel Ferrites for Gas Sensors Applications”, J. Phys., 1 2 (2012) 50 – 53.
59. E. Auzans, D. Zins, E. Blums and R Massart, “Synthesis and Properties of Mn-Zn Ferrite Ferrofluids”, Journal of Materials Science, 34 (1999) 1253-1260.
60. J. Li, D. Dai, X Liu, Y. Lin, Y. Huang and L. Bai, “Preparation and Characterization Of Self-Formed $CoFe_2O_4$ Ferrofluid”, Journal of Materials Research , 22 04 (2007) 886-892.
61. Girish Chitnis and Babak Ziaie, “A Ferrofluid-Based Wireless Pressure Sensor”, J. Micromech. Microeng. 23 (2013) 1-6
62. P. N. Vasambekar, C. B. Kolekar and A. S. Vaingankar, J. Magn. And Magn. Mater., 186 (1998) 333.
63. C.V. Gopal Reddy, S.V. Manorama and V. J. Rao, “Semiconducting Gas Sensor For Chlorine Based On Inverse Spinal Nickel Ferrite”, Sensor And Actuators B. 55 (1999) 90-95
64. N.Rezlesan. N. Iftimie, E. Rezfecu, C. Doroftei and P.D. Popa, “Semiconducting Gas Sensor For Acetone Based On The Fine Grained Nickel Ferrite”, Sensors And Actuators B, 114 (2006) 427-432

65. Z. Tiansha, P. Hing, Z. Jiancheng and K. Lingbing, “Ethanol Sensing Characteristics Of Cadmium Ferrites Prepared By Chemical Co-Precipitation”, Mater. Chem. Phys, 61 3 (1999) 192-198.
66. B. P. Ladgaonkar, P. N. Vasambekar and A. S. Vaingankar, “Effect of Zn^{2+} and Nd^{3+} Substitution On Magnetization And AC Susceptibility Of Mg Ferrite”, J. Magn. and Magn. Mater, 210 1-3 (2000) 289
67. E. Veena Gopalan, I.A.Al-Omari, K.A.Malini, P.A.Joy, D.SakthiKumar, YasuhikoYoshida and M.R.Anantharaman, “Impact of Zinc Substitution On The Structural And Magnetic Properties Of Chemically Derived Nanosized Manganese Zinc Mixed Ferrites”, J. Magn. and Magn. Mater., 321 (2009) 1092–1099.
68. M. Ul-Islam, T. Abbas, and M Ashraf Chaudhry, “Electrical Properties of Cd-Substituted Copper Ferrites”, Materials Letters, 53 1-2 (2002) 30-34.
69. S M Chavan, M K Babrekar, S S More and K M Jadhav,” Structural and Optical Properties of Nanocrystalline Ni–Zn Ferrite Thin Films”, J. Alloys Compd. 507 (2010) 21-25.
70. K. Bull, “Methods of Accurately Measuring Capacitive Rh Sensors”, 5th International Symposium on Humidity and Moisture – ISHM 2006 Brazil, May 02 – 05, 2006 – Rio de Janeiro, Brazil
71. C. B. Kolekar, A. Y. Lipare, B. P. Ladgaonkar, P. N. Vasambekar and A. S. Vaingankar, “The Effect of Gd3+ and Cd2+ Substitution On Magnetization Of Copper Ferrite,” J. Magnetism Magn. Mater., 247 (2002) 142-146.
72. A. B. Gadkari, T. J. Shinde and P. N. Vasambekar, “Structural and Magnetic Properties of Nanocrystalline Mg-Cd Ferrites Prepared By Oxalate Co-Precipitation Method,” Journal of Materials Science: Materials in Electronics, 21 1 (2010) 96-103.
73. A. Stognij, N. Novitskii, A. Sazanovich, N. Poddubnaya, S. Sharko, V. Mikhailov, V. Nizhankovski, V. Dyakonov, and H. Szymczak, “Ion-beam Sputtering Deposition And Magnetoelectric Properties Of Layered Heterostructures (FM/PZT/FM)n, where FM -- Co or Ni78Fe22 , Eur. Phys. J. Appl. Phys., 63:21301 (2013).
74. R. Valenzuela, “Novel Applications of Ferrites”, Physics Research International (2012) 1-9.

75. B. P. Ladgaonkar and A. S. Vaingankar, "X-ray Diffraction Investigation Of Cation Distribution In $Cd_xCu_{1-x}Fe_2O_4$ Ferrite System". Mater. Chem. and Phys., 56 (1998) 280
76. P. N. Vasambekar, C. B. Kolekar, A. S. Vaingankar, "X-ray Diffraction Data on CdxCo1-xFe2-yCryO4 System (x=0.50; y=0 and x=0.50; y=0.30)", 52-1798, 52-1799, Powder Diffraction File Release-2002, International Centre for Diffraction Data, U.S.A., (2002)
77. N. M. Deraz and A. Alarifi, "Preparation and Characterization of Nano-Magnetic Mn0.5Zn0.5Fe2O4 System", Int. J. Electro chem. Sci., 7 (2012) 5828 – 5836.
78. G Vaidyanathan, R Arulmurugan, S D Likhite, M R Anantharaman, M. Vaidya, S. Sendhilnathan and N D Senthilram, "Effect of Preparation On Magnetic Properties of Mn-Zn Ferrite", Indian Journal of Engineering & Materials Sciences, 11 (2004) 289-294.
79. H. Farahani, R. Wagiram and M. N. Hamidon, "Humidity Sensors Principle, Mechanism and Fabrication Technologies: A Comprehensive Review", Sensors, 14 (2014) 7881-7939.
80. J. Herran, G.G. Mandaya and E. Castano, "Semiconducting BaTiO3–CuO Mixed Oxide Thin Films for CO2 Detection", Thin Solid Films 517 (2009) 6192–6197.
81. A.Z. Sadek, S. Choopun, W. Wlodarski, S.J. Ippolito and K. Kalantar-zadeh, "Characterization of ZnO Nanobelt-Based Gas Sensor For H_2, NO_2, and Hydrocarbon Sensing", J. IEEE Sensors, 7 (2007) 919–924.
82. P. P. Dondapati, "An Automated Multi Sensored Green House Management", International Journal of Technological Exploration and Learning, 1 1 (2012) 21-24.
83. T. C. Korade and A. A. Shinde. "Study of Wireless Sensor Networks", International Journal of Electrical, Electronics and Data Communication, 2 3 (2014) 81-85.
84. Data Sheet Of Humidity Sensor SY-HS-220. http://www.dnatechindia.com/file/43-syhs220-humidity-sensor.html
85. A. Somov, A. Baranov, A. Savkinb, D. Spirjakin, A. Spirjakin and R. Passerone, "Development of Wireless Sensor Network For Combustible Gas Monitoring", Sensors and Actuators A, 171 (2011) 398– 405.
86. D. Bhattacharjee, P. Bhatnagar, S. Choudhury, "Design and Development of a Flexible Reliable Smart Gas Detection System" Intern. J. Computer Applications, 31.9 (2011)1-8.

87. L. K. Hema, Dr. D. Murugan and M. Chitra, “WSN based Smart System for Detection of LPG and Combustible Gases”, Int. J. Emerging Trends and Techn. in Comp. Sci. Special Issue of National Conference on Architecture, Software Systems and Green computing-2013(NCASG2013).
88. Oprea, N. Bârsan, U. Weima, J. Courbat, D. Briand and N.F. de Rooij, “Integrated Temperature, Humidity and Gas Sensors on Flexible Substrates for Low-Power Applications” , IEEE Sensors, (2007) 158-161.

*****

Topic 2

Preparation and Characterization of Polycrystalline Spinel Ferrites

Polycrystalline spinel ferrite, represented by the formula MFe_2O_4, where M is the divalent cation, is ubiquitous magnetic oxide. The ferrite compositions are depicting intrinsic properties, because of which it reveals wide spectrum of applications in diverse fields. During early days, applicability of these ferrite materials is constrained to the magnetic domain. However, recently, it is proved that, the ferrite materials are highly suitable for sensor based applications, due to its semiconducting behavior. Therefore, these materials are now pervasively becoming inevitable for development of smart sensors. It is known that, typical oxides can be deployed for development of the sensor. However, ferrite materials are featured with good reliability, easy to synthesize even in bulk size, low cost, good repeatability in the desired properties, enhanced stability, long durability, fast response timings etc. Therefore, these materials found more suitable for fabrication of the sensors. In fact, the major aim of present research work is to design smart sensor module, wherein embedded technology is realized, suitable for sensing the environmental parameters. For this purpose, it is essential to synthesize the materials of desired characteristics. On intensive study of properties of these materials, it found that, polycrystalline ferrites of spinel structure, nano particle sized, are most suitable for sensor based application. Therefore, it is proposed to synthesize polycrystalline spinel ferrites. Moreover, confirmation of formation of the materials of desired properties is also essential. The polycrystalline spinel ferrites of nano particle size are synthesized. The synthesized compositions are subjected to the process of characterization. The standards tools such as X-ray powder diffraction, FTIR absorption spectroscopy, Scanning Electron Microscopy etc are deployed for characterization. The details regarding synthesis and characterization are discussed in this topic through following points.

A. Preparation of compositions of polycrystalline spinel ferrites.
B. X-Ray Powder Diffraction
C. Infrared Absorption spectroscopy
D. Scanning Electron Microscopy

2.A) Preparation of compositions of polycrystalline spinel ferrites.

2.A.1 Introduction:

As discussed earlier, the ferrite materials belong to technologically important class of magnetic oxides. It exhibits interesting structural, electrical and magnetic properties. These intrinsic properties are strongly dependent on the chemical compositions, method of preparation, preparation conditions, sintering time, rate of sintering, sintering temperature, microstructural features, doping of the foreign ions, particle size, particle distribution etc[1-2]. By controlling these parameters, the compositions of the ferrites of desired features can be synthesized [3].The distribution of cations among crystallographic tetrahedral (A) and octahedral (B) site decides the electrical conduction mechanism, which is playing vital role for sensor based applications. Moreover, this cation distribution also significantly controls the magnetic properties, which arise due to magnetic interaction between these two sites. This cation distribution can be controlled by controlling preparation conditions [4, 5]. Therefore, for investigation of ferrites compositions, the preparation stage shows significant importance. Various methods have been suggested by different researchers. These methods are featured with their own advantages and limitations. The standard ceramic method is successfully proved as most suitable method for preparation of spinel ferrites [6, 7]. However, recently researchers are showing interest in chemical methods. Sláma et al have prepared nano crystalline compositions of NiZn ferrites by standard ceramic method [8]. Ismayadi et al have also used standard ceramic method for preparation of polycryatalline spinel ferrites [9]. They reported the suitability of the same for passive sensor based applications. Popescu et al have reported preparation of Zinc ferrite using co-precipitation method and investigated electromagnetic behavior of the compositions [10]. The $Mn_{0.2}Ni_{0.8}Fe_2O_4$ nanoparticles were synthesized by PEG assisted hydrothermal technique by Koseoglu et al [11]. They suggested the material`s suitability for humidity sensing.

Recently, it is found that, electrical properties of the ferrite materials are sensitive to the environmental gas. In principle, it can be deployed for development of an electronic nose. Therefore, many researchers have shown interest in preparation of nanosized ferrite materials suitable for various gases and other environmental

parameters sensing applications [11, 12]. Also, it was found that, the Mn addition in Ni ferrite improved the sensitivity to acetone [13]. This suggests that, substitution of the cations also plays vital role on the sensitivity of materials for gas. The sensing mechanism, for the reducing gases, reveals change of the electrical conductivity resulting from chemical reaction between the gas molecules and adsorbed oxygen onto the metal oxide surface [14]. Therefore, ferrite materials support surface phenomenon, wherein the process of adsorption is realized [15]. The polycrystalline ferrites are porous in nature, which favours the absorption mechanism as well [16]. Due to these properties ferrites play vital role in sensing mechanism. Employing various methods, the nanoparticle polycrystalline spinel ferrites have been synthesized by many researchers. These methods are summarized.

2.A.2 Methods of Preparation of Polycrystalline Ferrites:

As discussed earlier, the ferrites are highly sensitive to the preparation method, sintering condition, various additives, dopants and impurities etc [15-17]. The parameters of interest can be controlled by controlling preparation conditions. Hence, method of preparation and preparation conditions play vital role on the properties of the ferrites. Generally, preparation methods can be classified into two groups such as

- Physical Method
- ChemicalMethod

a) Physical Method :

The methods of generation of magnetic nanoparticles in the solid phase using high-energy treatment to the material are usually called physical method. This is also referred as standard ceramic method. Depending upon starting materials used, the standard ceramic method can also be classified into oxide methods and decomposition method. In oxide method, high purity oxides are used as starting materials. These materials are used in stoichiometric weight proportion. The materials are then ball milled to powder form and then subjected to the process of pre-sintering and sintering. The sintering temperature and sintering time decide the microstructure of the compositions under investigation. The standard ceramic method is the high temperature process, wherein solid state reaction is ensured at bulk level. Therefore, the resulting compositions are featured with porosity. Moreover, this method is very slow method of preparation of the ferrites materials. Instead of oxide as starting materials, if salts such as carbonates, nitrates, oxalates etc are considered, then it is decomposition method, wherein the decomposition of salts into oxide is essentially carried out.

In recent years, numbers of physical and chemical techniques have been developed to prepare nanosized materials [18]. The chemical techniques for the synthesis of nanostructured materials offer some advantages in comparison with the physical techniques in relation to simplicity, energy saving and product homogeneity [19].

Moreover, in physical method, the ceramic method, exact amount of constituent materials, to maintain stoichiometry, are homogeneously mixed using acetone base and ground. It is then subjected to the process of calcinations, wherein the carbonates undergo partial decomposition and also removes volatile impurities. In this pre-firing step the nucleation starts, which reduce the shrinkage in the final stage. In order to achieve uniform particle size the calcinated powder is again milled. Binders can be added at this stage. This method realizes the solid state reaction.

The traditional ceramic method suffers from a number of potential drawbacks. The grinding steps may introduce impurities and result in a broad distribution of particle sizes. Further, dry pressing can introduce porosity in the sintered parts. This method may be acceptable for producing materials for desired applications. There are other, more demanding applications that require low impurity content, uniform, small grain size, and low porosity. Moreover, ferrites of rather more particle size will be resulted. This causes to reduce the application potential and provide impediment to the pervasivity.

b) Chemical Method :

The limitations exhibited by the standard ceramic method can be overcome by employing chemical method. In Chemical method, the principle of co-precipitation of hydroxides, nitrides or acetates of constituents is carried out. Here the hydroxides of constituent materials are used and allowed to co-precipitate in either NaOH or NH_4OH as base. Use of NaOH would results into formation of the precipitate in jelicious form, for which washing becomes tedious job. Therefore, the NH_4OH is suggested to use as a base solution. The precipitate consists of the ferrite constituents. The precipitate is filtered and washed carefully. Washing is essential in order to remove cations of base solutions. The precipitate is then dried to specific temperature to remove hydroxyl or acetate group. The compositions are again milled to powder form. Now the powder is ready for final sintering.

The widely used chemical methods are electro deposition [20], co- precipitation [21], sol-gel route [22, 24], micro emulsion technique [23], hydrothermal method [26],

precursor method [25], reverse micelle technique [29], sucrose method [27, 28], self-combustion [30].

i) In hydroxide co-precipitation method, the hydroxides of constituent materials are allowed to co-precipitate in the base solution. The starting material may be chlorides [31], nitrides [32] or oxalates [33]. The materials, in stoichiometric proportion, are then simultaneously poured in to the NH_4OH. The pH of the reaction must be controlled. The precipitate comprises the hydroxides of the constituents of the desired ferrites. The precipitate is then dried initially at room temperature and then at some moderate temperature. It is milled properly and then subjected to the process of sintering. Sintering process is identical with that of standard ceramic method. On literature survey, it is found that, many researchers are employing this method for synthesis of nano particle sized spinel ferrites.

ii) Precursor method is also well proved method for preparation of the ferrites. Precursor is nothing but the solution of the compounds, containing metal ions such as M^{2+} and Fe^{3+} taken in desired concentration, decomposed to form the ferrites. Due to its preciseness and resulting fine grained structure with nanosized particles, this method was adopted by many researchers [34, 35, 36]. The precursors may be of oxalate or hydroxides. Nano crystalline nickel zinc ferrite was synthesized by a polymeric precursor method [39]. This method was first introduced by Pechini [37], wherein the citric acid is used as chelating agent and ethylene glycol as reaction medium in the formation of precursor [38]. It is based on polymerization of metallic citrate by using ethylene glycol. A hydrocarboxylic acid, such as citric acid, is used in an aqueous solution in order to chelate cations. Polymerizations, promoted by heating, results in a homogeneous resin in which metal ions are uniformly distributed throughout the organic matrix [39].

iii) It is found that, the sol-gel method is also employed for preparation of the ferrites. In this method a colloidal solution of constituents of the desired ferrite is prepared. On drying and then sintering of the gel the ferrite compositions could be resulted. The compositions of Mn-Zn ferrites have been prepared by sol gel technique and results are reported by Limin et al [40] and Azadmanjiri [41].

iv) Recently, self-combustion or auto combustion method is becoming more pervasive. It is because of the fact that, the ferrites of uniform and fine particles can be obtained by this method. Moreover, the compositions on the large scale can be prepared with very short time. Deploying this method, the compositions of polycrystalline spinel ferrites such as MgZn, NiZn and MnZn etc are synthesized by the researchers [40, 41, 42] and the results are attributed to the structural properties.

Since the reaction is taking place at molecular level, this co-precipitation process typically produces a sub-micron powder with narrow particle size distribution and with very low impurity content. The problems with this process are pertained to the dispersion of the oxygen gas, especially in large volumes of solution and complete removal of residual base from the precipitate. In particular, dispersion of oxygen in the solution is optimized by using a glass frit or "dispersion stone", which will break the gas stream into many small bubbles. This process creates considerable foaming action in the metal hydroxide gel. When carried out on a large scale, the foam can be difficult to remove. Complete removal of base from the product requires extensive washing as the alkyl ammonium hydroxides are not volatile and therefore are not readily removed by evaporation. Since the powders produced by this process are very fine, separation of powder from the liquid phase can be time consuming either by filtration or by centrifugation. As noted above, another approach to producing ferrites by co-precipitation involves precipitation of a solid solution of metal chlorides. In this approach, metal chlorides are dissolved in water. When carefully carried out, this procedure also results in a sub-micron powder with very low impurity content.

The method, for preparation of ferrite powders, which may be carried out at room temperature and permits the easy removal of the base, preferably by evaporation rather than washing, is needed. Such a method would substantially reduce the time and labor involved in the hydroxide precipitation method. Such a method must also be able to produce powders with low impurity content, uniform, small grain size and low porosity. From this study, it can be said that, co-precipitation method is most suitable method for preparation of the ferrites.

2.A.3 Preparation of ferrite compositions under investigation:

The compositions of polycrystalline spinel ferrite with chemical formula, $M_xZn_{1-x}Fe_2O_4$, where M are divalent cations such as Mg, Ni and Mn etc, have been prepared by using co-precipitation method. This results into three series of ferrites

compositions, $Mg_xZn_{1-x}Fe_2O_4$, $Ni_xZn_{1-x}Fe_2O_4$ and $Mn_xZn_{1-x}Fe_2O_4$ (x = 0.2, 0.4, 0.6 and 0.8). Following are the steps involved in preparation of the compositions under investigation. These steps involved are also pictorially depicted in figure 2.A.1.

i) Starting Materials :

The Chlorides of the starting materials, $MgCl_2$, $NiCl_2$, $MnCl_2$, $ZnCl_2$ and $FeCl_3$ of AR Grade were weighted by using electronic weighing balance. The compositions taken were in stoichiometric weight proportion and dissolved carefully in distilled water. Solutions were made ready for simultaneous mixing.

ii) Simultaneous mixing of the solutions :

The hydroxides were simultaneously mixed together. A magnetic stir is used to continuously stir the solution with uniform rate.

The 1 ml H_2O_2, as oxidizing agent, is added in the mixture of above solutions. In co-precipitation method the use of oxidizing agents helps to carry out the co-precipitation reaction at room temperature, simplify scale up, simplify washing of the powder, and eliminate waste products requiring special disposal. These improvements are accomplished without degrading the performance of the powders.

Thus, the co-precipitation could be modified with the use of H_2O_2 as oxidizing agent. This process entails dissolving metal salts in deaerated water and adding an aqueous base to precipitate the metal hydroxides. The preferred oxidizing agents such as H_2O_2 or $(NH_4)_2\ S_2\ O_8$ etc are more reactive than oxygen, which allows oxidation to be carried out at room temperature or slightly at higher temperature. Other oxidizing agents could leave residual transition elements behind with consequent which affect the magnetic or dielectric properties of the product. Second, using the preferred oxidizing agents, the reaction can be carried out at ambient temperature, which also permits use of NH_4OH as the base [15,16].

This process has several advantages over other co-precipitation methods for preparing these materials. For example, this reaction occurs rapidly at room temperature.

iii) Co-precipitation :

A 0.1 N solution of the base, ammonium hydroxide (NH_4OH), was slowly added into the mixture and allowed to co-precipitate the hydroxides of

constituents. The reaction mechanism realized during hydroxide co-precipitation is as given below.

$MgCl_2 + 2NH_4OH \quad =====> \quad Mg(OH)_2 + 2NH_4Cl$

$NiCl_2 + 2NH_4OH \quad =====> \quad Ni(OH)_2 + 2NH_4Cl$

$MnCl_2 + 2NH_4OH \quad =====> \quad Ni(OH)_2 + 2NH_4Cl$

$ZnCl_2 + 2NH_4OH \quad =====> \quad Zn(OH)_2 + 2NH_4Cl$

$FeCl_3 + 3NH_4OH \quad =====> \quad Fe(OH)_3 + 3NH_4Cl$

The mixture was continuously stirred with magnetic stirrer. The pH values are controlled to 8.5. It was confirmed that, the precipitation of the hydroxides of respective cations is completed. This is done taking sample of the liquid above precipitate and exposed same to ammonia. It is also confirmed by using H_2S test. The precipitate was allowed to settle and then filtered and washed carefully to remove ammonia. Use of ammonium hydroxide (NH_4OH) as a base solution avoids the formation of jelicious precipitate. This helped to enhance the washing process. Moreover, ammonia being volatile, would be removed during the process of drying.

iv) Drying and Presintering :

The precipitate was then subjected to drying process. In the beginning the precipitate was dried at room temperature for 4 hours. Then the same was heated to the temperature 80 ^{0}C for about 6 hours. The compositions are then milled carefully to achieve uniform distribution in the particles. However, at this temperature, the nucleation was not initiated. Therefore, the compositions were not in matrix of the spinel ferrites. Therefore, the powder is subjected to the process of sintering. The compositions were pre-sintered at 500 ^{0}C for 6 hours. It was then slowly cooled to the room temperature. After pre-sintering the compositions again milled to fine powder.

v) Sintering :

The compositions are subjected to the process of sintering. This sintering decides the microstructural features of the compositions. Actually, after pre-sintering the composition was exposed to X-ray diffraction. It was found that, the diffractogram

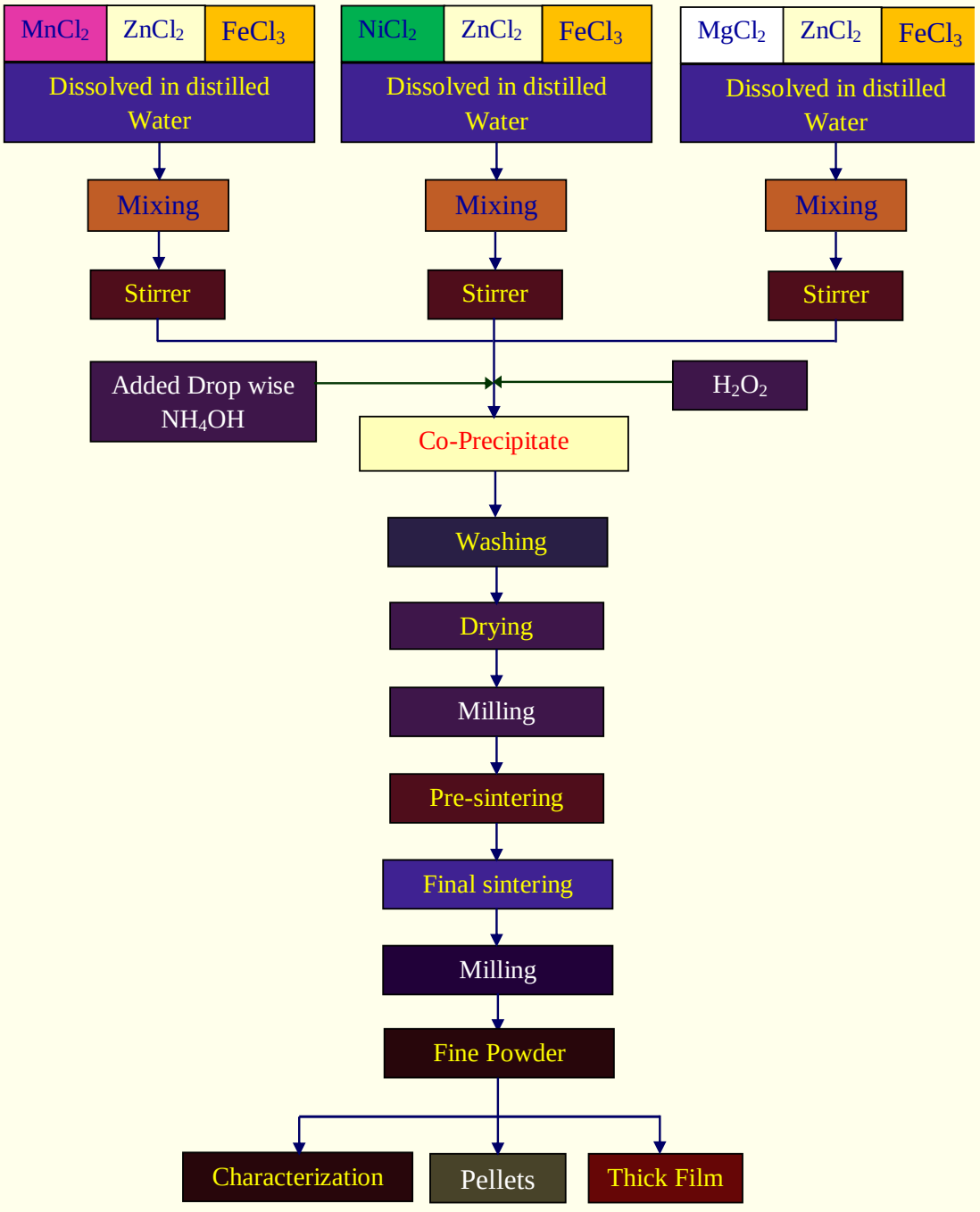

Figure 2.A.1: Flow diagram ensuring synthesis of the ferrite compositions under investigation.

comprises some additional reflections. Moreover, reflections are not well defined. The sintering temperature was optimized to 1000^0C. The final sintering was carried out at 1000 ^{0}C for 10 hours. This results into fine powder with nano particle size.

Fine powders of these compositions were subjected to X-ray diffraction for confirmation of formation of spinel ferrites. For further confirmation, FTIR Spectroscopy and Scanning Electrode Microscopy (SEM) are also employed.

vi) Preparation of the Samples :

To keep pace with the objectives, the investigation of electrical properties and designing of smart sensor module, ensuring an embedded technology, the compositions of the ferrites under investigation are shaped as per the requirement. For further investigation, the samples in pellet form and thick film form are prepared.

i) **Formation of the pellets:** The pellets were formed by pressing fine powder of the compositions under investigation into the die of 13 mm inner diameter. The pressure of about 10 tons/sq.in. was applied for 10 minutes. The Hydraulic Press (KBr Press) Techno Search Instruments Table model M 15 with Die of inner diameter 13mm is used to prepare the pellets. The pellets of the compositions were subjected final sintering. The sintering temperature was 1000 ^{0}C for 12 hours and then slowly cooled, at the rate of 80 ^{0}C per hr, to the room temperature. Thus prepared compositions were finished and used for further investigations.

ii) **Formation of the Thick Films:** To deploy the present sensor material for development of the sensor module, the sample in electrode form is essential. Therefore, a thick film of the compositions was prepared. The fine powder is mixed into PVA as a organic binder. By adopting screen printing technique the thick films of the compositions were prepared. A uniform thick film is developed on to the substrate. Moreover, a film realizing the theme of inter digitating electrode is also developed. In the beginning, the thick film was developed on the resign substrate. However, it is constrained for high temperature applications. Therefore, a glass is used as a substrate. Moreover, to ensure sensor applications, it is attempted to avail body of IC as the substrate. It is then interfaced to the electronic circuit.

2.B X-Ray Diffraction

2.B.1 Introduction:

In materials investigation, the characterization of the compositions has prime importance. It is an inevitable step of confirmation of formation of the desired material. The materials can be characterized by employing various tools. However, to explore the structural details of the compositions under investigation, the standard tools such as X-Ray diffraction, FTIR Spectroscopy, SEM etc are most recommended. Present investigation emphasizes the synthesis of polycrystalline ferrites materials suitable for typical sensor based applications. For investigation of structural details above tools are employed and results of investigation are interpreted through subsequent sections.

X-ray powder diffraction (XRD) is most widely used technique for qualitative as well as quantitative analysis of the materials [45]. It is known that, crystalline structure, single crystal or polycrystalline, reveals perfect and periodical geometry of points (Lattice points) called unit cell. Thus, crystal is periodic repetition of the unit cell in predetermined symmetry. Laue had suggested that, the crystal can act as a grating for X-ray [46]. The unit cell is featured with the parameters called lattice parameters, such as axial lengths (a, b and c) and interfacial angles (α, β, and γ). On possible combination of these parameters and possible arrangement of lattice points by maintaining periodicity, the French Crystallographer, Bravais demonstrated 14 lattice structures, which are popularized as 14-Bravais Lattice [47]. The symmetry operations, such as, rotation, reflection, Inversion etc, on these lattices results into 230 possible combinations, which are popularized as 230 space groups. The compositions of the polycrystalline spinel ferrites exhibit Fd3m (N0.227) space group [48]. From X-ray diffractometry information regarding structural details for materials under investigation, which can be used for prediction of their suitability for desired applications, can be explored. X- ray powder diffraction can be used to determine

- Phases of the composition
- Quantitative phase analysis.
- Unit cell lattice parameters
- Crystal structure and its symmetry space group
- Average crystallite size
- Cation distribution.

According to W.H. Bragg and W.L. Bragg, the X-ray diffraction is governed by the Bragg`s Equation [49],

$$2d \sin\theta = n\lambda. \quad (1)$$

where, the symbols d, θ, n and λ have their usual meanings. According to eq.1, the x-ray diffraction study can be implemented for study of single crystal (Laue method) or polycrystalline (Powder Diffractometry) materials. For investigation of polycrystalline materials, the X-Ray powder Diffractometry (XRD) is most suitable. In this method, the wavelength of the radiation is kept constant and the sample is kept rotating. The powdered compositions consist of the crystals of different orientations and hence the diffractograms shows numbers of peaks, satisfying Bragg`s condition, at different 'd' values. X-Ray powder Diffraction (XRD) tool is used for structural investigation of the materials under study.

2.B.2 Experimental :

The compositions, $Mg_xZn_{1-x}Fe_2O_4$, $Ni_xZn_{1-x}Fe_2O_4$ and $Mn_xZn_{1-x}Fe_2O_4$(x= 0.20, 0.40, 0.60 and 0.80) of ferrites were characterized by X-ray powder diffraction. Computerized X-ray diffractometer Bruker AXE Analytical Instrument Pvt. Ltd. Germany, modelD2 Phaser was used. The CuKα (λ_1 = 1.540 A^0) radiations have been used with Nickel as a filter to filtrate the K_β lines of the copper target. The source of 30 KV and 10 mA is used for excitation of the tube. The experimental arrangement is depicted in figure 2.B.1. The relative intensity (counts) is obtained by scanning. The angle (2θ) of scanning is ranging from 20^0 to

Figure 2.B.1: Experimental set up for X-Ray Powder Diffraction X-ray diffractometer Bruker AXE Analytical Instrument Pvt. Ltd. Germany, model D2 Phaser.

80^0within the step of 0.005 degree. The diffractograms obtained are used for characterization of the composition under investigation.

X-Ray diffractometer is schematically depicted in figure 2.B.2. The powder specimen is kept at the centre on the sample holder. This sample holder is capable of rotating about its axis perpendicular to the plane of the drawing. A beam of filtered X-ray, collimated by a slit is allowed to incident on the specimen. The diffracted beam, passing through focusing slits, is collected at the counter. The counter along with the slits is free to rotate about the center. The Goniometric arrangement is realized for rotation of the specimen and the counter as well. The specimen and counter are rotated through the scan limit and the data, counts against 2θ values, are recorded into the computer. This data is used to explore the structural details of the composition under investigation.

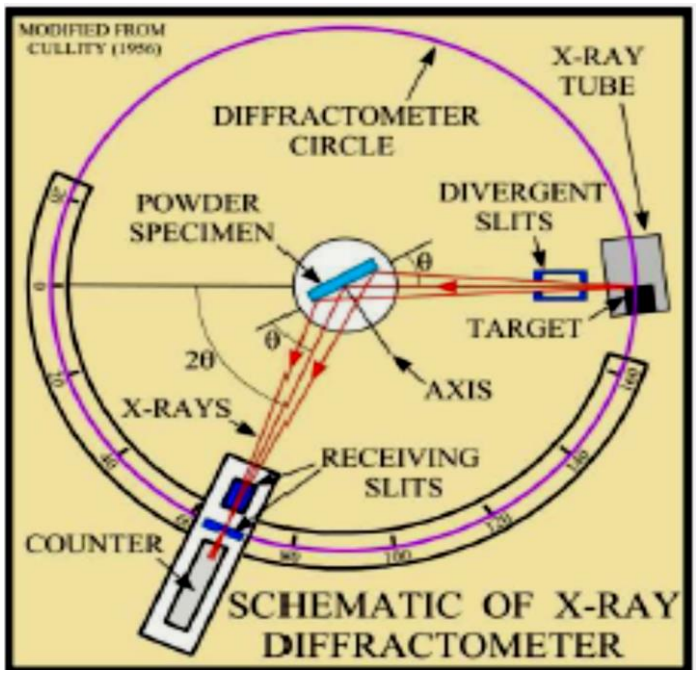

Figure 2.B.2: The Schematic of X-Ray Powder Diffractometer.

The diffractograms obtained from X-Ray diffractometer, reveals the information regarding intensity of the reflection (I) and Bragg`s angles (2θ). Availing this information the diffractograms are indexed. A method used for indexing depends upon nature of the crystal and its symmetry. The present investigation is related to the polycrystalline ferrites compositions, which are spinel in nature and depicts FCC structure [50]. Using Bragg`s angle of reflection (2θ) and employing expression 1, the observed 'd_{obs}' spacing is calculated by using equation 2.

$$d_{obs} = \frac{n\lambda}{2\sin\theta} \qquad (2)$$

It is reported by many investigators [51-54], that the predominant reflection for spinel structure is of the plane having indices (h, k, l) as 311. Therefore, reflection of maximum intensity, normally observed at angle about 2θ= 35.30 degree, is pre-assumed

as reflection from 311 plane. Then the value of lattice constant 'a' is calculated by deploying the expression

$$d_{hkl} = \frac{a}{h^2+K^2+l^2} \quad (3)$$

This 'a' value is used to determine the sum of squares of miller indices for all significant reflection. For FCC spinel structure the reported sum of squares are 2, 8, 11, 12, 16, 18, 20, 24, 27, 32 etc [55]. From observed sum of squares the 'd_{cal}' values are calculated. This process of indexing is iteratively performed to obtained sum of squares for which the observed and calculated d values are in close agreement.

$$a = [(\lambda^2/(4\sin^2\theta)) \times (h^2+k^2+l^2)]^{½} \quad (4)$$

Employing values of respective sum of squares for each significant reflection and using an expression 4 the lattice constant is determined for allowed reflections and then average value of 'a' is obtained and used for further interpretation.

The structural parameters such as cation-oxygen bond distances on tetrahedral (A-O) site and octahedral (B-O) site, ionic radii (r_A and r_B) of respective sites, physical density (ρ_P), X-ray density (ρ_x), porosity (P), and crystallite size (L) are also determined from X-ray diffraction data. Following expressions are used to calculate above structural parameters.

- **Cation – Oxygen Bond Distances on A and B sites of the spinel structure.**

$$A\text{-}O = (u - ¼)\, a\sqrt{3} \quad (5)$$

$$B\text{-}O = (5/8 - u)a \quad (6)$$

- **Ionic Radii on A and B sites**.

$$r_A = (u - ¼)\, a\sqrt{3} - r_{oxy} \quad (7)$$

$$r_B = (5/8 - u)a - r_{oxy} \quad (8)$$

Where u is oxygen ion parameters, ideally u = 0.375 [56,57] and r_{oxy} is ionic radius of the oxygen ion (r_{oxy}= 1.40A^0).

- **X-ray density (ρ_x) :**

$$\rho_x = \frac{8M}{N_o a^3} \quad (9)$$

Where, N_o is Avogadro`s number = 6.0225 x 10^{23}.

- **Porosity (P) in % :**

$$P = \frac{\rho_x - \rho_p}{\rho_x} * 100 \quad (10)$$

- **Crystallite size nm:**

  The size of the crystallites, particle size, for all compositions under investigation is estimated for employing Scherrer Equation [58,59,60],

$$L = \frac{K\lambda}{\beta\cos\theta} \quad (11)$$

Where λ is the X-ray wavelength in nanometer (nm), β is the FullWidth at Half Maxima (FWHM) in radians and K is a constant related to crystallite shape, normally taken as 0.9[61]. The value of β in 2θ axis of diffraction profile must be in radians. The θ can be in degrees or radians, since the $\cos\theta$ corresponds to thesame number.

2.B.3 Results and Discussion:

X-ray diffractograms of compositions, $Mg_xZn_{1-x}Fe_2O_4$, $Ni_xZn_{1-x}Fe_2O_4$ and $Mn_xZn_{1-x}Fe_2O_4$(x= 0.20, 0.40, 0.60 and 0.80) of polycrystalline ferrites, obtained from the diffractometer, are depicted in figure 2.B.2 -2.B.4. These diffractograms, show well defined reflections without any ambiguity. An intensity of 311 reflection is found maximum, supporting the fact that 311 reflection is predominant reflection. This is one of the features of the spinel structure [59]. The diffractograms are indexed by the process as discussed earlier. The miller indices, calculated for all compositions under investigation, exhibit close agreement with that of given by the FCC structure [60]. This confirms the formation of single phase spinel ferrite for all compositions under investigation. Employing process discussed earlier, d values are estimated for significant reflections and presented in tables 2.B.1-2.B.3. On inspection of these tables, it is found that, calculated ‘d’ values are closely matched with that of observed ‘d’ values. This confirms the process of indexing of the diffractograms. Lattice constants ‘a’ for all compositions under investigation are calculated by the process discussed earlier, and presented in tables 2.B.4-2.B.6.

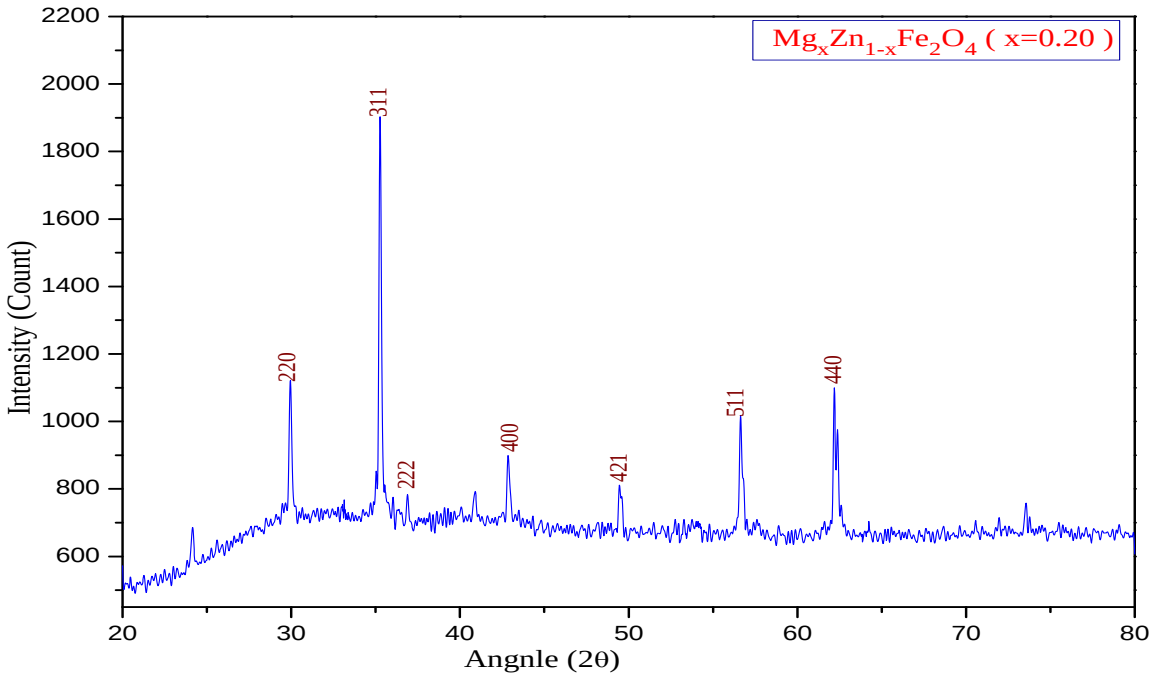

Figure 2.B.2(a) X-ray diffractogram for composition of $Mg_xZn_{1-x}Fe_2O_4$(x= 0.20)

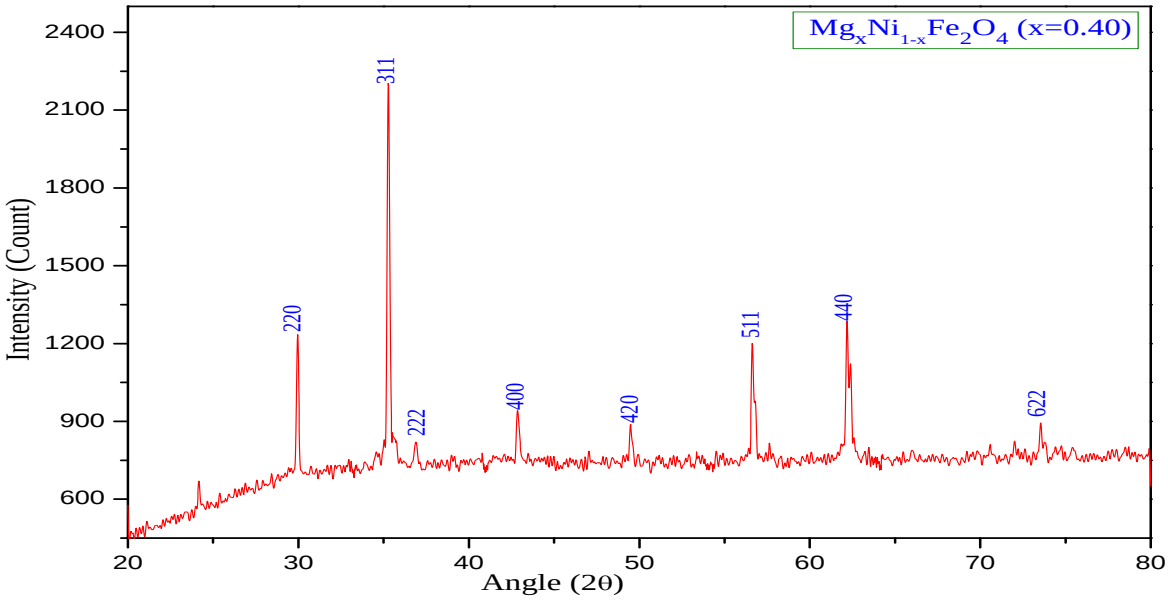

Figure 2.B.2(b) X-ray diffractogram for composition of $Mg_xZn_{1-x}Fe_2O_4$(x= 0.40)

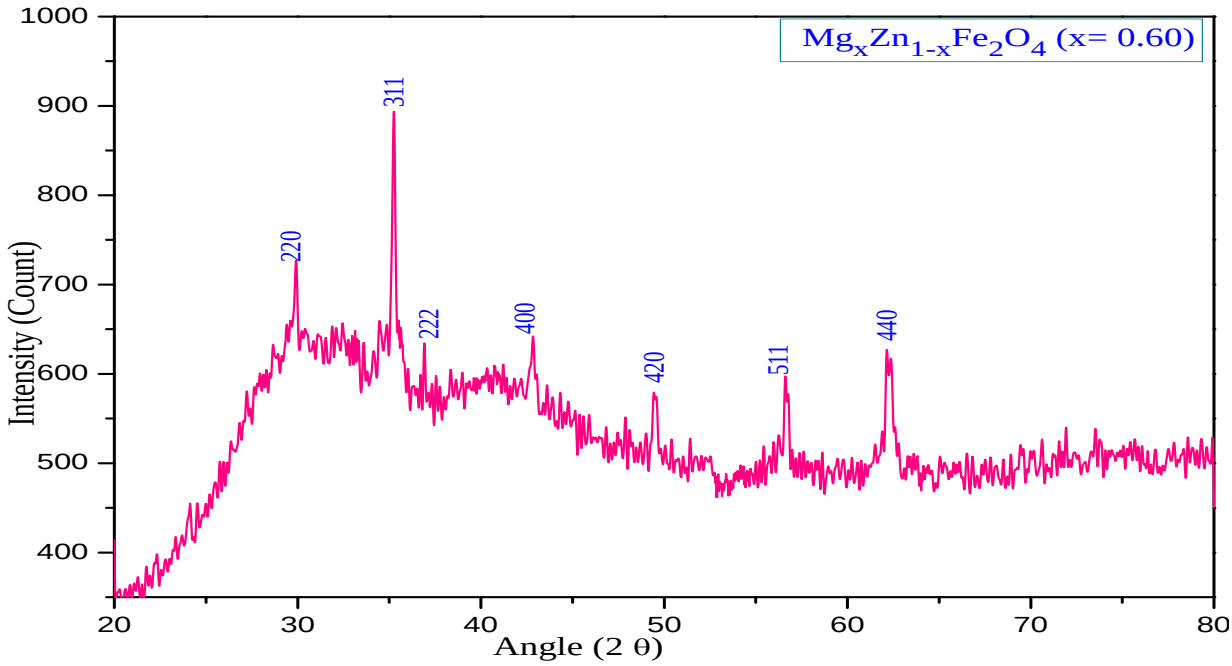

Figure 2.B.2(c) X-ray diffractogram for composition of $Mg_xZn_{1-x}Fe_2O_4$(x= 0.60)

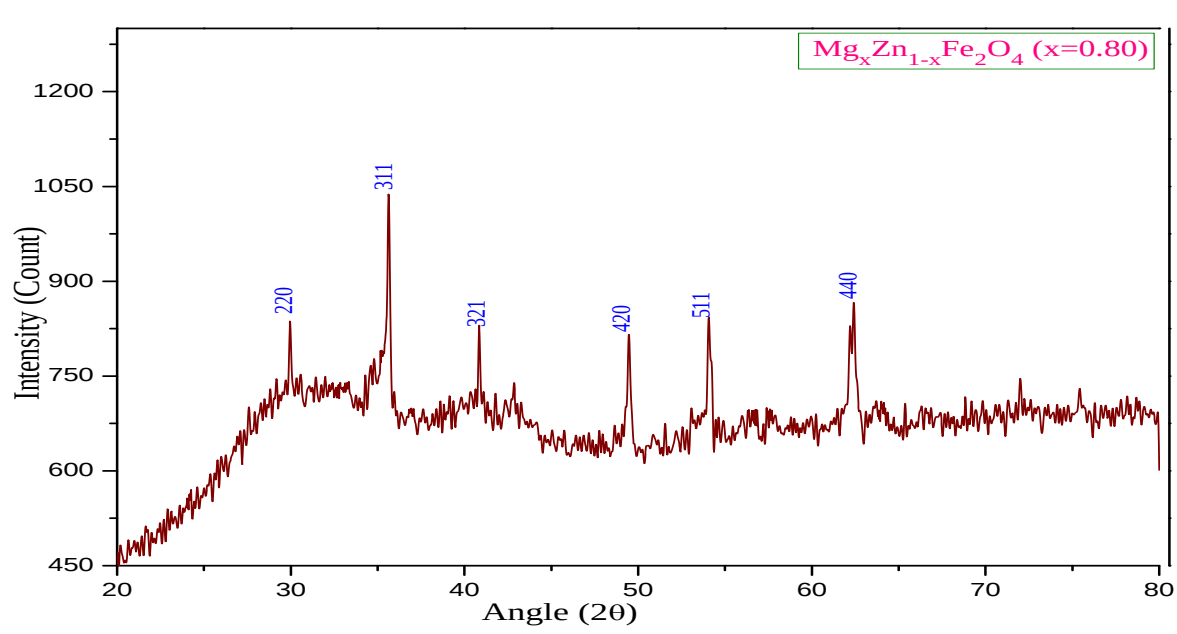

Figure 2.B.2(d) X-ray diffractogram for composition of $Mg_xZn_{1-x}Fe_2O_4$(x= 0.80)

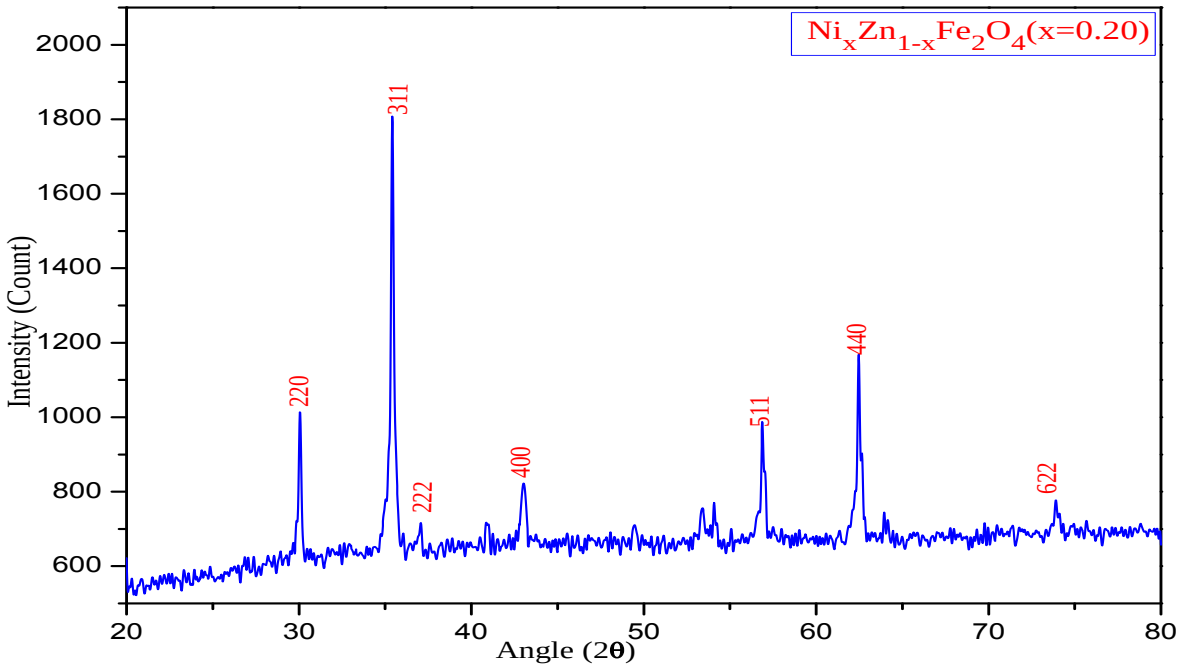

Figure 2.B.3(a) X-ray diffractogram for composition of $Ni_xZn_{1-x}Fe_2O_4$(x= 0.20)

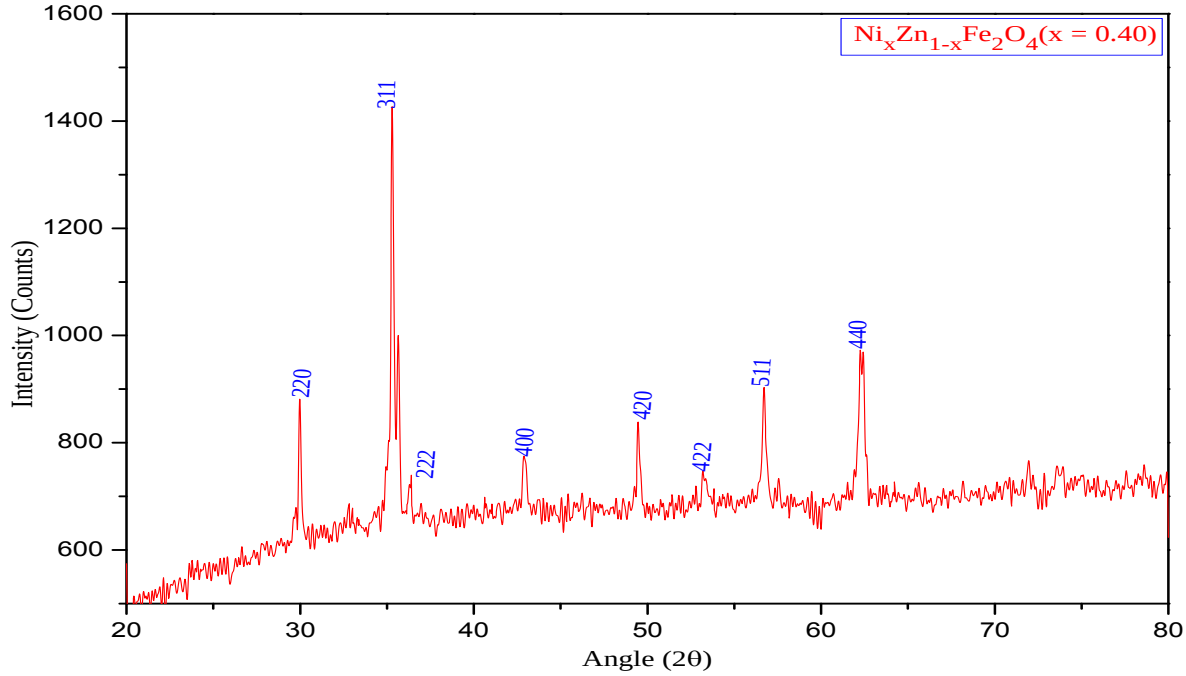

Figure 2.B.3(b) X-ray diffractogram for composition of $Ni_xZn_{1-x}Fe_2O_4$(x= 0.40)

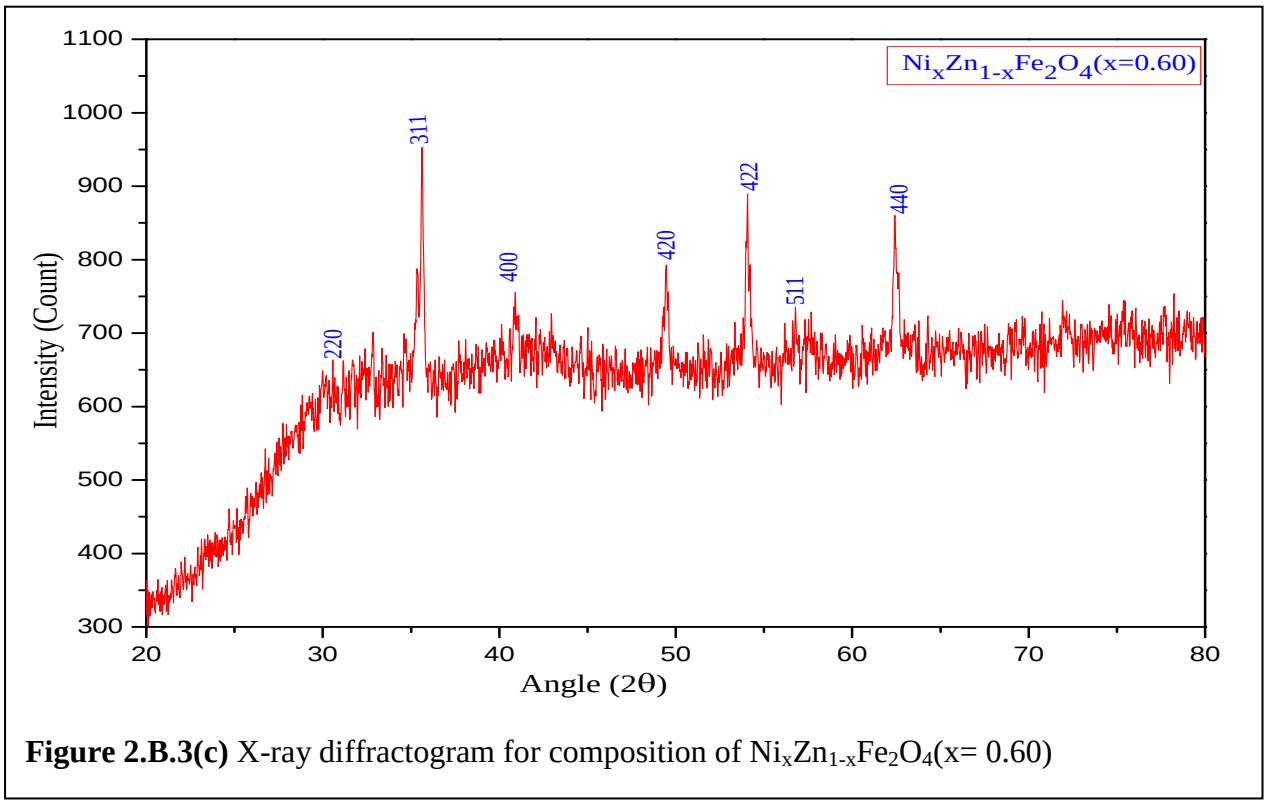

Figure 2.B.3(c) X-ray diffractogram for composition of $Ni_xZn_{1-x}Fe_2O_4$(x= 0.60)

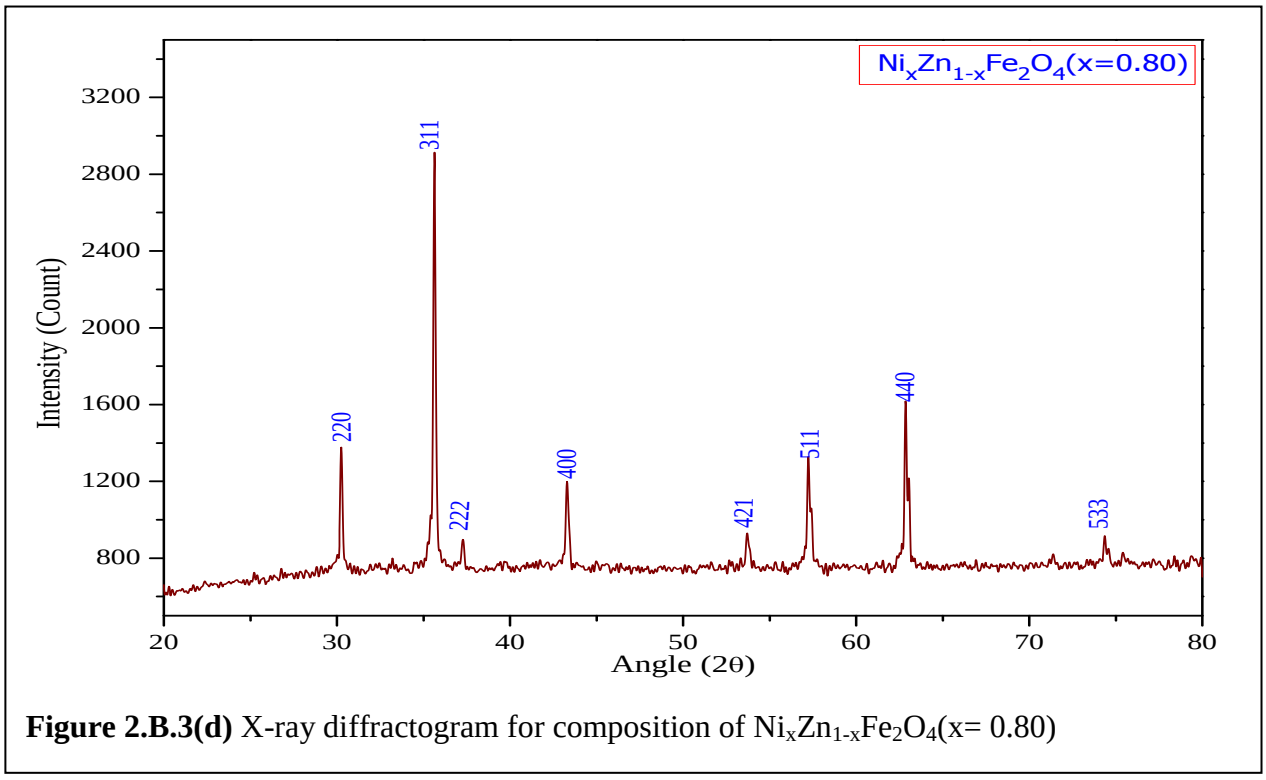

Figure 2.B.3(d) X-ray diffractogram for composition of $Ni_xZn_{1-x}Fe_2O_4$(x= 0.80)

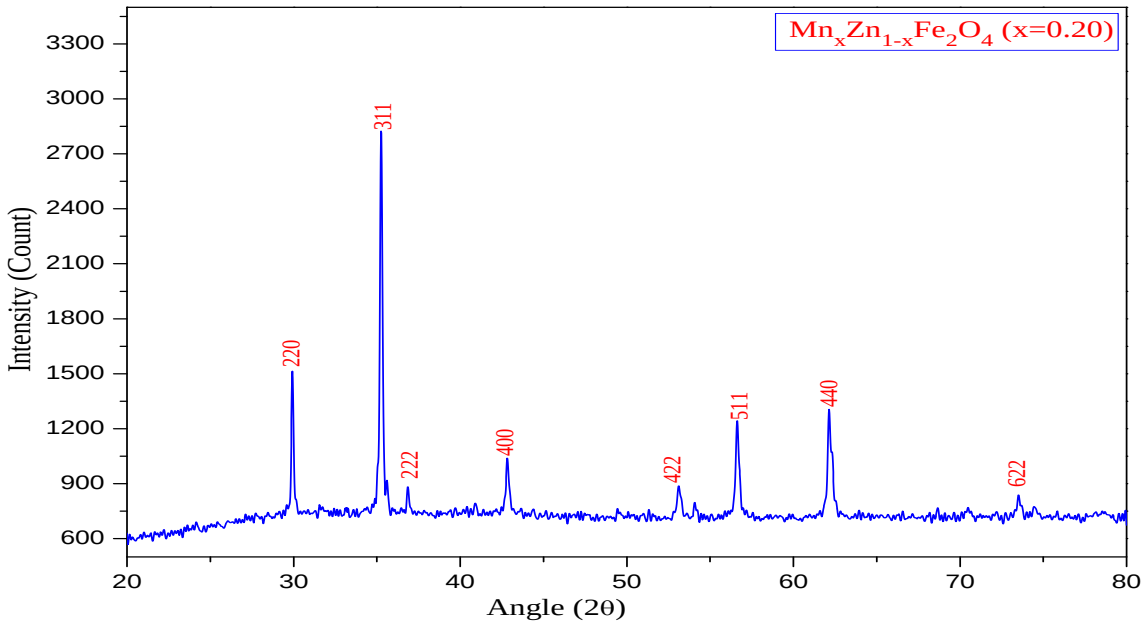

Figure 2.B.4(a) X-ray diffractogram for composition of $Mn_xZn_{1-x}Fe_2O_4$(x= 0.20)

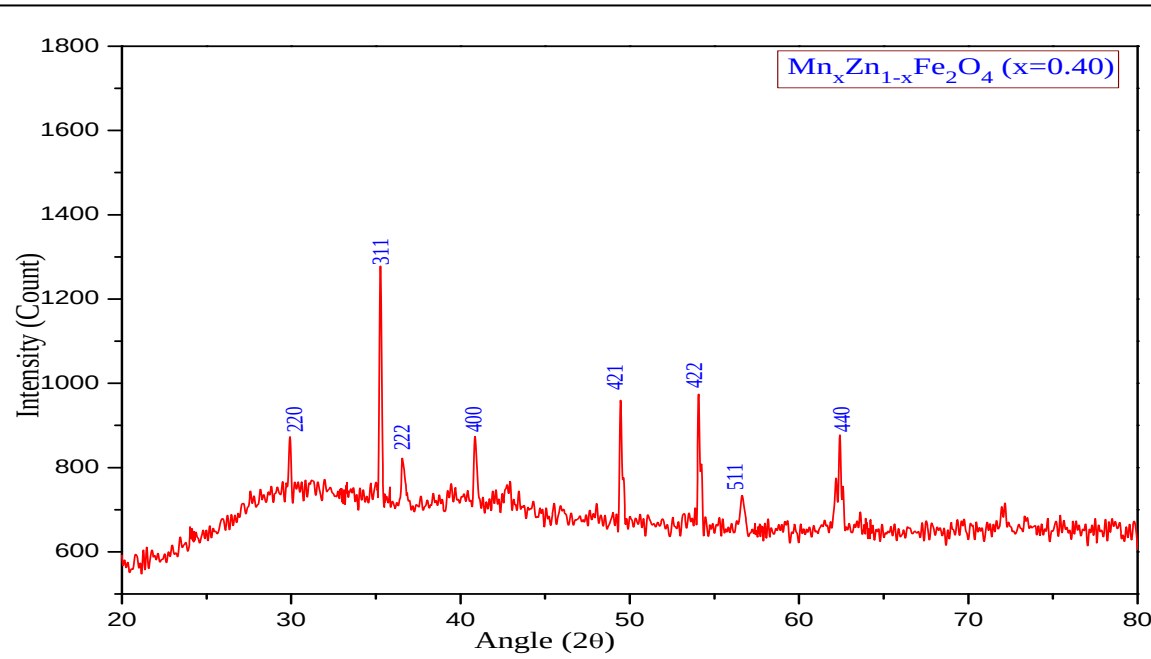

Figure 2.B.4(b) X-ray diffractogram for composition of $Mn_xZn_{1-x}Fe_2O_4$(x= 0.40)

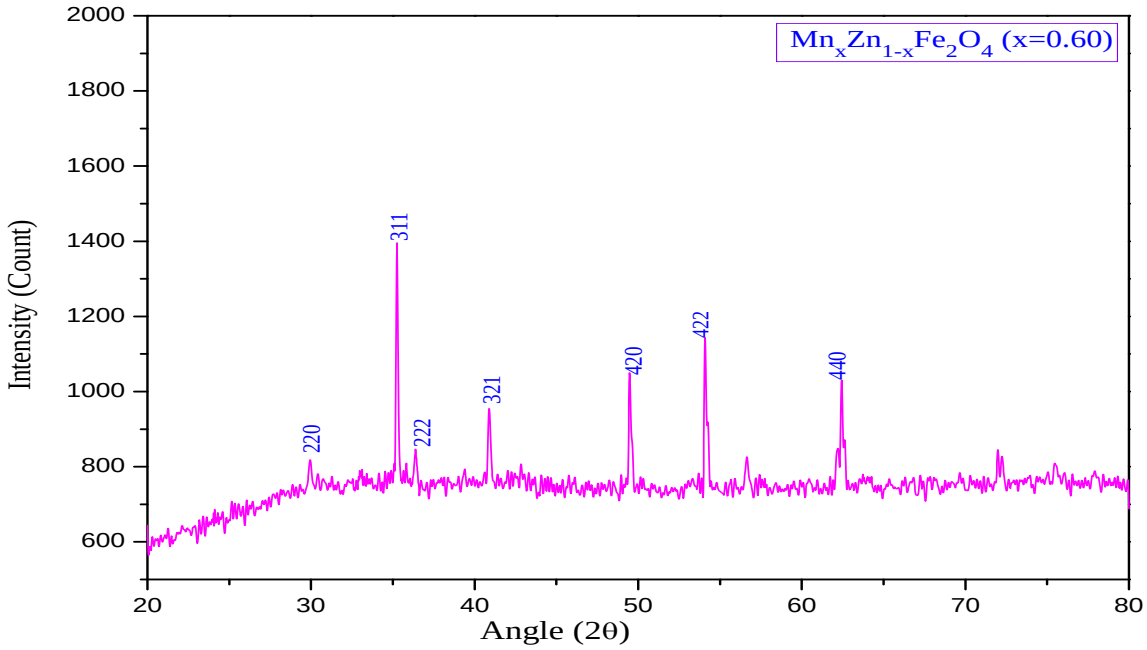

Figure 2.B.4(c) X-ray diffractogram for composition of $Mn_xZn_{1-x}Fe_2O_4$(x= 0.60)

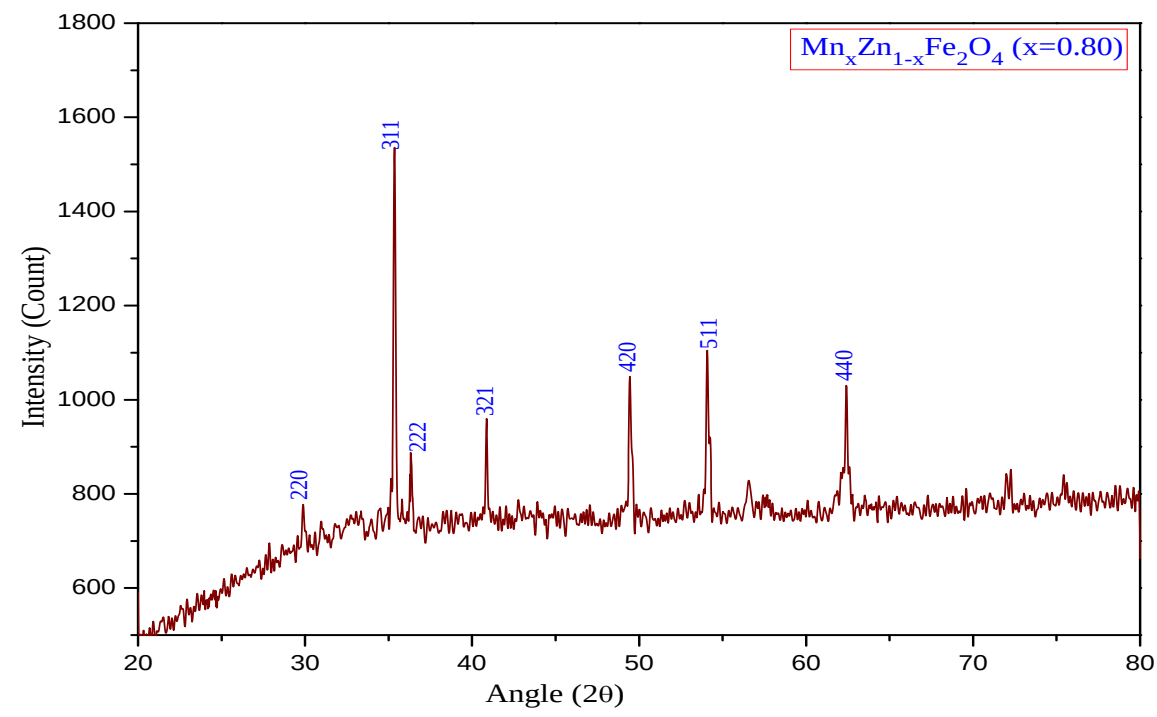

Figure 2.B.4(d) X-ray diffractogram for composition of $Mn_xZn_{1-x}Fe_2O_4$(x= 0.80)

On inspections of the tables 2.B.4-2.B.6, it is found that, the lattice constants reveal its compositional dependence.

It is also found that, the values of the lattices constant show close agreement with the earlier reports [61, 62,63]. Table 2.B.4 shows that, the lattice constant 'a', for the compositions $Mg_xZn_{1-x}Fe_2O_4$ decreases with increase in the concentration of Magnesium ion. It is known that, the ionic radius of Zn^{2+} is 0.83 A^0[64], whereas that of Mg^{2+} is 0.66 A^0 [65]. The ionic radius of Fe^{3+} is 0.67 A^0 [66]. That mean, the zinc ion is bigger than magnesium ion. Also, the zinc ferrites are normal ferrites depicting strong occupancy of zinc ion on tetrahedral (A) site of the spinel structure. Moreover, the magnesium ion preferentially distribute among A and B sites [67, 68, 69]. By increasing concentration of magnesium ion (x), the concentration of zinc ion reduces. Thus, on substitution of magnesium ion an amount of zinc ion(r_{Zn2+} = 0.83 A^0), the bigger ion, on tetrahedral site decreases, which results into increase in the concentration of Fe^{3+} ion (r_{Fe3+} = 0.67 A^0). This may cause to decrease ionic radius on tetrahedral site. Hence, the lattice constant, 'a', decreases with increase in the concentration of magnesium ion. This reduction of lattice constant with increase in magnesium in MgZn ferrites are also reported by the investigator [70,71]

On inspection of Table 2 B.5, it is found that, the lattice constant 'a', for the compositions $Ni_xZn_{1-x}Fe_2O_4$also reveals the compositional dependency. It known that, the nickel ferrite is the good example of inverse ferrites exhibiting strong occupancy of nickel on octahedral (B) site of the spinel structure [70]. Thus, nickel ion (r_{Ni2+} = 0.69A^0) when substituted resides on B site and displaces proportional amount of Fe^{3+} ion from B site to A site. Thus, increase in the concentration of nickel results into decrease in the concentration of zinc ion on tetrahedral site. The proportional amount of Fe^{3+} is shifted from A site to B site. Distribution of these cations results into slight decrease in the lattice constant. Similar results are also reported by many investigators [71,72]. Similar results (Table 2.B.6) of decrease in the lattice constant due to increase in preferentially distributed (among A and B sites) manganese ion in $Mn_xZn_{1-x}Fe_2O_4$ are also reported. This can assigned to the change in the ionic radii of tetrahedral (A) and octahedral (B) site due to cation distribution.

Cation-oxygen bond distances for tetrahedral site (A-O) and that of octahedral site (B-O) are also estimated by the process discussed earlier. The values of these bond (A-O & B-O), distances for compositions under investigations, are presented in tables 2.B.4 to 2.B.6. From these tables, it can be said that the bond distances depict

compositional variations. From FTIR spectroscopy studies, it is also found that variation of the bond distances is reflected on the spectra revealing the positions of absorption bands attributed to the tetrahedral and octahedral sites. The values of ionic radii for both tetrahedral and octahedral sites are calculated and presented in table 2.B.4 to 2.B.6. According to Sorescua et al [73, 74], the ionic radii on tetrahedral and octahedral sites significantly depends upon cation distribution. Therefore, the cation distribution can be predicted from calculation of ionic radii of the respective sites.

TABLES 2.B.1 (a-d):X-ray diffraction data for the compositions $Mg_xZn_{1-x}Fe_2O_4$ (x= 0.20, 0.40, 0.60 and 0.80)

a) $Mg_xZn_{1-x}Fe_2O_4$ (x =0.20)				b) $Mg_xZn_{1-x}Fe_2O_4$ (x =0.40)			
2θ Degree	**Miller Indices h k l**	**Observed d_{Obs} A^0**	**Calculated d_{cal} A^0**	**2θ Degree**	**Miller Indices h k l**	**Observed d_{Obs} A^0**	**Calculated d_{cal} A^0**
29.934	220	2.983	2.985	29.934	220	2.983	2.985
35.265	311	2.543	2.545	35.245	311	2.545	2.546
36.907	222	2.434	2.435	36.867	222	2.436	2.438
42.907	400	2.106	2.108	42.846	400	2.109	2.111
49.455	421	1.841	1.843	49.475	420	1.841	1.842
54.076	422	1.695	1.696	53.144	422	1.722	1.723
56.630	511/333	1.624	1.625	56.63	511/333	1.624	1.625
62.205	440	1.491	1.492	62.185	440	1.492	1.493

c) $Mg_xZn_{1-x}Fe_2O_4$ (x =0.60)				d) $Mg_xZn_{1-x}Fe_2O_4$ (x =0.80)*			
2θ Degree	**Miller Indices h k l**	**Observed d_{Obs} A^0**	**Calculated d_{cal} A^0**	**2θ Degree**	**Miller Indices h k l**	**Observed d_{Obs} A^0**	**Calculated d_{cal} A^0**
29.954	220	2.981	2.983	29.934	7.736	2.983	2.985
35.245	311	2.545	2.546	35.286	10.655	2.542	2.544
36.887	222	2.435	2.437	35.63	10.857	2.518	2.520
42.887	400	2.107	2.109	40.88	14.146	2.206	2.208
49.576	420	1.838	1.839	49.455	20.295	1.842	1.843
56.63	511/333	1.624	1.625	56.691	26.146	1.623	1.624
62.306	440	1.489	1.490	62.225	30.969	1.491	1.492
				64.009	32.579	1.454	1.455

TABLES 2.B.2 (a-d): X-ray diffraction data for the compositions $Ni_xZn_{1-x}Fe_2O_4$ (x= 0.20, 0.40, 0.60 and 0.80)

a) $Ni_xZn_{1-x}Fe_2O_4$ (x =0.20)				b) $Ni_xZn_{1-x}Fe_2O_4$ (x =0.40)			
2θ Degree	**Miller Indices h k l**	**Observed d_{Obs} A^0**	**Calculated d_{cal} A^0**	**2θ Degree**	**Miller Indices h k l**	**Observed d_{Obs} A^0**	**Calculated d_{cal} A^0**
30.056	220	2.971	2.973	29.954	220	2.981	2.983
35.387	311	2.535	2.536	**35.306**	311	2.540	2.542
43.029	400	2.101	2.102	42.988	400	2.103	2.104
56.894	511/333	1.617	1.618	49.475	420	1.841	1.842
62.468	440	1.486	1.487	53.326	422	1.717	1.718
74.793	622	1.269	1.269	56.712	511/333	1.622	1.623
				62.306	440	1.489	1.490

c) $Ni_xZn_{1-x}Fe_2O_4$ (x =0.60)				d) $Ni_xZn_{1-x}Fe_2O_4$ (x =0.80)			
2θ Degree	**Miller Indices h k l**	**Observed d_{Obs} A^0**	**Calculated d_{cal} A^0**	**2θ Degree**	**Miller Indices h k l**	**Observed d_{Obs} A^0**	**Calculated d_{cal} A^0**
33.157	310	2.700	2.702	30.258	220	2.952	2.954
35.63	311	2.518	2.520	35.63	311	2.518	2.520
40.13		2.246	2.247	37.232	222	2.413	2.415
49.455	420	1.842	1.843	43.292	400	2.089	2.090
54.076	422	1.695	1.696	53.711	421	1.705	1.707
62.428	440	1.487	1.488	57.259	511/333	1.608	1.609
63.989	530	1.454	1.455	62.853	440	1.478	1.479
				74.367	533	1.275	1.276

TABLES 2.B.3 (a-d): X-ray diffraction data for the compositions $Mn_xZn_{1-x}Fe_2O_4$ (x= 0.20, 0.40, 0.60 and 0.80)

a) $Mn_xZn_{1-x}Fe_2O_4$ (x =0.20)				b) $Mn_xZn_{1-x}Fe_2O_4$ (x =0.40)			
2θ Degree	**Miller Indices h k l**	**Observed d_{Obs} A^0**	**Calculated d_{cal} A^0**	**2θ Degree**	**Miller Indices h k l**	**Observed d_{Obs} A^0**	**Calculated d_{cal} A^0**
29.934	220	2.983	2.985	29.934	220	2.983	2.985
35.245	311	2.545	2.546	35.245	311	2.545	2.546
36.867	222	2.436	2.438	49.455	421	1.842	1.843
42.826	400	2.110	2.112	54.076	422	1.695	1.696
53.103	422	1.723	1.725	62.408	440	1.487	1.488
56.651	511/333	1.624	1.625	63.968	541	1.454	1.455
62.144	440	1.493	1.494				
73.496	622	1.288	1.289				

c) $Mn_xZn_{1-x}Fe_2O_4$ (x =0.60)				d) $Mn_xZn_{1-x}Fe_2O_4$ (x =0.80)			
2θ Degree	**Miller Indices h k l**	**Observed d_{Obs} A^0**	**Calculated d_{cal} A^0**	**2θ Degree**	**Miller Indices h k l**	**Observed d_{Obs} A^0**	**Calculated d_{cal} A^0**
24.177		3.679	3.681	29.894	220	2.987	2.989
35.265	311	2.543	2.545	35.225	311	2.546	2.548
40.88	321	2.206	2.207	40.86	321	2.207	2.208
49.495	420	1.840	1.842	49.475	420	1.841	1.842
54.097	422	1.694	1.695	54.076	422	1.695	1.696
62.448		1.486	1.487	62.408		1.487	1.488
63.989	440	1.454	1.455	63.948	440	1.455	1.456

TABLES 2.B.4: X-ray diffraction data; Lattice constant, Cation- Oxygen Bond Distance and Ionic radii for the compositions $Mg_xZn_{1-x}Fe_2O_4$ (x= 0.20, 0.40, 0.60 and 0.80)

X **A**	**Lattice constant 'a' A^0**	**CationOxygen Bond Distance A^0**		**Ionic Radii A^0**	
		Tetrahedral (A) site (A-O)	**Octahedral (B) site (B-O)**	**Tetrahedral (A) site (r_A)**	**Octahedral (B) site (r_B)**
0.20	8.191	1.759	2.056	0.359	0.656
0.40	8.173	1.755	2.051	0.355	0.651
0.60	8.184	1.758	2.054	0.358	0.654
0.80	8.115	1.669	1.951	0.269	0.551

TABLES 2.B.5: X-ray diffraction data; Lattice constant, Cation- Oxygen Bond Distance and Ionic radii for the compositions $Ni_xZn_{1-x}Fe_2O_4$ (x= 0.20, 0.40, 0.60 and 0.80)

X B	Lattice constant 'a' A^0	Cation oxygen Bond Distance A^0		Ionic Radii A^0	
		Tetrahedral (A) site (A-O)	Octahedral (B) site (B-O)	Tetrahedral (A) site (rA)	Octahedral (B) site (r_B)
0.2	8.151	1.751	2.046	0.351	0.646
0.4	8.163	1.753	2.049	0.353	0.649
0.6	8.006	1.720	2.010	0.320	0.610
0.8	8.088	1.737	2.030	0.337	0.630

TABLES 2.B.6: X-ray diffraction data; Lattice constant, Cation- Oxygen Bond Distance and Ionic radii for the compositions $Mn_xZn_{1-x}Fe_2O_4$ (x= 0.20, 0.40, 0.60 and 0.80)

X C	Lattice constant 'a' A^0	Cation oxygen Bond Distance A^0		Ionic Radii A^0	
		Tetrahedral (A) site (A-O)	Octahedral (B) site (B-O)	Tetrahedral (A) site (rA)	Octahedral (B) site (r_B)
0.2	8.457	1.816	2.123	0.416	0.723
0.4	8.457	1.816	2.123	0.416	0.723
0.6	8.307	1.784	2.085	0.384	0.685
0.8	8.228	1.767	2.065	0.367	0.665

TABLES 2.B.7: Physical Density, x-ray density, Porosity and Particles of the compositions $Mg_xZn_{1-x}Fe_2O_4$ (x= 0.20, 0.40, 0.60 and 0.80)

X A	Physical density ρ_p gm/cm^3	X-ray density ρx	Porosity P %	Particle Size L
0.2	4.0487	5.665	28.53	48.17
0.4	4.1418	5.443	23.91	44.92
0.6	4.3660	5.231	16.53	40.32
0.8	4.8253	5.893	18.12	46.74

TABLES 2.B.8: Physical Density, x-ray density, Porosity and Particles of the compositions $Ni_xZn_{1-x}Fe_2O_4$ (x= 0.20, 0.40, 0.60 and 0.80)

X B	Physical density ρ_p gm/cm^3	X-ray density ρ_x	Porosity P %	Particle Size L
0.2	4.548	5.880	22.65	44.17
0.4	4.473	5.821	24.01	35.67
0.6	4.230	6.135	31.05	75.96
0.8	3.579	5.916	22.60	52.80

TABLES 2.B.9: Physical Density, x-ray density, Porosity and Particles of the compositions $Mn_xZn_{1-x}Fe_2O_4$ (x= 0.20, 0.40, 0.60 and 0.80)

X C	Physical density ρ_p gm/cm^3	X-ray density ρ_x	Porosity P %	Particle Size L
0.2	3.913	5.248	25.44	44.01
0.4	3.312	5.202	36.35	54.73
0.6	3.992	5.441	26.66	52.27
0.8	4.558	5.549	17.88	56.59

Emphasizing investigation of the structural details, the X-Ray diffraction is also employed to calculate the values of X-ray density (ρ_x) by using expression 9. The values of physical density are obtained from the physical dimensions of the samples under investigation. Deploying equation 10, the porosities (P) of the compositions are determined. Values of these parameters are presented in tables 2.B.7 - 2.B.9 for the compositions under investigation. The porosities are in range from 17 % to 36%. The porosity values observed for present investigation show good agreement with that of earlier reports [75, 76]. In fact, present investigation emphasizes the development of materials suitable for development of electronic sensor. For detection of environmental parameters like humidity the compositions of high porosity are essentially suitable [77]. Thus, on structural study, it can be said that, the compositions under investigation are suitable for humidity sensor.

Using Scherrer expression, equation 11, the particle size of all compositions arecalculated. According to Scherrer the β (FWHM) values for significant reflections are measured. For measurement of β (FWHM) value, the reflection observed at Bragg`s angle 2θ, is selected and magnified as depicted in figure 2.B.5. From figure 2.B.5, it is cleared that, the reflections reveal Guassian distribution indicating symmetry about the Braggs angle. Employing relation $\beta = 2\theta_2 - 2\theta_1$, the values of FWHM for significant reflections are obtained. Deploying the Scherrer relation, values of particle size are calculated for each of the reflections. These values are averaged to obtain resultant particle size (L) in nanometer. Values of the size of particle (L) in nm are presented in tables 2.B.7-2.B.9. On inspection of these tables, it can be said that, the compositions reveal the formation of nano-sized particles. The particle diameter varies from 35 nm to 75 nano meter. The size of crystallites observed for present investigation show good agreement with that of earlier reports [77,78]. Thus, X-ray powder diffraction is suitably employed to explore the structural details of the compositions under investigation.

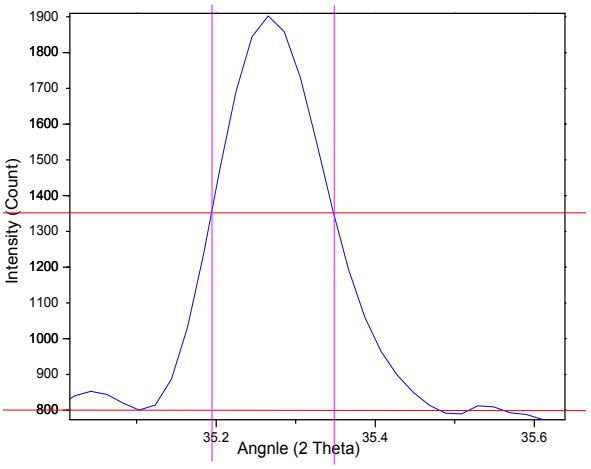

Figure 2.B.5 Representation of the reflection to measure FWHM

2.B.4 Conclusion:

The compositions under investigation are characterized with standard tool, the X-ray powder diffraction. The diffractograms reveal the formation of the single phase compositions without any ambiguity. On characterization, it is found that, the compositions are cubic spinels with F3dm space group symmetry. Close agreement of observed and calculated d values supports the indexing process. Lattice constants for compositions under investigation depict compositional dependence. Cation-Oxygen band distance and ionic radii supports the results obtained from FTIR spectroscopy. The porosities are within the range from 17% to 36%. Using Debye-Scherer relation, the particles size of compositions are estimated and it is in the range from 35nm to 75 nanometer. From results of investigation, it can be concluded that, the synthesized composition reveal polycrystalline, single phase, nano particle size structure, which would be suitable for development of the sensor.

2.C FTIR Spectroscopy

2.C.1 Introduction:

Major objective of present investigation is to synthesize polycrystalline ferrite materials suitable for sensor based applications and deployment of the same for development of smart sensor module, wherein the embedded philosophy is ensured. For confirmation of preparation of materials, it is essential to characterize the same with the standard tools [79]. The compositions under investigation are already characterized with X-ray powder diffractometry, which reveals the formation of spinel compositions. For further confirmation, FTIR spectroscopy is employed and materials under investigation are characterized.

Infrared absorption spectroscopy is an important, non-destructive and rapid method of characterization and it provides the information regarding functional group and their linkages [80]. The modes of lattice vibrations are the intrinsic characteristics of any crystalline material. These modes of vibrations reflect the structural details and group complexes as well. The heavy metal oxides and inorganic compounds absorb the radiation in the frequency range from 200 cm^{-1} to 800 cm^{-1}, significantly [81]. Ferrite materials are the good example of metal oxides and therefore, the structural details are explored within this range of investigation. The absorption band, from which the structural information can be explored, is found to be dependent on atomic mass, cationic radius, cation-anion bond distances, method of preparation, chemical compositions etc [82]. Waldron was the first, who proved that the IR spectroscopy is mostly suitable to explore the details regarding group complexes, existing in the polycrystalline spinel ferrite materials [80] . On investigation of strength of the bonds, he attributed high frequency absorption band to tetrahedral (A) site and low frequency absorption band to the group complexes existing at octahedral (B) site of the spinel structural [83,84].

Normally, in case of spinel structure, the four absorption bands may be observed within the range from 200 cm^{-1} to 800 cm^{-1}. These bonds are denoted as ν_1, ν_2, ν_3 and ν_4. The absorption band (ν_1), observed around 600 cm^{-1} is assigned to the intrinsic vibrations of tetrahedral (A) site [85], whereas the second band (ν_2) observed at about 400 cm^{-1} is attributed to the octahedral metal-oxygen group complexes [86]. The bond (ν_3) near about band (ν_2) is due to the vibrations in the divalent metal oxygen

complexes in the octahedral site [87]. Moreover, the bond γ_4 is attributed to the mass of divalent cation on tetrahedral site. Recently, investigators are characterizing the compositions of the ferrite materials by using FTIR within the range from 400cm^{-1} to 4000cm^{-1}[88]. In higher frequency region the significant absorption bands are also observed [89]. These bands are attributed to dedicated reason.

IR spectroscopy is non-destructive and reliable method of material characterization. Therefore, many investigators have investigated the structural details and results of investigation are reported. Kumar et al have characterized the composition of MnZn ferrite by IR absorption spectroscopy and reported the existence of lattice vibration within the range from 400 cm^{-1} to 4000 cm^{-1} [90]. A thin film of $NiFe_2O_4$, nanosized ferrite, was synthesized by Gunjakar et al and explored the structural detail by employing FT-IR spectroscopy [91]. They reported absorption bands at different frequencies and attributed the result to the spinel structure of the ferrite, revealing two crystallographically significant sites, tetrahedral (A) site and octahedral (B) site [92]. Two absorption bands ν_1 and ν_2 observed at 597.12 cm^{-1} and 417.13 cm^{-1} , are respectively attributed to the group complexes of tetrahedral site and octahedral sites [91]. In addition to these significant absorption bands, Gunjakar et al have also found two bands at frequency 3400 $cm^{-1}$and 1814 cm^{-1}. They assigned these bands to the existence of hydroxide group [91]. FTIR spectroscopic analysis of nanosized nickel zinc ferrites was carried out by Saafan et al [93]. They reported four significant absorption bands. Out of four bands two bands, ν_1 and $\nu_2$are attributed to the tetrahedral and octahedral metal-oxygen complexes [94]. Moreover, remaining two bands ν_3 and ν_4 are due to divalent metal ion-oxygen complexes in octahedral sites and lattice vibration of the tetrahedral cations [93,94]. Nickel ferrite is the inverse ferrite, exhibiting occupancy of the nickel on octahedral (B) site of the spinel structure [101,102]. This results into shifting of Fe^{3+} ion on A site. Broadening of the band may be due to asymmetric stretching of the bonds [100]. Emphasizing the synthesis of material suitable for sensor based application, Thangaraj et al have studied zinc oxide nano powder by IR spectroscopy [98]. The results of IR spectroscopic studies of ferrite/ polypyrrole composites are reported by Saafan et al [99].

In present work, FTIR spectroscopy of the compositions, under investigation, are extensively studied for their suitability as a sensor material and the results are interpreted in this report.

2.C.2 Experimental:

Figure 2.C.1 The Experimental set FTIR absorption spectroscopic studies

The FTIR spectra of the compositions $Mg_xZn_{1-x}Fe_2O_4$, $Ni_xZn_{1-x}Fe_2O_4$ and $Mn_xZn_{1-x}Fe_2O_4$ ferrites were obtained in the range from 400 cm^{-1} to 4000 cm^{-1} by using FT-IR spectrometer, NICOLET 6700, USA, wherein the IR source Alum Standard ETC Ever-Glo is used. The resolution was configured to 0.125cm^{-1} to 320 cm^{-1}. The Experimental setup is shown in figure 2.C.1. The spectrometer is configured in absorption mode. So, the resulted spectrographs, transmittance (%) against wave number (cm^{-1}) reveal the absorption bands, significantly.

2.C.3 Result and Discussion:

Infrared absorption spectra, Transmittance (T) (%) against wave number (ν) (cm^{-1}), for the compositions under investigation, are obtained from FT-IR spectrometer, NICOLET 6700, USA and presented in Figures 2.C.2 – 2.C.4 respectively for $Mg_xZn_{1-x}Fe_2O_4$, $Ni_xZn_{1-x}Fe_2O_4$ and $Mn_xZn_{1-x}Fe_2O_4$ ferrites compositions.

A) **IR spectroscopic study of $Mg_xZn_{1-x}Fe_2O_4$ compositions:**

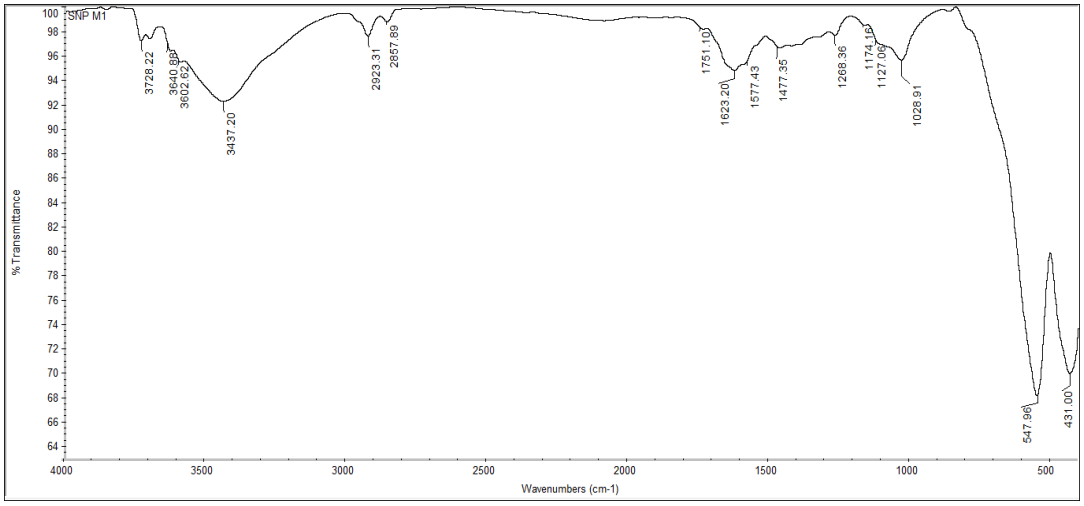

Figures 2.C.2 (a) IR absorption spectra of the composition $Mg_xZn_{1-x}Fe_2O_4$ (x=0.20)

As depicted in figures 2.C.2 (a-d), the FTIR spectra for the compositions $Mg_xZn_{1-x}Fe_2O_4$, show significant absorption bands, ν_1 and ν_2, at frequency about 545 cm^{-1} and 450cm^{-1}. The absorption bands observed within this specific limit reveal the formation of spinel structure [101,102,103]. The absorption band (ν_1), observed at frequency about 545 cm^{-1} is attributed to the tetrahedral (A) site whereas that of ν_2 observed at about 450cm^{-1} is assigned to the cation oxygen group complexes of the

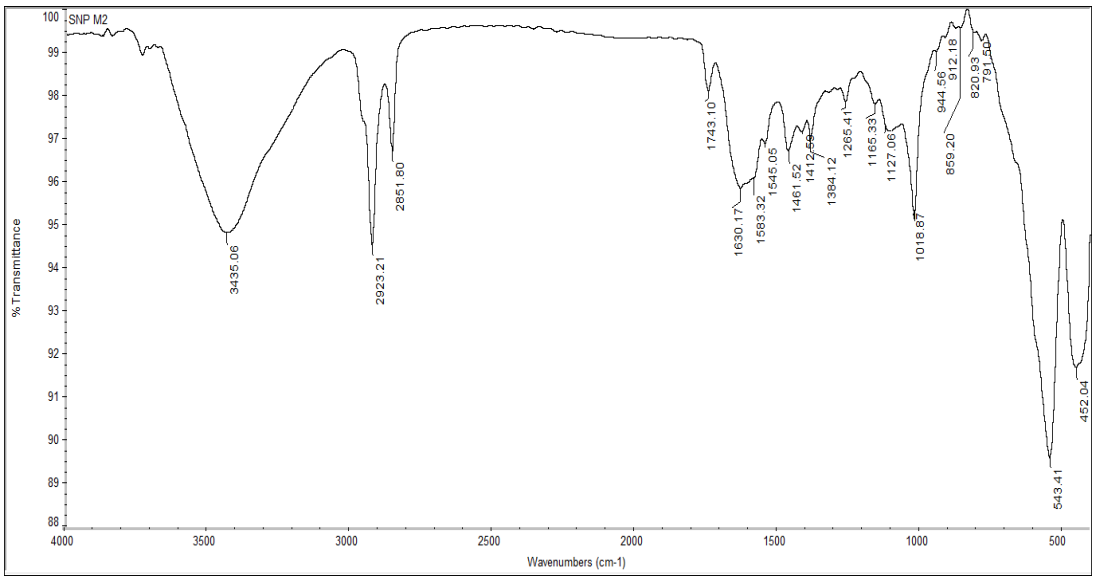

Figures **2.C.2 (b)** IR absorption spectra of the composition $Mg_xZn_{1-x}Fe_2O_4$ (x=0.40)

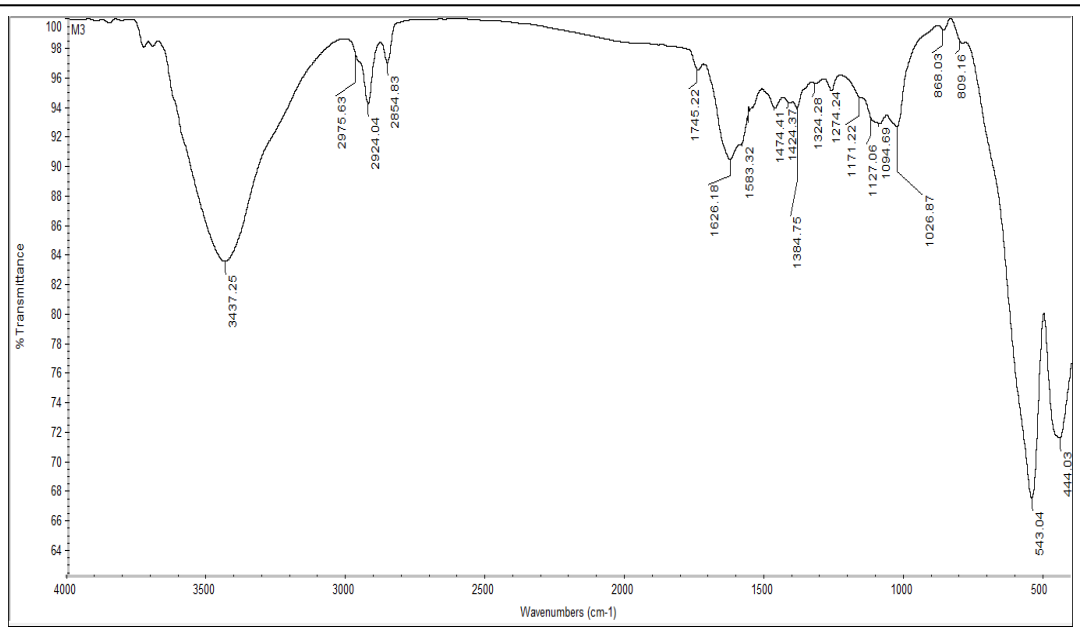

Figures **2.C.2 (c)** IR absorption spectra of the composition $Mg_xZn_{1-x}Fe_2O_4$ (x=0.60)

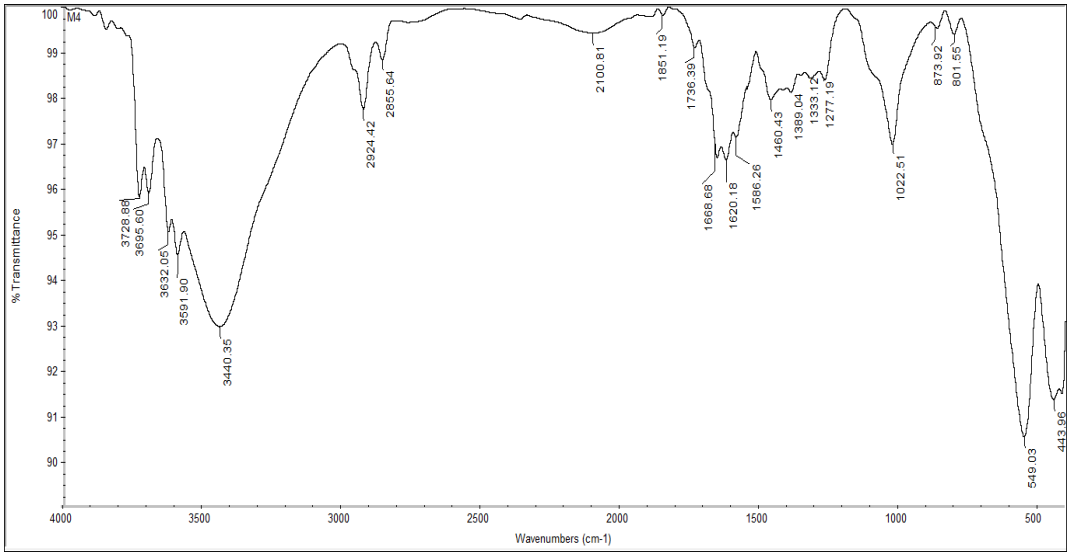

Figures **2.C.2 (d)** IR absorption spectra of the composition $Mg_xZn_{1-x}Fe_2O_4$ (x=0.80)

octahedral (B) sites [103]. The positions of these bands are presented in the table 2.C.1. Frequencies of the absorption show close agreement with the previous reports [104, 105, 106]. On inspection of table 2.C.1, it is found that, the frequency of $\nu_1$band is more than that of ν_2 band. This can be attributed to cation oxygen bond distances of the

TABLE 2.C.1 IR absorption spectroscopy data for the compositions $Mg_xZn_{1-x}Fe_2O_4$ (x= 0.20, 0.40, 0.60 and 0.80)

Conc. of Mg (x)	Frequency of Vibration (ν) cm^{-1}					
	Absorption Band (ν_1)	Absorption Band (ν_2)	Absorption Band (ν_3)	Absorption Band (ν_4)	Absorption Band (ν_5)	Absorption Band (ν_6)
0.20	547.96	431.00	-	1623.20	2923.31	3437.20
0.40	543.41	452.04	-	1630.17	2923.21	3435.06
0.40	543.04	444.03	-	1626.18	2924.04	3437.25
0.80	549.03	443.96	-	1668.68	2924.42	3440.35

respective sites [107]. The cation oxygen bond distance on tetrahedral site (A-O) is about 1.755 A^0. However, the cation oxygen bond distance on octahedral site (B-O) is about 2.054 A^0. This supports the fact that, more stretching of the bond needs less energy to break [108]. Table 2.C.1 also shows that, the frequencies of the absorption bands are compositional dependent. This may be due to cation distribution among tetrahedral site and octahedral site [109]. It is reported that, the Zinc ferrite is the normal ferrite [110] depicting strong occupancy of Zinc ion on tetrahedral site. Moreover, the magnesium ion exhibit preferential occupancies among on A and B sites [111]. The ionic radii of the cations distributed among A and B sites are different.

Therefore, cation distribution significantly affects the ionic radii and hence cation oxygen bond distances (A-O & B-O) of respective sites [112]. Thus, the position of the absorption band can be attributed to the compositional dependency and cation distribution as well. On inspection of the FTIR spectra 2.C.2 (a-d) and the table 2.C.1, it is found that, three absorption bands ν_4, ν_5 and ν_6, at higher frequencies are also observed. These absorption bands are observed at about 1600 cm^{-1}, 2900 cm^{-1} and 3400 cm^{-1}, respectively. Many researchers have reported such spectral bands at higher frequencies [113,114,115]. It is known that, the nonlinear, triatomic molecule of water has three significant modes of vibrations; symmetric stretching, asymmetric stretching and scissoring type stretching [92, 117]. The water absorption spectrum is rather complex [118]. FTIR spectroscopy of water vapour, Humidity, has been studied by Bernath [119] and Tennyson et al [120] and reported various kinds of vibration modes and their combination as well [117]. Particularly in the moisture state, the vibrations involves combination of both symmetric stretch and asymmetric stretch of the Hydrogen oxygen bonds. Moreover, along with the stretching, the hydrogen bond also exhibits the bending of the bond. Due to these different modes of vibration of the water molecules, the absorption bands are observed at different frequencies. Due to asymmetric stretch in the O-H bond, the absorption band is observed at frequency (ν_7) about 3750cm^{-1} [117]. The symmetrical stretching in the water molecule results into the band of frequency (ν_6) about 3440 cm^{-1}[115, 116]. The absorption band observed at frequency (ν_4) about 3440 cm^{-1} can be attributed to the bending of the O-H bond [117]. The existence of C-H is reflected by the absorption band at frequency (ν_5) about 2920 cm^{-1}. Thus, absorption bands found at higher frequencies can be attributed to the different vibration modes of the water molecule, either in water form or in water vapour form. It is known that, the compositions of the ferrites exhibit hygroscopic nature. Therefore, water molecules may be trapped into the matrix of the compositions realizing the absorption phenomenon. The FTIR spectra shown in figure 2.C.2 reveal the absorption bands at higher frequencies, which could be attributed to existence of the water molecules in the compositions of the ferrites under investigation. These water molecules, moisture, contribute the electrical conduction process. This supports the fact that the polycrystalline ferrite compositions can suitably used as sensor materials for humidity sensor.

B) IR spectroscopic study of $Ni_xZn_{1-x}Fe_2O_4$ compositions:

As depicted in figures 2.C.3 (a), the FTIR spectra for the compositions $Ni_xZn_{1-x}Fe_2O_4$, show significant absorption bands, ν_1 and ν_2, at frequency about 590 cm^{-1} and 414 cm^{-1}. The absorption bands observed within this specific limit reveal the formation of spinel structure [121, 122]. The absorption band (ν_1), observed at frequency about 590 cm^{-1} is attributed to the tetrahedral (A) site whereas that of ν_2 observed at about 414 cm^{-1} is assigned to the cation oxygen group complexes of the octahedral (B) sites [123]. The positions of these bands are presented in the Table 2.C.2. Frequencies of the absorption show close agreement with the previous reports [121, 122, 123]. On inspection of table 2.C.2, it is found that, the frequency of $\nu_1$band is more than that of ν_2 band. This can be attributed to cation oxygen bond distances of the respective sites. On comparison, Table 2.C.1 and Table 2.C.2, it is observed that, frequency of absorption bands ν_1 attributed to tetrahedral site NiZn ferrites is more than that of observed for MgZn ferrites. On X-diffraction studies, it is found that the cation oxygen bond distances on tetrahedral site for NiZn ferrite is less. Therefore, increase in the frequency of ν_1 can assigned to reduction in the cation oxygen bond length of the tetrahedral site.

TABLE 2.C.2 IR absorption spectroscopy data for the compositions $Ni_xZn_{1-x}Fe_2O_4$(x= 0.20, 0.40, 0.60 and 0.80)

Conc of Ni (x)	Frequency of Vibration (ν) cm^{-1}					
	Absorption Band (ν_1)	Absorption Band (ν_2)	Absorption Band (ν_3)	Absorption Band (ν_4)	Absorption Band (ν_5)	Absorption Band (ν_6)
0.20	550.10	422.33	-	1653.63	2920.48	3441.62
0.40	567.55	424.80	-	1627.52	2930.32	3429.34
0.60	570.08	428.11	-	1625.15	2928.30	3432.70
0.80	590.21	414.72	414.72	1627.46	2923.65	3437.62

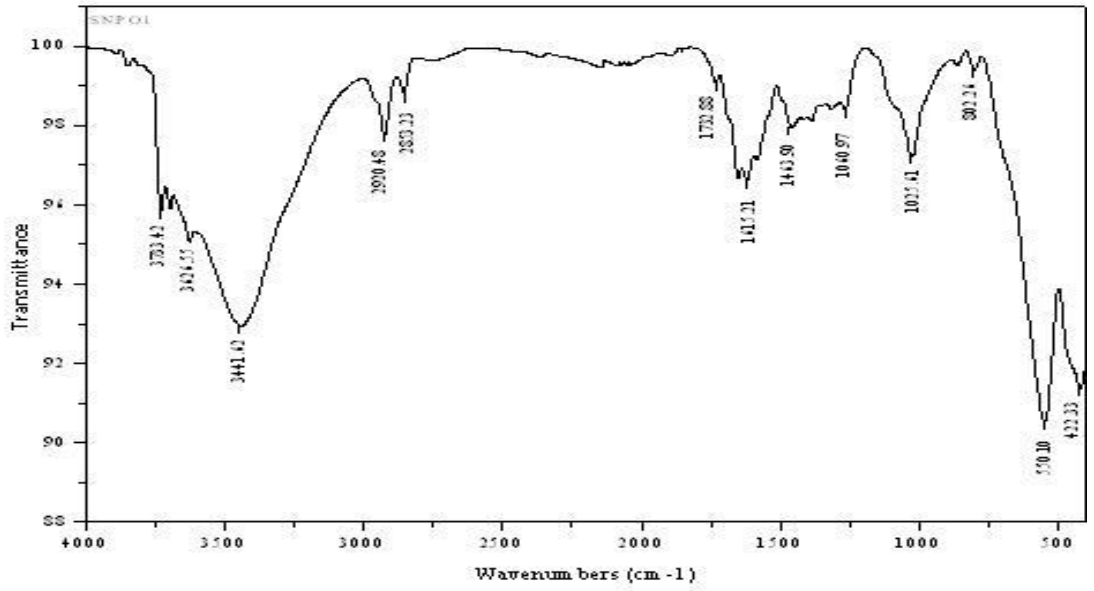

Figures **2.C.3 (a)** IR absorption spectra of the composition $Ni_xZn_{1-x}Fe_2O_4$ (x=0.20)

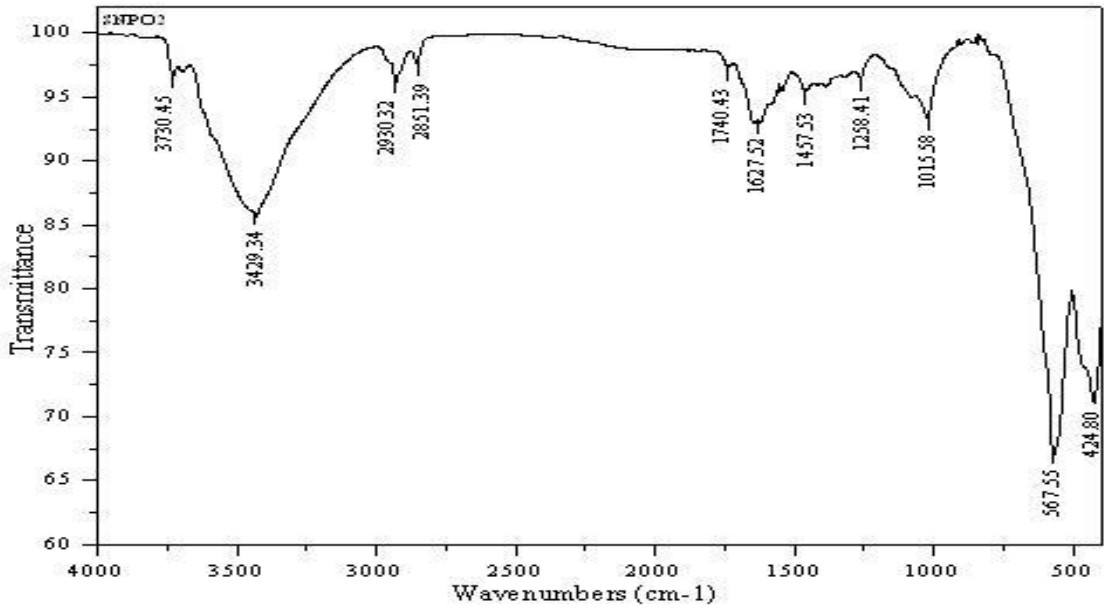

Figures **2.C.3 (b)** IR absorption spectra of the composition $Ni_xZn_{1-x}Fe_2O_4$ (x=0.40)

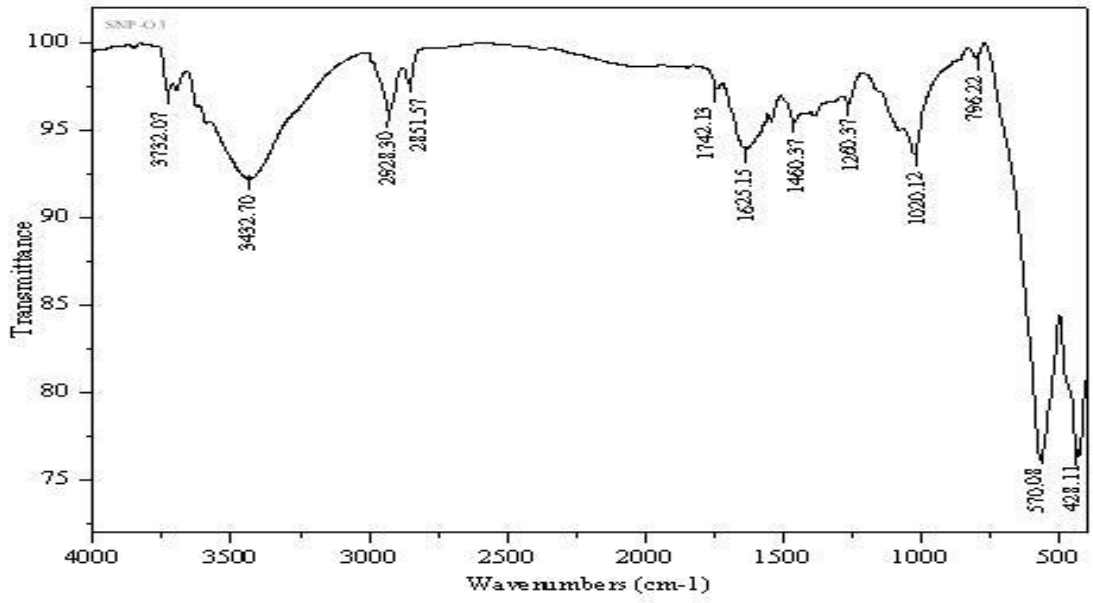

Figures **2.C.3 (c)** IR absorption spectra of the composition $Ni_xZn_{1-x}Fe_2O_4$ (x=0.60)

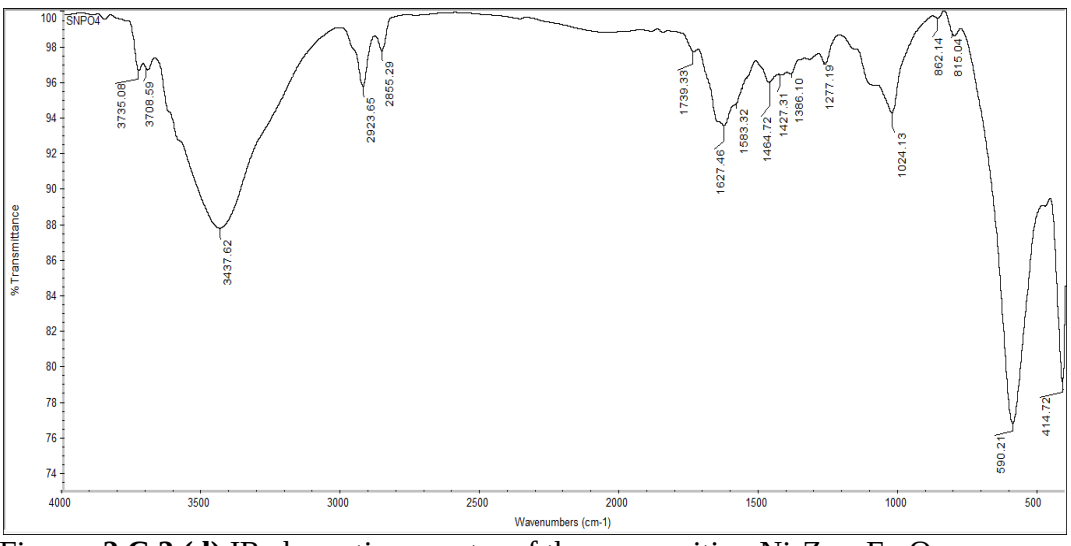

Figures **2.C.3 (d)** IR absorption spectra of the composition $Ni_xZn_{1-x}Fe_2O_4$ (x=0.80)

As discussed earlier, the FTIR spectra of NiZn ferrites also depicts the significant absorption bands at higher frequencies. Such absorption bands are also reported by many investigators [121, 122, 123]. These absorption band are attributed to the different vibration modes of water molecule, vapour or moisture, trapped into the matrix of the ferrite composition under investigation. In fact, the compositions of the ferrites exhibit hygroscopic nature. The FTIR spectra shown in figure 2.C.3 (a-d) reveal the absorption bands at higher frequencies, which could be attributed to existence of the water molecules in the compositions of the ferrites under investigation. These water molecules can contribute the electrical conduction process. This supports the fact that the polycrystalline ferrite compositions are also most suitable as sensor materials for humidity sensor.

C) IR spectroscopic study of $Mn_xZn_{1-x}Fe_2O_4$ compositions:

As depicted in figures 2.C.4 (a-d), the FTIR spectra for the compositions $Mn_xZn_{1-x}Fe_2O_4$, show significant absorption bands, ν_1, ν_2, ν_3, ν_4, ν_5, and ν_6. On inspection of these spectra, it is found that, there are two groups of absorption bands; one is at lower frequencies and second is observed at higher frequency region. These two groups can be respectively attributed to metal-oxygen bonds of tetrahedral and octahedral sites of the spinel structure and to the different vibration modes of the triatomic water molecules. The frequencies of the absorption bands for the compositions under investigation are presented in Table 2.C.3. On inspection of table 2.C.3, it is found that, compositions show only two absorption band, at lower frequencies, ν_1 and ν_2 except x = 0.60. The composition for x = 0.60 depicts the existence the third band ν_3, which can be assigned to the vibrations in the divalent metal oxygen complexes in the octahedral site of the spine structure. This also supports the cation distribution [124].

TABLE 2.C.3 IR absorption spectroscopy data for the compositions $Mn_xZn_{1-x}Fe_2O_4$(x= 0.20, 0.40, 0.60 and 0.80)

Conc of Mn (x)	Frequency of Vibration (ν) cm^{-1}					
	Absorption Band (ν_1)	Absorption Band (ν_2)	Absorption Band (ν_3)	Absorption Band (ν_4)	Absorption Band (ν_5)	Absorption Band (ν_6)
0.20	547.99	410.66	-	1626.73	2972.69	3444.82
0.40	550.40	460.05	438.27	1623.13	2924.05	3435.57
0.40	546.15	466.50	-	1627.75	2923.61	3445.00
0.80	547.38	464.02	-	1627.05	2923.38	3442.68

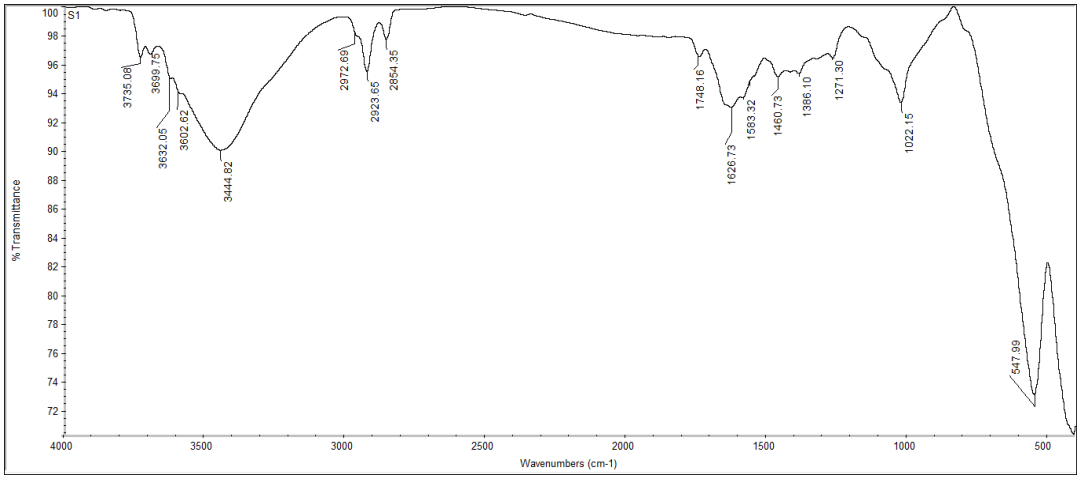

Figures **2.C.4 (a)** IR absorption spectra of the composition $Mn_xZn_{1-x}Fe_2O_4$ (x=0.20)

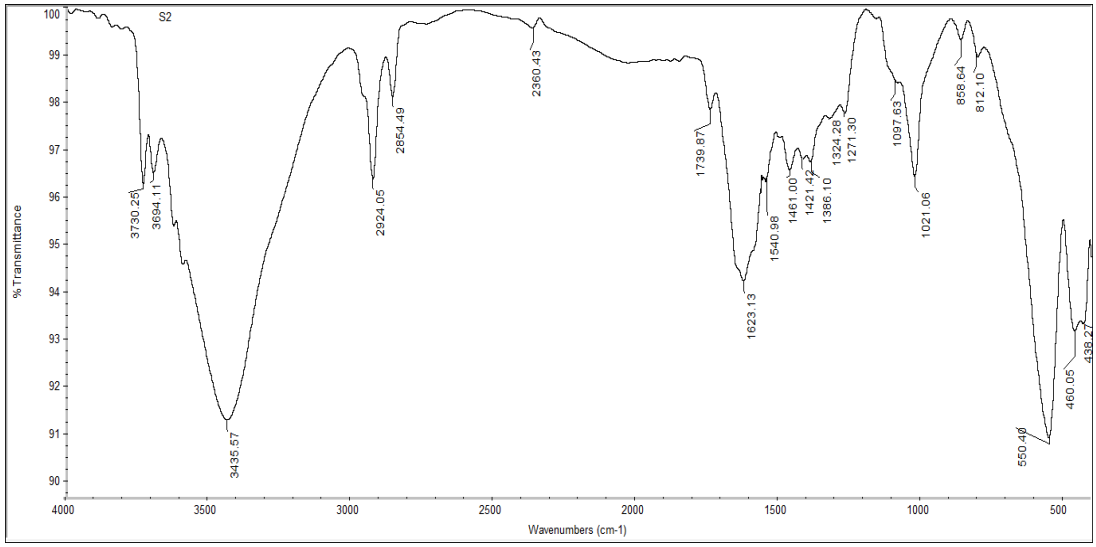

Figures **2.C.4 (b)** IR absorption spectra of the composition $Mn_xZn_{1-x}Fe_2O_4$(x=0.40)

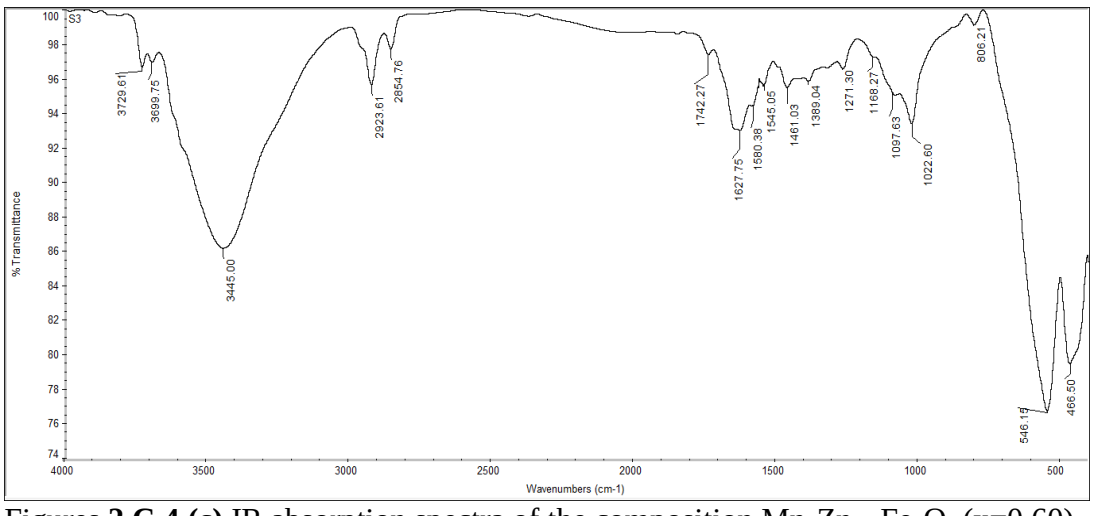

Figures **2.C.4 (c)** IR absorption spectra of the composition $Mn_xZn_{1-x}Fe_2O_4$ (x=0.60)

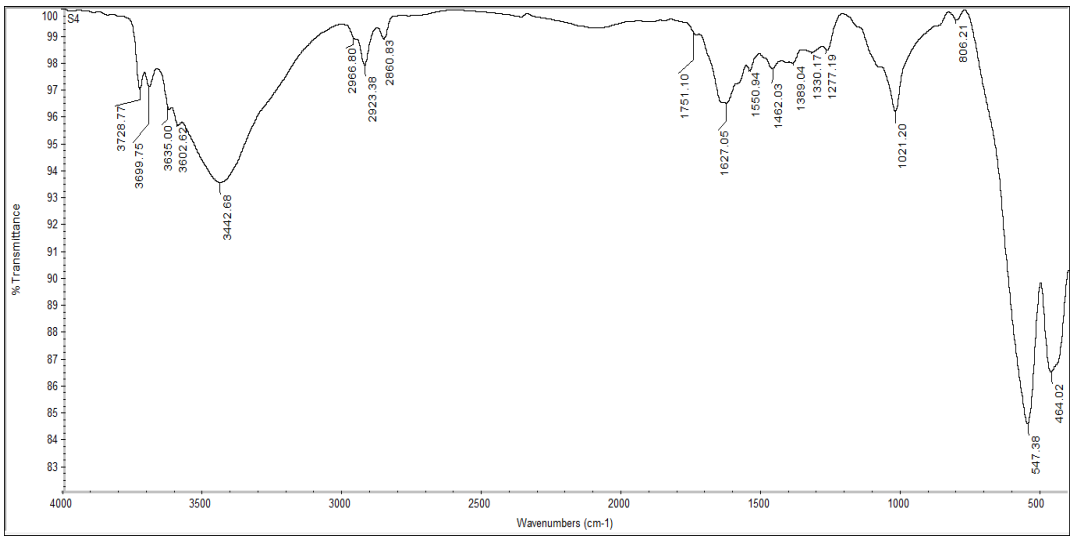

Figures **2.C.4 (d)** IR absorption spectra of the composition$Mn_xZn_{1-x}Fe_2O_4$ (x=0.80)

For higher frequencies, the compositions under investigation also reveal the three significant absorption bands, ν_4, ν_5 and ν_6. Table 2.C.3 shows the frequencies of these bands. However, as discussed earlier, these absorption bands can be attributed to the different vibration modes of the water molecule (moisture) trapped into the matrix of the compositions. This supports the fact that, the ferrites compositions are hygroscopic in nature. The existence of water molecules suggests the protonic kind of electrical conductivity. Therefore, it can be said that, the ferrite materials are most suitable for humidity sensor. Emphasizing this fact into account, the humidity sensor is developed and results of interpreted in topic 4.

2.C.4 Conclusion:

The composition of polycrystalline $Mg_xZn_{1-x}Fe_2O_4$, $Ni_xZn_{1-x}Fe_2O_4$ and $Mn_xZn_{1-x}Fe_2O_4$ nano ferrites are also characterized by Infrared absorption spectroscopy. The spectrophotographs show significant absorption bands, which are attributed to existence of different modes of vibrations. The values of absorption bands, supports the spinel nature of the compositions. Absorption bands observed at higher frequencies reveal the existence of significant modes of vibrations, such as symmetric stretching, asymmetric stretching and scissoring type of stretching of non-linear triatomic molecule of the water in vapour form. It can be concluded that, the compositions are spinels and most suitable for development of humidity sensor.

2.D Scanning Electron Microscopy (SEM)

2.D.1 Introduction:

Along with X-ray diffraction and IR spectroscopy, the results of Scanning Electron Microscopy (SEM) studies help to explore the microstructural details of the composition under investigation. Present investigation is not merely structural investigation. But deployment of the materials for sensor development is the major objective of present research work. Therefore, before implementation, confirmation of formation of the materials, of desired features, is essential. For confirmation of formation, the compositions are characterized with the standard tools such as X-ray diffraction and IR absorption spectroscopy etc. On inspection of results obtained from XRD and FTIR spectroscopy, it is confirmed that, the single phase nano-sized polycrystalline ferrite with spinel structure is formed without any ambiguity. Moreover, in order to supports above results, the scanning electron microscopic studies of typical compositions, representative of each series, are carried out and the results obtained are interpreted.

It is known that, electrical as well as magnetic properties of the spinel ferrites are found to be sensitive to their microstructure. The intrinsic properties decide the application areas of the compositions under investigation. For sensor based applications, the electrical properties are playing vital role. These electrical properties are sensitive to the microstructure of the compositions. Moreover, the pores and voids significantly affect the electrical properties of the ferrites [125]. In fact, the microstructure depends on the method of preparation and preparation condition. The microstructure, which includes, the grain size, grain distribution, gain boundaries, pores, voids etc, can be studied by means of Scanning Electron Microscopy (SEM). It is known that, magnetic properties of the ferrite compositions are sensitive to the grain growth, grain boundaries. The Scanning Electron Microscopy (SEM) is most suitable tool to explore microstructural details, because it has very high magnification and resolving power and great depth of the focus.

It permits the observations and characterization of heterogeneous organic and inorganic bulk materials in nanometer scale. The finer grains give more grain to grain contacts. However, the excessive grain growth reduces grain to grain contact. Porosity, the inherent property of the ceramic materials, depends upon the grain structure.

Porosity is also playing key role in the electrical properties; those are suitable for sensor based applications.

In fact, the microstructure develops during sintering process. Therefore, the sintering temperature and sintering time play significant role on the microstructure of the composition under investigation. The sintering temperature should be sufficiently high to complete the solid state reaction. An excessive sintering temperature may results into evaporation of some constituent such as Zn, Li etc [126]. It is known that, the microstructure with large pores is developed at lower sintering rate [127]. To reduce porosity, the rate of sintering can be increased, but it is constrained by rate of oxygen diffusion, which may be affected on the stoichiometry of the compositions. Thus, the sintering process can be control to achieve desired microstructure. Grain growth is nothing but the change in the size and morphology of the grain with time. There are two types of grain growths; exaggerated grain growth and duplex grain structure. The grain size and grain surface area are important features, which decides the sensor based applications. Kumara et al synthesized the composition of magnesium ferrite with exaggerated grain growth and found decrease in the surface area and the grain boundary [128]. If a giant grains are formed in the matrix of fine grains then it is referred as duplex grain structure.

The electrical resistance of polycrystalline ferrite is due to presence of grain boundaries [129]. Therefore, the grain size and porosity would significantly affect the electric properties. Increase in the porosity may results in decrease into physical density of the compositions. Existence pore and voids affect the electrical properties of the ferrites. The compositions, when exposed to the humidity, the water vapor in the air, then the water molecule may be trapped into a pore, which may causes reduction in the performance of the sensor at higher humidity. Due to water tapped into pores, the response as well as recovery time of the humidity sensor may be adversely affected [130]. The ferrite compositions, being magnetic semiconductor, the eddy current must be very low [131]. To achieve this, essentially the small grains and large grain to grain contact must be present.

Sarangi et al have synthesized Ni-Zn ferrite nano powder by co-precipitation method and reported the results of microstructural investigation [132]. They reported the effect of sintering temperature on microstructure of the Ni-ZN ferrites. They showed that, the lower sintering temperature causes very less grain growth with agglomerated grains and inter granular porosity. However, increase in the sintering

temperature results into formation of well defined grains with reduction in the porosity. They also suggested that, excessive sintering temperature results into decrease in concentration of zinc and hence disturbance in stoichiometry [132].

An effect of microstructure on electrical resistance of magnesium ferrite was investigated by Shah et al, with various humidity in %RH [133]. They reported that the doping of CeO_2 results into increase in the intergranular porosity. In the absorption process, first a water molecule chemically adsorbed on the active site, leading to granular formation of stable chemisorbed OH^- ions on the surface. Once first layer is formed, the physical adsorption occurs to form subsequent layers of the water molecules. Physisorbed water molecule dissociates due to high electrostatic fields in the chemisorbed OH^- layers [134] and protonic conduction taken place in the physisorbed water layers. [135]. Due to existence of mesopores the capillary condensation of water vapour may takes place for higher humidity. Khedr [136], investigated the effect of sintering temperature of microstructure of the nickel ferrite. He reported the existence of this high porosity may provide impediment to the gas diffusion. Rezlescu et al [137], have investigated the microstructural properties of MgZn ferrites and reported that the porous ceramic can easily exhibit absorption and condensation of water vapours. This is already proved from IR spectroscopic study, wherein the IR spectra depict the absorption band at frequency at about 3400 cm^{-1}, which is assigned to stretching of the O-H bonds. Effect of microstructure has studied by Iftimie et al and reported the suitability of porous nickel ferrite for sensing applications [138,139]. KashiViswanath et al have studied the microstructure of Ni-Zn, Mg-Zn ferrites and reported the formation of finer grained structure with little agglomeration [140]. During investigation of magnetic permeability of the copper substituted Ni-Zn ferrites Jun and Mi [141] have explored the microstructure of the compositions. They attributed the results of magnetic properties to the microstructure of the compositions. Microstructure of the nickel and samarium substituted zinc ferrite is studied by Naidu et al [142]. They interpreted the effect of grain size on the magnetic properties. Effect of microstructure on magnetic properties of the cadmium substituted nickel copper ferrites was studies by Belavi et al [143]. They attributed the fact of increase in the magnetization to the decrease in the porosity. The sensing mechanism is a combination of the porous characteristics and the semiconductivity of the material under investigation. Particularly, in the case of a humidity sensor, a higher surface area is desirable, because, it provides more sites for water adsorption [144]. Considering this fact into account,

Arshaka et al have synthesized Mn Zn ferrites suitable for development of humidity sensor. They attributed the results regarding sensitivity and response time of the microstructural properties of the compositions.

2.D.2 Experimental:

To explore the details regarding microstructural properties such as, grain size, shape, grain growth, cracks, voids, pores etc, the compositions of $Mg_xZn_{1-x}Fe_2O_4$, $Ni_xZn_{1-x}Fe_2O_4$ and $Mn_xZn_{1-x}Fe_2O_4$ (x= 0.20, 0.40, 0.60 and 0.80) spinel ferrites were studied by Scanning Electron Microscopy (SEM) by using JSM-6360A, Jeol Japan model at Pune. The sample were fractured to expose the inside portion and mounted on the standard specimen mounting stub. The micrographs of the typical samples with EHT field about 20 KV and the resolution was configured to 3.00 nm. The experimental arrangement is depicted in Figure 2.D.1.

Figure 2.D.1 The experimental set up for Scanning Electron Microscopy studies.

2.D.3 Results and Discussion:

The Scanning Electron Microscopy (SEM) study of the two compositions, as representatives of the series $Mg_xZn_{1-x}Fe_2O_4$, (x=0.20 and 0.40), $Ni_xZn_{1-x}Fe_2O_4$(x=0.20 and 0.80) and $Mn_xZn_{1-x}Fe_2O_4$ (x=0.20 and 0.60) was carried out. The micrographs of the compositions under investigation are shown in figures 2.D.2 to 2.D.4. On inspection of the micrographs, shown in the figure 2.D.2 to figure 2.D.4, it can be said that, the compositions are formed without any exaggerated grain growth. The compositions comprise well defined grains with uniform grain distribution. From figure 2.D.2 (a) & (b), it is found that, an average grain diameter of NiZn ferrites is ranging from few nanometers to 2 μm, approximately. As depicted in figure 2.D.3 (a) & (b), the grain diameter for Mn-Zn ferrite is approximately 1 μm. It is also found that, agglomeration of the grains in the structure is rare. Moreover, the compositions of MgZn ferrites reveal the uniformly distributed grains. The size of the grains is also in the range of nanometer

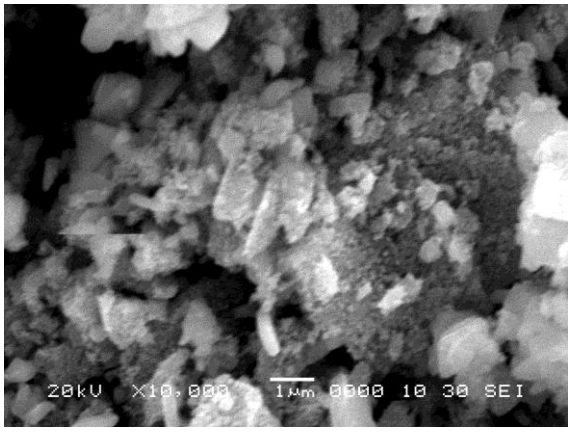

Figure 2.D.2(a) X-ray diffractogram for composition of $Ni_xZn_{1-x}Fe_2O_4$(x= 0.20)

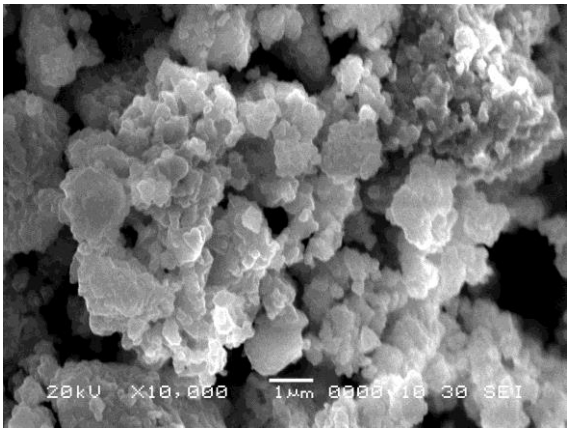

Figure 2.D.2(b) X-ray diffractogram for composition of $Ni_xZn_{1-x}Fe_2O_4$(x= 0.80)

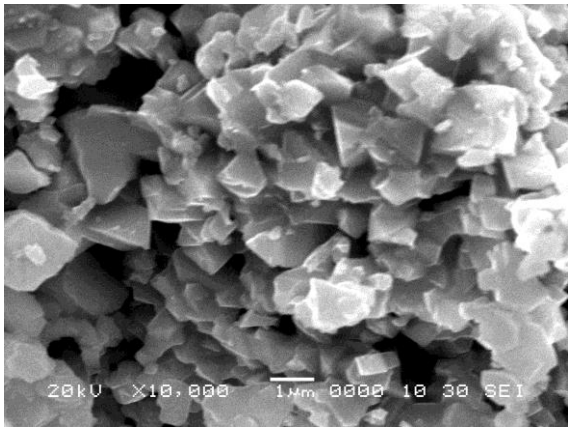

Figure 2.D.3(a) X-ray diffractogram for composition of $Mn_xZn_{1-x}Fe_2O_4$(x= 0.20)

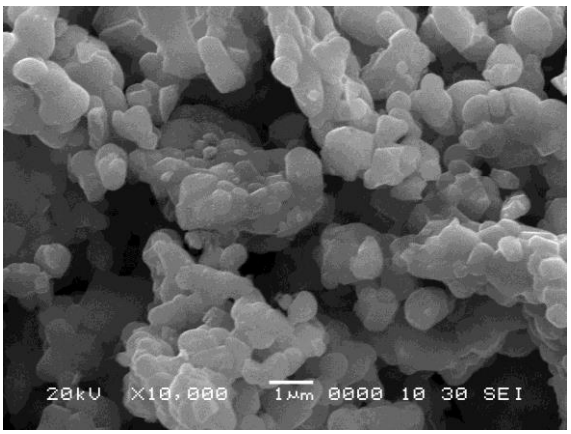

Figure 2.D.3(b) X-ray diffractogram for composition of $Mn_xZn_{1-x}Fe_2O_4$(x= 0.60)

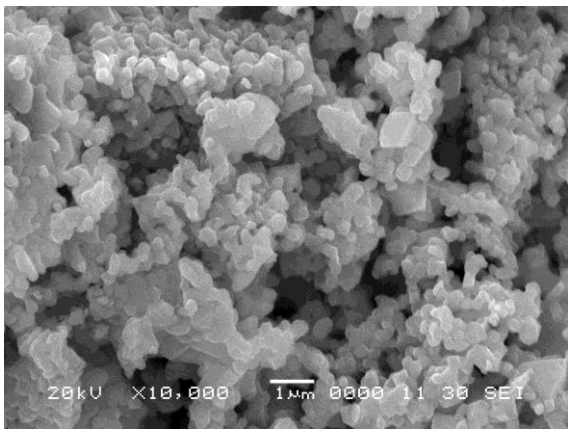

Figure 2.D.4(a) X-ray diffractogram for composition of $Mg_xZn_{1-x}Fe_2O_4$(x= 0.20)

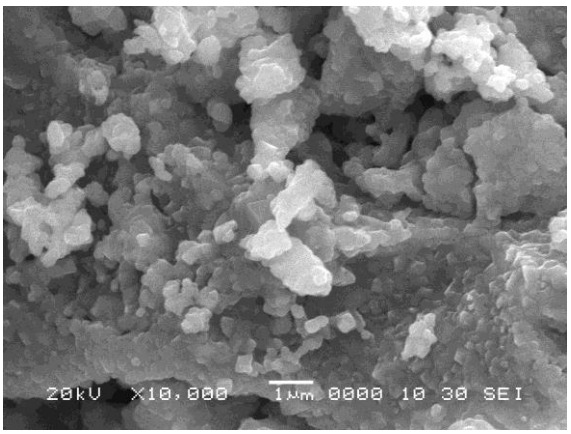

Figure 2.D.4(b) X-ray diffractogram for composition of $Mg_xZn_{1-x}Fe_2O_4$(x= 0.40)

Also, the excessive grain growth is not observed. Obviously, the grains diameters observed by SEM are several times larger than the particle diameters calculated using XRD patterns, which indicates that each grain observed by SEM consists of several particles [145,146].

On inspection of the micrographs, it is found that the compositions are porous. However, the mesopores are absent. The compositions reveal the existence of inter granular micro pores and pores are formed at the grain boundary. The pore size varies from few nanometer to approximately 2 to 4 μm. This behavior could be attributed to the fact that the samples with high porosity contain many pores.

Present investigation emphases, the development of sensors for detection of humidity and typical gases as well. For these purpose, the electrical conductivity property is investigated (topic 3). From this investigation, it is found that, the compositions with the porosity are most suitable for sensor based applications, wherein the process of absorption and adsorption is realized. Present materials reveal the existence of inter granular porosity. Therefore, these materials are suitable for sensor development.

2.D.4 Conclusion:

To confirm the formation and to investigate microstructural details, the compositions are subjected to scanning electron microscopy study. It is found that, the compositions with uniform grain distribution and small grain size are formed. The pore size varies from few nanometer to approximately 2 to 4 μm. It also depicts the existence of inter granular micropores without intragranular pores. Due to uniform grain distribution and increase in effective area of the surface, the process of adsorption and absorption favors, which suggests the suitability of the material for development of gas sensor.

References:

1. A. Dias, R. L. Moreira, N. D. S. Mohallem and A. I. C. Persiano, "Microstructural Dependence Of The Magnetic Properties Of Sintered Nizn Ferrites From Hydrothermal Powders", J. Magn. andMagn. Mater, 172 (1997) L9-L14.
2. Y. Qu, H. Yang, N. Yang, Y. Fan, H. Zhu and G. T. Zou, "The Effect of Reaction Temperature on the Particle Size, Structure and Magnetic Properties of Co-precipitated $CoFe_2O_4$ Nanoparticles",Mater. Lett., 60 29-30 (2006)3548-3552.
3. K. Raj, R. Moskowitz, R. Casciari, "Advances In Ferrofluid Technology", J. Magn. Magn. Mater. 149(1995) 174.
4. P. L. Phillips, J. C. Knight, B. J. Mangan, P. St. J. Russell, M. D. B. Charlton and G. J. Parker, "Near-Field Optical Microscopy of Thin Photonic Crystal Films",J. of Appl. Phys., 85(1999)6338-6345.
5. M. H. Sousa and F. A. Tourinho, "New Electric Double- Layered Magnetic Fluids Based on Copper, Nickel, and Zinc Ferrite Nanostructures",J. Phys. Chem. B, 105 6 (2001)1168-1175.
6. Mazaleyrat and L. K. Varga, "Ferromagnetic Nano-Composites," J. Magn.andMagn. Mater., 215-216 (2000)253-259.
7. D. E. Speliotis, "Magnetic Recording Beyond the First 100 Years," J. Magn. andMagn. Mater., 931-3(1999)29-35.
8. J. Sláma, A. Grusková , M. Ušáková, E. Ušák, J.Šubrt and J. Luká, "Substituted NniZzn Ferrites for Passive Sensor Applications", J. ELECT. Engg.,57 8/S (2006), 159-162.
9. I. Ismayadi, M. Hashim, A.M. Khamirul and R. Alias, "The Effect of Milling Time on $Ni_{0.5}Zn_{0.5}Fe_2O_4$ Compositional Evolution and Particle Size Distribution", Amer. J. Appl. Sci., 6 8(2009) 1548-1552.
10. S. A. Popescu, P. Vlazan, S. Novaconi, I. Grozescu and P. V. Noţingher, "Electromagnetic Behavior of Zinc Ferrites Obtained By A Coprecipitation Technique",U.P.B. Sci. Bull., Series C, 73(2011)247-256.
11. Y. Koseo glu, I. Aldemir, F. Bayansal, S. Kahraman and H. A. Çetinkara, "Synthesis, Characterization and Humidity Sensing Properties of $Mn_{0.2}Ni_{0.8}Fe_2O_4$ Nanoparticles", Mater. Chem. and Phys., 139 (2013) 789-793.

12. Petrila and F. Tudorache, “Humidity Sensor Applicative Material Based On Copper-Zinc-Tungsten Spinel Ferrite”, Mater.Lett.,108(2013)129–133.
13. T. G. G. Maffeis, “Nano-Crystalline SnO2 Gas Sensor Response to O2 and CH4 At Elevated Temperature Investigated by XPS”, Surface Science, 520 1 (2002)29–34
14. R. Martins, E. Fortunato, P. Nunes, I. Ferreira, and A. Marques, “Zinc Oxide as an Ozone Sensor”, J. Appl. Phys., 96 3(2004)1398–1408.
15. N. Rezlescu, N. Iftimie, E. Rezlescu, C. Doroftei, and P.D. Popa, “Semiconducting Gas Sensor For Acetone Based On The Grained Nickel Ferrite”, Sensors and Actuators B, 114 1 (2006) 427–432.
16. Gurlo, N. Barsan, and U. Weimar, “Mechanism of NO_2Sensing on SnO_2 and In_2O_3Thick Film Sensors As Revealed By Simultaneous Consumption And Resistivity Measurements”, The 16th European Conference on Solid-State Transducers, Prague, Czech. Republic, 15–18 (2002)970–973.
17. A.B. Gadkari, T.J. Shinde, P.N. Vasambekar, “Structural Analysis of Y3+ Doped Mg-Cd Ferrites Prepared by Oxalate Co-precipitation Method”, Materials Chemistry and Physics, 114 2-3 (2009)505-510.
18. L Gama, A. P.Diniz, A Costa, S. M.Rezende, A.Azevedo and D. R.Cornejo, “Magnetic Properties Of Nanocrystalline Ni–Zn Ferrites Doped With Samarium”,Physica B: Condensed Matter, 384 1 (2006) 97-99.
19. T. J. Shinde, A. B. Gadkari and P. N.Vasambekar, “Effect of Nd3+ Substitution On Structural And Electrical Properties Of Nanocrystalline Zinc Ferrite”, J. Magn. Magn. Mater., 322 (18) (2010) 2777-2781.
20. U. Erb, “ElectrodepositedNanocrystals: Synthesis, Properties and Industrial Applications”,Nanostructured Materials, 6 5(1995)533-538.
21. Wei-Chih Hsu, S.C Chen, P.C Kuo, C.T Lie and W.S Tsai, “Preparation of NiCuZn Ferrite Nanoparticles From Chemical Co-Precipitation Method And The Magnetic Properties After Sintering”, Materials Science and Engineering: B, 111 2–3 (2004) 142–149.
22. R. Sridhar, D. Ravinder and K. V. Kumar, “Synthesis and Characterization of Copper Substituted Nickel Nano-Ferrites by Citrate-Gel Technique”, Adv. Mat. Phy. and Chem., (2012) 2 192-199.
23. M. Pal and D. Chakravorty, “Nanocrystalline Magnetic Alloys and Ceramics,” Sadhana, 281 2 (2003)283-297.

24. Chatterjee, D. Das, S. K. Pradhan and D. Chakravarty, “Synthesis of Nanocrystalline Nickel-Zinc Ferrite by the Sol-Gel Method”,J. Magn. andMagn. Mater., 127 1-2 (1993)214-218.
25. J. Chargles, N. O’Connor, E. Kolesnichenko, C. Carpenter, S. W. Zheu, A. Kumbhar, S. Jessica and A. Fabrice, “Fabrication and Properties of Magnetic Particles with Nanometer Dimensions”,Synthetic Metals, 122 3 (2001)547-555.
26. Dias, “Microstructural Evolution of Fast-Fired Nickel- Zinc Ferrites from Hydrothermal Nanopowders”,Materials Research Bulletin, 35 9 (2000)1439-1446.
27. R. N. Das, “Nanocrystalline Ceramics from Sucrose Process”,Materials Letters, 47 6(2001)344-350.
28. Caizer and M. Stefanescu, “Magnetic Characterization of Nanocrystalline Ni-Zn Ferrite Powder Prepared by the Glyoxylate Precursor Method”,J. Phys.D: Appl. Phys., 3523 (2002)3035-3040.
29. S. Gubbala, H. Nathani, K. Koizol and R. D. K. Misra, “Magnetic Properties of Nanocrystalline Ni-Zn, Zn-Mn, and Ni-Mn Ferrites Synthesized by Reverse Micelle Technique”,Physica B, 348 1-4 (2004)317- 328.
30. Qian Chen, Piyi Du,a Wenyan Huang, Lu Jin, Wenjian Weng, and Gaorong Han, “Ferrite with extraordinary electric and dielectric properties prepared from self-combustion technique”, Applied Physics Letters, 90 132907 (2007).
31. S. A. Popescu, P. Vlazan, P. V. Notingher, S. Novaconi, I. Grozescu, A. Bucur and P. Sfirloaga, “Synthesis, Morphology and Magnetic Characterization of Zn Ferrite Powders”, J. Electromagnetic Analysis & Applications, 2(2010)598-600.
32. A. D. Sheikh and V. L. Mathe, “Anomalous Electrical Properties of Nanocrystalline Ni–Zn Ferrite”, J. Mater. Sci., 43 (2008)2018-2025.
33. N. S. Shinde, S. S. Khot, B. P. Ladgaonkar, B. B. Kale, S. Apte, P. M. Tamhankar, S. C. Watawe, “Effect of Oxalate Precursor Formation Temperature on Magnetic Properties of NiCuZn Ferrites”, Mater. Sci. and Appl., 2(2011)1097-1108.
34. A.Verma, T.C.Goel, R.G.Mendiratta and P.Kishan, “Magnetic Properties Of Nickel–Zinc Ferrites Prepared By The Citrate Precursor Method”,J. Magn. andMagn. Mater., 208 1–2(2000)13–19.

35. A. Thakurand andM. Singh, “Preparation and Characterization Of Nanosize$Mn_{0.4}Zn_{0.6}$ Fe_2O_4 Ferrite By Citrate Precursor Method”, Ceramics International, 29 5 (2003)505–511.
36. I. Szczygieł and K.Winiarska, “Synthesis and Characterization Of Manganese–Zinc Ferrite Obtained By Thermal Decomposition From Organic Precursors”, J. Thermal Analysis and Calorimetry, 115 1 (2014)471-477.
37. M. Galceran, M. C. Pujol, M. Aguilo and F. D´ıaz, “Sol-gel Modified Pechini Method For Obtaining Nanocrystalline KRE(WO4)2 (RE = Gd and Yb)”, J. Sol-Gel Sci. Techn., 42 (2007)79–88.
38. Xian-ming Liu and Wen-Liang Gao, “Preparation and Magnetic Properties of $NiFe_2O_4$Nanoparticles by Modified Pechini Method”, Mater. Manuf. Processes,27 9 (2012) 905-909.
39. P. Pramanik, “A Novel Chemical Route for the Preparation of Nanosized Oxides, Phosphates, Vanadates, Mo- lybdates and Tungstates Using Polymer Precursors”,Bulletin of Mater. Sci., 22 3 (1999)335- 339.
40. D. Limin , H. Zhidong, Z. Yaoming, W Ze, and Z. Xianyou, “ Preparation and Sinterability of Mn-Zn Ferrite Powders by Sol-Gel Method”, J. Rare Earths, 24 11(2006)54–56.
41. J. Azadmanjiri, “Preparation of Mn–Zn Ferrite Nanoparticles From Chemical Sol–Gel Combustion Method And The Magnetic Properties After Sintering”, J. Non-Crystalline Solids**,** 353 44–46 (2007) 4170–4173.
42. P. M. PrithvirajSwamy, S. Basavaraja, A.Lagashetty, N. V. Srinivasrao, R. Nijagunappa and A. Venkataraman, “Synthesis and Characterization Of Zinc Ferrite Nanoparticles Obtained By Self-Propagating Low-Temperature Combustion Method”, Bull. Mater. Sci., 34 7 (2011)1325–1330.
43. M. N. Akhtar, N. Yahya and P. B. Hussain, “Structural and Magnetic Characterizations of Nano Structured $Ni_{0.8}Zn_{0.2}Fe_2O_4$ Prepared By Self Combustion Method”, Intern. J. Basic & Applied Sci., 9 9(2009) 37-40.
44. M. Houshiar, F Zebhi, Z. J. Razi, Ali Alidoust andZohrehAskari, “Synthesis of Cobalt Ferrite ($CoFe_2O_4$) Nanoparticles Using Combustion, Coprecipitation, And Precipitation Methods: A Comparison Study Of Size, Structural, And Magnetic Properties”, J. Magn.Magn. Mater., 371(2014)43–48.

45. D. Carta, M. F. Casula, A. Falqui, D. Loche, G. Mountjoy, C. Sangregorio and A. Corrias, "A Structural and Magnetic Investigation of the Inversion Degree in Ferrite Nanocrystals MFe_2O_4 (M= Mn, Co, Ni)", J. Phys. Chem. C, 113 (2009) 8606–8615.
46. G. Hildebrandt, "The Discovery of the Diffraction of X-rays in Crystals — A Historical Review", Cryst. Res. Techno., 28 6(1993) 747–766.
47. http://en.wikipedia.org/wiki/Crystal_system
48. B. P.Ladgaonkar andA.S. Vaingankar, "X-ray Diffraction Investigation of Cation Distribution in $Cd_xCu_{1-x}Fe_2O_4$Ferrite System", Mater. Chem.Phys.,56(1998)280.
49. W. H. Bragg and W. L. Bragg, "The Reflection of X-rays by Crystals-I", Proceed.of the Cambridge Philosophical Society, A,88 (1913) 43-57.
50. S.P. Dalawai, A.B. Gadkari, T.J. Shinde and P.N. Vasambekar, "Effect Of Sintering Temperature On Structural And Electrical Switching Properties Of Cadmium Ferrite", Adv. Mat. Lett., 4 7 (2013) 586-590.
51. N. M. Deraz and A. Alarifi, "Preparation and Characterization of Nano-Magnetic $Mn_{0.5}Zn_{0.5}Fe_2O_4$ System", Int. J. Electrochem. Sci., 7 (2012) 5828 – 5836.
52. S. V. Bangale, D. R. Patil and S. R. Bamane, "Preparation and Electrical Properties OfNanocrystalline$MgFe_2O_4$ Oxide By Combustion Route", Archives of Appl. Sci. Res., 3 5 (2011) 506-513.
53. R. Iyer, R. Desai and R. V.Upadhyay, "Low Temperature Synthesis OfNanosized$Mn_{1-x}Zn_xFe_2O_4$Ferrites And Their Characterizations", Bull. Mater. Sci., 32 2 (2009) 141–147.
54. M. Menzel, V. Sepelak and K. D. Becker, "Mechanochemical Reduction of Nickel Ferries", Solid State Ionics, 141-142 (2001) 663-669.
55. A. R. Tanna and H. H. Joshi, "Computer Aided X-Ray Diffraction Intensity Analysis for Spinels: Hands-On Computing Experience", World Academy of Science, Engg. and Techno.,7 3 (2013)70-77.
56. B. P. Ladgaonkar, P.N. Vasambekar and A.S.Vaingankar, "Cation Distribution and Magnetization Study of Nd^{3+} Substituted Zn-Mg Ferrites", Turkish J. Phys., 25 (2001) 129.

57. M. Kumar, P. Apparao, M. ChaitanyaVarma, G. Choudary and K. H. Rao, "Cation Distribution in $Co_{0.7}Me_{0.3}Fe_2O_4$ (Me = Zn, Ni and Mn) J. Modern Phys., 2(2011)1083-1087.
58. G. Aravind and D. Ravinder, "Preparation and Structural Properties of Aluminium Substituted Lithium Nano Ferrites By Citrate-Gel Auto Combustion Method", Int. J. Engg. Res. Appl., 3 6 (2013)1414-1421.
59. S.T.Mahmud, A.K.M. AktherHossain, , A.K. M. Abdul Hakim, M. Seki, T. Kawai, and H. Tabata, "Influence of Microstructure On The Complex Permeability Of Spinel Type Ni–Zn Ferrite", J. Magn. Magn. Mater., 305 (2006) 269– 274.
60. A. Monshi, M. R. Foroughi and M. R. Monshi, "Modified Scherre Equation to Estimate More Accurately Nano-crystallite Size using XRD", World j. Nano Sci. and Engg.,2(2012) 154-160.
61. I. H Gul, W. Ahmed, and A. Maqsood, "Electrical and Magnetic Characterization OfNanocrystalline Ni-Zn Ferrite Synthesis Byco-Precipitation Route", J.Magn.andMagn.Mater., 3203 4 (2008)270–275.
62. S. M. Attia, "Study of Cation Distribution of Mn-Zn Ferrites", Egypt. J. Solids, 29 2(2006) 329-340.
63. M. Manjurul Haque, M. Huq and M.A. Hakim, "Effect of Zn2+ Substitution of the Magnetic Properties of Mg_{1-}xZnxFe2O4Ferrtie", Phys. B: Condensed Matter, 404(2009) 3915–3921.
64. K. Rama Krishna, D. Ravinder, K. Vijaya Kumar and Ch. Abraham Lincon, "Synthesis, XRD & SEM Studies of Zinc Substitution in Nickel Ferrites by Citrate Gel Technique", J. Condensed Matt. Phys., 2(2012)153-159
65. R. Ali, A. Mahmood, M.Azhar Khan, A. H. Chughtai, M. Shahid, I. Shakir, and M. F.Warsi, "Impacts of Ni–Co Substitution On The Structural, Magnetic And Dielectric Properties Of Magnesium Nano-Ferrites Fabricated By Micro-Emulsion Method" , Journal of Alloys and Compounds, 584 (2014) 363–368.
66. V.K. Mittal, P. Chandramohan, S. Bera, M.P. Srinivasan, S. Velmurugan and S.V.Narasimhan, "CationDistribution in Ni x Mg 1− x Fe_2 O_4Studied by XPS and Mössbauer Spectroscopy", Solid State Commun., 137 (2006) 6–10.
67. N. Chen and M.Gu, "Microstructure and Microwave Absorption Properties of Y-Substituted Ni-Zn Ferrites", J. of Metal., 2(2012)37-41.

68. C.Venkataraju,"Effect of Nickel on the Structural Properties ofMn Zn Ferrite Nano Particles", Appl. Phys. Res., 1 1(2009)40-45.
69. S. J. Azhagushanmugam, N. Suriyanarayanan and R. Jayaprakash, "Chemical Synthesis Route and Analysis of Dielectric Property of Nanocrystalline $Ni_{0.6}$ $Zn_{0.4}$ (Fe_2 O_4) Spinel Ferrite", J. Environ. Res. Develop., 7 1A (2012)421-425.
70. B.P. Ladgaonkar, P.N. Vasambekar and A.S. Vaingankar, "Effect of Zn^{2+} and Nd^{3+}Substitution on Magnetization and AC Susceptibility OfMg Ferrite", J. Magn. andMagn. Mater., 210 1-3 (2000)289.
71. K. Velmurugana,V.S.K. Venkatachalapathyand S. Sendhilnathan, " Synthesis of Nickel Zinc Iron Nanoparticles by Coprecipitation Technique", Materials Research., 13 3 (2010)299-303.
72. M.R. Anantharaman, S. Jagatheesan,K.A. Malini, S. Sindhu,A. Narayanasamy, C.N. Chinnasamy, J.P.Jacobs, S. Reijne, K. Seshan, RHH. Smits and H HBrongersma, "On the Magnetic Properties Of Ultra-Fine Zinc Ferrites", J. Magn. Magn. Mater., 189 1(1998) 83-88.
73. M. Sorescua, L. Diamandescua, R. Peelamedub, R. Royb and P. Yadojic "Structural and Magnetic Properties of NiZnFerrites Prepared By Microwave Sintering", J.Magn.Magn.Mater., 279 (2004) 195–201
74. M. P. Reddy, G. Kim, D. S. Yoo, W. Madhuri, N. R. Reddy, K. V. Siva Kumar, and R. Ramakrishna Reddy, "Characterization and Electromagnetic Studies on NiZn and NiCuZn Ferrites Prepared by Microwave Sintering Technique", Materials Sciences and Applications, 3 (2012) 628-632.
75. X.L. Jiao, D.R. Chen and H.Y. Hu, "Hydrothermal Synthesis of Nanocrystalline $M_xZn_{1\_x}Fe_2O_4$ Powders", Mater. Res. Bull., 37 9 (2002) 1583-1588.
76. Y.L. Liu, Z.M. Liu and Y. Yang, "Simple Synthesis of MgFe2O4 Nanoparticles as Gas Sensing Materials", Sensor. Actuat. B-Chem., 107 (2005) 600–604.
77. R. Sridhar, D. Ravinder and K. Vijaya Kumar, "Synthesis and Characterization of Copper Substituted Nickel Nano-Ferrites by Citrate-Gel Technique", Advan. Mater. Phys.& Chem., 2(2012)192-199.
78. M. Ahmadipour and K.VenkateswaraRao "Preparation of Nano Particle $Mg_{0.2}Fe_{0.8}O$ by Solution Combustion Method and Their Characterization", Int. J. Engg. & Adv. Techno., 1 6 (2012) 135-137.

79. A.Sukta, A. Borisova, J. Kleperies, G. Menzinskis, D. Jakovlevs and Juhnevica, “Effect of Nickel Addition OnColour Of Nanometer Spinel Zinc Ferrite Pigments”, J Australian Ceram. Soc., 48 2(2012) 150-155.
80. R. D. Waldron, “Infra-Red Spectra of Ferrites”, Phys. Rev., 99(1955) 1727.
81. B. P. Ladgaonkar, C. B.Kolekar and A. S. Vaingankar, “Infrared Absorption Spectroscopic Study of Nd3+ Substituted Zn-Mg Ferrites”, Bull. Mater. Sci., 25 4 (2002) 351-354.
82. S. S. Khot, N. S. Shinde, B. P. Ladgaonkar, B. J. Kale and S. C. Watawe, “Effect of Temperature Of Synthesis On X-ray, Infrared Spectroscopic Study And Magnetic Properties of Magnesium Zinc Ferrites”, Key Engg Mater., 547 (2013)57-69.
83. A. Pradeep and G. Chandrashekaran, “FTIR Study of Ni, Cu and Zn Sunstituted Nano-Particles of $MgFe_2O_4$”, Mater. Lett., 60 (2006)371-374.
84. S. G. Bachhav, R. S. Patil, P. B. Ahirrao, A. M. Patil and D. R. Patil, “Microstructure and Magnetic Studies of Mg-Ni-Zn-Cu Ferrites”, Mater. Chem. Phys. 129 (2011) 1104-1109.
85. Amarjeet and V. Kumar, “Synthesis, Thermal and FTIR Study of Zn-Fe Nano Ferrites”, Intern. J. Latest Res.Sci.andTechn., 3 1 (2014) 61-63.
86. C. A. Ladole, “Preparation and Characterization of Spinel Zinc Ferrite $ZnFe_2O_4$”, Int. J. Chem. Sci., 10 3(2012)1230-1234.
87. M. Sertkol, Y. Koseoglu, A. Baykal, H. Kavas and M. S. Toprak,“Synthesis and Magnetic Characterization of $Zn_{0.7}Ni_{0.3}Fe_2O_4$Nanoparticles ViaMicrowave-Assisted Combustion Route”, J. Magn. Magn. Mater., 322, (2010)866-871.
88. M. Gharagozlou, “Synthesis, Characterization And Influence Of Calcination Temperature On Magnetic Properties Of Nanocrystalline Spinel Co-Ferrite Prepared By Polymeric Precursor Method,” Journal of Alloys and Compounds, 486 1-2 (2009) 660–665.
89. N. Kumar, V. Kumar, M. Arora, M. Sharma, B. Singh and R.P. Pant, “Synthesis of $Mn_{0.2}Zn_{0.8}Fe_2O_4$Particals by High Energy Ball Milling And Their Applications”, Ind. J. Engg. Mater. Sci., 16 (2009) 410-414.
90. J. L. Gunjakar, A. M. More, K.V. Gurav and C.D. Lokhande, “Chemical Synthesis of Spinel Nickel Ferrite ($NiFe_2O_4$) Nano-Sheets”, Appl. Surface, Sc., 254 (2008) 5844-5848.

91. M. Gotic, I. Czako-Nagy, S. Poponic and S. Music, “Formation of Nanocrystalline $NiFe_2O_4$”, Philos. Mag. Lett., 78 3 (1998) 193-201.
92. S. A. Saafan, T. M. Meaz, E.H. El. Ghazzawy, M. K. El. Nimr, M. M. Ayad and M. Bakr, “AC and DC Conductivity of NiZnFerrite Nanoparticles In Wet And Dry Conditions”, J. Magn. Magn. Mater., 322 (2010) 2309-2374.
93. P. Priyadharsini, A. Pradeep, P.S. Rao and G. Chandrasekaran, “Structural, Spectroscopic And Magnetic Study Of Nanocrystalline Ni-Zn Ferrites Mater, Chem. Phys., 116 (2009) 207.
94. S. A. Mazon, S.F. Mansour, E. Dhahri, H.M.Zoki and T. A. Elmosalambi, “The Infrared Absorption And Dielectric Properties of Li–GaFerrite”, J. Alloys, Compd., 470 (2009) 294.
95. M. Kaiser, “Effect of Nickel Substitutions On Some Properties of Cu—Zn ferrites”, J. Alloys. Compd., 468 (2009) 15-21.
96. P. V. Reddy and V. D. Reddy, “Far-Infrared Spectral Studies Of Some Lithium-Nickel Mixed Ferrites”, J. Magn, Magn. Mater., 136 (1994) 279-283.
97. P. Thangaraj, J. Rajan, S. Durai, S. Kumar, A. Ratnaphani and G. Neri, “The Role Of Al Album (Egg White) In Controlled Particle Size And Electrical Conductivity Behavior Of Zinc Oxide Nanoparticles”, Vaccum, 86 (2011) 140-143.
98. S. A. Saafan, T. M. Meaz, and E.H. El-Ghazzawy, “Study of DC Conductivity and Relative Magnetic Permeability of Nanoparticle $NiZnFe_2O_4$/ppyComposites”, J. Magn. Magn. Mater., 323 (2011) 1517-1524.
99. J. Jiang, L. Li and F. Xu, “Polyaniline–LiNiFerrite Core–Shell Composite: Preparation, Characterization and Properties”, Mater Sc. Engg A, 456 (2007) 300-304.
100. S.W. Caoa, Y.J. Zhua, G.F. Cheng and Y.H. Huang, “$ZnFe_2O_4$ Nanoparticles: Microwave-Hydrothermal Ionic Liquid Synthesis and Photocatalytic Property Over Phenol”, J. Hazard. Mater., 171 1-3 (2009) 431–435.
101. M. Mouallem-Bahout, S. Bertrand and O. Peńa, “Synthesis and Characterization of $Zn_{1-x}Ni_xFe_2O_4$ Spinels Prepared By A Citrate Precursor”, J. SolidState Chem., 178 4 (2005) 1080–1086.
102. T. Jahanbi, M. Hashim, K.A. Matoria and S.B.Waje, “Influence of Sintering Temperature On the Structural, Magnetic And Dielectric Properties of

$Ni_{0.8}Zn_{0.2}Fe_2O_4$ Synthesized by Co-precipitation Route", J. Alloys Compd., 503 1 (2010)111–117.

103. R.C. Kambale, N. R. Adhate, B.K. Chougule and Y.D. Kolekar, "Magnetic and Dielectric Properties Of Mixed Spinel Ni–Zn Ferrites Synthesized By Citrate–Nitrate Combustion Method", J. AlloysCompd., 491 1-2 (2010) 372–377.
104. N. Kaur and M. Kaur, "Comparative Studies On Impact Of Synthesis Methods On Structural And Magnetic Properties Of Magnesium Ferrite Nanoparticles", Processing and Application of Ceramics, 8 3 (2014) 137–143.
105. A.Loganathana and K.Kumarb, "Structural, optical and dielectric properties of nanosized $Mg_{0.88}Sr_{0.12}Fe_2O_4$ ferrite nanoparticles", Int. J. Adv. Res. Biol.Sci., 2 5 (2015) 112–118.
106. Binod B. Dora, Sanjay Kumar and Mahesh C. Sahu, "Size Controlled Synthesis and Magnetic Behaviour of Mg-Zn Nano Ferrites by Using Aloe vera Extract Solution", Int. J. Pharm. Sci. Rev. Res., 29 2 (2014) 307-311.
107. I. D. Brown and K. K. Wu, "Empirical Parameters For Calculating Cation-Oxygen Bond Valences", Acta Cryst. (1976). B32, 1957-1959.
108. Gurdip Singh, I.P.S. Kapoor, Shalini Dubey, Prem Felix Siril, Jian Hua Yi, Feng-Qi Zhao and Rong-Zu Hu, "Effect of mixed ternary transition metal ferrite nanocrystallites on thermal decomposition of ammmonium perchlorate", Thermochimica Acta, 477 1–2 (2008) 42–47.
109. Arthur Miller, "Distribution of Cations in Spinels", J. Appl. Phys. 30 S24 (1959).
110. M. G.Naseri, E. B. Saion, M.Hashim, A. H. Shaari and H. A. Ahangar, "Synthesis And Characterization Of Zinc Ferrite Nanoparticles By A Thermal Treatment Method", Solid State Communications, 151 14–15 (2011) 1031–1035.
111. G.V.S. Rao, C.N.R. Rao, J.R. Ferraro, Appl. Spectrosc. 24 436 (1970)
112. S. Hafner, Z. Kristallogr. 115 331 (1961)
113. M.Mouallem-Bahout, S. Bertrand and O. Peña, "Synthesis and Characterization of $Zn_{1-x}Ni_xFe_2O_4$ Spinels Prepared By A Citrate Precursor", J. Solid State Chem., 178 4(2005)1080–1086.
114. S. Maensiri, M. Sangmanee and A. Wiengmoon, "Magnesium Ferrite ($MgFe_2O_4$) Nanostructures Fabricated by Electrospinning", Nanoscale Res Lett., 4 (2009) 221–228.

115. Manju Kurian and Divya S. Nair, “Effect Of Preparation Conditions On Nickel Zinc Ferrite Nanoparticles: A Comparison Between Sol–Gel Auto Combustion And Co-Precipitation Methods”, Journal of Saudi Chemical Society, (2013).
116. M C Chhantbar, U N Trivedi, P V Tanna, H J Shah, R P Vara, H H Joshi and K B Modi, “Infrared Spectral Studies of Zn-substituted CuFeCrO4 Spinel Ferrite System”, Indian J. Phys., 78A (3) (2004) 321-326.
117. http://www1.lsbu.ac.uk/water/water_vibrational_spectrum.html
118. D. A. Skoog, “Principles of Instrumental Analysis”, Saunders Golden Sunburst Series, (1985).
119. P. F. Bemath, “The Spectroscopy of Water Vapou: Experimental, Theory And Application”, Phys. Chem. Chem.. Phys., 4(2002) 1501-1509.
120. J. Tennyson, P. F. Bernath, L. R. Brown, A. Campargue, A. G. Csaszar, L. Daumont, R. R. Gamache, J.T. Hodges, O. V. Naumenko, O. L. Polyansky, L. S. Rothman, A. C. Vandaele and N. F. Zoboy, “A Database Of Water Transitions From Experiment And Theory (IUPAC Technical Report)”, Pure Appl. Chem., 86 (2014) 71-83.
121. B. P. Jacob, A. Kumar, R. P. Pant, S. Singh and E. M. Mohammed, “Influence of Preparation Method On Structural And Magnetic Properties Of Nickel Ferrite Nanoparticles”, Bull. Mater. Sci., 34 7 (2011)1345–1350.
122. A.T. Raghavender, N. Biliškov, Ž. Skoko, “XRD and IR Analysis Of NanocrystallineNi–Zn Ferrite Synthesized By The Sol–Gel Method, Mater.Lett., 65 (2011) 677–680.
123. S. Zahi, “Synthesis, Permeability and Microstructure of the Optimal Nickel-Zinc Ferrites by Sol-Gel Route”, J. Electromagnetic Analysis and Applications, 2 (2010) 56-62.
124. E. V.Gopalan, I.A. Al-Omari , K.A. Malini, P.A. Joy, D. Sakthi Kumar, Y. Yoshida and M.R. Anantharaman, “Impact Of Zinc Substitution On The Structural And Magnetic Properties Of Chemically Derived Nanosized Manganese Zinc Mixed Ferrites”, J. Magn. andMagn.Mater., 321 (2009) 1092–1099.
125. John T. S. Irvine, Alfonso Huanosta, Raul Valenzuela and Anthony R. West, “Electrical Properties of Polycrystalline Nickel Zinc Ferrites”, Journal of the American Ceramic Society, 73 3 (1990) 729–732.

126. Qi Chen, Z. John Zhang, Size-dependent super paramagnetic properties of MgFe2O4 spinel ferrite nanocrystallites, Appl Phys Lett 73:3 (1998) 156.
127. P. Yadoji, R. Peelamudu, D. Agrawal and R. Roy, "Microwave Sintering of Ni-Zn Ferrites: Comparison With Conventional Sintering", Materials Science and Engineering:B, 98 (2003) 269-278.
128. A. Kumar, M. Arrora, M. S. Yadav and R. P Panta, "Induced Size Effect on Ni doped Nickel-Ferrite nanoparticles", Physics Proceeding, 9 (2010) 20-23.
129. R. S. Totagi, N. J. Choudhari, S. S. Kakati, C. S. Hiremath, S. B. Koujalagi and R. B. Pujar "Electrical properties of Ni-Mg-Cu nanoferrites synthesized by sucrose precursor technique", Der Pharma Chemica, 7 3 (2015)11-15.
130. J. Shah, M. Arora, L.P. Purohit and R.K. Kotnala, "Significant increase in humidity sensing characteristics of praseodymium doped magnesium ferrite", Sensors and Actuators A: Physical 167 2 (2011)332–337.
131. Gul, I. H., W. Ahmed, and A. Maqsood, \Electrical and magneticcharacterization of nanocrystalline Ni-Zn ferrite synthesis by co-precipitation route," J. Magn. Magn. Mater.,320(2008), 270-275,2008.
132. P.P Sarangi, S.R. Vader, M.K. Patra and N.M. Ghosh, "Synthesis and Characterization of pure single phase Ni-Zn Ferrites Nanopowders by Oxalate Based Precursor Method", Power Technology, 203 (2010) 348-353..
133. P.P Sarangi, S.R. Vader, M.K. Patra and N.M. Ghosh, "Synthesis and Characterization of Pure Single Phase Ni-Zn Ferrites Nanopowders by Oxalate Based Precursor Method", Power Technology, 203 (2010) 348-353.
134. J. Shah, R.K. Kotnala, B. Singh and H. Kishan, "Microstructure- Dependent Humidity Sensitivity of Porous $MgFe_2O_4$-CeO_2 Ceramic", Sensors and Actuators B: Chemical, 128 (2007) 306-311.
135. W.J. Fleming, "A Physical Understanding of Solid State Humidity Sensor", Proceed. Int. Automotive Meeting, SAE Detroit MI (1981) 51-62.
136. J.G. Paik, M.J. Lee and S.H. Hyun, "Reaction Kinetics and Formation Mechanism of Magnesium Ferrites", ThermochimActa, 425 (2005) 131-136.
137. M.H. Khedr, "Isothermal Reduction Kinetics at 900-1100 ^{0}C of $NiFe_2O_4$Sintered at 1100 to 1200 ^{0}C", J. Anal. Appl. Pyrolysis, 73 (2005) 123-129.

138. N. Rezlescu, E. Rezlescu, P. Popaand F. Tudorache, “On The Humidity Sensitivity Of A Ceramic Element Structure And Characterization”, PhysicaStarili Condensate, (2001-2002) 89-97.
139. N. Iftimie, E. Rezlescu, P.D. Popa and N. Rezlescu, “Gas Sensitivity of Nanocrystalline Nickel Ferrite”, J. Optoelectronics and Adv. Mater., 8 3 (2006) 1016-1018.
140. N. Rezlescu, E. Rezlescu, F. Tudorache and P.D. Popa, “Gas Sensing Properties of Porous Cu-Cd and Zn Ferrites”, Romanign Reports in Phys., 612 (2009) 223-234.
141. V. Kasiviswanath, Y. L. N. Murthy, K. Tata and R. Singh, “Synthesis and Characterization of Nano Ferrites By Citrate Gel Method”, Int. J. Chem. Sci., 11 1 (2013) 64-72.
142. H. U. Jun and Y. A. N Mi, “Preparation of High-Permeability NiCuZn ferrite”,J. Zhejiang Univ. Sci. 6B, 6 (2005) 580-583.
143. V. Naidu, S.K.A.Ahamed, M.SheikDawood and M.Suganthi, “Magnetic Properties of Nano Crystalline Nickel, Samariumdoped Zinc Ferrite”, Int. J. of Comp. Appl., 24 2 (2011) 18-22.
144. P.B. Belavi, G.N. Chavan, L.R. Naik, R. Somashekar and R.K. Kotnala, “Structural, Electrical And Magnetic Properties Of Cadmium Substituted Nickel–Copper Ferrites”, Mater. Chem. and Phys., 132 (2012) 138– 144.
145. K. Arshaka , K.Twomey and D.Egan, “A Ceramic Thick Film Humidity Sensor Based on MnZn Ferrite”, Sensors 2 (2002) 50-61.
146. S. A. Mazen and T. A. Elmosalami “Structural and Elastic Properties of Li-Ni Ferrite”, ISRN Condensed Matt. Phys., 20 11 (2011)9
147. S. C. Watawe, B. D. Sarwade, S. S. Bellad, B. D. Sutar, and B. K. Chaugule, “Microstructure and Magnetic Properties of Li-Co Ferrites,” Mater. Chem. & Phys., 65 2 (2000) 173–177.
148. A. Dhahri, J. Dhahri, S. Zemni, M. Oumezzine, M. Said, and H. Vincent, “Synthesis, Structural, Magnetic And Electrical Properties of $La1-xCdxMnO_3$ Manganites ($0.1\leq x\leq 0.5$)”, J. Alloys and Compounds, 450 1-2 (2008) 12–17.

*****

Topic 3

Electrical Properties

Electrical properties of the polycrystalline spinel ferrites reveal the materials` suitability for sensor based applications. Development of Smart Sensor Module is the major objective of present research work. For this purpose, it is also proposed to design own sensors of required characteristics. To develop the sensor, the sensing materials play vital role. Therefore, the polycrystalline spinel nano ferrites have been synthesized, and used to develop the sensors. On confirmation of formation of single phase compositions of nano particles, it is essential to investigate the electric properties of the same. It is found that, electrical properties, such as DC resistivity, dielectric constant, activation energies, Fermi energies, Curie temperatures etc are depend upon preparation methods, preparation condition, cation substitution, cation distribution, nature of composition either in bulk or thick film from, temperature and other environmental parameters. Therefore, the electrical properties of the compositions are investigated. Moreover, it is also found that, the ferrite materials, depicts the phenomenon of chemisorption and absorption. This surface phenomenon plays significant role on the electrical conduction mechanism, presenting protonic and electronic conductivity as well.

These properties of ferrite materials, reveals their suitability for sensor based application. Emphasizing sensor based applications, the electrical properties of the compositions under investigation are investigated and results of the investigation are interpreted through the following points

I) Temperature Sensitive Electrical properties
II) Humidity Sensitive Electrical properties
III) Gas Sensitive Electrical properties

A. Temperature Sensitive Electrical Properties

3.A.1 Introduction:

The possibility of preparing ferrites in the form of nanoparticles has open a new and exciting research field, with revolutionary applications in the electronic technology. Deployment of the ferrites for sensor based applications is the novel field for the researchers. Polycrystalline ferrites exhibit interesting electrical properties, wherein the semiconducting behavior is realized. Measurement of dc conductivity is essentially important technique to explore the transport process in ferrites. The electrical properties such as dc resistivity, dielectric polarization, mobility etc are the intrinsic properties and these properties are found to be dependent on the chemical compositions, preparation conditions, substitution of divalent or trivalent cations in the parent lattice, temperature, environmental conditions etc. These ferrite materials are highly resistive and its resistivity is mostly sensitive to the microstructure of the compositions. The microstructure usually develops at the sintering stage. Therefore, sintering conditions play significant role on the electrical properties of the ferrites. Thus, by controlling preparation condition, the electrical properties can be optimized. It is also reported that, the electrical properties are sensitive to the distribution of cations among tetrahedral (A) and octahedral (B) sites of the spinel structure [1]. For example, the zinc in zinc ferrite, being normal, could not participate in conduction process. Therefore, zinc ferrites are highly resistive ferrites. Moreover, the substitutions of cations such as nickel, exhibiting high degree of inverse, results into slight decrease in the resistivity.

The exponential dependence of electrical conductivity of ferrites with temperature can be attributed to the semiconducting nature. However, the semiconducting nature of spinel ferrites is quite different than that of semiconductors. This is because of the fact that, in semiconductor the conductivity is because of thermally generated charge carriers. However, in case of the ferrites the electrical conductivity is due to thermally activated charge carriers in the ionic lattice, which can be explained on the basis of hopping model [2,3]. The activation energy for electrical conduction is considerably reduced if the crystallattice intrinsically contains cations of one element in more than one valence state. According to Verway et al, the conduction in the ferrite composition is due to electron hopping between Fe^{3+} and Fe^{2+} ions

localized at crystallographic octahedral (B) site [4]. During this electron exchange the valence states of two cations are exchanged. However, this conductivity is very low, which can be attributed to the lower mobility of the charge carriers. The cations are not free to leave the lattice sites. However, due to lattice vibrations, these cations come enough close together to transfer the electrons as $Fe^{2+} \Leftrightarrow Fe^{3+} + e^-$. The number of electrons contributing the conduction process depends upon the concentration of the Fe^{2+} ion of octahedral site. Therefore, in ferrous ferrite the concentration of Fe^{2+} ions is same as that of Fe^{3+} ions on octahedral site. Therefore, it favours the conduction process and results into low resistivity. Moreover, as discussed earlier, on substitution, the nickel ion is also contributing electron hopping mechanism as $Ni^{2+} + Fe^{3+} \Leftrightarrow Ni^{3+} + Fe^{2+}$[5]. However, this is also featured with low mobility. Because of the thermal energy, the mobility of charge carriers increases significantly. Hence, electrical conduction significantly depends upon temperature. In addition to electron hoping model, other models are also suggested by the investigators [6,7]. Polaron, electron with strain field, hopping mechanism is suggested by Ul-Islam et al [6] and Chavan [7] to explain the conduction phenomenon, due to thermally activated mobility [8,9]. Thus, the electrical conductivity of the ferrite compositions strongly depends upon the temperature. In mixed ferrites, the conductivity is found to be dependent on the availability of Fe^{2+}/Fe^{3+} ions andM^{2+}/M^{3+} pairs in octahedral sites. Thus, cation distributions along with their characteristic oxidation states play a dominant role in the conduction process. The cation distribution is distinctly different in ferrite nanoparticles as compared with the bulk. The presence of Mn^{3+} ions along with Mn^{2+} ions will also affect the cation distribution in MnZn ferrites. In zinc substituted $Mn_{1-x}Zn_xFe_2O_4$, the zinc ions are likely to occupy the tetrahedral sites. In the case of samples prepared using ceramic techniques, the zinc ions were found to exist only in the tetrahedral sites (A sites) [13]. Moreover, for nano particle ferrites, prepared by the chemical route, the zinc ion showed its preferential distribution among A & B sites [14]. The occupancy of zinc ions in octahedral sites plays a major role in deciding the overall electrical properties of the nanosized manganese zinc ferrite. [14,15].

The temperature dependence of electrical resistivity obeys Wilson`s relations [10],

$$\rho = \rho_o \exp(\Delta E/KT) \qquad (1)$$

where ΔE is the activation energy and K is the Boltzman constant. An expression 1 depicts the fact that, the ferrite compositions reveal semiconducting nature with negative temperature coefficient of resistance. The graph of logρ against 1/T is the straight line with discontinuities in the slope at certain temperatures, which can be attributed to the Curie points. Thus, the electrical conductivity is strongly influenced by the magnetic ordering as well [11].

The temperature dependence of dc resistivity of the Mg-Zn-Cu ferrites was studied by Bachhav et al [12] and reported three significant regions in the graph of logρ against 1/T. The nature of graph is attributed to the effect of magnetic interaction on electrical conduction. The transport properties of nanoparticle $Mn_{1-x}Zn_xFe_2O_4$mixed ferrite, synthesized by co-precipitation method, were intensively studied by Gopalan et al and results obtained are attributed to the cation distribution [16].Temperature dependent electrical resistivity of CuNi nanoferrites, synthesized by using citrate gel auto combustion technique, was investigated by Vijayakumar et al [17] and reported that, electrical conduction is due to electron hopping for lower temperature. Moreover, the behaviour of resistivity for elevated temperature is attributed to the polaron hopping conduction mechanism. They reported that the activation energy at paramagnetic region is more than that of at ferrimagnetic region [18]. Effect of chromium substitution on electrical properties of nickel ferrites was studied by Choudhuri et al [19] and reported that, the substituted chromium resides on B site and results into decrease in the concentration of Fe^{2+} ions. The nickel ion is contributing the conduction process. The electrical properties of Ni-Mg-Cu nanoferrites synthesized by sucrose precursor technique are intensively studied by Totagi et al [20]. The variations in the logρ against 1/T curve depict the semiconducting nature with two regions referred as ferri region and para region. They reported that, the substitution of Mg results into decrease in the Curie temperature, which could be attributed to the decrease in the magnetic interaction. The substitution of rare earth element in spinel ferrites causes to increase in the resistivity [21,22, 23]. This may be due to stable valence of the rare earth ions. Nanosized cobalt ferrite was synthesized by sol-gel method by Gul and Maqsood and behaviour of dc resistivity is explained with Verway electron hopping mechanism. [24]. Temperature dependent electrical conductivity of chromium substituted NiZn ferrites was studied by Sayyd [25] and behaviour is attributed to electron hopping mechanism. The effect of excessive iron ion on electrical properties of Ni-Zn nanoferrites was investigated by

Sukta et al [26] and showed increase in the electrical resistivity. The electrical properties of Ni-Zn nanoferrites, synthesized by sol gel method, were investigated by Munir et al [27]. The temperature dependant variation of electrical conductivity is assigned with the Maxwell-Wagner model [27]. Nano crystalline cobalt substituted lithium ferrites have been synthesized by Arvind et al [28] by using citrate gel auto combustion method. The straight graph of log (σT) against inverse of temperature is assigned to the semiconducting behavior of prepared ferrite compositions.

Thus, it is found that, to decide applicability of the nanoferrites, the study of dc electrical properties and its temperature dependence is essential. Therefore, electrical properties of the ferrites under investigation are studies and results are reported in this topic.

3.A.2 Experimental :

The measurement of electrical resistance (R) of the pelletized compositions of the polycrystalline, $Mg_xZn_{1-x}Fe_2O_4$, $Ni_xZn_{1-x}Fe_2O_4$ and $Mn_xZn_{1-x}Fe_2O_4$ (x= 0.20, 0.40, 0.60 and 0.80) spinel ferrites were carried out from room temperature to 600 K using two probe method. An experimental arrangement is shown in figure 3.A.1. The measurements are carried out using samples in pellet (disk) form. The schematic of the electrode designed in the laboratory is depicted in figure 3.A.2. A silver paste is used to achieve Ohmic contacts. Highly precise digital meter, Tektronix Make model DMM4050, 6.5 Digit Resolution, Accuracy up to

Figure 3.A.1: Experimental set up to measure temperature dependent electrical resistance.

0.0024%, 10 Ω to 1.2 GΩ Range, with 10 μΩ Resolution, is used for resistance measurement. Automatic controlled electric furnace, Make Modern Scientific, Mumbai, is used and temperature of the furnace is measure by Cromel-Alumel thermocouple.

The thick films of the compositions under investigation are prepared by the method discussed earlier. The temperature dependent electrical resistance (R) of the thick films is also measured from room temperature to 150^{o}C. This is proposed range of investigation for sensor based application. The sensors are designed by employing two types of substrates, the glass and ceramic. The temperature dependent electrical properties of both these sensor are studied. The results obtained are used to decide the suitable range of their implementation.

Figure 3.A.2: The Schematic of Electrode designed to measure resistance of the compositions using two probe methods.

3.A.3. Results and Discussion:

I) Investigation of DC Electrical Resistivity of Pelletized Compositions:

The DC electrical resistance 'R', of the pelletized compositions under investigation, is measured in temperature range from 300K to 675K. To explore the details regarding conduction mechanism the values of resistivity 'ρ', in Ωcm, are obtained from resistance data and values of logρ are plotted against inverse temperature (1000/T) and presented in figures 3.A.3- 3.A.5, respectively, for the compositions polycrystalline, $Mg_xZn_{1-x}Fe_2O_4$, $Ni_xZn_{1-x}Fe_2O_4$ and $Mn_xZn_{1-x}Fe_2O_4$(x= 0.20, 0.40, 0.60 and 0.80) spinel nanoferrites. On inspection of these figures, it is found that, the graphs of logr against 1/T are almost linear obeying Wilson relation. The figures reveal semiconducting nature by exhibiting decrease of resistivity due to increase in the temperature. As depicted in the figure 3.A.3 (a-d), the compositions of $Mg_xZn_{1-x}Fe_2O_4$ ferrites exhibit decrease in the resistivity with increase in the temperature. The graphs of logρ against inverse temperature (1000/T) are almost linear with two significant breaks at distinct temperatures. This decrease in the resistivity with increase in the temperature can be attributed to the conduction mechanism, wherein conductivity due to thermally activated mobility of the charge carriers is ensured. It is known that, the

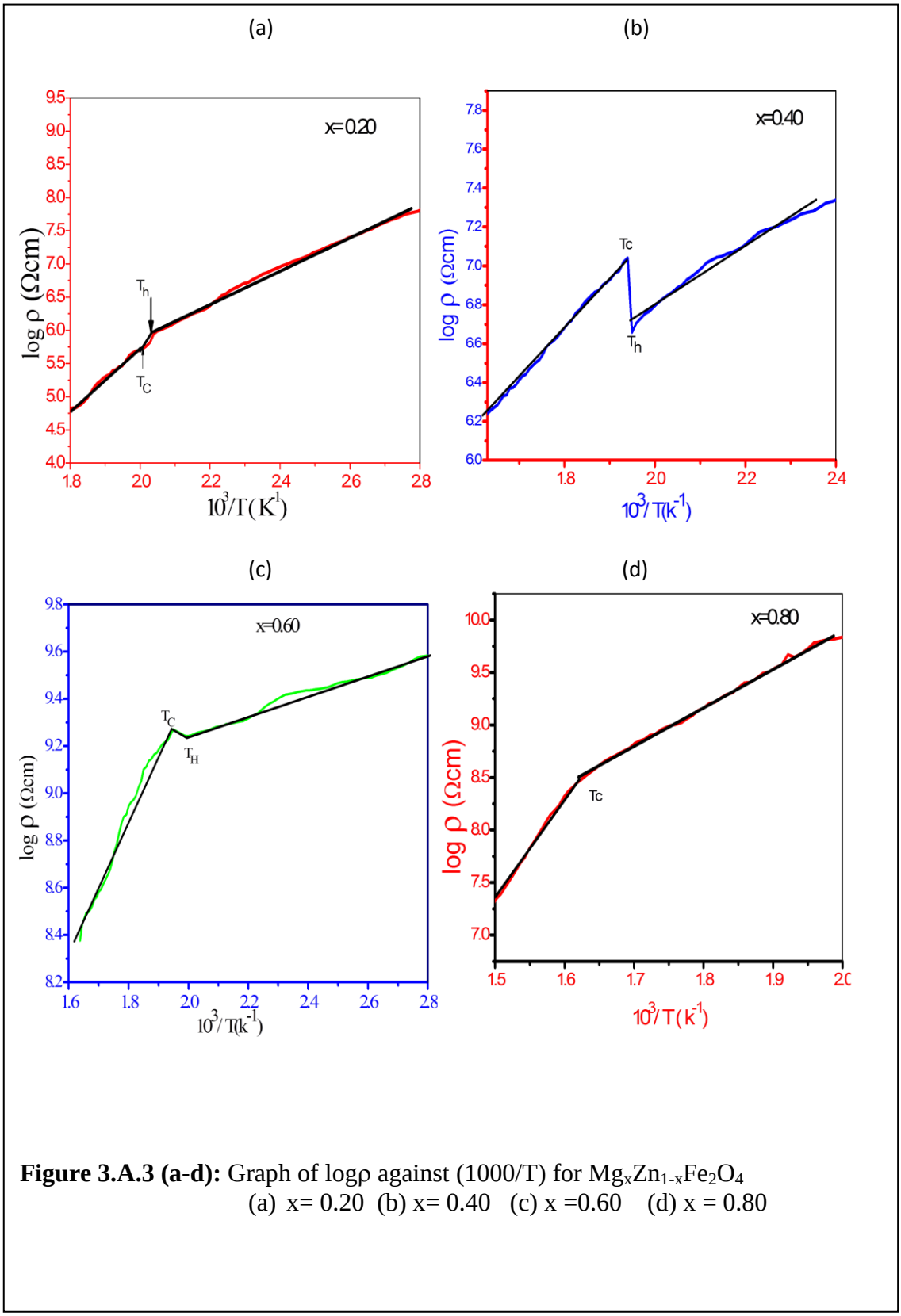

Figure 3.A.3 (a-d): Graph of logρ against (1000/T) for $Mg_xZn_{1-x}Fe_2O_4$
(a) x= 0.20 (b) x= 0.40 (c) x =0.60 (d) x = 0.80

zinc ions prefer to reside on A site, whereas magnesium ions preferentially distribute among A and B site. Moreover, valency of Mg ion remains stable. Therefore, the conduction is due to hopping of electrons between Fe^{3+} and Fe^{2+} ions on octahedral site [5]. On inspection of figure 3.A.3 (a-d), it is found that, the linear relationship of logρ against 1/T graph shows two significant breaks Tp and Tc for the compositions for x = 0.20, 0.40 and 0.60. Moreover, the composition for x = 0.80 depicts one break at a temperature Tc. Such two breaks are also reported by Bachhav et al [29] and Varalaxmi and Sivakumar [30]. These two temperatures, Tp and Tc, are called magnetic phase transition temperature and Curie temperature, respectively. The magnetic interaction is sensitive to the thermal energy and hence at a typical temperature, the disordering of interaction begins. Due to this disorder an amount of energy required for activation of the hopping is increased and hence the graph depicts the change in the slope. Moreover, at Curie temperature, the magnetic interaction vanishes. Therefore, the compositions become paramagnetic at which more amount of disorder is realized. This results into increase in the slope of the graph of log ρ against inverse of temperature (T). This reveals the fact that, the electrical conductivity is strongly influenced by magnetic interaction. Therefore, the region of the graph before Curie temperature is called ferri region and that of after Curie temperature is called Para region. Thus, the graphs of logρ against 1000/T, figure 3.A.3 (a-d) clearly depict the ferri and para magnetic nature of the compositions.

The Curie temperature values are obtained from temperature dependant electrical resistivity data and presented in table 3.A.1. On inspection of this table, it is found that, the Curie temperature values reveal compositional dependence. Pure zinc ferrite is paramagnetic in nature [31]. Moreover, occupancy of magnesium ion on B site displaces proportional amount of iron ion from B site to A

Table 3.A.1: The Curie temperature and activation energy values for the composition $Mg_xZn_{1-x}Fe_2O_4$.

X	Activation energy ΔE (eV)		Curie Temperature (Tc) K
	Ferri region	Para region	
0.20	0.0840	0.0949	499
0.40	0.024	0.102	515
0.60	0.010	0.135	602
0.80	0.135	0.377	626

site, which causes to increase in the magnetic interactions [32]. Therefore, increase in concentration of magnesium ion (x), the concentration of Zinc ion decreases. Therefore, magnetic interaction becomes more favorable. Thus, increase in the Curie temperature, due to increase in the magnesium ion, can be attributed to the increase in the magnetic interactions [33]. Activation energies for both ferri region as well as para region are estimated from the slope of log ρ against inverse temperature graphs and presented in the table 3.A.1. On inspection of the table 3.A.1, it is found that, the activation energies observed for present investigation found close match with that of earlier reports [32, 33]. From, this table, it is also found that, the activation energy for para region is more than for ferri region. This supports the statement that electrical properties are strongly influenced by magnetic ordering.

To investigate electrical characteristics of compositions of $Ni_xZn_{1-x}Fe_2O_4$ nanoferrites the values of logρ are plotted against inverse temperature (1000/T) and depicted in figure 3.A.4 (a-d). On close inspection of the figure 3.A.4 (a-d), it is observed that, the resistivity of the compositions decreases with increase in the temperature. This can be attributed to semiconducting nature of the compositions. The figures 3.A.4 (a-d), show almost linear relationship of logρ with 1/T with two significant breaks Tp and Tc for all compositions. Such change in the slope of the resistivity graph for NiZn ferrites is also reported by Ahmed et al [34]. They attributed these graphs to the ferri region and para region and temperature values are assigned to magnetic phase transition temperature (Tp) and Curie temperature (Tc), respectively. In fact, the conduction in ferrites is due to hopping of electrons, wherein

Table 3.A.2: The Curie temperature and activation energy values for the composition $Ni_xZn_{1-x}Fe_2O_4$.

X	Activation energy ΔE(eV)		Curie Temperature (Tc) K
	Ferri region	Para region	
0.20	0.051	0.091	402
0.40	0.022	0.113	479
0.60	0.024	0.235	519
0.80	0.457	0.582	650

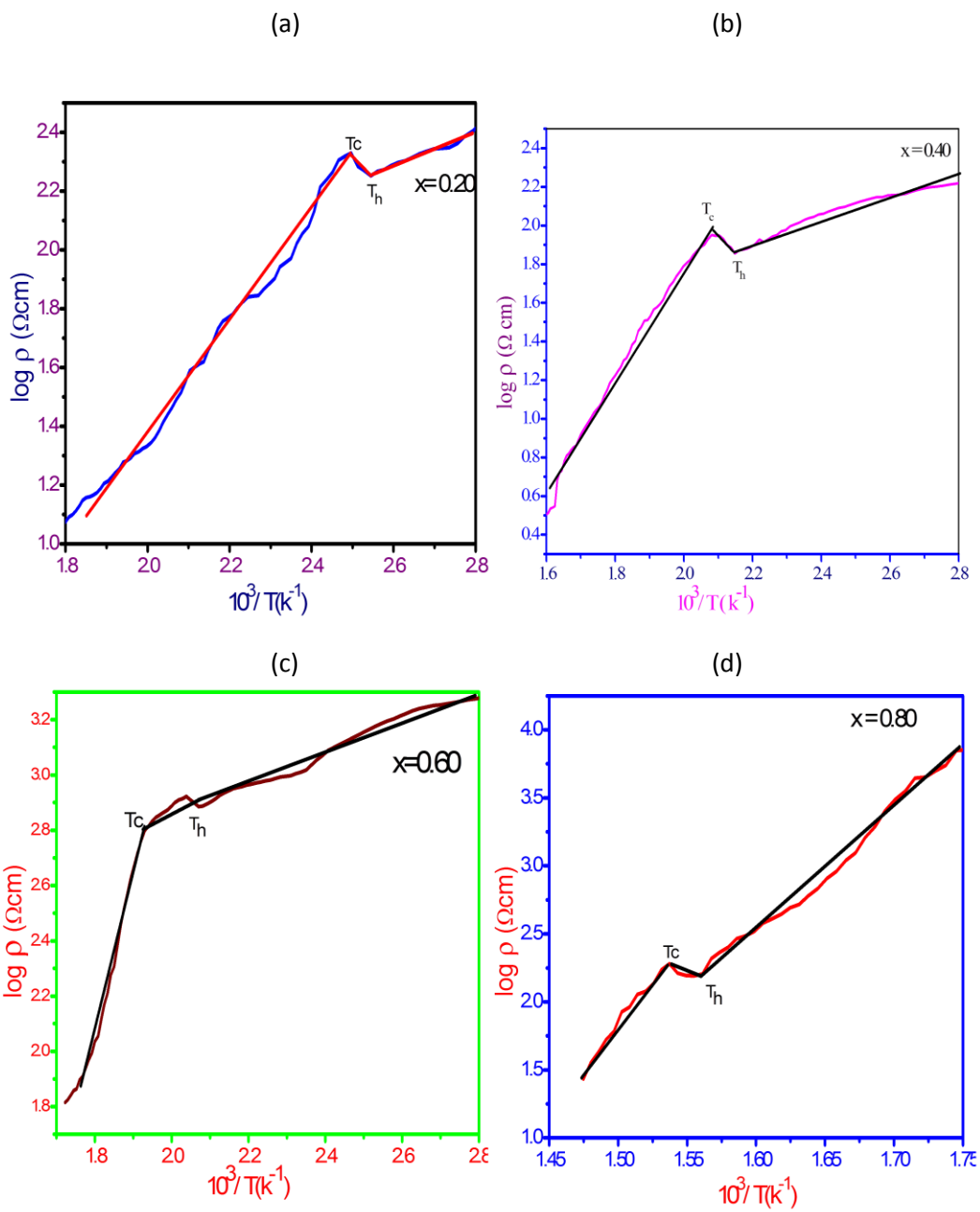

Figure 3.A.4 (a-d): Graph of logρ against (1000/T) for $Ni_xZn_{1-x}Fe_2O_4$
(a) x= 0.20 (b) x= 0.40 (c) x =0.60 (d) x = 0.80

thermal activation to increase the mobility is ensured. During para region the disorder between the ions increases considerably and therefore probability of hopping of electrons reduces. However, to realize the conduction, more activation energy (ΔE) is required. Hence, the slope of the graph during para region is greater than that of ferri region. The values of activation energies are obtained from the slope of the resistivity graphs and presented in table 3.A.2. Deploying the resistivity graphs, the values of Curie temperatures are obtained and presented in table 3.A.2. On inspection of the table 3.A.2, it is found that, the Curie temperatures Tc for Ni-Zn ferrites show compositional dependence. As discussed earlier, the zinc ion strongly occupies A site, whereas nickel exhibit its inverse nature. Therefore, nickel prefers to occupy B site. For lower concentration of nickel (x=0.20), the magnetic interactions are very weak, which results into decrease in the Curie temperature. Moreover, for higher nickel concentration, the magnetic interactions are favorably increased. Therefore, the values of Curie temperatures increase with increase in the nickel concentration. The Curie temperature values observed for present investigation showed close match with that of reported by Ahmed et al [34].The electrical characteristics, temperature dependent electrical resistivity (ρ) of compositions of $Mn_xZn_{1-x}Fe_2O_4$ nanoferrites, are also investigated. The temperature dependent resistance 'R' of the pelletized compositions is measured with respected to the temperature T in K. By availing this data, the values of logρ are calculated and plotted against inverse temperature (1000/T). These resistivity graphs are presented in figure 3.A.5 (a-d). On close inspection of the figure 3.A.5 (a-d), it is observed that, the resistivity of the compositions decreases with increase in the temperature. This can be assigned to semiconducting

Table 3.A.3: The Curie temperature and activation energy values for the composition $Mn_xZn_{1-x}Fe_2O_4$.

X	Activation energy ΔE (eV)		Curie Temperature (Tc) K
	Ferri region	Para region	
0.20	0.045	0.254	430
0.40	0.085	0.116	555
0.60	0.019	0.260	586
0.80	0.006	0.345	590

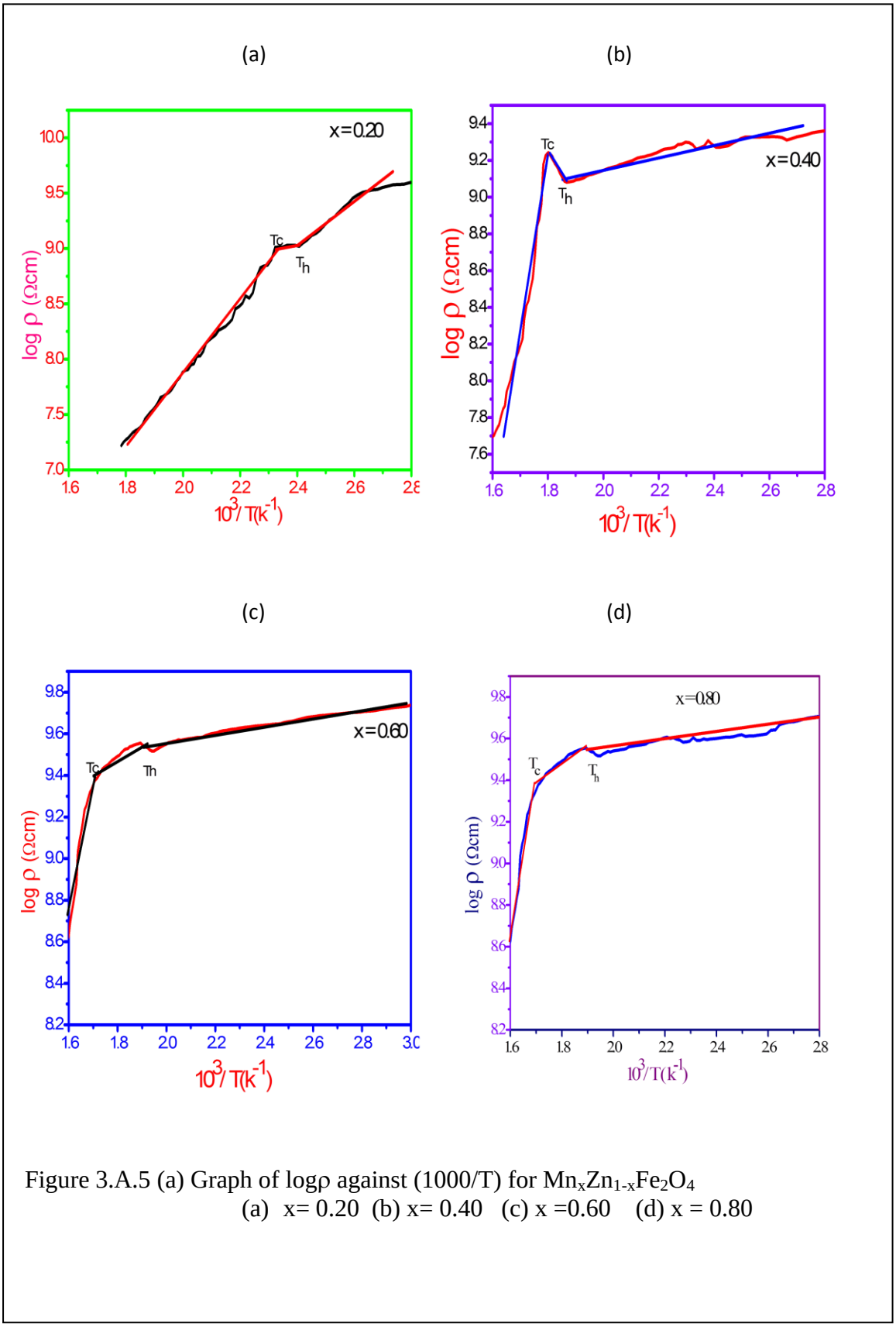

Figure 3.A.5 (a) Graph of logρ against (1000/T) for $Mn_xZn_{1-x}Fe_2O_4$
(a) x= 0.20 (b) x= 0.40 (c) x =0.60 (d) x = 0.80

nature of the compositions. The conduction is due to hopping of the electrons between cations of octahedral Sites. The figures 3.A.5 (a-d), show significant change in the slope of the graphs at temperature called Curie temperature. These graphs reveal two regions, ferri region and para-region, attributing to the fact that, the electrical properties of the ferrites are strongly influenced by magnetic interaction of the cations situated on A and B sites. The values of Curie temperatures (Tc) are obtained from these graphs and presented in table 3.A.3. These values of Curie temperatures show good agreement with that of earlier reports for MnZn ferrites [35, 36]. From this table, it is observed that, values of Curie temperatures increases with increase in the manganese ion concentration. This Mn^{2+} ion favorably participate in magnetic interaction. Therefore, increase in the Curie temperature can be attributed to the increase in the magnetic interaction, due to manganese ion. The activation energies of the compositions for both ferri as well as para region are obtained from slope of the resistivity graphs and presented in table 3.A.3. From, this table, it is found that, activation energy for para region is more than that of ferri region, which is as expected.

The values of Curie temperatures (Tc) for all compositions under investigation, obtained from resistivity graphs, are plotted against concentration (x) of Mg, Ni and Mn, the substituted cations and depicted in figures 3.A.6. On close inspection of the figure 3.A.6, it is found that, the Curie temperature strongly depends upon substitution of cations into basic compositions. It is known that, magnetic moment of Zn^{2+} is 0 μB and that of Mg^{2+} is also 0 μB [37]. Moreover, theoretically magnetic moments of Ni^{2+}, Fe^{2+}, Mn^{2+} and Fe^{3+} are 2 μB, 4 μB, 5 μB and 5 μB respectively [38]. Therefore, magnetic interactions due to Mn^{2+}, Fe^{2+} and Fe^{3+} ions are

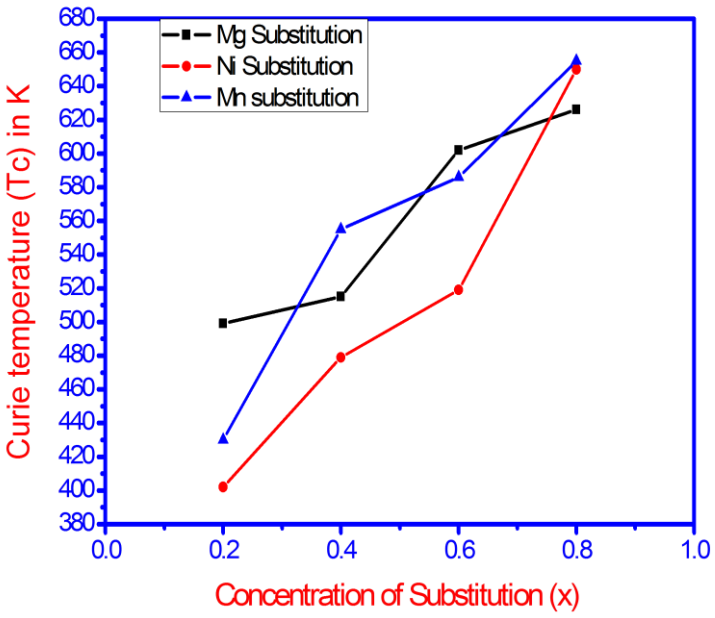

Figure 3.A.6: Graph of Curie temperatures against concentration of substituted cations in Zinc ferrites

stronger than that of nickel ion. It is known that, stronger magnetic interaction needs more thermal energy to collapse the same. The figure 3.A.6 reveals the effect of Mg, Mn and Ni substitution on Curie temperature of the zinc ferrite. As concentration (x) of substituted ion increases, the Curie temperature increases. Pure Zinc ferrite is paramagnetic in nature. The substitution of cations results into ferri magnetic behaviour into the compositions. It is also found that, Curie temperatures of Mn substituted compositions are higher than that of Ni substituted compositions. This can be attributed to the fact that, the Mn exhibits strong magnetic interaction than that of Ni ion. Moreover, nickel ion strongly occupy B site, whereas occupancy on Mn is about 80% to the tetrahedral site [39, 40]. The substitution of magnesium also affected to increase the Curie temperature. This may be due to cation distribution among A & B site of the spinel structure of MgZn ferrites.

II) Investigation of DC Electrical Properties suitable for Sensor Based Applications:

The major objective of the present research work is to study and deploy polycrystalline nanoferrite materials for development of the sensor for typical application. Employing the ferrite materials the sensors have been designed, wherein thick film technology is ensured. Emphasizing the application areas and nature of measurand, the sensors are prepared, by thick film technology, wherein different substrates have been employed. It was attempted to develop the sensors on different substrates. However, emphasizing the salient features needed for present embedded system design, it is proposed to deploy the glass and ceramic materials as substrate.

a) **Temperature dependent Electrical properties of the sensor developed on Glass Substrate :**

Deploying glass substrate the sensor is developed. Availing screen printing technique, as discussed earlier, a thick film of the composition under investigation is deposited on the glass substrate in cylindrical shape. The Schematic of the sensor is depicted in figure 3.A.7. A specially designed Heating Element (HH) is installed along

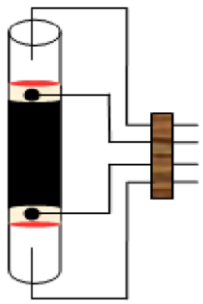

Figure 3.A.7 The Schematic of the sensor designed by using polycrystalline ferrites materials

the axis of the sensor. In order to achieve Ohmic contacts the rings of silver paste are deposited at both sides of the thick film. From these silver electrodes the leads are developed to ensure electrical contacts. Thus, the sensing element is developed. Highly precise digital meter, Tektronix Make model DMM4050, 6.5 Digit Resolution, Accuracy up to 0.0024%, 10 Ω to 1.2 GΩ Range, with 10 μΩ Resolution , is employed to measure the resistance of the Sensing Element (SS) (Thick film of the composition). The digital thermometer is used to measure temperature in degree centigrade. Heating element is energized with separate source of 5V. A current through HH is gradually increased to increase the temperature of the sensing element (SS). The Resistance, R, of the sensing element is measured within the temperature range from room temperature to 150 ^{0}C. It is aimed to designed sensor module, realizing embedded technology, to sense the environmental parameters. Therefore, range of temperature for sensor development is constrained to 150 ^{0}C.

Temperature dependant resistance R of the sensor element, designed by employing the compositions of $Mg_xZn_{1-x}Fe_2O_4$ nanoferrite, is measured within the temperature range from room temperature to 150^{0}C. The resistance R is plotted against temperature and depicted in figure 3.A.8. On close inspection of the figure 3.A.8, it is found that, the resistance R exponentially decreases with increase in the temperature. This negative temperature coefficient realizes the semiconducting nature. The temperature sensitivity (S_t) of the composition for x ≥ 0.40 is significantly high below 100 ^{0}C. However, above 100 ^{0}C, the trend of decrease in the resistance with temperature is found low. The sensitivity for composition x = 0.20 is high for entire range of investigation. Thus, sensors developed by using fine powdered compositions of MgZn ferrites can be suitably deployed as

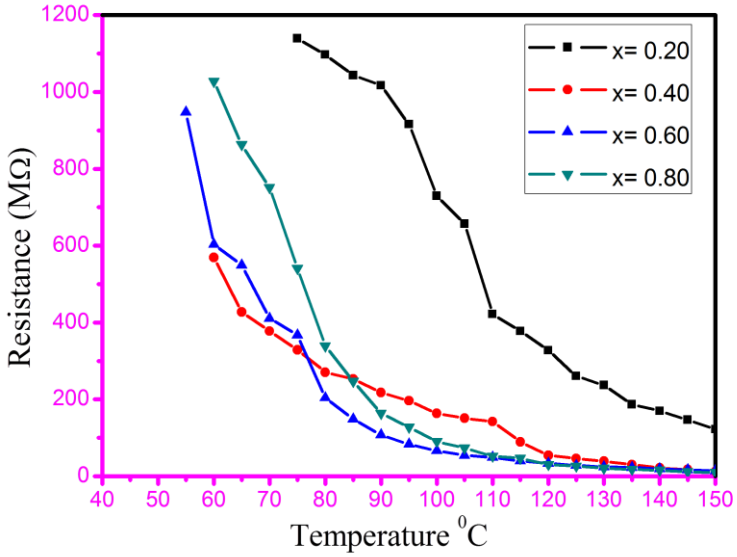

Figure 3.A.8: Graph of Resistance (R) against Temperature (t) in ^{0}C for the Compositions $Mg_xZn_{1-x}Fe_2O_4$

temperature sensor for development of sensor module. Further, the process of calibration is also carried out. The details regarding calibration and implementations are interpreted in next topic.

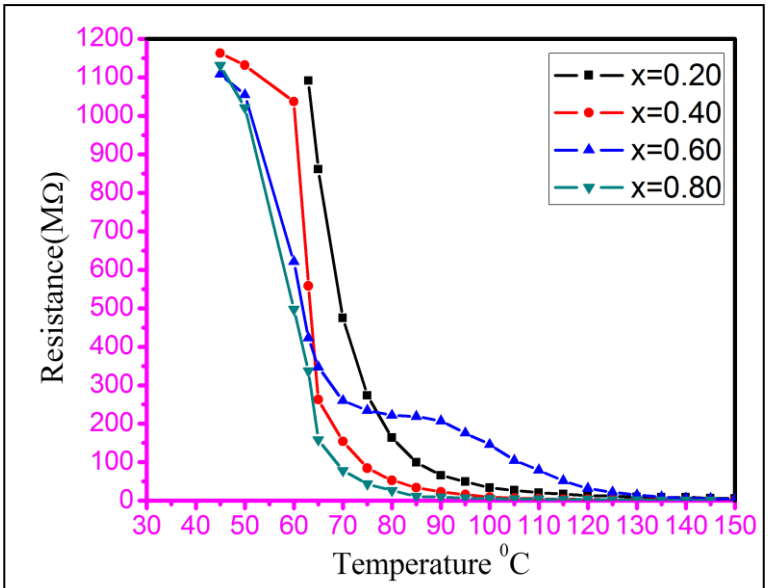

Figure 3.A.9: Graph of Resistance (R) against Temperature (t) in ^{0}C for the Compositions $Ni_xZn_{1-x}Fe_2O_4$

Similarly, the resistance of the sensors designed by availing compositions of $Ni_xZn_{1-x}Fe_2O_4$ is measured with temperature from room temperature to 150^{0}C and graph of resistance R against temperature is shown in figure 3.A.9. The figure shows exponential variation of resistance with temperature. In fact, for temperature below 90^{0}C, the resistance suddenly drops, whereas after 90 ^{0}C the resistance slowly decreases. This behaviour must be considered during calibration of the system. By employing suitable process of calibration, the sensor can be deployed as environmental temperature sensor.

Further, using the compositions of $Mn_xZn_{1-x}Fe_2O_4$ ferrites, the sensors have been developed and implemented for temperature dependent resistance measurement. The values of resistance are plotted against temperature and depicted in figure 3.A.10. As expected, the graphs of resistance against temperature reveal exponential behaviour, which is further considered for process of calibration.

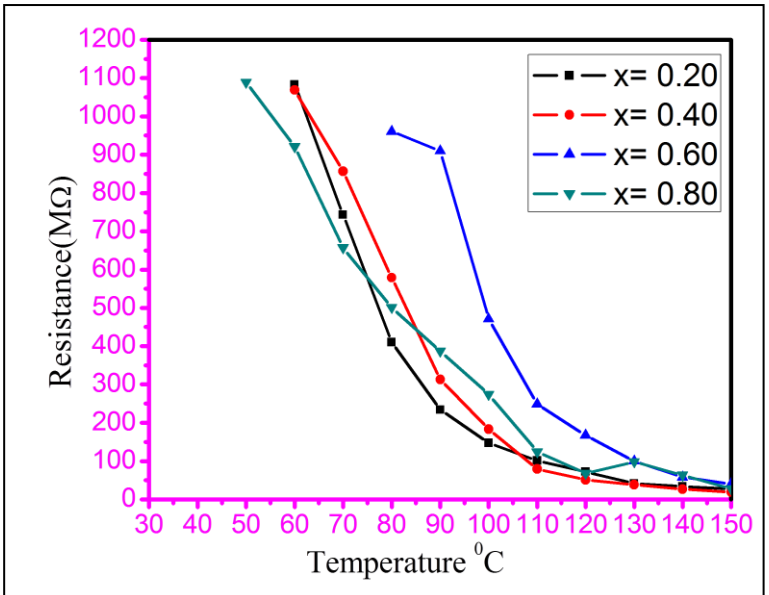

Figure 3.A.10: Graph of Resistance (R) against Temperature (t) in ^{0}C for the Compositions $Mn_xZn_{1-x}Fe_2O_4$

The sensitivity is high before temperature about 100 ^{0}C. It found declined above this

temperature. Therefore, as per proposal these sensors can be used as temperature sensor with the range of investigation.

From the results, it can be said that, the compositions of the polycrystalline ferrites can be suitably used to design temperature as well as gas sensors. By developing software the exponential response can be essentially linearized to realize the process of calibration and implementation.

b) Temperature dependent Electrical properties of the sensor developed on Ceramic Substrate:

To keep pace with the objectives of the present research work, the design of polycrystalline nanoferrite based sensor, for typical parameters and deployment of the same to design an embedded system to ensure smart sensor module, the thick film of the compositions is also developed on the ceramic substrate. It is known that, the ceramic materials such as Alumina are highly resistive ($\rho > 10^{14}\Omega$cm) [41]. Moreover, it is highly rigid in nature. The materials used for IC packaging are highly resistive and exhibit good thermal conductivity [42]. Therefore, these materials are mostly suitable as a substrate material for development of the thick film sensor. It is emphasized to develop temperature sensor, humidity Sensor and gas sensor. Moreover, the design of these sensors should suitable for interfacing to electronic circuit. Therefore, ensuring the device fabrication, by using screen printing technology, the thick film of the compositions is deposited on ceramic substrate. The schematic of the sensor is as presented in the figure 3.A.11. A thick film (4mm) of the sensor material is deposited on the rectangular substrate, of size 10mm x 5mm x 3mm, and slowly heated to the 300 ^{0}C. The bands of silver paste are deposited on both ends of the film to establish the electrical contacts. This sensor is employed for further investigation.

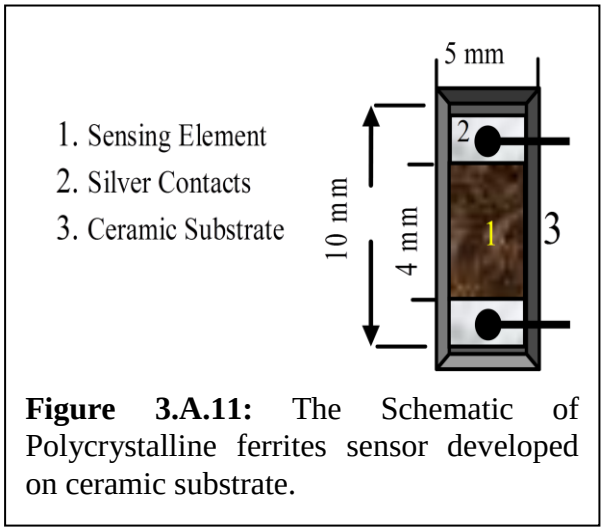

Figure 3.A.11: The Schematic of Polycrystalline ferrites sensor developed on ceramic substrate.

Deploying the compositions of polycrystalline $Mg_xZn_{1-x}Fe_2O_4$spinel ferrites, the sensors are developed, wherein a ceramic substrate of ultra high resistivity and good thermal conductivity is employed. The electrical resistance of the sensor (Rt) is

measured with the temperature (t) from 30^0C to 150^0C. This range of investigation is also considered for designing of analog part of the electronic circuit. The values of resistance are plotted against temperature and presented in figure 3.A.12. From figure 3.A.12, it is found that, the resistance exponentially decreases with the temperature within the range of investigation. The sensors for the compositions x= 0.20 and 0.80 show high resistance. This can be attributed to the resistivity of the compositions. The resistance of the compositions for x = 0.40 and 0.60 is comparatively low. Therefore, the sensors developed by using ferrite compositions for x = 0.40 and 0.60 reveal its suitability as temperature sensor with the range from room temperature to about 100 ^{0}C. The relative variation in the resistance (ΔR), in percentage, of the sensors is calculated by using an expression 2.

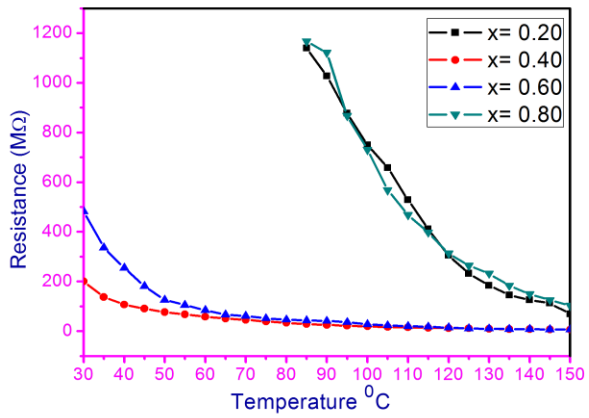

Figure 3.A.12: Graph of Resistance (R) against Temperature (t) in ^{0}C for thick film of Compositions $Mg_xZn_{1-x}Fe_2O_4$ deposited on Ceramic substrate

$$\Delta R = \frac{(Ra - Rt)}{Ra} \times 100\ \% \qquad (2)$$

Where, Ra is resistance at ambient temperature, Rt is temperature dependent resistance. The values of the sensitivities, St = (ΔR/Δt)x 100 %, [43] can be determined from the slope of the graph of relative resistance (ΔR) plotted against temperature and depicted in figure 3.A.15. The variation in the sensitivity can be attributed to the exponential nature of the resistance- temperature graph. While interfacing to the circuit, this behaviour of the sensor is

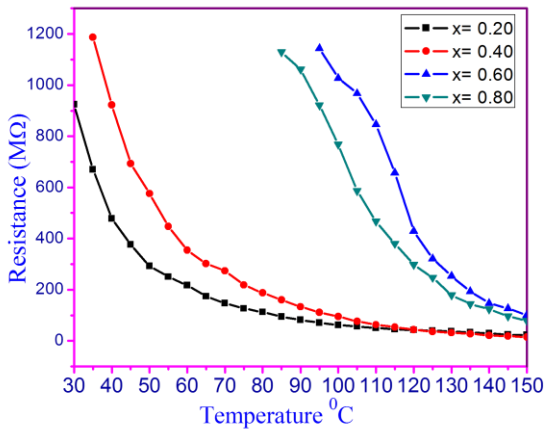

Figure 3.A.13: Graph of Resistance (R) against Temperature (t) in ^{0}C for thick film of Compositions $Ni_xZn_{1-x}Fe_2O_4$ deposited on Ceramic substrate

considered. The sensors developed using compositions of $Mg_xZn_{1-x}Fe_2O_4$ for x = 0.40 and x = 0.60 are employed for development of smart sensor module.

Based on ceramic substrate the sensors are prepared, wherein the thick film of the compositions of $Ni_xZn_{1-x}Fe_2O_4$nanoferrites have been deposited. A method of preparation is illustrated earlier. The electrical resistances (Rt) for these sensors are measured with the temperature (t) from 30^0C to 150^0C and graph of resistance against temperature is depicted in figure 3.A.13. These graphs help to confirm the range of temperatures for which the devices could be suitably deployed. From inspection of these graphs, it is found that, for x = 0.20 and x = 0.40 are most suitable for development of sensors for temperature range from room temperature to 100 ^{0}C. The sensitivity obtained from figure 3.A.15, also supports this argument. The sensor, developed by employing compositions for x = 0.60 and x =0.80,reveal their suitability for upper range of temperature. With suitable electronic circuit, as illustrated in next topic, these sensors can also be deployed for lower range of temperatures.

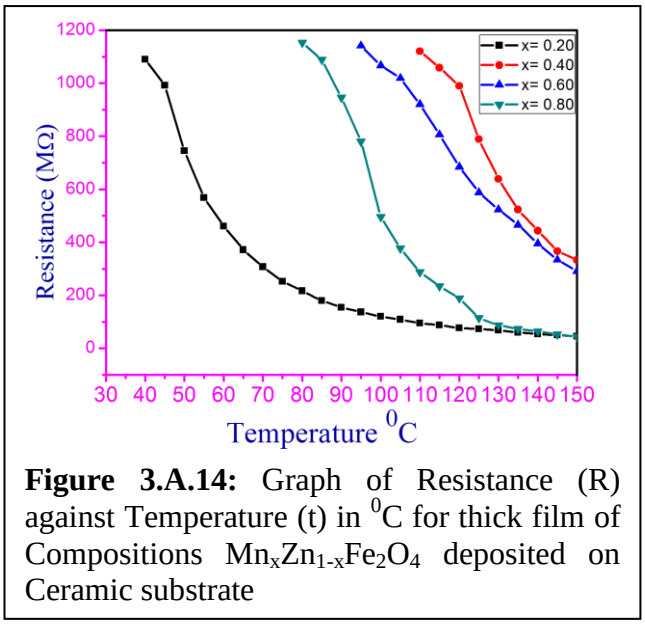

Figure 3.A.14: Graph of Resistance (R) against Temperature (t) in ^{0}C for thick film of Compositions $Mn_xZn_{1-x}Fe_2O_4$ deposited on Ceramic substrate

To confirm the suitability of the materials for development of temperature sensor, the thick film of compositions $Mn_xZn_{1-x}Fe_2O_4$ is developed on ceramic substrate, by the process discussed earlier. The temperature dependent electrical resistances (Rt) for these sensors are measured with the temperature (t) from 30^0C to 150^0C. The values of Rt are plotted against temperature t and presented in figure 3.A.14. As depicted in figure 3.A.14, the

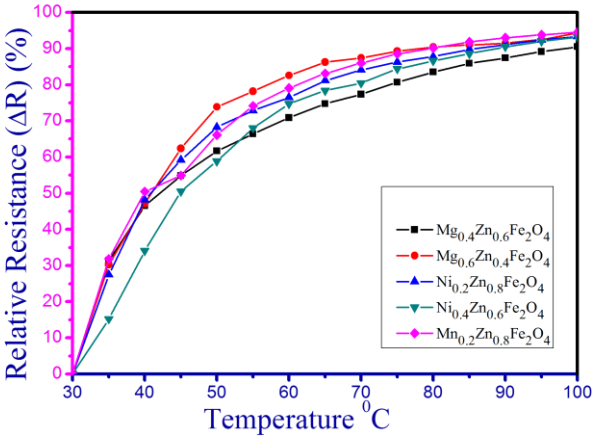

Figure 3.A.15: Graph of Sensitivity (St) against Temperature (t) in ^{0}C for thick film of Compositions of nanoferrites deposited on Ceramic substrate

response of the sensor to the applied temperature is exponential. This is attributed to the semiconducting nature of the sensing element, the thick film of the ferrite materials. It is also found that, the sensor developed with x = 0.20 is suitable for detection of lower temperatures. However, for compositions $x \geq 0.40$, the suitable modifications in the analog part of the hardware, is essential. Application of proper biasing potential and use of accurate resistive divider arrangement can make devices applicable for expected range of temperature. The sensitivity obtained from the Figure 3.A.15, also supports the suitability of these devices for development of sensor module to measure environmental temperature along with other parameters.

3.A.4 Conclusion:

Temperature dependent electrical properties of the compositions of $Mg_xZn_{1-x}Fe_2O_4$, $Ni_xZn_{1-x}Fe_2O_4$and $Mn_xZn_{1-x}Fe_2O_4$ nano ferrites were investigated for suitability of these materials as the sensing element for designing of sensors. The D.C electrical resistivity of the pelletized compositions shows, semiconducting behavior, which is attributed to the electron hopping mechanism. This electrical conductivity exhibit the influence of magnetic ordering at and about Curie temperature. The values of curie temperatures and activation energies show good agreement with the earlier reports. The Curie temperature values depict the compositional dependence. Keeping pace with the objectives of present research, the sensors are developed, employing thick film technology, wherein the compositions of the ferrite under investigation are used as sensing elements. It is attempted to design the sensors on different substrates, Such as epoxy resin, glass and ceramic. Temperature dependent electrical properties of the sensor developed on glass substrate are investigated. The resistance of sensing element shows negative temperature coefficient within the range of investigation. From the results, it can be concluded that, the present ferrite materials are suitable for sensing element. Moreover, the thick film of the sensing material is developed on ceramic substrate of ultrahigh resistivity. The temperature dependent D.C resistance of the sensor developed on ceramic substrate is measured. It is proposed to deploy the sensor within the temperature range from 30^0C to 100^0C. The sensitivities of the compositions are also studied. From the results of investigation, it is concluded that, the sensor developed on ceramic substrate are most suitable for temperature sensor and deployment of the same for designing of smart sensor module.

3.B. Humidity Sensitive Electrical Properties

3.B.1 Introduction:

Humidity, a concentration of water vapors in the air, is most significant parameter to be measured. Precise measurement of humidity exhibits prime importance in various sectors such as sugar and paper based industries, chemicals and medicine industries, automotive industries, climatology, HVAC systems, agriculture etc. [44]. Recently, the term precision agriculture is evolving, wherein crops are grown in controlled environment. The humidity of polyhouse environment should be monitored and controlled to the deterministic level. For meteorological applications the collection and processing data, in real time, regarding humidity of the environment is most essential, which may help to predict about the precipitation, Dew or Fog [45]. The information can be suitably availed to avoid catastrophic disaster due to heavy precipitation. To have desirable surrounding atmosphere, it is essential to monitor and control the ambient humidity under various conditions related to the temperature and concentration of other environmental gases [46]. In paper manufacturing industry, the humidity of environment plays significant role on the quality of the paper. Furthermore, in hardboard manufacturing industries, the finishing paper sheet is laminated in controlled humidity condition. It is found that, for food processing industries, the controlling of humidity of the environment plays vital role on the quality of the food product. In semiconductor industries, the performance of the photo-resist is highly dependent on the humidity. Utilization of intelligent electronic systems and network of sensors for monitoring humidity of the environment as well as soil moisture is the most challenging area of the research. To realize the preciseness in the measurement, the humidity sensor should be of prominent features. The sensing material and sensing principle play a key role on the specification of the sensor. The state- of-art of recent technologies is to develop smart sensor module, wherein the features of the devices are optimized by using electronic technologies. The state-of-art for present technology is to synthesize the humidity sensing material of promising features and by deploying same the designing of electronic system to realize precise measurement of the humidity of the desired environment.

The major objective of the present research work is to synthesize the materials suitable for humidity sensing and fabrication of the smart humidity sensor module,

which may realize the greater applicability. Therefore, based on polycrystalline nanoferrite materials, synthesized in the laboratory, the humidity sensors are fabricated and investigated for their performance.

a) Basics of the Humidity :

Humidity is defined as the amount of water vapour in an atmosphere of air or other gases. Humidity can be expressed in different ways, such as Absolute humidity, relative humidity, ppm, etc. Absolute Humidity expresses directly the amount of water either in volumetric unit or gravimetric units. Relative Humidity (abbreviated as RH) is defined as ratio of the partial pressure of water vapour in the air (Pa) to the partial pressure of water vapour in saturated air (Ps) at a given temperature and pressure [47]. It is expressed in terms of percentage (%). The relative humidity (%RH) can be calculated by using expression [24]

$$\text{Relative Humidity (\%RH)} = \frac{Pa}{Ps} \text{ x } 100 \text{ \%} \qquad (3)$$

Thus, the water molecule in the gaseous form (H_2O) realizes the adsorption as well as absorption mechanism with the sensing materials. As discussed in the mechanism of conduction due to humidity, these water molecules contribute the electrical conduction, wherein either protonic or electronic or both conductions are ensured [48].

b) Review of the Literature :

The synthesis and characterization of materials, suitable for humidity sensing, is carried out by many researchers and the results obtained are reported. It is known that variety of materials, classified as polymers, electrolytes, porous ceramics, organic polymers, acoustics and optics [49, 50] can be suitably deployed for development of humidity sensors. It was suggested that, the ceramic and polymer materials are most suitable for humidity sensor [50]. Emphasizing the development of humidity sensor, many researchers have synthesized ceramic oxides based materials of different characteristics. However, the research work carried out by some researchers, as a representative, is reviewed. On literature survey, it is found that, the polycrystalline spinel ferrite materials of nano particle size exhibit humidity sensing properties. Lipare et al have investigated the effect of LiCl substitution on humidity dependent electrical properties of CuZn spinel ferrites [51]. They reported that, substitution of LiCl results into enhancement of the performance of the materials to the humidity. Wang et al [52] have studied lanthanum ferrite/polymer quarternary acrylic resin composite materials

for humidity dependent electrical properties. They reported improvement in the response timing due to addition of polymer in lanthanum ferrites. They also reported the hysteresis effect and relaxation behavior in dielectric response of the material under investigation. The effect of substitution of multivalent cations (Sn & Mo) in Mg ferrites was investigated by Rezlescu et al [53]. They synthesized the materials by sol-gel auto combustion method and reported nanocrystallite structure. They reported that, the Sn ion enhances the humidity sensitivity of the magnesium ferrite. Emphasizing the features of ceramic materials, Faia et al [54] investigated the humidity sensing properties of thick film titania prepared by spin deposition technique. The behaviour of the materials to the humidity is attributed to the existence of protonic conduction mechanism. Kotnala et al studied the humidity response of Li Mg ferrites [55]. They claimed that, substitution of lithium causes to enhance humidity sensitivity of magnesium ferrites. Deploying self combustion method the compositions of magnesium copper ferrites have been synthesized by Rezlescu et al [56] and effect of Y^{3+} , Ga^{3+} and La^{3+} on performance of sensitivity for humidity is investigated. They reported that, substitution of Ga in MgCu ferrites results into increase in the range of humidity. Shah et al have doped the rare earth elements like Pr in magnesium ferrites [57] and reported the reduction in the lower limit of humidity detection range. Widening of the range of utilizations is attributed to the contribution of Pr in the process of adsorption. The humidity sensitive electrical properties of pure and K^{+} doped LaCo ferrite thick film deposited on ceramic substrate have been studied by Wang et al [58] and reported that, the doping of K^{+} ion results into four order decreases in the resistance. Moreover, the hysteresis loop is also narrowed. They reported the suitability of the material to prepare interdigitated sensor for humidity measurement. Humidity sensing properties of α-Fe_2O_3 have been studied by Tulliani and Bonville [59] and reported the results on investigation of humidity dependent electrical properties of the screen printed thick film sensor. They suggested the suitability doping of alkali and alkaline earth oxides for improvement in the performance of the sensors. Bagum et al [60] have synthesized compositions of CuZn nano ferrites with doping of 0.05 wt% of $MgCl_2$ and deployed to study resistance humidity characteristics of the same. Electrical properties of the compositions are attributed to the microstructure and porosity of the compositions. Nanocrystallite Mg-Cd spinel ferrite samples were prepared by Gadkari et al by oxalate co-precipitation method [61]. They investigated the humidity sensitive electrical

properties and reported good performance for wide range of humidity. Emphasizing the applicability of the ferrite materials for development of humidity sensor, Petrila and Tudorache have synthesized nanostructured tungsten substituted CuZn ferrites [62]. The exponential behavior of the resistance against humidity attributed to the conduction mechanism. They reported the expression $R=Ro\ Exp\ (-K_{RH}t)$ for resistance curve and $C = Co\ Exp(K_{CH}t)$ for capacitance curve. Cavalieri et al [63] studied effect of substitution of small amount of Cu in place of Fe^{3+} ion in LaSr ferrites and reported improvement in response of the samples for water vapour proving its suitability for development of humidity sensor. The compositions of nanostructure MgZn ferrites were synthesized by Rezlescu et al using standard ceramic method and the results regarding humidity dependent electrical characteristics are reported [64]. The behaviour of electrical conductivity is attributed to the microstructure of the samples. A thick film of Mn Zn spinel ferrite was deposited on ceramic substrate by Arshaka et al [65]. They prepared thick film sensors, wherein two layers; one of interdigitated electrode and second of sensing element, have been deposited. The investigation regarding their performance for humidity proves its suitability for sensor based applications. It was also reported that, the accuracy of capacitive sensor is more than that of resistive type sensor. However, the response times of capacitive sensor is large than that of resistive sensor. The complex electronic circuit is required to interface capacitive sensor [66,67]. Köseo_glu et al [68] intensively studied the humidity sensing properties of MnNi ferrites prepared by chemical route using nitrides of the constituents. They reported that the $Mn_{0.2}Ni_{0.8}Fe_2O_4$ is sensitive for ethanol, acetone LPG and some oxidizing gases as well. However, the sensitivity of this material for water vapour is significantly high than other gases. Hence, these materials are suitable for humidity sensor. In addition to the ferrites, other ceramic oxides are studied for humidity characteristics by different researchers [69]. Moreover, the material depicting carbon nano tube structure also suitable for humidity sensor [70]. It is found that, ferrites materials, realizing promising electrical characteristics, are most sensitive to the humidity. The synthesis and characterization of the ferrite compositions for humidity are reported. However, reports on fabrication of the devices and deployment of the same to design sensor module, wherein embedded technology is ensured, are rather rare. Therefore, present investigation emphasizes the utilization of ferrites material to design humidity sensor module of promising characteristics.

c) Mechanism of Humidity Dependent Electrical Conduction:

Polycrystalline spinel ferrite, the semiconducting oxides, due to its microstructural properties such as porosity, nanoparticles, larger surface area, uniform grain size etc, are most suitable for electrochemical sensor applications [71]. It is known that, the current through ferrite sample is temperature dependent [3.A]. However, the electrical conduction through the ferrite compositions also depends upon humidity of the atmosphere. In fact, electrical conduction in the ceramic can be classified as ionic conduction, electronic conduction and solid-electrolyte, wherein surface phenomenon is realized. In case of FTIR studies, it is also found that, the ferrites as hygroscopic in nature, supported by existence of absorption band at higher domain of frequencies.

In ferrites, humidity dependent electrical conduction depends upon the phenomenon of water vapour adsorption based on chemical adsorption (chemisorption), physical adsorption (physisorption) and capillary condensation processes.[44]. It is surface phenomenon. When ferrites are exposed to atmospheric moist air, in the first stage of the interaction a few water vapour molecules are chemically adsorbed (chemisorption) at the neck of the crystalline grains on activated sites of the surface, which is accompanied with a dissociative mechanism of vapour molecules to form hydroxyl groups (two hydroxyl ions per water molecule) as shown in figure 3.B.1. The H^+ ion is referred as proton. As an interaction between the surface ions of the grain necks and the adsorbed water, the hydroxyl group of each water molecule is adsorbed on metal cations, which are present in the grains` surfaces and possess high charge carrier density and strong electrostatic fields, providing mobile protons. The proton transfer takes place. The protons migrate from site to site on the surface. The released H^+ ion immediately combines with another H_2O molecule to form hydronium ion H_3O^+. This transfer mechanism is called Grotthus mechanism and can be illustrated as

$$H_2O = H^+ + OH^-$$

$$H^+ + H_2O = H_3O^+$$

In environment is with low humidity levels, very small amount of water is adsorbed, resulting into hydroxyl ion and proton (hydrogen ion). The proton proceeds by hopping between adjacent hydroxyl ions of the sites, as shown in figure 3.B.1(a). Thus, the electrical conduction favours due of protonic hopping. This protonic conduction exists for low level of humidity. The chemisorbed layer is the first formed layer. So, once it has formed on the surface, it may not be affected further by exposure to humid air.

As a second stage, after completion of chemical adsorption (the first layer), subsequent water vapour layers are physically adsorbed (physisorption) on the first formed hydroxyl layer and results into the stack of physisorbed hydroxyl layers. As water vapour continues to increase on the surface, extra layers form on the first physisorbed layer. Therefore, the physisorption changes from monolayer to multilayer, which result into increase in the concentration of protons and hence increase in the conductivity. During this region of humidity, the dielectric properties become more significant.

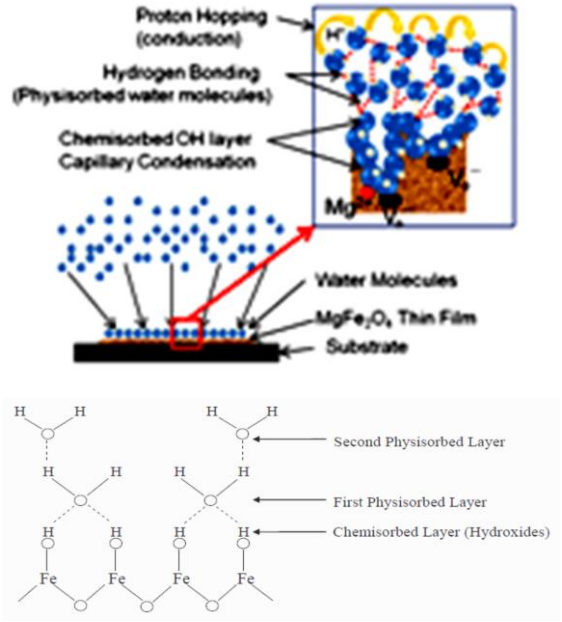

Figure 3.B.1(a and b): Realization of Humidity dependent Electrical Conductivity mechanism

Therefore, the slight variations of conductivity with humidity adsorption can be due to a water protonation and protonic conduction mechanism on the surface. Multilayer formation due to water vapour physisorption can be attributed increase in the conductivity. Figure 3.B.1(b) shows multilayer structure of adsorbed water vapour molecules on the surface of ferrite materials.

The porous structure of ferrites plays a decisive role in the interactions and physisorption of water vapor molecules. The humidity easily adsorbs throughout the open porosities and leads to water condensation within the capillary pores which are distributed between the grains. The water condensation tends to take place on the neck of the pores, and the amount of condensed water is mostly dependent on the pores volume, pore sizes and distributions. If the pore of sufficient size is available, then capillary condensation may takes place. The water condensation occurs in all the pores to form capillaries more easily. This conductivity is called as capillary condensation.

3.B.2 Experimental :

The electrical resistance (R_H) of the compositions of the polycrystalline, $Mg_xZn_{1-x}Fe_2O_4$, $Ni_xZn_{1-x}Fe_2O_4$ and $Mn_xZn_{1-x}Fe_2O_4$ (x= 0.20, 0.40, 0.60 and 0.80) nanoferrites were measured with variable relative humidity in the range from 30%RH to 95%RH. A sophisticated humidity chamber, Gayatri Scientific, Mumbai, having temperature range from 20ºCto 80ºC with 1ºCaccuracy and Humidity range from 30% RH to 95% RH with accuracy of 3% RH, is used to apply variable humidity to the compositions under investigation. The humidity chamber is also facilitated with precise control of the temperature. An experimental arrangement is shown in figure 3.B.2. For realization of humidity sensor, thick films of above compositions are prepared on the substrate, PCB (Epoxy resin with FR4 Standard), in interdigitated form. The photograph of the typical sensor is depicted in figure 3.B.3. The highly precise digital meter, Tektronix Make model DMM4050, 6.5Digit Resolution, Accuracy up to 0.0024%, 10 Ω to 1.2 GΩ Range, with 10 μΩ Resolution, is used for resistance measurement.

Figure 3.B.2: Experimental arrangement for measurement of humidity dependent characteristics of the composition under investigation.

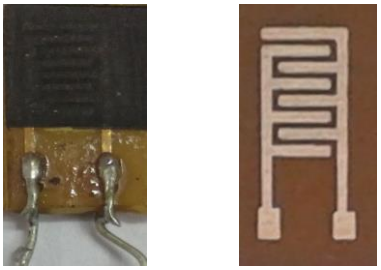

Figure 3.B.3: Photograph of typical humidity sensor wherein interdigitated technique is ensured

As discussed earlier, using screen printing technology, the sensing element, the thick film of the compositions is also deposited on ceramic substrate. The schematic of the sensor is as presented in the figure 3.A.11. This sensor is employed for investigation of humidity dependent electrical properties of the compositions. Humidity dependent capacitance, exhibited by the sensing element, developed by using compositions of polycrystalline nanoferrites, is also measured with variable relative humidity from

30%RH to 95%RH. The Precision LCR meter model TH2816A is used for capacitance measurement.

3.B.3 Results and discussion :

I) Humidity Sensitive Electrical properties of the sensors, developed on epoxy resin substrate:

The Humidity dependent resistance 'R_H', of the thick film sensors, deposited on epoxy resin substrate of FR4 standard is measured with variable relative humidity from 30 % RH to 95%RH. The temperature is controlled at 35 ^{0}C. To interpret humidity dependent conductivity mechanism, the values of resistance 'R_H' in MΩ are plotted against applied relative humidity (%RH) and presented in figures 3.B.4 - 3.B.6, respectively, for the compositions of polycrystalline, $Mg_xZn_{1-x}Fe_2O_4$,$Ni_xZn_{1-x}Fe_2O_4$and $Mn_xZn_{1-x}Fe_2O_4$(x= 0.20, 0.40, 0.60 and 0.80) nanoferrites. From these graphs, it is found that the resistance of the compositions under investigation exponentially decreases with increase in the relative humidity. Such nature of curve of R_H against -H is reported by various researchers for ferrites compositions [64, 65, 68, 69].

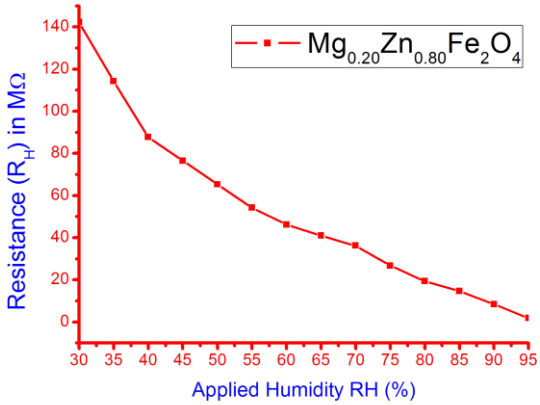

Figure 3.B.4(a): Graph of Humidity dependent resistance R_H against applied relative humidity (%RH) for thick film of Compositions of $Mg_{0.20}Zn_{0.80}Fe_2O_4$nanoferrites deposited on

The compositions of polycrystalline, $Mg_xZn_{1-x}Fe_2O_4$are exposed to the environment of various humidity levels and the values of resistances are recorded with applied humidity at constant temperature of 35 ^{0}C. The graph of humidity dependent resistance R_H plotted against applied humidity is depicted in figure 3.B.4.(a & b). The figure 3.B.4(a) depicts the variation of resistance with humidity for the composition x = 0.20. Moreover, these graphs for compositions x = 0.40, 60 and 0.80 are shown in figure 3.B.4 (b). On inspection of figure 3.B.4(a), it is found that, decrease of resistance R_H within lower level of humidity is more than that of for upper range. During 40 % RH to 70 %RH, the trend of variation in the R_H is deviates from earlier range. Moreover, after 70%RH the resistance significantly decreases with applied RH. Thus, for x = 0.20, the three significant regions are observed. This existence of three regions can be attributed to the conduction mechanism. For lower

humidity level, the conduction in the spinel ferrites is due to protonic hopping [72]. During this region, one chemisorbed layer and few physisorbed layers may be formed. Moreover, this protonic conduction mechanism becomes more favorable for increase in the water vapor. This can be attributed to the formation of multiple physisorbed layers of hydroxyl ions. It is known that, the electrical conductivity is mostly sensitive to the porosity. The compositions depicts existence of inter granular pores. Therefore, the water molecule may be trapped at the neck of the pores. This favors the conduction process and results into decrease in the resistance R_H for high humidity level. The behaviour of humidity dependent resistance for the composition x = 040, 0.60 and 0.80 is depicted in figure 3.B.4(b). The graphs depict exponential decrease in the resistance with increase humidity. On close inspection of these graphs, it is found that, the resistance R_H-H curves show two regions. As discussed earlier, these regions can be attributed to the protonic conduction mechanism. Moreover, the composition for x = 0.80 shows drastic decrease in the resistance with increase in the humidity. This may due existence of capillary condensation of water molecules in to the pores [73]. From figure 3.B.4 a & b, it is also observed that, the resistance of composition for x = 0.20 is significantly high than that of other members of the series. The same observations are also recorded during temperature dependent electrical studies. The composition for x = 0.20 is zinc rich composition. The zinc ion prefers to reside on A sites and does not participate into conduction. Therefore, the zinc compositions are exhibiting more resistance. The compositions exhibit reproducible relation with applied humidity and therefore, these are most suitable to develop humidity sensor. The above characteristics are primarily considered for developing electronic part of the module and while designing of the necessary firmware as well.

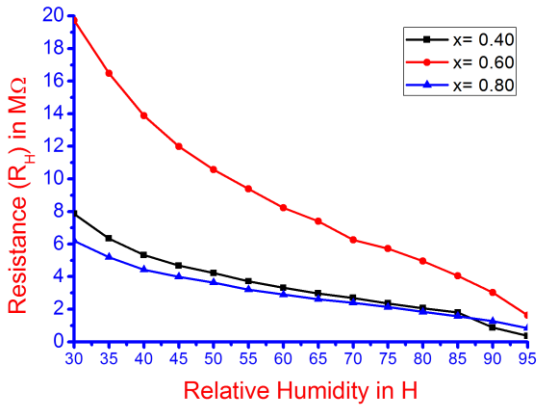

Figure 3.B.4(b): Graph of Humidity dependent resistance R_H against applied relative humidity (%RH) for thick film of Compositions of $Mg_xZn_{1-x}Fe_2O_4$nanoferrites deposited on epoxy resign

Similarly, thick films, sensing element, of compositions of $Ni_xZn_{1-x}Fe_2O_4$ ferrites, deposited on epoxy resin substrate, are also exposed to the environment of variable humidity using sophisticated humidity chamber. The humidity dependent values of R_H are recorded with increasing humidity (RH) and graph of R_H plotted against relative humidity RH is presented in figure 3.B.5 (a & b). The graph of R_H against RH for x = 0.20 is presented in figure 3.B.5(a). This graph also shows the existence of three regions of conductivity, which may attributed to the conduction mechanism. Such three regions in resistance (R_H) –Humidity (%RH) curve for MgZn ferrite is also reported by Gumano et al [74]. Lower region of the humidity is attributed to the proton hopping conduction mechanism. For higher humidity level, the decrease in the resistance value is significantly more than that of lower level. This may be due to either trapping of water molecules in the pores or due to the capillary condensation of water molecules or both. The variation of resistance due to applied humidity for compositions x = 0.40 and 0.60, 3.B.5.b, also shows the exponential variation. It was also studied for hysteresis effect to the applied humidity. The compositions for x = 0.40 and 0.60 show, low hysteresis effect. Hence, these sensors are more suitable for implementation to design smart sensor module.

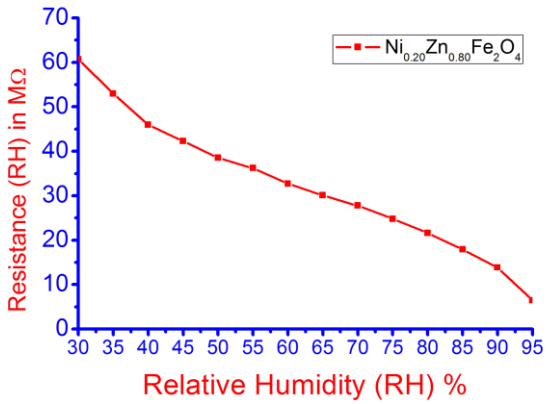

Figure 3.B.5(a): Graph of Humidity dependent resistance R_H against applied relative humidity (%RH) for thick film of Compositions of $Ni_{0.20}Zn_{0.80}Fe_2O_4$nanoferrites deposited on epoxy resign

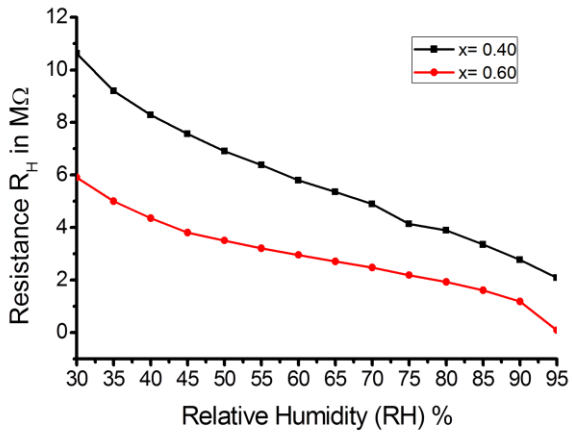

Figure 3.B.5(b): Graph of Humidity dependent resistance R_H against applied relative humidity (%RH) for thick film of Compositions of $Ni_xZn_{1-x}Fe_2O_4$nanoferrites deposited on epoxy resign

The thick films of compositions of $Mn_xZn_{1-x}Fe_2O_4$ ferrites, deposited on epoxy resin substrate, are used for investigation of humidity sensitive properties. The humidity dependent resistance values are measured against applied humidity in % RH and the data obtained are availed to predict the suitability of the materials for development of sensors. The humidity dependent values of R_H are recorded with increasing humidity (RH) from 30 %RH to 95%RH and graph of R_H plotted against relative humidity RH is presented in figure 3.B.6. On inspection of the figure 3.B.6, it is cleared that, the composition of MnZn ferrites are most suitable for development of humidity sensor. The graph of resistance of the film plotted against the relative humidity exhibit exponential behavior. Moreover, the resistance values recorded for lower humidity is less than 200 MΩ for thick films under investigation. The uniform and smooth decrease in the resistance proves its suitability for interfacing of the device to the electronic circuit, which also helps to calibrate the the sensor module. From this investigation, it is confirmed that the compositions are suitable of development of the sensor.

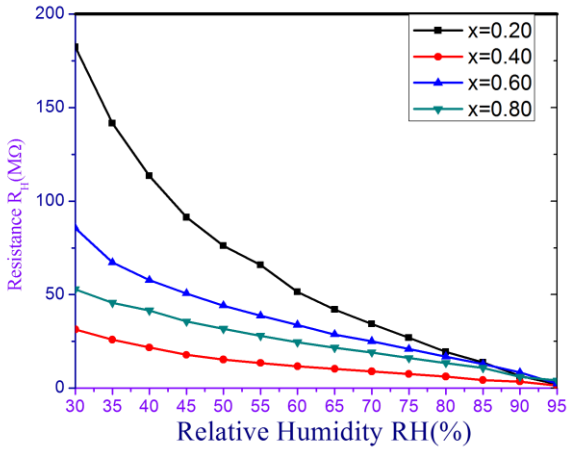

Figure 3.B.6: Graph of Humidity dependent resistance R_H against applied relative humidity (%RH) for thick film of Compositions of $Mn_xZn_{1-x}Fe_2O_4$nanoferrites deposited on epoxy resign

The study of Relative Deviation in the Resistance, RDR, (ΔR_H), of the samples under investigation, are also determined by employing the expression

$$\Delta R_H = \frac{R_{1H} - R_H}{R_{1H}} \times 100\ \% \qquad (4)$$

where, R_{1H} is the resistance of the sample measure at lower humidity (RH = 30%RH) and R_H is the resistance of the composition at any humidity in RH%. The Values of ΔRH are estimated for entire range of investigation and plotted against applied humidity (%RH). The Graph of Relative Deviation in the Resistance (RDR) against humidity, are depicted in figure 3.B.7 – 3.B.9, respectively for three series, $Mg_xZn_{1-x}Fe_2O_4$, Ni_xZn_{1-}

$_xFe_2O_4$ and $Mn_xZn_{1-x}Fe_2O_4$nanoferrites. From these graphs, it can be said that, the values of RDR increases with increase in the humidity.

The values of Relative Deviation in the Resistance (RDR) are calculated from humidity dependent resistance data, for the thick film sensor deposited on epoxy resin, for compositions of $Mg_xZn_{1-x}Fe_2O_4$nanoferrites and the graphs of RDR against RH are presented in the figure 3.B.7. The figure 3.B.7 shows two significant regions. Within humidity range from 30 % RH to 40 %RH the graph is almost linear with intensive slope. Moreover, from 40%RH onwards the graph changes its slope. This can be attributed to the sensitivity of the compositions to the humidity.

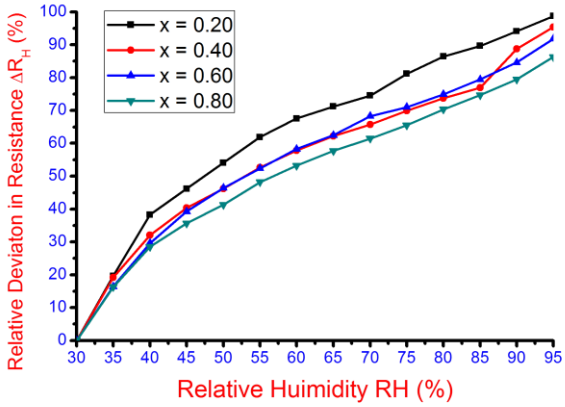

Figure 3.B.7: Graph of Relative Deviation in Resistance (ΔR_H) against applied relative humidity (%RH) for thick film of Compositions of $Mg_xZn_{1-x}Fe_2O_4$ nanoferrites deposited on epoxy resign.

The Humidity Sensitivity (S_H) is defined as the change in the resistance of the sample per unit change in the applied relative humidity. It can be expressed as

$$S_H = \frac{\Delta R}{\Delta RH} \qquad (5)$$

Where, S_H is the humidity sensitivity in MΩ/%RH, ΔR is the change in the resistance within the range ΔRH. The Humidity Sensitivity for the sensors is determined for different ranges and values of S_H are presented in Table 3.B.1. From inspection of the table, it found the Humidity sensitivity (S_H) of the samples for range from 30 to 40 %RH is high. This is also supported by the

TABLE 3.B.1: Humidity sensitivity SH for different ranges of humidity for the samples of $Mg_xZn_{1-x}Fe_2O_4$ ferrites

Humidity Range (%RH)	**Humidity Sensitivity (ΔR/ΔH) (MΩ/%RH) for the composition for**			
	x = 0.20	**x = 0.40**	**x = 0.60**	**x = 0.80**
30-40	5.32	0.20	0.52	0.15
40-50	2.25	0.09	0.28	0.07
50-60	1.60	0.08	0.23	0.06
60-70	0.95	0.06	0.23	0.05
70-80	1.49	0.06	0.15	0.06
80-90	1.27	0.19	0.20	0.06

graph of RDR. The humidity sensitivity after 40RH% is small. However, it depicts uniform distribution for entire range of investigation. The table 3.B.1 also depicts that the Humidity sensitivity is also compositional dependent. Such variation in the humidity sensitivity is also reported by Gumano et al [74]. Therefore, the present sensors can suitably be deployed for further development of the electronic part. The average values of Humidity sensitivities (in MΩ/%RH), determined over the range of relative humidity RH from 40% RH to 95%RH, are 1.51, 0.10, 0.22 and 0.06 for x = 0.20, 0.40, 0.60 and 0.80, respectively.

Moreover, the values of RDR are estimated for the composition of $Ni_xZn_{1-x}Fe_2O_4$ ferrites are estimated by using expression 4 and plotted against applied relative humidity RH. The graphs of RDR against RH, shown in figure 3.B.8, reveal the effect of conduction mechanism on RDR values. Within the range from 30%RH to about 40%RH the trend of RDR variation is almost linear. Variation in the R_H-RH is also reflected in the variation the RDR-RH curve. Moreover, sudden increase in the RDR above 90% RH may be attributed to the sudden decrease in the resistance due to condensation of water molecule at the neck of the pores, which ensures the capillary conduction due high humidity.

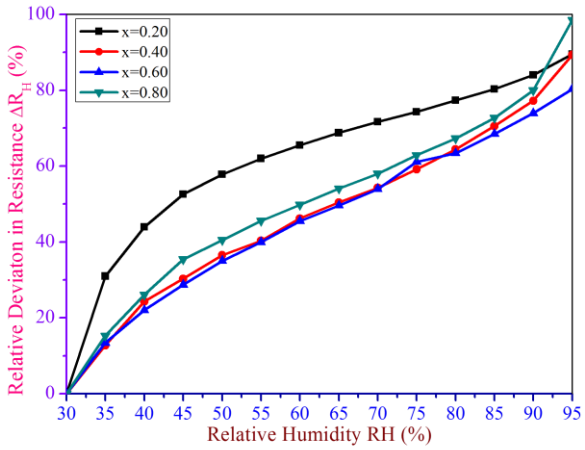

Figure 3.B.8: Graph of Relative Deviation in Resistance (ΔR_H) against applied relative humidity (%RH) for thick film of Compositions of $Ni_xZn_{1-x}Fe_2O_4$nanoferrites deposited on epoxy resign.

The values of Humidity sensitivities are estimated by employing expression 5 and tabulated in Table 3.B.2. The table shows that, the S_H is

TABLE 3.B.2: Humidity sensitivity SH for different ranges of humidity for the samples of $Ni_xZn_{1-x}Fe_2O_4$ ferrites

Humidity Range (%RH)	Humidity Sensitivity (ΔR/ΔH) (MΩ/%RH) for the composition for			
	x = 0.20	x = 0.40	x = 0.60	x = 0.80
30-40	1.40	0.18	0.13	0.36
40-50	0.76	0.13	0.06	0.15
50-60	0.71	0.12	0.05	0.10
60-70	0.46	0.10	0.05	0.08
70-80	0.64	0.05	0.05	0.09
80-90	0.81	0.12	0.09	0.11

high for lower range of humidity. However, the trend of variation of SH for higher humidity ranges is uniform. An average humidity sensitivity S_H (in MΩ/%RH) for the composition for x = 0.20 (Average S_H= 0.80) is high in comparison with that of other members of the series (Average S_H= 0.12, 0.07 and 0.15 for x= 0.40, 0.60 and 0.80). This can be assigned with high resistivity of the composition, resulted due to porosity. This realizes the fact that, the humidity characteristics of the samples significantly depends upon microstructure of the same. Thus, availing this data the suitability of the composition for sensor development can be predicted.

Similarly, in order to explore further details regarding characteristics of materials for humidity, the values of Relative Deviation in Resistance (RDR) are estimated by using equation 4 for thick film sensing element of $Mn_xZn_{1-x}Fe_2O_4$ ferrites and plotted against RH. The graphs of RDR against RH are depicted in figure 3.B.9. As expected the values of RDR becomes significantly high for higher range of the humidity. This can be attributed to the conduction mechanism, wherein formation of multiple physisorbed layers is ensured. The increase in the concentration of protons hoping between neighbouring hydroxide groups results into increase in the conductivity. From this graph, it can be concluded that, the sensors of MnZn ferrites are suitable for interfacing to the electronic circuit to realize embedded technology based sensor module design. The Humidity Sensitivities are calculated from resistance data,

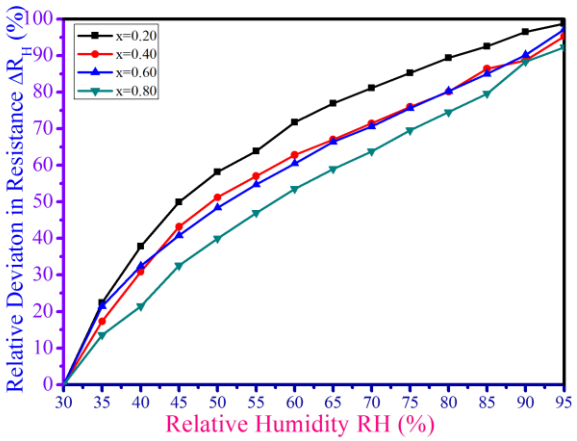

Figure 3.B.9: Graph of Relative Deviation in Resistance (ΔR_H) against applied relative humidity (%RH) for thick film of Compositions of $Mn_xZn_{1-x}Fe_2O_4$nanoferrites deposited on epoxy resign.

TABLE 3.B.3: Humidity sensitivity SH for different ranges of humidity for the samples of $Mn_xZn_{1-x}Fe_2O_4$ ferrites

Humidity Range (%RH)	**Humidity Sensitivity (ΔR/ΔH) (MΩ/%RH) for the composition for**			
	x = 0.20	**x = 0.40**	**x = 0.60**	**x = 0.80**
30-40	5.63	0.85	1.88	0.83
40-50	3.02	0.51	1.30	0.78
50-60	2.89	0.37	0.99	0.69
60-70	1.55	0.28	0.72	0.51
70-80	1.51	0.26	0.80	0.52
80-90	1.44	0.14	0.89	0.93

employing expression 5 and presented in Table 3.B.3. From this table, it is found that, Humidity Sensitivities (S_H) of the compositions for lower range of humidity (30 %RH to 40%RH) is high for all samples. This can be attributed to the protonic conductivity. The compositional dependence of S_H values helps to predict about suitability of the sensors. The values of average Humidity sensitivities (in MΩ/%RH), averaged over the range from 40%RH to 95%RH, are 2.08, 0.31, 0.94 and 0.69 for respective samples.

II) Humidity Sensitive Electrical properties of the sensors, developed on Ceramic substrate:

To keep pace with the objectives of the present research work, wherein implementation of sensors to design sensor module is emphasized, the sensors are also fabricated by deposition of the thick film, as a sensing element, using printing technology, of the compositions, on the ceramic substrate. The ceramic substrate of ultra high resistivity and good thermal conductivity is used. Moreover, this substrate is insensitive to the humidity. The rectangular surface between two electrodes, the sensing elements, is exposed to the humidity. As discussed earlier, a sophisticated humidity chamber is used to apply humidity in controlled manner. The highly precise digital meter, Tektronix Make model DMM4050, 6.5Digit Resolution, Accuracy up to 0.0024%, 10 Ω to 1.2 GΩ Range, with 10 μΩ Resolution, is used for humidity dependent resistance measurement.

The humidity dependent resistance (R_H) of the Thick Film Sensor (TFS), wherein the thick film of compositions of $Mg_xZn_{1-x}Fe_2O_4$nanoferrites is deposited, is measured for Relative Humidity (RH) within the range from 30%RH to 95%RH. The values of R_H, in MΩ, are plotted against relative humidity (%RH) and presented in the figure 3.B.10. On investigation of the figure 3.B.10, it is found that, the resistance of the sample (TFS) exponentially varies with applied

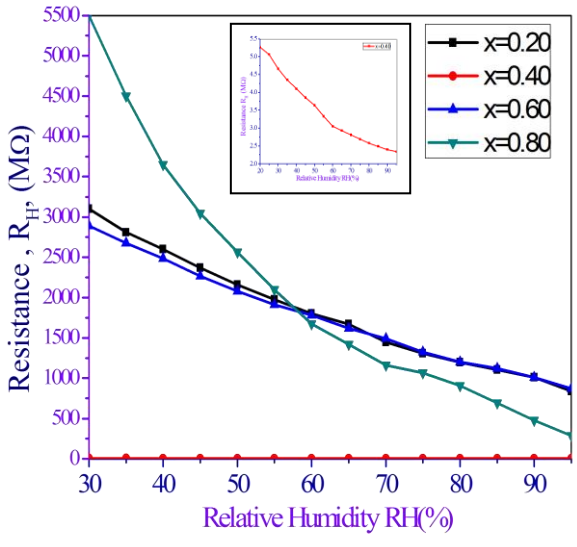

Figure 3.B.10: Graph of Resistance (R_H) against applied relative humidity (%RH) for thick film of compositions of $Mg_xZn_{1-x}Fe_2O_4$nanoferrites deposited on ceramic substrate

relative humidity (%RH). The graphs reveal two regions, which can be attributed to the conduction mechanism, wherein the principles of chemisorption and physisorption of the water molecules on the crystallite sites are ensured. As shown in the figure 3.B.10, the ambient resistance of the sample for x = 0.40 is very small as compared to the other members. Therefore, the graph plotted this composition is expanded and shown in the said figure. The resistances of the sensing element at humidity about 30%RH for x= 0.20, 0.60 and 0.80 are substantially high, whereas that of x = 0.40 is about 5.5MΩ. Moreover, the trend of variation is almost similar. Since, the resistance of the sensing element for 0.20, 0.60 and 0.80 are high, the impedance matching becomes difficult. This may adversely affect on the performance of the sensor module. Therefore, it is attempted to deploy the sensing element developed by using ferrites composition of x = 0.40.

The Relative Deviation in the Resistance (RDR), (Eq. 4), is obtained from R_H-RH data and plotted against relative humidity from 30%RH to 95%RH. The graphs of RDR against RH for all compositions are shown in figure 3.B.11. On observation of the figure 3.B.11, it is noticed that, the values of RDR (%) increases with increase in the relative humidity. Within the range of investigation, the variation in RDR is wide (up to 80% to the initial value) for samples except x = 0.40. For x = 0.40 the deviation is very narrow and linear. This may be due to the resistance of the sensor observed at ambient conditions. The RDR for sensing elements developed by using MgZn ferrites for x = 0.20, 0.60 and 0.80 is high. This may causes to increase the sensitivity of the sensor. However, the resistances of these sensors are very high and therefore difficult to ensure the interfacing. The Humidity sensitivity S_H is calculated by employing expression 5 and presented in table 3.B.4. On inspection of table 3.B.4, it is found that, humidity sensitivity of the compositions for x = 0.20 and 0.80 is substantially high than that of x

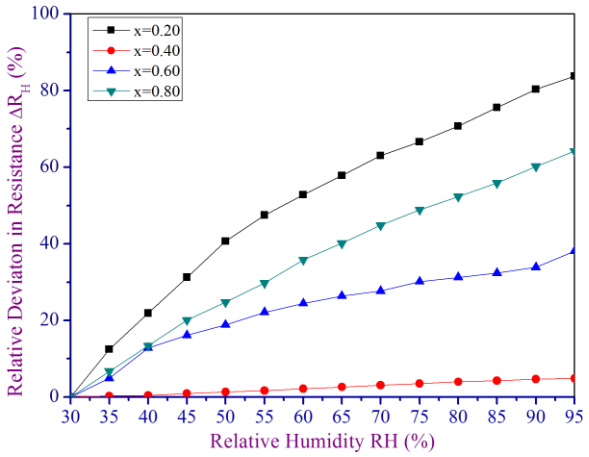

Figure 3.B.11: Graph of Relative Deviation in Resistance (RDR) against applied relative humidity (%RH) for thick film of compositions of $Mg_xZn_{1-x}Fe_2O_4$nanoferrites deposited on ceramic substrate

= 0.40 and 0.60. This may be due to resistance of the sensing element observed at ambient conditions. This data about humidity sensitivity of the sensing element and resistance at ambient conditions are most useful for designing of an analog part of the electronic circuit.

TABLE 3.B.4 : Humidity sensitivity S_H for different ranges of humidity for the samples of $MgZn_{1-x}Fe_2O_4$ ferrites

Humidity Range (%RH)	Humidity Sensitivity (ΔR/ΔH) (MΩ/%RH) for the composition for			
	x = 0.20	x = 0.40	x = 0.60	x = 0.80
30-40	60.00	0.08	16.80	40.00
40-50	60.00	0.09	5.80	28.00
50-60	34.00	0.10	5.00	36.00
60-70	33.40	0.11	2.80	28.00
70-80	26.20	0.11	2.40	20.60
80-90	30.60	0.09	3.20	26.00

Further, the thick film sensors (TFS) are developed by depositing thick film of compositions of $Ni_xZn_{1-x}Fe_2O_4$nanoferrites on ceramic substrates and deployed for investigation of their humidity dependent characteristics. The humidity dependent resistance (R_H) of the sensing element developed on ceramic substrate is measured with variable Relative Humidity (%RH) within the range from 30%RH to 95%RH. The values of R_H, in MΩ, are plotted against RH (%) and presented in the figure 3.B.12. Moreover, the values of relative deviation in resistance (RDR), in %, is calculated for all compositions by using expression 4 and plotted against relative humidity (%RH). The graphs of RDR against RH are presented in figure 3.B.13. From inspection of figure 3.B.13, it is found that, the RDR values of the sensing element, developed by employing compositions of x = 0.20 and 0.60, show almost linear behaviour for entire range of investigation. This supports the applicability of the present sensor for development of sensor unit. This nature of the graph simplifies the process of calibration, discussed in topic 5. The Humidity sensitivities, S_H, are obtained from R_H data for various ranges relative humidity and presented in the table

TABLE 3.B.5 : Humidity sensitivity S_H for different ranges of humidity for the samples of $Ni_xZn_{1-x}Fe_2O_4$ ferrites

Humidity Range (%RH)	Humidity Sensitivity (ΔR/ΔH) (MΩ/%RH) for the composition for			
	x = 0.20	x = 0.40	x = 0.60	x = 0.80
30-40	42.00	0.050	38.00	170.00
40-50	42.00	0.042	37.00	96.00
50-60	35.00	0.056	26.00	85.00
60-70	44.00	0.024	26.00	51.80
70-80	23.00	0.022	24.40	32.00
80-90	19.20	0.018	22.40	42.60

3.B.5. The table reveals the compositional dependence of the sensitivity. The value can be attributed to the resistance level at ambient conditions. The sensitivity of sensing element for x = 0.40 is less. However, the ambient resistance of the sample is less. Therefore, it is highly suitable for interfacing to the analog circuit, wherein impedance matching will be realized [75].

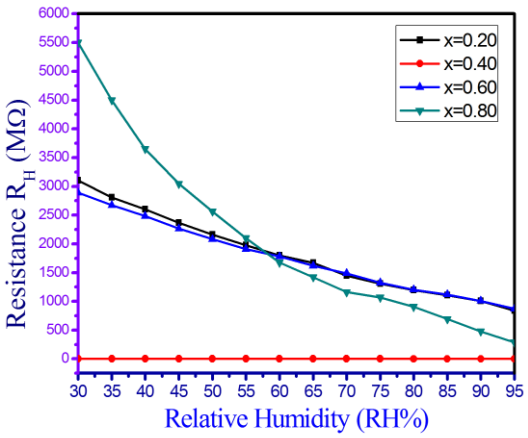

Figure 3.B.12: Graph of Resistance (R_H) against applied relative humidity (%RH) for thick film of compositions of $Ni_xZn_{1-x}Fe_2O_4$nanoferrites deposited on ceramic substrate

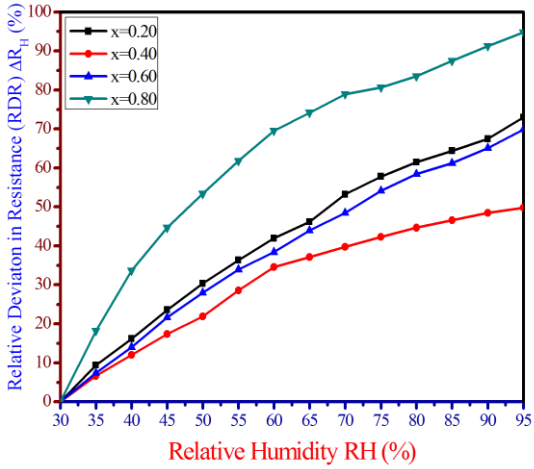

Figure 3.B.13: Graph of Relative Deviation in Resistance (RDR) against applied relative humidity (%RH) for thick film of compositions of $NI_xZn_{1-x}Fe_2O_4$nanoferrites deposited on ceramic

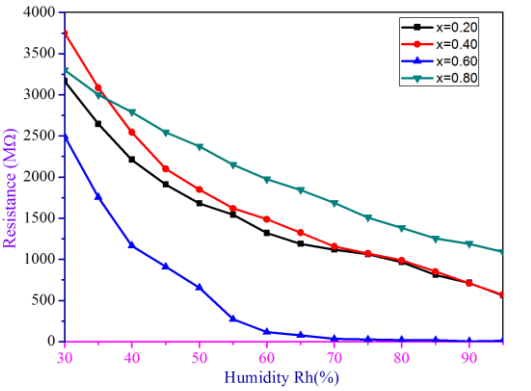

Figure 3.B.14: Graph of Resistance (R_H) against applied relative humidity (%RH) for thick film of compositions of $Mn_xZn_{1-x}Fe_2O_4$nanoferrites deposited on ceramic substrate

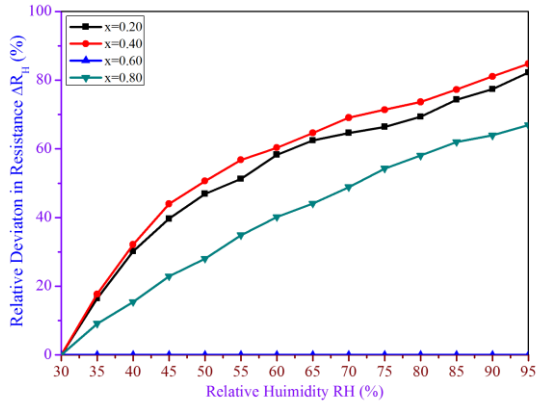

Figure 3.B.15: Graph of Relative Deviation in Resistance (RDR) against applied relative humidity (%RH) for thick film of compositions of $Mn_xZn_{1-x}Fe_2O_4$nanoferrites deposited on ceramic substrate

The sensors are also prepared by depositing the thick film of the compositions $Mn_xZn_{1-x}Fe_2O_4$ ferrites, as a sensing element, on ceramic substrate. The schematic of the sensor is presented in figure 3.A.11. These thick film sensors, TFS, are used to explore the behaviour with relative humidity. The humidity dependent resistance of the sensing element (R_H) is measured with application of relative humidity within the range from 30%RH to 95%RH. To study the behavior at a glance, the R_H values, for all sensors, are plotted against relative humidity and presented in figure 3.B.14. Similar to the response of interdigitated thick films, developed on epoxy resin, the present sensor, developed on ceramic substrate, shows exponential relation with relative humidity. The nature of the graph can be attributed to the existence of protonic conduction mechanism. Köseo_glu et al have studied MnZn ferrites for humidity and reported exponential variation in the R_H values [68]. The slope of graph of logR against applied humidity is named as sensitivity. As shown in figure 3.B.14, the R_H for x = 0.60 exhibit sudden drop at and above 60 %RH. This may be due to existence of capillary condensation of water. Within this region conduction may be due to both proton hopping and capillary condensation of water molecules. The values of relative deviation in the resistance RDR are obtained from R_H-RH data. Figure 3.B.15 shows the response of RDR with relative humidity. The nature of graph helps to calibrate the sensor module for humidity measurement. Employing method described earlier, the Humidity sensitivity, S_H, values are estimated from the expression 5 for different ranges of the humidity. The S_H values are presented in table 3.B.6. The table depicts compositional dependence of the humidity sensitivity. This data is used to design an analog part of the electronic circuit and its calibration.

TABLE 3.B.6: Humidity sensitivity S_H for different ranges of humidity for the samples of $Mn_xZn_{1-x}Fe_2O_4$ ferrites

Humidity Range (%RH)	**Humidity Sensitivity (ΔR/ΔH) (MΩ/%RH) for the composition for**			
	x = 0.20	**x = 0.40**	**x = 0.60**	**x = 0.80**
30-40	87.00	108.00	117.60	41.40
40-50	46.00	50.00	50.80	34.00
50-60	44.40	26.60	31.20	35.00
60-70	14.00	33.40	8.40	31.60
70-80	18.80	16.80	1.08	25.20
80-90	19.40	28.60	2.80	12.60

III) Humidity Sensitive Dielectric properties:

In fact, in case of ferrite materials, conductivity mechanism for humidity realizes the formation of chemisorbed layer with ions of crystal sites. Moreover, due to increase in the humidity level, multiple physisorbed layers are formed. Formation of these layers may results into formation of the dipoles, which exhibit dielectric properties. Emphasizing this behaviour of ferrites, the researchers have investigated the humidity dependent dielectric properties of the materials under investigation [77-78]. Capacitance of the sensing element, TFS, deposited on epoxy resin substrate, is

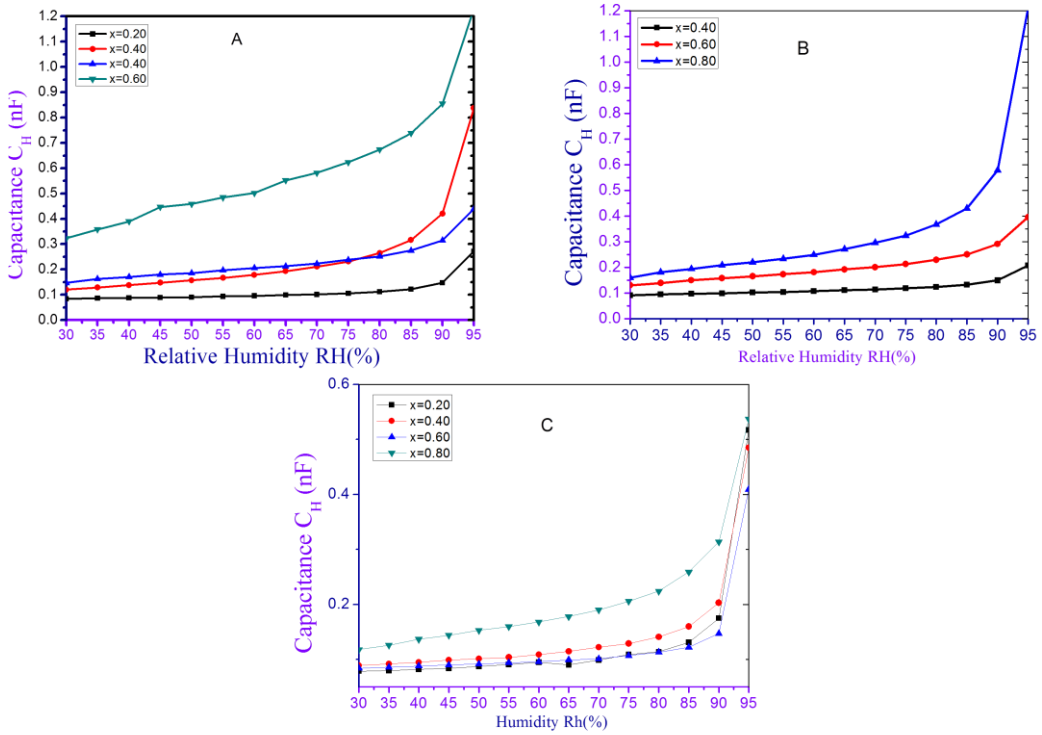

Figure 3.B.16: Graph of Capacitance (C_H) against applied relative humidity (%RH) for thick film of compositions of nanoferrites, (A) $Mg_xZn_{1-x}Fe_2O_4$, (B) $Ni_xZn_{1-x}Fe_2O_4$and (C) $Mn_xZn_{1-x}Fe_2O_4$deposited on epoxy resin

measured against relative humidity within the range from 30 % RH to 95 %RH at frequency 100Hz. The capacitance values are plotted against relative humidity and depicted in figure 3.B. 16. On inspection of figure 3.B.16, it is found that, the humidity of the environment plays significant role on the capacitance of the sensing element. On increase in the concentration of water molecules, the concentration of charge carriers, the protons, increases, which results into increase in the dielectric constant and hence capacitance of the sensing element. At elevated humidity, the value of capacitance significantly increases. This can be attributed to the conduction mechanism, wherein both capillary condensation and protonic conduction are ensured.

Thus, compositions under investigation are also suitable for development of capacitive sensors. However, for present development, only resistive sensors are developed and implemented.

IV) Timing Characteristics:

A sensor, once developed, should be studied for its timing parameters. Two parameters, response time (T_{RES}) and recovery time (T_{REC}) play significant role on features of the sensors [65]. The time response of a sensor can vary from seconds to minutes and it is of great interest to determine it [76, 79, 80, 81]. Therefore, these parameters for the sensors under investigation are measured and presented in table 3.B.7. The time response of the samples to RH% was determined by inserting the samples into the humidity chamber at the different settings and the time required for the sensing element to sense the correct RH% is recorded. Initially, the appropriate time was allowed for the chamber to reach equilibrium. A Pulse of relative humidity 90%RH is applied for about 120 sec to the sensing element, deposited on ceramic substrate, and the values of humidity dependent resistance (R_H) against time, in second, are recorded. From these observations, the response time (T_{RES}) and recovery time (T_{REC}) are estimated. The schematic of the measurement is depicted in figure 3.B.17. The response time (T_{RES}) is time required to decrease the resistance up to 37% of ambient resistance R_{1H}. The recovery time (T_{REC}) is time required for increase the resistance up to ambient resistance. These timing parameters have been measured, for all sensing elements of the ferrite composition under investigation, developed on ceramic substrate. Table 3.B.7 presents the values of timing parameters.

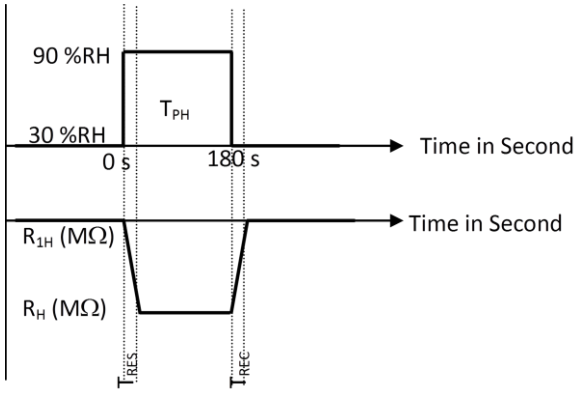

Figure : 3.B.17: Realization of Response and recovery timing

TABLE 3.B.7: Response time (T_{RES}) and Recovery time (T_{REC}) for sensing elements of ferrite compositions for 90 %RH.

Conc. x	$Mg_xZn_{1-x}Fe_2O_4$		$Ni_xZn_{1-x}Fe_2O_4$		$Mn_xZn_{1-x}Fe_2O_4$	
	Response Time (T_{RES}) in Sec	Recovery Time (T_{REC}) in Sec	Response Time (T_{RES}) in Sec	Recovery Time (T_{REC}) in Sec	Response Time (T_{RES}) in Sec	Recovery Time (T_{REC}) in Sec
0.20	9	7	10	5	10	5
0.40	13	9	31	14	11	8
0.60	13	7	10	7	12	9
0.80	12	7	14	6	9	7

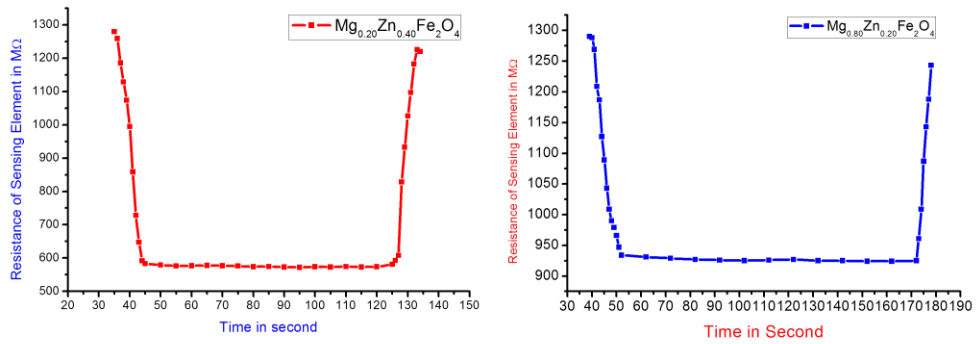

Figure 3.B.18: Timing Response of the compositions of $Mg_xZn_{1-x}Fe_2O_4$ ferrite thick film deposited on ceramic substrate typically for x = 0.20 and 0.80.

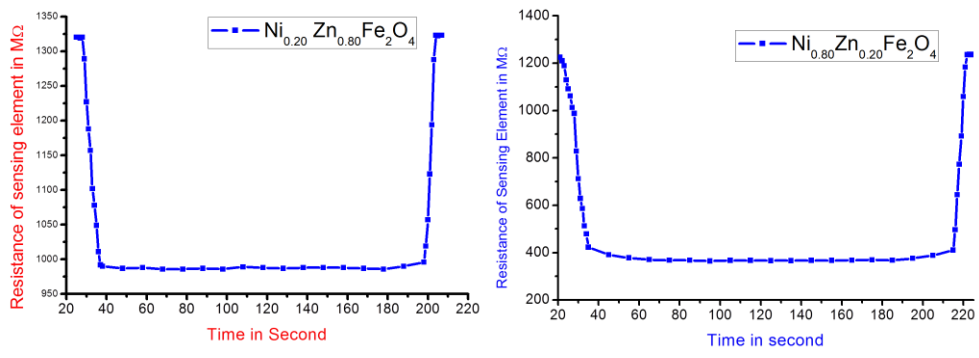

Figure 3.B.19: Timing Response of the compositions of$Ni_xZn_{1-x}Fe_2O_4$ ferrite thick film deposited on ceramic substrate typically for x = 0.20 and 0.80.

The instantaneous values of resistance (R_H) of the sensing element are recorded for the compositions under investigation and plotted against time. Figure 3.B.18, 19 and 20 show the response of the sensor with time. As discussed earlier, the pulse of humidity of variable duration is applied. On application of pulse the resistance starts

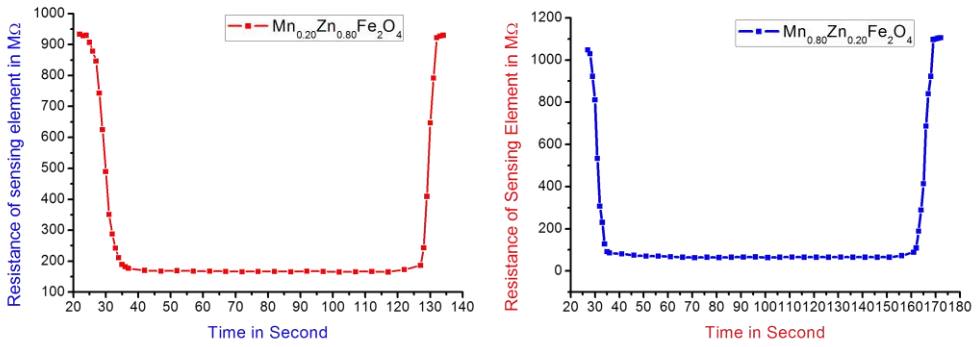

Figure 3.B.20: Timing Response of the compositions of$Mn_xZn_{1-x}Fe_2O_4$ ferrite thick film deposited on ceramic substrate typically for x = 0.20 and 0.80.

rapidly decreasing and reaches to its minimum value. The minimum and maximum value of resistance depends upon concentration of applied humidity. After pre-determined time the sensing element is suddenly exposed to the normal environment. The resistance rapidly increases [Figure 3.B.18-20]. Using these graphs the response timing are measured and presented in table 3.B.7. On inspection of table 3.B.7, it is found that, both Response time (T_{RES}) and Recovery time (T_{REC}) are very small. This supports the conclusion, that present sensor are very fast sensor. Table 3.B.7, shows that, the response times are ranging from 13 second to 5 second, depending upon the compositions of sensing materials. This data is obtained at 90% RH relative humidity, which is near to the saturation limit.

It was also found that, the response time depends upon the level of applied humidity. Therefore, in addition to present response timings for full scale limit, the instantaneous values of response timing are also determined at various points. It was found that, for 10% RH variation, the response time is less than 1 second. This supports the statement that, the humidity sensor developed by employing compositions of ferrite on ceramic substrate are very fast and hence it can be implemented to develop Smart Sensor Module of Promising features.

3.B.4 Conclusion:

Emphasizing adsorption and absorption sensitive electrical properties of polycrystalline ferrites, the electrical resistance (RH) of the compositions $Mg_xZn_{1-x}Fe_2O_4$, $Ni_xZn_{1-x}Fe_2O_4$ and $Mn_xZn_{1-x}Fe_2O_4$ nanoferrites have been investigated. The sensing element is fabricated by developing thick film of the materials on the substrate such as epoxy resin, glass and ceramic substrate. The compositions show decrease in the resistance with increase in the relative humidity. The natures of the graphs are attributed to existence of conducting mechanism, wherein the protonic conductivity is realized. At elevated relative humidity level, the conductivity may due to capillary condensation in to the pores of sufficient size. The relative deviation in the resistance values and humidity sensitivity are also studied. On investigation of results obtained, it is confirmed that, the sensor developed on ceramic substrate are most suitable for deployment of the same to design the Smart Sensor Module. The timing response data reveal the fact that, present sensor are fast sensor, which help to enhance the features of SSM.

3.C. Gas Sensing Properties

3.C.1 Introduction:

During recent days, due to progressively increasing atmospheric pollution, the detection and quantification of the various gases, is the need of hour. To cater this need an electronic system of great preciseness, wherein promisingly featured sensors are deployed, is required. However, the cost of such sensors and hence entire systems is unaffordable. Therefore, the research is going on in the development of the sensing materials to fabricate the gas sensor of good quality. While synthesizing the sensor materials, the design requirements of electronic systems are also considered. Several kinds of gas sensors have been developed based of different kinds of materials such as zinc oxides, tin oxides, tungsten oxides etc [82]. However, chemiresistive semiconducting oxides, such as polycrystalline spinel nanoferrites, are potential candidates due to their salient features such as very low cost, high sensitivity, fast response and recovery time, simple electronic interface, wide ranges of compositions, high selectivity etc. Therefore, the researchers are showing interest in synthesizing the polycrystalline ferrite based gas sensitive materials [83]. The ferrite materials of nanostructure exhibit nano particles and very small grains with uniform grain distribution. This leads to increase in the effective surface area. The gas sensing properties are mostly based on the surface phenomenon such as chemisorption and physisorption. The surface of ferrite materials at typical operating temperature reveals chemisorption of the oxygen species needed for physisorption of oxidizing or reducing gases [84]. Therefore, these materials are suitable for gas sensing applications. The characteristics of the sensing materials can be optimized by controlled preparation conditions, chemical compositions, doping of catalytic element etc. Therefore, the features of the sensors can be suitably improved. The responses of the sensing element, developed by using nanoferrites is significantly depend upon the size and shape of the film and operating temperature as well [85].

Emphasizing the development sensor module, wherein embedded philosophy is realized, the polycrystalline ferrite based sensing materials are synthesized and studied for their gas sensing properties. The results of the investigation are interpreted in this section.

a) Review of the Literature :

Deploying fundamental principle of electrical conduction, the MgMn ferrite of nanocrystallite is synthesized by Iftimie et al and investigated the gas sensing properties of the same [86, 87]. They studied the response of Mg $Mn_{0.2}Fe_{1.8}O_4$ ferrites for the gases such as LPG, ethyl alcohol, formaldehyde, methane ammonia etc and reported that, the composition is most sensitive for LPG at temperature about 450^0C [86]. The gas sensing properties of polycrystalline Cu, Cd substituted Zn ferrites are investigated by Rezlescu et al [88] and reported that the Zinc ferrite is suitable for ethanol detection. They showed that, the sensitivity of the compositions is temperature dependent. They reported the optimum sensitivity at temperature about 350^0C. They used pelletized samples and results regarding gas sensitivity are attributed to the microstructure of the compositions. However, the sensitivity of the compositions is good at higher temperatures. The operating temperature must be suitably low. The gas sensing properties of nanostructured thin films of copper ferrites have been investigated by Chapelle et al [89]. They showed that these ferrite compositions reveal good sensitivity to the hydrogen gas. They observed maximum sensitivity at temperature about 280^0C. They found increase in the resistance of the film due to presence of the H_2 gas. This may be attributed to the fact that, the H_2 gas undergoes reduction on reaction with chemisorbed layer of oxygen at lattice sites [90, 91]. The ceramic materials like ferrites are mostly sensitive to the reducing gases. Emphasizing this nature, the gas sensing properties of Lanthanum ferrites were investigated by Kong and Shen [92] and reported increase of resistance of the sensing element due to existence of the reducing gas. The suitability of semiconducting metal oxides as sensors for environmentally hazardous gases is reviewed by Wetchakan et al [93]. The response of the sensor is mostly sensitive to the reduction-oxidation reaction with the surface of the sensing material under investigation. The conductance response of the nano crystalline $MgFe_2O_4$thick films were measured by exposing the films to the reducing gases like methane (CH_4), H_2S, LPG, ethanol (C_2H_5OH) by Liu et al [94]. They reported that the magnesium ferrites exhibit good sensitivity to the H_2S and ethanol. It was also reported that, the zinc ferrites show significant response to the H_2S gas [95]. Gopal Reddy et al, have synthesized nickel ferrite by using co-precipitation method and investigated the response of the nickel ferrite for various gases [96]. They reported that the Nickel ferrite is most sensitive to the chlorine gas with best selectivity as well. They demonstrated that, the timing parameters such as response time and recovery time etc

are also significant. Based on nitrates of the constituents, Rezlescu et al have synthesized cobalt substituted MnNi ferrite by employing auto combustion sol-gel method [97]. They doped the composition with CaO in 1 Wt%. They concluded that, these compositions are sensitive to the various reducing gases such as ethanol, methane, acetone (CH_3COCH_3) and LPG. Moreover, the composition for $Ni_{0.99}CO_{0.01}Mn_{0.02}Fe_{1.98}O_4$ exhibits significant sensitivity to the acetone at operating temperature about 488K. Tianshu et al have synthesized the cadmium ferrite by using co-precipitation method [98] and investigated the electrical properties for ethanol (C_2H_5OH). They found that, at 200 ppm and at 380^0C the sensitivity of the material is about 90%. Therefore, these compositions exhibited good selectivity with respect to other gases. Nano crystalline nickel ferrite was synthesized by Kamble and Mathe by adopting chemical co-precipitation method [99]. They reported that, the $NiFe_2O_4$ thick film sensor showed commendable response than that of pelletized composition. The results are attributed to the surface phenomenon. The Nickel ferrite is most suitable for detection of chlorine gas. Gadkari et al [100], emphasizing electrical characteristics, have synthesized, the spinel ferrite materials using chemical route. They investigated the gas sensing properties of the ferrites and reported that the ferrites are the novel material for fabrication of gas sensing mechanics. They also reported that the composition of $Mg_{0.6}Cd_{0.4}Fe_2O_4$ exhibits about 78% sensitivity to the LPG gas at 225^0C [101]. Chromium substituted MgCd ferrite was investigated by Masti et al [102] for their performance to the LPG Gas. They optimized the temperature required to complete the process of adsorption of oxygen at crystallite site by the phenomenon of chemisorption. The existence of porosity favours the process of adsorption [102]. Polycrystalline nanostructured CuZn ferrites have been prepared by Jain et al to investigate their suitability as LPG gas sensor [103]. They reported that, the copper zinc ferrites showed maximum sensitivity that the composition exhibited was up to 55% at 250^0C. The sensitivity was determined at 0.6 vol% of LPG. Employing citrate sol-gel method, the compositions of NiZn ferrites have been synthesized by Kapse et al and reported that the thick film sensors developed by using composition under investigation are mostly suitable for ethanol sensor. They attributed the phenomenon to the reducing nature of gaseous species to react with the chemisorbed oxygen on the surface, which is heated to pre determined operating temperature [104, 105]. Manganese and Nickel doped zinc ferrite of nano-crystallite size was synthesized by Gawas et al and reported the formation of single phase spinel ferrites with particle size of about 13nm [106].

They reported that the thick film of the composition $Mn_{0.3}Ni_{0.3}Zn_{0.4}Fe_2O_4$ showed good response for ammonia at room temperature. The selectivity for NH_3 is also well suited to the requirements of development of the sensor. Wan-li and Lei have studied the gas sensing properties of Ni Fe_2O_4ferrite and reported its suitability for acetone gas. They claimed that, the sensors developed on ceramic cylindrical tube show very fast response time and recovery time as well [107]. Gas sensing properties of MgZn ferrite nano particles were extensively studied by Bharti et al and reported that the composition are sensitive for the Co gas. They attributed the properties of electrical conduction to adsorption process [108].

b) Gas Sensing Mechanism in the Polycrystalline ferrite materials:

Semiconducting metal oxides, such as zinc oxide, tin oxide, tungsten oxide etc, are successfully proved as gas sensor materials. However, recently, many reports are appeared in the literature, wherein the investigation of characteristics of ferrite materials suitable for sensor based applications is emphasized. The polycrystalline spinel ferrite materials play significant role in the development of the gas sensors of salient features and interfacing of the same to electronic circuit for realization of sensor module. It is essential to explore the details regarding gas sensing mechanism of the ferrite material.

Gas sensing is the realization of surface phenomenon, wherein the phenomenon of chemisorption and physisorption is ensured. When the sensing element is heated to the sufficient temperature then the adsorption of the oxygen at the crystallographic sites of surface of the grains of polycrystalline material takes place. This is called as the chemisorption of the oxygen to form ionic species such as O^-, O_2^- and O^{2-}, which have acquired electrons from the conduction band of the surface material. The adsorption mechanism can be described through reaction path [109-111].

$$O_{2(gas)} \Leftrightarrow O_{2(Adsorbed)}$$

$$O_{2(Adsorbed)} + e^- \Leftrightarrow O_2^-$$

$$O_2^- + e^- \Leftrightarrow 2O^-$$

$$O^- + e^- \Leftrightarrow O^{2-}$$

Thus, three types of oxygen ions may be formed at the surface of the sensing element. The operating temperature favours the formation of these ionic species. These oxygen ions, O_2^-, O^- and O^{2-} are stable below 100 ^{0}C, in between 100 ^{0}C to 300 ^{0}C and

above 300 ^{0}C, respectively [112]. The electron transfer from conduction band of the sensing element to the chemisorbed oxygen results into decrease in the concentration of electrons, the charges carriers, of the sensing element. Therefore, for n-type semiconducting metal oxides, an increase in the resistance of the sensor is observed [93]. Moreover, in case of p-type metal oxides, the transfer of electrons results into formation of the holes at valence band and favours the electrical conduction. This reveals the decrease in the resistance of the sensor film. The operating temperature plays vital role on the adsorption and desorption rate of the oxygen ion at surface of the ferrite film. Moreover, this also depends upon the nature of the gases to be sensed. As per the properties, generally, the gases could be classified into two groups such as oxidizing gases and reducing gases. The gases such as NO_2, NO, N_2O, CO_2 etc are oxidizing gases. However, the gases such as NH_3, H_2S, CH_4, ethanol, acetone etc are come under the group of reducing gases.

When the sensing element of the ferrite material is exposed to the oxidizing gases such as CO_2, then it reacts with chemisorbed O^- ion at the surface of the film. The oxidation reaction between metal oxide and oxidizing gas follow the reaction paths [113].

$$CO_{2(gas)} + e^- \Leftrightarrow CO_2^-{}_{(Adsorbed)} \quad (6)$$

$$CO_2^-{}_{(Adsorbed)} + O^- + 2e^- \Leftrightarrow CO(gas) + 2O^{2-} \quad (7)$$

The adsorbed O^- ions play an interesting role of assisting the oxidizing ions to take electrons from surface of the ferrite films, which results into reduction in the concentration of electrons. Hence, resistance of the sensing element increases with increase in the concentration of oxidizing gas molecules. This is for n-type metal oxide thick films. Therefore, the gas sensing response for oxidizing gas is normally defined as $S = (R_a/R_{og})$. Where, R_{og} is the resistance in presence of the oxidizing gas and Ra is the resistance at ambient condition for pure and dry air.

When the surface of the polycrystalline ferrite material is exposed to the reducing gases, such as NH_3, H_2S etc, then the reducing gas reacts with chemisorbed oxygen thereby releasing electrons back into the conduction band of the ferrite film. The Reaction mechanism between reducing gases and chemisorbed oxygen species are given below [114, 115].

$$2NH_{3(gas)} + 3O^{-}_{(Adsorbed)} \Leftrightarrow N_2 + 3H_2O + 3e^{-} \quad (8)$$

$$2NH_{3(gas)} + 3O^{2-}_{(Adsorbed)} \Leftrightarrow N_2 + 3H_2O + 6e^{-} \quad (9)$$

and

$$H_2S_{(gas)} + 3O^{-}_{(Adsorbed)} \Leftrightarrow H_2O + SO_2 + 3e^{-} \quad (10)$$

$$H_2S_{(gas)} + 3O^{2-}_{(Adsorbed)} \Leftrightarrow H_2O + SO_2 + 6e^{-} \quad (11)$$

These reactions reveal the donation of electrons to the conduction band of the sensing material. As a result the concentration of electrons on the surface of the ferrite film increases and resistance of the sensing element decreases. Therefore, the gas sensing response for reducing gases is normally defined as $S = (R_{rg}/R_a)$. Where, R_{rg} is the resistance in presence of the reducing gas and Ra is the resistance at ambient condition for pure and dry air. As discussed above, gas sensing is the result of adsorption mechanism. This adsorption significantly depends upon operating temperature. During temperature range from 200 ^{0}C to 350^{0}C the adsorption favours. However, for higher temperature, the desorption of the species occurs, which results into decrease in the sensitivity of the sensor to the test gas.

3.C.2 Experimental:

Gas sensing properties of polycrystalline nanoferrite compositions of $Mg_xZn_{1-x}Fe_2O_4$, $Ni_xZn_{1-x}Fe_2O_4$ and $Mn_xZn_{1-x}Fe_2O_4$ (x= 0.20, 0.40, 0.60 and 0.80) were studied by measuring electrical resistance (R_g) of the sensing element by exposing to the gases. The test gases are CO_2, NH_3 and H_2S. The sensor is fabricated by deposition of thick film (10mm length), of the respective compositions, using screen printing technique, on cylindrical tube. The schematic of the sensor is depicted in the figure 3.C.1. As shown in the figure, 3.C.1, the sensing element is deposited on the cylindrical tube of length 20mm, outer diameter 6 mm and inner diameter 4mm. A specially designed Heating Element (HH) is installed along the axis of the sensor to provide temperature to realize the process of chemisorption. Use of cylindrical shape sensing element helps to improve the response of the sensors to the various gases. In order to achieve Ohmic contacts the rings of silver paste are deposited at both sides of the thick film. From these silver electrodes the leads are developed to ensure electrical contacts and connected to the male of the connector to ensure the interfacing to the Smart sensor module.

Thus, prepared sensor is deployed to explore the gas sensitive properties of the composition under investigation.

The thick film sensing element is exposed to the carbon dioxide (CO_2) gas by using sophisticated Carbon dioxide chamber [Figure 3.C.2], Thermo Scientific Ltd USA, Model Midi 40. The specifications of this CO_2 chamber are presented in table 3.C.1 [116]. An experimental arrangement is shown in figure 3.C.2. The CO_2 Gas, in percentage unit (%), is applied in the controlled manner to the sensor. The operating temperature is controlled by controlling current through heating element (HH). The gas sensitive resistance (R_g) of the sensing element is measured with respect to variable concentration of CO_2 gas. The precise digital meter, Tektronix Make model DMM4050, 6.5Digit Resolution, Accuracy up to 0.0024%, 10 Ω to 1.2 GΩ Range, with 10 μΩ Resolution, is used for resistance measurement. The Resistance against concentration of CO_2 data is employed for further interpretation.

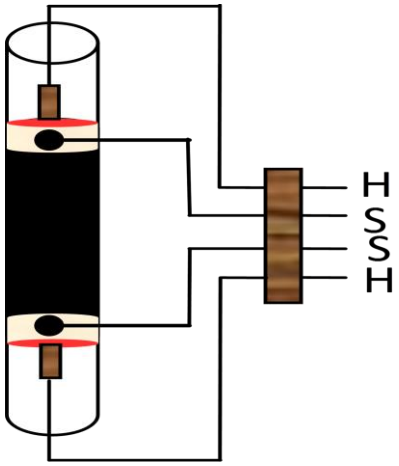

Figure 3.C.1: The schematic of the sensor to explore the gas sensitive properties of the compositions

Figure 3.C.2: Experimental arrangement to study CO_2 gas sensitive properties of the sensors

TABLE 3.C.1: Specification of CO2 Gas Chamber

Sr. No.	Parameters	Specifications
1.	Manufacturer	Thermo Scientific, USA
2.	Model	Midi 40
3.	Capacity	1.4 cu. ft. (39.6 L)
4.	Cabinet configuration	Benchtop
5.	Chamber and cabinet	Stainless Steel
6.	Interior	Non-corrosive stainless steel, type 304, mirror finish
7.	CO_2 Sensor	Thermal conductivity sensor
8.	CO_2 Concentration Range	0-20%
9.	Control accuracy	± 0.1%
10.	Uniformity	0.10%
11.	Inlet pressure required	15 PSIG (1.0 bar)
12.	Inlet air filtration	0.3 micron antimicrobial filter
13.	Alarm	User programmable high/low
14.	Relative Humidity Range	To 95% RH at 37°C
15.	Temperature Range	5°C above ambient to 60°C
16.	Control accuracy	± 0.1°C
17.	Uniformity	± 0.4°C @ 37°C
18.	Outputs	RS-485 signal output and audible and visual alarm functions ensure proper operations
19.	Microcontroller	IntrLogic™ II

Moreover, ferrites compositions under investigation, deposited on glass tube, are exposed to the reducing gases such as ammonia and hydrogen sulfide. The change in the resistance of the sensing element is recorded by exposing the sensing element to ammonia and H_2S gas. The operating temperature is optimized by studying temperature dependent sensitivity for both gases. The sensitivities are estimated for all compositions under investigation.

3.C.3 Results and Discussion:

I) Carbon dioxide gas Sensitive electrical properties:

The thick films of the sensing element of compositions of $Mg_xZn_{1-x}Fe_2O_4$, $Ni_xZn_{1-x}Fe_2O_4$ and $Mn_xZn_{1-x}Fe_2O_4$ nanoferrites, deposited on cylindrical glass tube, are exposed to the CO_2 gas of variable concentration from 0.1 % to the 15% and resistance

of the sensing element (R_{CO2}) is measured. The measurements are also carried out for variable operating temperature.

The values of electrical resistance (R_{CO2}), in MΩ, of the sensor developed by using thick film of $Mg_xZn_{1-x}Fe_2O_4$ (x=0.20, 0.40, 0.60 and 0.80) are measured against concentration of carbon dioxide gas in % unit. In fact, for gas sensor, the operating temperature plays significant role on the performance of the sensor. Therefore, before investigation of gas sensitive properties, the operating temperature is optimized. For optimization of operating temperature, concentration of carbon dioxide is kept constant, with the help of above mentioned sophisticated CO_2 chamber and values of electrical resistance are measured. The sensitivity is defined as relative change in the measuring value of the parameter [117]. Therefore, the expression for sensitivity of the materials for carbon dioxide gas is given by [113]

$$S_G = \frac{R_{CO2} - R_a}{R_{CO2}} \times 100\ \% \qquad (12)$$

Where, Ra is the resistance of the sensing element for ambient condition. By employing formula given by expression 12, the sensitivities are estimated. The temperature dependent sensitivity is recorded. From this data the operating temperature is decided. Operating temperature is supposed to be the temperature of the sensing element at which maximum sensitivity is observed. The operating temperature for MgZn ferrite is optimized to 220^0C. It is known that, this would be the temperature range within which the chemisorbed oxygen species depict good stability. Above this temperature, the desorption initiates, which causes to decrease the sensitivity. This value of the operating temperature shows close agreement with the earlier reports for magnesium substituted ferrites [86, 87, 94]. As discussed earlier, the carbon dioxide gas is oxidizing gas and takes the electrons from conduction band of the sensing element [113]. This results into decrease in the concentration of the electron in conduction band. Therefore, the resistance value increases with increases in concentration of carbon dioxide gas.

The sensitivity values for all compositions under investigation are determined, at constant operating temperature (T_{OP}) of 220 ^{0}C. The electrical resistance (R_{CO2}) is measured for variable concentration of carbon dioxide gas and plotted. The graphs of

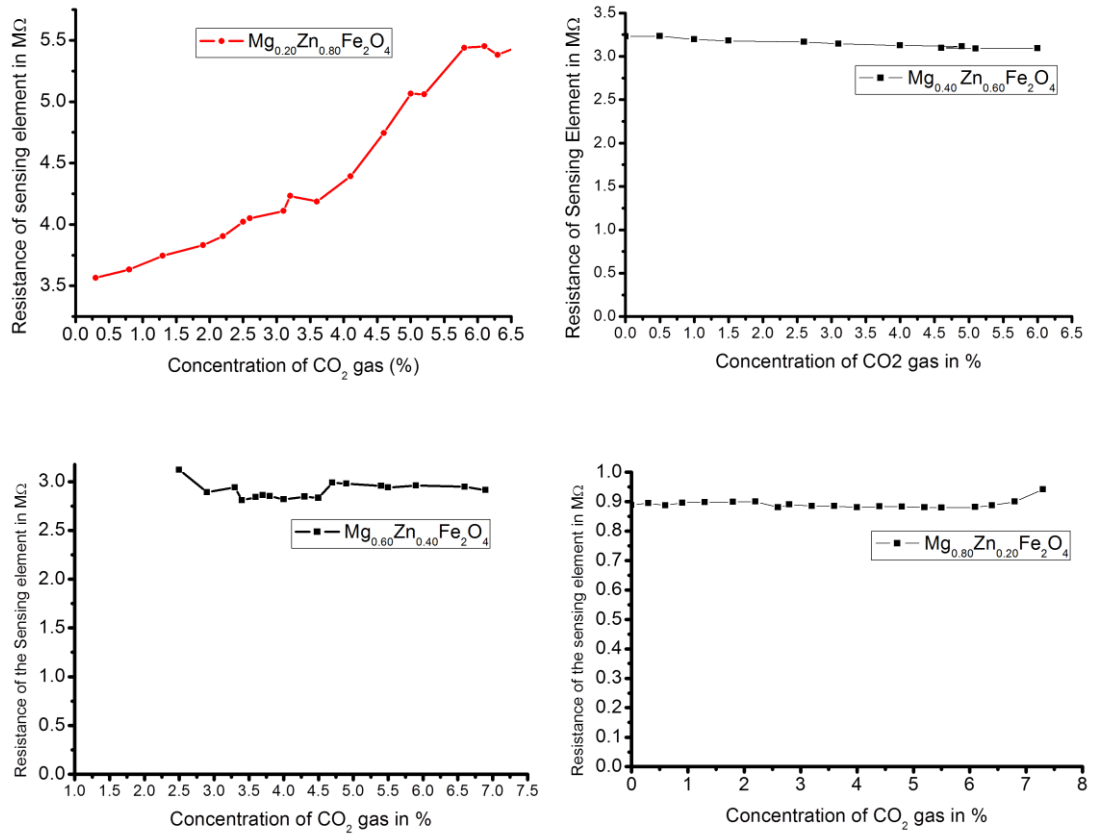

Figure 3.C.3: The Graph of Resistance of Sensing Element, R_{CO2}, in MΩ, against concentration of carbon dioxide gas in % at operating temperature about 220 ^{0}C.

observed resistance of sensing material against concentration of CO_2 gas (in %) are depicted in figure 3.C.3. On inspection of figure 3.C.3, it is found that, the sensing element for x=0.20, i.e $Mg_{0.20}Zn_{0.80}Fe_2O_4$ ferrite, shows significant sensitivity for carbon dioxide gas. However, other candidates, for x= 0.40, 0.60 and 0.80, found less sensitive to the carbon dioxide gas. Liu et al [94] have investigated MgZn ferrite for carbon dioxide gas and reported that, the composition of lower concentration of magnesium are most sensitive to the carbon dioxide. Employing expression (12) the sensitivity, S_G, (in%) are estimated for composition of MgZn ferrites. It is found that the sensitivity of the composition for x=0.20 measured at operating temperature 220 ^{0}C is more that 65%. However, remaining candidates reveal very small sensitivity. On inspection of the figure 3.C.3, it is found that, resistance of the sensing element for x=0.20 increases with increase in concentration of carbon dioxide gas. This nature of

the graph can be attributed to the oxidizing nature of the CO_2 gas. The carbon dioxide gas is oxidizing gas. When it comes in contact with the chemisorbed oxygen species, then it takes electron from the conduction band. The reaction mechanism is given in expression 6 and 7. Due to this, the concentration of electrons of the conduction bands decreases, which results into decreases in the electrical current and hence increases in the resistance R_{CO2} [118] , due to increase in the concentration of CO_2, is observed. This mechanism favours for n-type semiconducting metal oxides [118]. The graphs, depicted in figure 3.C.3, for $x \geq 0.40$, show slight dependence on CO_2 gas concentration. The resistance of the sensing element for x=0.20 shows increasing trend with CO_2 concentration. This increase in the resistance occur up to the 6.9 % CO_2 gas. Thereafter, the saturation is depicted. It is known that, the chemisorptions of oxygen species favours at typical range of operating temperature [119, 120]. At typical operating temperature the concentration of oxygen species are constant. Therefore, the saturation of chemisorptions takes place. Therefore, after typical concentration of the CO_2 gas the saturation in the response is observed. This behavior of the sensing material should be considered, while designing of the Smart Sensor Module for CO_2gas measurement.

Thus, from this, it can be concluded that, the sensor developed by employing the sensing element of $Mg_{0.2}Zn_{0.8}Fe_2O_4$nanoferrite is most suitable for development of Smart Sensor Module to detect the carbon dioxide gas.

The sensors, developed by depositing thick films of $Ni_xZn_{1-x}Fe_2O_4$ (x=0.20, 0.40, 0.60 and 0.80) polycrystalline spinel nanoferrites are also used to carry out investigation of carbon dioxide gas sensitive electrical properties. The resistances, R_{CO2} of the compositions under investigation are measured against concentration of carbon dioxide gas from 0% to 15% by deploying sophisticated carbon dioxide gas chamber. In the beginning, the operating temperature is optimized by studying operating temperature dependent sensitivities of compositions under investigation. The temperature at which

TABLE 3.C.2: Operating Temperature, sensitivities and Saturation limit for sensing element of NiZn ferrites

Concentration of Ni ion (x)	**Operating temperature ^{0}C**	**Sensitivities S_G (%)**	**Saturation limit of concentration of CO_2 gas in %**
0.20	180	70.26	8
0.40	190	24.56	9
0.60	220	18.14	7.5
0.80	180	21.69	8

the sensitivity found maximum is called operating temperature. The operating temperature for NiZn ferrite is optimized and presented in table 3.C.2. For gas sensing mechanism this operating temperature plays vital role on the performance of the sensor. The operating temperature shows close agreement with earlier report [102, 104, 105]. After determination of operating temperature, the compositions are subjected to investigation of CO_2 sensitive electrical properties.

On investigation of carbon dioxide gas sensitive electrical properties, it is found that, the compositions for x=0.20 and x=0.40 are most sensitive to the CO_2 gas. Therefore, typically the sensors of these two compositions are used for further investigation. The values of electrical resistance (R_{CO2}) against concentration of CO_2 gas are recorded at respective operating temperatures and plotted against concentration of CO_2 gas. The graphs of typical compositions for x =0.20 & 0.40, are presented in figure 3.C.4On inspection of the figure 3.C.4, it is found that, the resistance of the sensing element increases with increase in the concentration of CO_2 gas. This could be attributed to oxidizing nature of the carbon dioxide gas. As discussed earlier, during process of chemisorptions, the CO_2 gas accepts the electrons from conducting bands of the sensing element. The decrease in the concentration of electrons results into increase in the resistance of the sensing element.

From the figure 3.C.4, it is also found that at and above typical limit of the

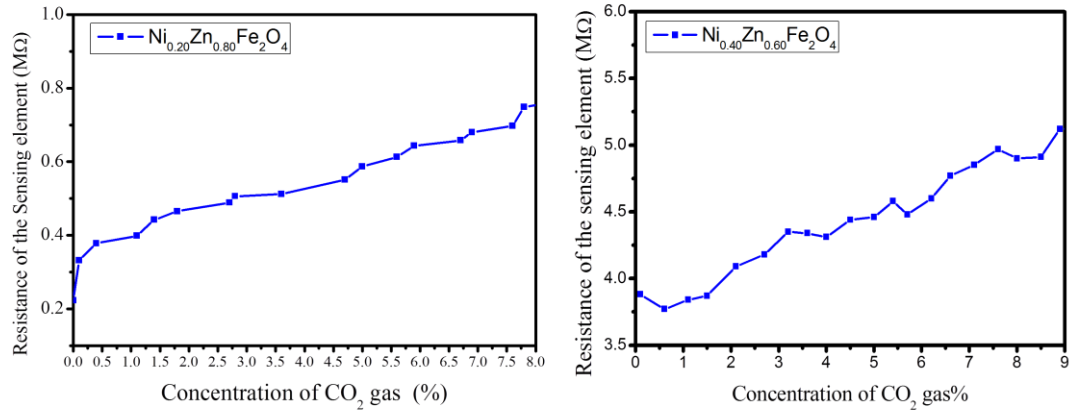

Figure 3.C.4: The Graph of Resistance of Sensing Element, R_{CO2} , in MΩ, against concentration of carbon dioxide gas in %, at respective operating temperature, typical for x = 0.20 and 0.40.

CO_2gas, saturation in the resistance value takes place. This may be attributed to the saturation in the concentration of chemisorbed oxygen ion species. Along with the sensitivities the saturation levels are also depicted in the table 3.C.2

From this investigation, it can be conclude that, the sensors developed by employing the sensing element of $Ni_{0.2}Zn_{0.8}Fe_2O_4$ and $Ni_{0.4}Zn_{0.6}Fe_2O_4$ nano ferrites are most suitable for development of the smart sensor module for detection of the CO_2 gas.

Further, the sensors are developed by depositing thick film of $Mn_xZn_{1-x}Fe_2O_4$ (x=0.20, 0.40, 0.60 and 0.80) polycrystalline spinel ferrites. Investigation of electrical properties of these sensors, with respect to the carbon dioxide gas is carried out. Deploying sophisticated carbon dioxide gas chamber, a variable concentration of CO_2 gas is applied to the sensors under investigation and resistance values (R_{CO2}) exhibited by the sensing element are recorded. As discussed earlier, the operating temperature is optimized and it is about 205^0C for all compositions of this series. Controlling temperature of sensing element to the operating temperature, CO_2 dependent resistance values are recorded and graph of resistance of sensing element $R_{CO2,}$ plotted against concentration of CO_2 gas, are presented in figure 3.C.5. On inspection of the figure 3.C.5, it is found that the resistance values increases with increase in the concentration

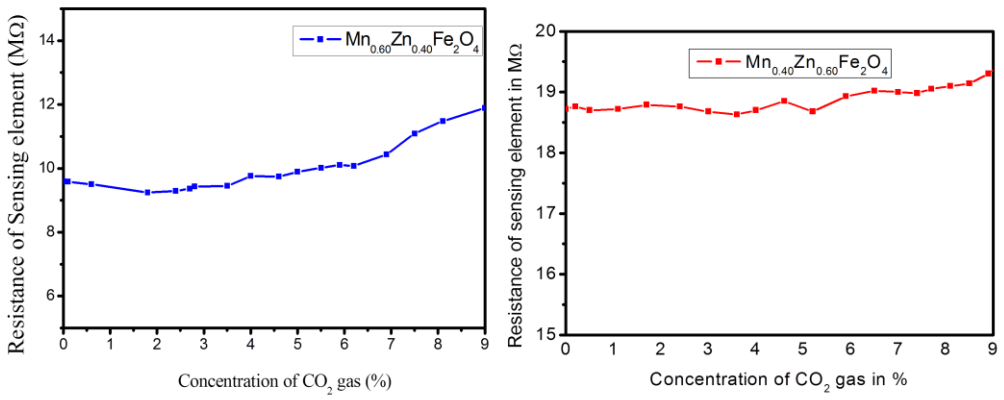

Figure 3.C.5: The Graph of Resistance of Sensing Element, R_{CO2} , in MΩ, against concentration of carbon dioxide gas in %, at respective operating temperature, , typical for x = 0.40 and 0.60.

of CO_2 gas. It is as expected. The nature of the graph is attributed to oxidizing behavior of the carbon dioxide gas. On observation of these graphs, it is also found that, the sensitivities are significantly less. The sensitivities of these compositions are lesser than that of compositions of NiZn ferrites. From graph, it is also observed that, the saturation in the resistance takes place at typical value of concentration of CO_2 gas. The sensitivity of these compositions are less. However, the saturation limits are extended to about 8.4 % of CO_2 gas. From results obtained, it can be concluded that, the

composition of MnZn ferrites are less sensitive to carbon dioxide gas, as compared to the typical candidates of MgZn and NiZn ferrites.

II) H_2S gas Sensitive electrical properties:

With the view to develop a sensor for detection of reducing gas, electrical properties of the compositions under investigation are studied for Hydrogen Sulfide (H_2S) gas. There are various gases, such as ethanol, LPG, Methane etc, who are categorized as reducing gases. It is known that, the hydrogen sulfide gas is also reducing gas. It can participate in chemisorption phenomenon by reacting with the chemisorbed oxygen species. The reaction mechanism is given in the expression 10 and 11. According to this reaction mechanism the H_2S gas donate electrons to the conduction band of the sensing material. This is for n-type metal oxides [118]. This results into increase in the concentration of electrons in the conduction band. Therefore, the resistance of the composition decreases [119]. Band theory as applied to gas sensors has been the subject of intense study for a number of years [121, 122]. The target gas interacts with the surface of the metal oxide film (generally through surface adsorbed oxygen ions), which results in a change in charge carrier concentration of the material. This change in charge carrier concentration serves to alter the conductivity (or resistivity,) of the material. An n-type semiconductor is one where the majority charge carriers are electrons, and upon interaction with a reducing gas an increase in conductivity occurs. Conversely, an oxidising gas serves to deplete the sensing layer of charge carrying electrons, resulting in a decrease in conductivity. Thus, on exposer to the H_2S gas, the sensing material depicts the reduction in the resistance. This is the realization of conduction mechanism for n-type semiconducting metal oxides. The sensitivity (S_{H2S}) in % of the materials for H_2S gas is given by

$$S_{H2S} = \frac{R_a - R_{H_2S}}{R_a} \times 100\ \% \qquad (13)$$

Where, Ra is the resistance of the sensing element at ambient condition and $R_{H2S}$is the resistance of sensing element measured on exposing same to the H_2S gas.

The values of Ra and R_{H2S}, for all compositions under investigation, are measured by using highly precise digital multimeter model Tektronix Make model DMM4050, 6.5Digit Resolution, Accuracy up to 0.0024%, 10 Ω to 1.2 GΩ Range, with 10 μΩ Resolution.

Experimental arrangement used to realize the detection of H_2S gas is depicted in figure 3.C.6. As shown in the figure 3.C.6, the H_2S gas is hold in the jar and it is conveyed towards the sensor through tube. A typical valves are fitted to make the gas ON and OFF.

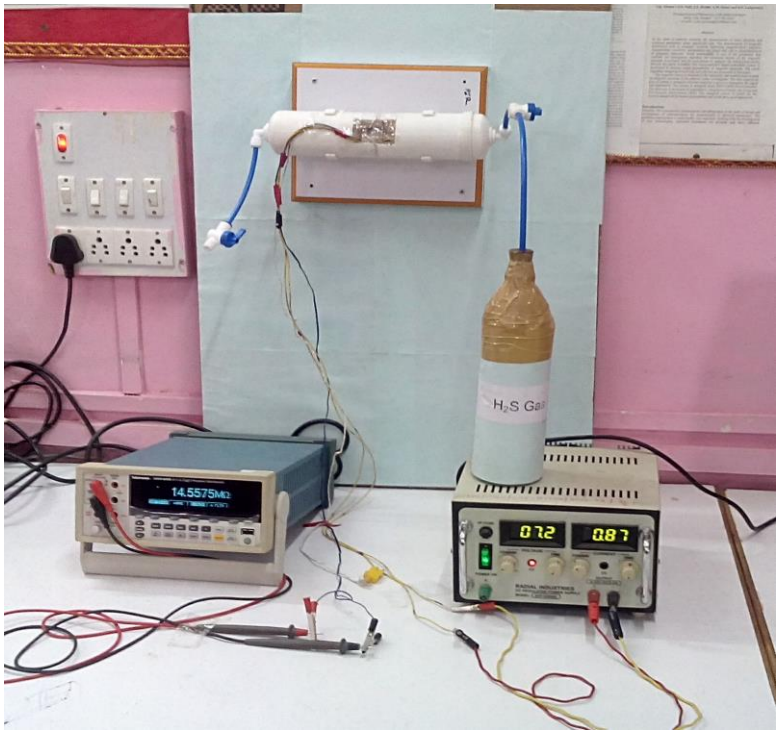

Figure 3.C.6: Experimental arrangement for detection of the H_2S gas

The sensing element of the sensor for H_2S gas detection is developed by adopting thick film technique, wherein the compositions of polycrystalline $Mg_xZn_{1-x}Fe_2O_4$, $Ni_xZn_{1-x}Fe_2O_4$ and $Mn_xZn_{1-x}Fe_2O_4$ spinel nanoferrites have been employed as sensing materials. The resistance of the sensing element is measured at ambient condition and assigned to Ra. By opening valve, the H_2S gas is applied to the sensing element and resistance is measured and recorded as $R_{H2S.}$ Then, employing expression 13 the sensitivities (S_{H2S}) are estimated. The sensitivities of the composition are calculated for different values of temperature of the sensing element. The sensitivity of the compositions under investigation are plotted against temperature and depicted in figure 3.C.7, 3.C.8 and 3.C.9 for MgZn, NiZn and MnZn ferrites respectively. From, these graphs, it is found that, sensitivity increases with increase in the temperature and become maximum at a typical temperature called operating temperature. From figures 3.C.7, 3.C.8 and 3.C.9, it is found that, compositions depict the operating temperature at about 150^0C. All compositions, except x=0.20 and x=0.60 of MnZn ferrites, the sensitivity is maximum at about 150^0C.

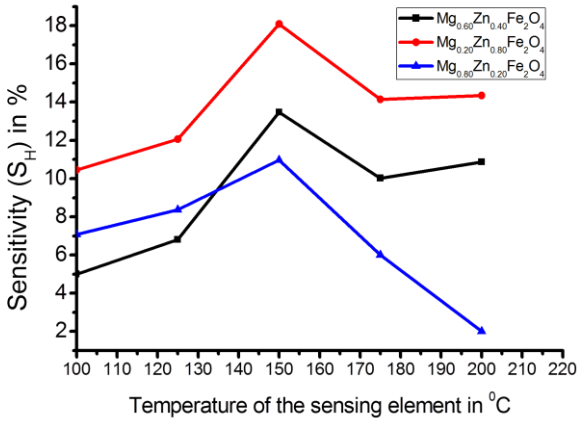

Figure 3.C.7: Graph of Sensitivity for S_{H2S} gas against temperature of the sensing element in ^{0}C

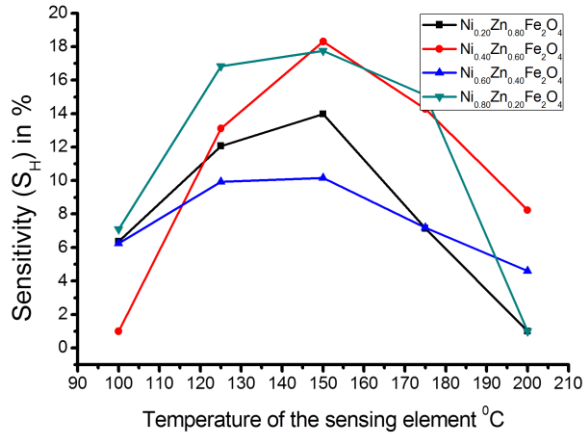

Figure 3.C.8: Graph of Sensitivity for S_{H2S} gas against temperature of the sensing element in ^{0}C

Therefore, the operating temperature of the sensor should be 150^{0}C. While implementation of these sensors to develop smart sensor module, this feature of sensor should be consider. The sensitivity of the sensor, which is developed by employing the sensing element of $Mn_{0.20}Zn_{0.80}Fe_2O_4$ and $Mn_{0.60}Zn_{0.40}Fe_2O_4$materials, is optimum at 125^{0}C. Therefore, for said sensor the operating temperature would be 125^{0}C. Thus, the reduction of operating temperature is observed for MnZn ferrites. The sensitivity values and operating temperature values are shown in the table 3.C.4

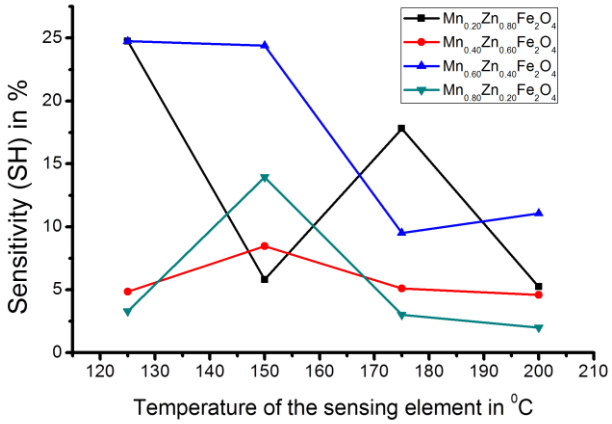

Figure 3.C.9: Graph of Sensitivity for S_{H2S} gas against temperature of the sensing element in ^{0}C

From, the results of this investigation, it can be concluded that, the compositions under investigation can be suitably used for deployment of Smart Sensor Module for detection of H_2S gas.

III) NH_3 gas Sensitive electrical properties:

Polycrystalline ferrite materials are sensitive to ammonia, NH_3, gas. Ammonia, NH3 is a caustic and hazardous colourless gas with a characteristic pungent odour. Ammonia gas is reducing gas and hence it plays s remarkable role of the properties of

the spinel ferrite materials. Nanto et al [123] reported a zinc oxide thin film sensor

TABLE 3.C.4: Operating temperature and sensitivity of the materials for H_2S gas

Concentration 'x'	$Mg_xZn_{1-x}Fe_2O_4$		$Ni_xZn_{1-x}Fe_2O_4$		$Mn_xZn_{1-x}Fe_2O_4$	
	Sensitivity S_{H2S}(%)	Operating Temperature 0C	Sensitivity S_{H2S}(%)	Operating Temperature 0C	Sensitivity S_{H2S}(%)	Operating Temperature 0C
0.20	18.06	150	13.98	150	24.74	125
0.40	-	-	18.30	150	8.40	150
0.60	13.44	150	17.35	150	24.75	125
0.80	10.99	150	10.09	150	13.90	150

prepared by sputtering. The material was doped with aluminum, gallium and indium. The response of these materials was compared with the un-doped film. Large negative responses are reported in reaction to the presence of ammonia, with positive responses to other gases depending on the material [124]. The detection of ammonia gas is essential in various industries and for environmental prediction as well. Therefore, it is proposed to develop Smart Sensor Module for detection of ammonia gas, wherein the sensor, developed with use of thick film of ferrite materials, is deployed. With the view to develop a sensor for detection of ammonia gas, electrical properties of the compositions under investigation are studied. It is known that, the ammonia, NH_3, is reducing gas. It can participate in chemisorption phenomenon by reacting with the chemisorbed oxygen species. The reaction mechanism is given in the expressions 8 and 9. According to this reaction mechanism the ammonia gas donate electrons to the conduction band of the sensing material [124]. This is for n-type metal oxides [118]. This results into increase in the concentration of electrons in the conduction band. Therefore, the resistance of the composition decreases [125]. Thus, on exposing to the ammonia gas, the sensing material depicts the reduction in the resistance. This is the realization of conduction mechanism for n-type semiconducting metal oxides. The sensitivity (S_{NH3}) in % of the materials for NH_3 gas is given by

$$S_{NH3} = \frac{R_a - R_{NH3}}{R_a} \times 100\ \% \qquad (14)$$

Where, Ra is the resistance of the sensing element at ambient condition and R_{NH3} is the resistance of sensing element measured on exposing same to the ammonia gas.

The values of Ra and R_{NH3}, for all compositions under investigation, are measured by using highly precise digital multimeter model Tektronix Make model DMM4050, 6.5 Digit Resolution, Accuracy up to 0.0024%, 10 Ω to 1.2 GΩ Range, with 10 μΩ Resolution. Experimental arrangement used to ensure the detection of ammonia gas is presented in figure 3.C.10. As shown in the figure 3.C.10, the ammonia gas is hold in the jar and it is conveyed towards the sensor through tube. Typical valves are fitted to make the gas ON and OFF.

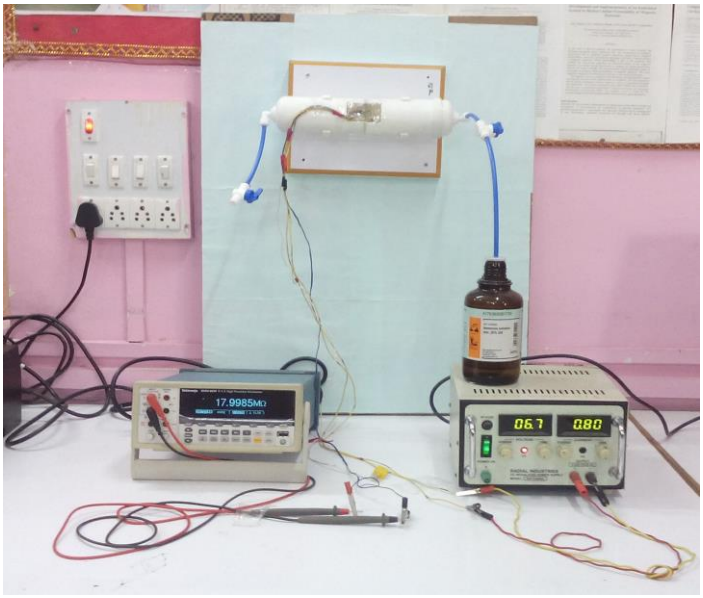

Figure 3.C.10: Experimental arrangement for detection of the NH_3 gas

The sensing element of the sensor for ammonia gas detection is developed by depositing thick film of compositions of polycrystalline $Mg_xZn_{1-x}Fe_2O_4$,$Ni_xZn_{1-x}Fe_2O_4$ and $Mn_xZn_{1-x}Fe_2O_4$ spinel nanoferrites on cylindrical tube, wherein heating element is kept exactly at the center of tube.

The resistance of the sensing element is measured at ambient condition and assigned to Ra. On exposing the sensing element to the ammonia the resistance is measured and recorded as R_{NH3}. Then, employing expression 14 the sensitivities (S_{NH3}) are estimated. The sensitivities of the composition are calculated for different values of temperature of the sensing element. The sensitivity of the compositions under investigation are plotted against temperature and depicted in figure 3.C.11, 3.C.12 and 3.C.13 for MgZn, NiZn and MnZn ferrites

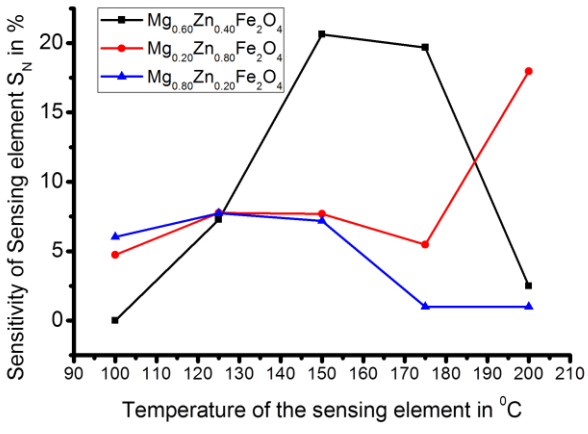

Figure 3.C.11: Graph of Sensitivity for S_{NH3} gas against temperature of the sensing element in ^0C

respectively. From, these graphs, it is found that, sensitivity increases with increase in the temperature and becomes optimum at a typical temperature called operating temperature. On intense study of these figures, it is observed that the compositions of MnZn ferrites are most sensitive to ammonia gas. It is also observed that, the operating temperature required for compositions of MnZn ferrites is less that of other candidates under investigation. As depicted in figure 3.C.11, the sensing elements of MgZn ferrites reveal compositional dependent sensitivity and operating temperature required. The composition for x = 0.40 & 0.60 are successfully operating at temperature about 150^0C.

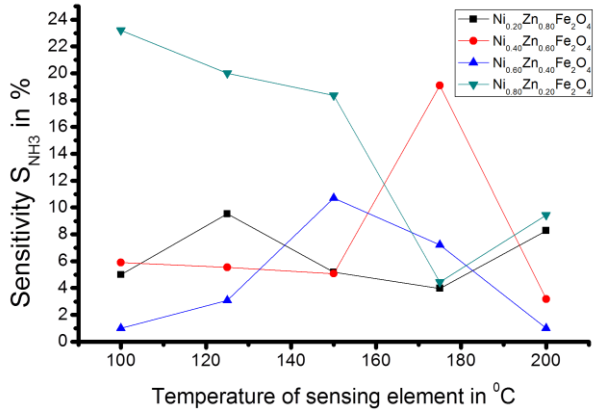

Figure 3.C.12: Graph of Sensitivity for S_{NH3} gas against temperature of the sensing element in ^{0}C

However, the operating temperature for x = 0.20 is about 200 ^{0}C. The gas sensor with lower operating temperature is always recommendable. Operating temperature and sensitivity values are presented in table. 3.C.5 . As shown in figure 3.C.12, the operating temperatures of the sensors developed by the use of NiZn ferrites are also compositional dependent. The sensitivity of the sensing element for x = 0.80 is highest as compared with other members of the series. Moreover, value of operating temperature is about 125^0C. As discussed earlier, this sensing element is most suitable for detection of the ammonia gas. Operating temperatures and values of sensitivities are presented in table 3.C.5. While implementation of these sensors to develop smart sensor module, this feature of sensor should be consider.

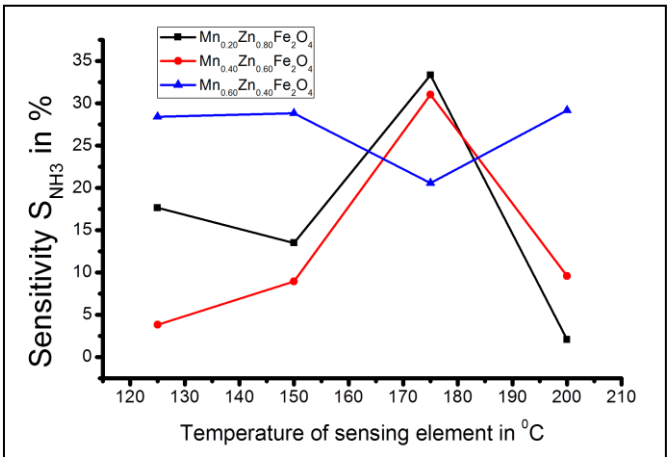

Figure 3.C.13: Graph of Sensitivity for S_{NH3} gas against temperature of the sensing element in ^{0}C

The sensitivity of the sensor, developed by employing the sensing element of $Mn_{0.60}Zn_{0.40}Fe_2O_4$ is optimum at 125^0C. Therefore, for said sensor the operating temperature would be 125^0C. Moreover, the sensitivity of this sensing element is high. Thus, the reduction of operating temperature is always acceptable. The sensitivity values and operating temperature values are shown in the table 3.C.5

TABLE 3.C.5: Operating temperature and sensitivity of the materials for ammonia gas

Concentration 'x'	$Mg_xZn_{1-x}Fe_2O_4$		$Ni_xZn_{1-x}Fe_2O_4$		$Mn_xZn_{1-x}Fe_2O_4$	
	Sensitivity S_{NH3}(%)	Operating Temperature 0C	Sensitivity S_{NH3} (%)	Operating Temperature 0C	Sensitivity S_{NH3} (%)	Operating Temperature 0C
0.20	7.72	150	9.39	125	33.38	175
0.40	-	-	18.99	175	31.11	175
0.60	20.69	150	10.58	150	28.85	150
0.80	7.11	150	23.27	100	-	-

From, the results of this investigation, it can be concluded that, the compositions under investigation can be suitably used for deployment of Smart Sensor Module for detection of ammonia gas.

3.C.4 Conclusion:

As per the objectives, development of the sensor for gas sensing, electrical properties of the compositions of polycrystalline $Mg_xZn_{1-x}Fe_2O_4$, $Ni_xZn_{1-x}Fe_2O_4$ and $Mn_xZn_{1-x}Fe_2O_4$ nanoferrites have been investigated. Employing these materials, the sensing elements are developed on epoxy resin, cylindrical glass tube, ceramic etc substrates. The sensing elements are demonstrating the phenomenon of chemisorption at specific operating temperature. The materials are n-type metal oxides and depict increase in the resistance due to presence of oxidizing gas and decrease in the resistance due to existence reducing gas. Emphasizing this fact, sensing elements of the ferrite materials are exposed to the carbon dioxide gas, hydrogen sulfide gas and ammonia gas and results obtained are interpreted. The resistance of the compositions is increasing for CO_2 gas. The sensitivities are also estimated. From results obtained, it can be concluded, the compositions of NiZn ferrites are most suitable for development of carbon dioxide gas sensor. Moreover, the composition $Mg_{0.20}Zn_{0.80}Fe_2O_4$ is also suitable

for fabrication of carbon dioxide gas sensor. Operating temperature determined for MgZn ferrites is 220 ^{0}C. Moreover, reduction in the operating temperature is observed for NiZn ferrite. Good sensitivity with low operating temperature, suggest implementation of NiZn ferrites for carbon dioxide gas sensor. Moreover, the MnZn ferrites reveal less sensitivity to CO_2 gas. The performances of the sensing elements are also tested for two reducing gases, the H_2S and NH_3. On application of these gases, the reduction is the resistance takes place, which is attributed to existence of n-type of conductivity at operating temperature. The sensitivities of all sensing elements are estimated for various temperatures. The operating temperatures are obtained for all sensing element. The compositions under investigations are showing good sensitivities. However, the sensitivity observed for MnZn ferrites for both gases is remarkable. Therefore, it can be concluded that, the sensing elements MnZn ferrites are most suitable for fabrication of H_2S and NH_3 gas sensor. It is also found that, the operating temperature is significantly reduced. For H_2S gas sensing, for MnZn ferrites, the operating temperature is reduced to 125 ^{0}C. On investigation of results obtained, it is confirmed that, the sensors developed on cylindrical glass tubes are most suitable for deployment of the same to design the Smart Sensor Module.

3. D. Selection of Materials for Sensing Elements of the Sensors:

To develop Smart Sensor Module, the sensors of promising features are required. To cater this need, the compositions $Mg_xZn_{1-x}Fe_2O_4$, $Ni_xZn_{1-x}Fe_2O_4$ and Mn_x-$Zn_{1-x}Fe_2O_4$of polycrystalline spinel ferrites have been synthesized by employing co-precipitation method. On successful characterization, the electrical properties are essentially investigated. The electrical properties are investigated for their suitability to design the sensor for desired parameters. For present investigation, it is proposed to design Smart Sensor Module for the parameters such as relative humidity, environmental temperature, carbon dioxide gas, hydrogen sulfide gas and ammonia gas, wherein the features of IEEE standards 1451 are realized. Therefore, it is essential to design sensors for above parameters. Emphasizing the deployment of the sensing elements for sensors for above parameters, the materials are investigated. The results of investigation are interpreted in earlier sections. The materials under investigation are demonstrating suitability for sensing of said parameters. However, it is essential to select specific sensing material for desired sensor. For selection of the sensing materials for development of typical sensor, the specifications such as range, sensitivity, operating temperature, nature of substrate, ambient conditions etc are ensured. Emphasizing above selection criteria, the sensing materials, suitable for respective sensor are selected and presented in table 3.D.1. The sensing elements, as presented in

TABLE 3.D.1: Selection of the sensing materials for development of sensors.

Sr. No.	Name of the Sensor	Materials for Sensing Elements	Substrate used
1	Relative Humidity	$Ni_{0.40}Zn_{0.60}Fe_2O_4$	Ceramic Substrate
		$Ni_{0.80}Zn_{0.20}Fe_2O_4$	Ceramic Substrate
2	Environmental Temperature	$Mg_{0.40}Zn_{0.60}Fe_2O_4$	Ceramic Substrate
		$Mg_{0.60}Zn_{0.40}Fe_2O_4$	Ceramic Substrate
3	Carbon dioxide gas	$Ni_{0.40}Zn_{0.60}Fe_2O_4$	Cylindrical Glass Tube
		$Ni_{0.60}Zn_{0.40}Fe_2O_4$	Cylindrical Glass Tube
4	H_2S gas	$Mn_{0.20}Zn_{0.80}Fe_2O_4$	Cylindrical Glass Tube
		$Mn_{0.60}Zn_{0.40}Fe_2O_4$	Cylindrical Glass Tube
5	NH_3 gas	$Mn_{0.40}Zn_{0.60}Fe_2O_4$	Cylindrical Glass Tube
		$Mn_{0.60}Zn_{0.40}Fe_2O_4$	Cylindrical Glass Tube

table 3.D.1, are deployed to fabricate the sensor for respective parameters. Employing these sensors the Smart Sensor Module is designed. The designing issues are interpreted in next topic.

References:

1. T.J. Shinde, A.B. Gadkari, P.N. Vasambekar, "DC resistivity of Ni–Zn ferrites prepared by oxalate precipitation method", Mater. Chem. and Phys. 111 1(2008) 87-91.
2. Y.-P. Fu and S.-H. Wu, "Electrical and Magnetic Properties of Magnesium-Substituted Lithium Ferrite the Ceramic," Ceramics International,36 (2010)1311- 1317.
3. M. E. Shabashy, "DC Electrical Properties of Zn-Ni Ferrites," J. Magn. and Magn. Mater., 172 1-2 (1997)188-192.
4. V. R. K. Murthy andJ. Sobhanadri, "Electrical conductivity of some nickel-zinc ferrites, Physica Status Solidi (a) 38 2 (2006) 647-651.
5. E. Veena Gopalan, I.A.Al-Omari, K.A.Malini, P.A.Joy, D.SakthiKumar, YasuhikoYoshida and M.R.Anantharaman, "Impact of zinc substitution on the structural and magnetic properties of chemically derived nanosized manganese zinc mixed ferrites", J. Magn.and Magn.Mater., 321(2009) 1092–1099.
6. M. Ul-Islam, T. Abbas, and M Ashraf Chaudhry, "Electrical properties of Cd-substituted copper ferrites", Materials Letters, 53 1-2 (2002)30-34.
7. S M Chavan, M K Babrekar, S S More and K M Jadhav," Structural and optical properties of nanocrystalline Ni–Zn ferrite thin films", J. Alloys Compd. 507(2010)21-25.
8. T. J. Shinde, A. B. Gadkari, P. N.Vasambekar, "Effect of Nd^{3+} substitution on structural and electrical properties of nanocrystalline zinc ferrite", J. Magn. Magn. Mater., 322 18 (2010)2777-2781
9. B.V. Bhise, A. K. Ghatage, B. M. Kulkarni, S. D. Lotke, S. A. Patil, "Conduction in Mn substituted Ni-Zn ferrites," Bull. Mater. Sci., 193(1996)527-531.
10. P.N.Vasambekar, C.B.Kolekar and A.S.Vaingankar, "Crystallographic and dc electrical resistivity study of Cd-Co and Cr^{3+} substituted Cd-Co ferrites," Journal of Materials Science: Materials in Electronics, 10(1999)667-671.
11. A Narayanasamy and N Sivakumar, "Influence of mechanical milling and thermal annealing on electrical and magnetic properties of nanostructured Ni–Zn and cobalt ferrites", Bull. Mater. Sci., 31 3 (2008)373–380.

12. S.G. Bachhav, A.A. Patil and D.R. Patil, “Electric and Dielectric Properties of Ni Substituted Mg-Zn-Cu Ferrites”, Adv. Ceram. Sci. and Engg (ACSE), 2 2(2013) 89-94.
13. S D Shenoy, P A Joy and M R Anantharaman, “Effect of mechanical milling on the structural, magnetic and dielectric properties of coprecipitated ultrafine zinc ferrite”,J. Magn. Magn. Mater. 269 (2004)217–226
14. M. George, S. S Nair, A. M. John, P. A. Joy and M R Anantharaman, “Structural, magnetic and electrical properties of the sol-gel prepared $L_{i0.5}F_{e2.5O4}$ fine particles”, J. Phys. D: Appl. Phys. **39(**2006) 900.
15. V. E. Gopalan, K.A.Malini, D. Sakthi Kumar, Y. Yoshida, I. A. Al-Omari S. Saravanan and M. R. Anantharaman, “On the dielectric dispersion and absorption in nanosized manganese zinc mixed ferrites”, J. Phys. Condens. Matter, 21 (2009) 146006.
16. E Veena Gopalan, K A Malini, S Sagar, D Sakthi Kumar, Y. Yoshida, I A Al-Omari and M R Anantharaman, “Mechanism of ac conduction in nanostructured manganese zinc mixed ferrites”, J. Phys. D: Appl. Phys., 42 (2009) 165005-165013.
17. K. Vijaya Kumar, R Sridhar, D. Ravinder, and K. Rama Krishna, “Structural Properties and Electrical Conductivity of Copper Substituted Nickel Nano Ferrites”, Intern. J. Appl. Phys. and Maths., 4 2 (2014) 113-117.
18. K. Rama Krishna, K. Vijaya Kumar, Dachepalli Ravinder, “Structural and Electrical Conductivity Studies in Nickel-Zinc Ferrite”, Adv. Mater. Phys. and Chem., 2(2012)185-191.
19. S. C. Chaudhari and A. K. Ghatage, “Electrical and dielectric behaviour of chromium substituted nickel ferrite”, Der Chemica Sinica, 4 3 (2013)47-51.
20. R. S. Totagi, N. J. Choudhari, S. S. Kakati, C. S. Hiremath, S. B. Koujalagi and R. B. Pujar “Electrical properties of Ni-Mg-Cu nanoferrites synthesized by sucrose precursor technique”, Der Pharma Chemica, 7 3 (2015)11-15.
21. G. S. V. R. K. Choudary, M. Chaitanya Varma, and K. H. Rao, “Effect of Nd^{3+}on Electrical resistivity and dielectric properties of NiZnferrites”, National Conference on Advanced Functional Materials and Computer Applications in Materials Technology (2014) 36-41.

22. B.P. Ladgaonkar, P.N. Vasambekar andA.S. Vaingankar, “Structural and dc electrical resistivity study of Nd^{3+} substituted Zn-Mg ferrite”, J. Mater. Sci. Lett., 19(2000)1375.
23. A.B. Gadkari, T.J. Shinde and P.N. Vasambekar, “Structural analysis of Sm^{3+} doped nanocrystalline Mg–Cd ferrites prepared by oxalate co-precipitation method”, Materials Characterization 60 11 (2009)1328-1333.
24. I.H. Gul and A. Maqsood, “Structural, magnetic and electrical properties of cobalt ferrites prepared by the sol–gel route”,J. Alloys and Compounds**”,** 4651–2 (2008)227–231.
25. A.M. El-Sayed, “Electrical conductivity of nickel–zinc and Cr substituted nickel–zinc ferrites, Materials Chemistry and Physics**”,** 82 3 (2003) 583–587.
26. A Sutka, G Mezinskis and A Lusis, “Electric and dielectric properties of nanostructured stoichiometric and excess-iron Ni–Zn ferrites” Physica Scripta *Phys. Scr* A, 87 2 (2013). 87.
27. A. Munir, F. Ahmed, M. Saqib and M. Annis Ur Rehman, “Electrical Properties of Ni Zn Nanoparticles prepared by simplified sol gel method”,J. Super Cond. Nov Magn., 28(2015)983-987.
28. G.Aravind, Abdul Gaffoor, D. Ravinder and V. Nathanial, “Impact of transition metal ion doping on electrical properties of lithium ferrite nanomaterials prepared by auto combustion method”, Adv. Mater. Lett., 6 2 (2015)179-185.
29. S.G Bachhav, R.S Patil, P.B Ahirrao, A.M Patil and D.R. Patil, “Microstructure and magnetic studies of Mg–Ni–Zn–Cu ferrites”, Mater. Chem. Phys. 129 (2011) 1104-1109.
30. N.Varalaxmi and K.V. Sivakumar, “Studies on AC and DC Electrical Conductivity Andthermo-Electric Power of NiMgCuZn Ferrite”,Int. J. Nanoparticles, 3 4 (2010)349
31. B.P. Ladgaonkar, P.N. Vasambekar and A.S. Vaingankar, “Effect of Zn^{2+} and Nd^{3+} substitution on magnetization and ac susceptibility of Mg ferrite”, J. Magn. and Magn. Mater, 210 1-3 (2000)289.
32. F. Li, H. Wang, L. Wang, J. Wang, “Magnetic properties of ZnFe2O4 nanoparticles produced by a low-temperature solid-state reaction method”, J .Magn .Magn. Mat. 309 (2007) 295-299.
33. P A Jadhav, R S Dewan, Y D Kolekar, B K Chougule, J Phys And Chem Of Solids, 2009, 70, 396-400

34. M.A. Ahmed, E. Ateia., L.M. Salah, A.A. El-Gamal, "Structural and electrical studies on La^{3+} substituted Ni–Zn ferrites", Mater. Chem. and Phys., 92(2005)310–32.
35. G. Vaidyanathan , R. Arulmurugan , S. D. Likhite , M R Anantharamanc, M.Vaidya , S. Sendhilnathan and N. D. Senthilram, "Effect of preparation on magnetic properties of Mn-Zn ferrite", Ind. J. Engg. & Mater. Sci., 11(2004)289-294
36. N. T. Lan, T. D. Hien, N.P. Duong and D. V. Thruong, "Magnetic Properties of $Mn_{1-x}Zn_xFe_2O_4$ ferrites nanoparticles prepared by using Co-precipitation", J. of Korean Phys. Society, 52 5 (2008) 1522-1525.
37. http://web.uvic.ca/~djberg/Chem324/Chem324-12.pdf
38. https://www.unf.edu/~michael.lufaso/chem3610L/inorganic_lab_exp_8.pdf
39. A Mahesh Kumar , TRK Pydi Raju , P Appa Rao , M Chaitanya Varma , GSVRK Choudary , K. Srinivasa Rao and KH Rao, "Cation Distribution in $Mn_{0.7}Me_{0.3}Fe_2O_4$ (Me = Ni, Co and Zn)", Int. J. Adv. Res. Sci. Technol.,1 1(2012)1-4.
40. O. M. Hemeda, "Structural and Magnetic Properties of $Co_{0.6}Zn_{0.4}Mn_xFe_{2-x}O_4$", Turk. J. Phys., 28 (2004)121 – 132.
41. Intel Physical Constants of IC Package Materials Packaging Data book, 2000
42. www.national.com, Semiconductor Packaging Assembly Technology, August, 1999.
43. K. Arshaka , K.Twomey and D.Egan, "A Ceramic Thick Film Humidity Sensor Based on MnZn Ferrite", Sensors 2 (2002) 50-61.
44. H. Farahani, R. Wagiram and M. N. Hamidon, "Humidity sensors principle,mechanism and fabricaition technologies: a comprehensive review", Sensors, 14 (2014) 7881-7939.
45. Chairperson Publication Board, "Guide to meteorological Instrument and method of observations", 7th Edn, World Meteorological organization, Geneva, Switzerland, 2008.
46. J. R. Stetter, W. R. Penrose and S. Yao, "Chemical Sensors, Electromagnetic Sensors and ECS", J. Electrochem.Soc., 150(2003) S11.
47. J. Fraden, " Handbook of Modern Sensor", Springer Newyork, NY, (2010)

48. N. Rezlescu, C. Dorofti and P. D. Popa, "Humidity Sensing Electrical Resistivity of $MgFe_2O_4$ and $Mg_{0.9}Sn_{0.1}Fe_2O_4$ Porous Ceramics", Romania J. Phys., 52 3-4 (2007)353-360.
49. E. Traversa, "Ceramic Sensors For Humidity Detection: The state of Art and Future Developments", Sensors and Actuators B Chemical, 23 (1995) 135-156.
50. Z. Chen and C. Lu, "Humidity Sensors: A Review Of Materials And Mechanism", Sensor Letters, 3 (2005) 274-295.
51. A.Y Lipare' ,P.N Vasambekar, A.S Vaingankar**,** "Dielectric Behavior and A.C. Resistivity Study Of Humidity Sensing Ferrites", Materials Chemistry and Physics**,** 81 1 (2003)108–115.
52. J. Wang , F. Wu, K.Shi, X.Wangand P. Sun, "Humidity Sensitivity Of Composite Material Of Lanthanum Ferrite/Polymer Quaternary Acrylic Resin", Sensors and Actuators B: Chemical, 99, 2–3, (2004)586–591.
53. N. Rezlescu' , C. Doroftei, E. Rezlescuand P.D. Popa**,** "Structure and Humidity Sensitive Electrical Properties of the Sn^{4+} and/or Mo^{6+} Substituted Mg Ferrite", Sensors and Actuators B: Chemical**,**115 2 (2006)589–595.
54. P.M. Faia' , C.S. Furtado, and A.J. Ferreira**,** "Humidity Sensing Properties Of A Thick-Film Titania Prepared By A Slow Spinning Process", Sensors and Actuators B: Chemical**,**1011–2, 15(2004)183–190.
55. R.K. Kotnala' , Jyoti Shah, Bhikham Singh, Hari kishan, Sukhvir Singh, S.K. Dhawan and A. Sengupta, "Humidity Response Of Li-Substituted Magnesium Ferrite", Sensors and Actuators B: Chemical,129 2 (2008) 909–914.
56. E. Rezlescu' , N. Rezlescuand P.D. Popa**,** "Fine-grained MgCu Ferrite With Ionic Substitutions Used As Humidity Sensor", J. Magn.and Magn. Mater.290–291 2 (2005)1001–1004.
57. J. Shah, M. Arora, L.P. Purohit and R.K. Kotnala**,** "Significant Increase In Humidity Sensing Characteristics Of Praseodymium Doped Magnesium Ferrite", Sensors and Actuators A: Physical167 2 (2011)332–337.

58. Z.Wang, C.Chen, T.Zhang, H. Guo, B. Zou R. Wang and F.Wu' "Humidity Sensitive Properties of K^+-doped nanocrystalline $LaCo_{0.3}Fe_{0.7}O_3$",Sensors and Actuators B: Chemical126 2-1 (2007)678–683..
59. J.M. Tullianiand P. Bonville' "Influence of the dopants on the electrical Resistance Of Hematite-Based Humidity Sensors" Ceramics International, 31 4 (2005)507–514.
60. N.Bagum, M. A. Gafur, A. H. Bhuiyan and D. K. Saha,"$MgCl_2$ doped $Cu_xZn_{1-x}Fe_2O_4$ ferrite humidity sensors", Phys. Status Solidi (a), (2010). 10.
61. A. B Gadkari, T.J Shinde and P. N. Vasambekar, " Electrical and Humidity Sensing Study of Nanocrtsyallite Mg-Cd Ferrites", Sensors & Transducers 137 2 (2012) p145
62. I. Petrila and F. Tudorache, Humidity sensor applicative material based on copper-zinc-tungsten spinel ferrite", Mater.Lett., 108(2013)129-133.
63. A. Carvalievi, T. Caronna, I. Natali Sora and J. M. Tulliani, " Electrical characterization of room temperature humidity sensor in $La_{0.8}Sr_{0.2}Fe_{1-x}Cu_xO_3$ (x=0, 0.05 and 0.10)", Ceramic International, 38(2012)2865-2872.
64. N Rezlescu, E Rezlescu, C Doroftei and P D Popa, "Study of some Mg-based ferrites as humidity sensors", J. Physics: Conference Series, 15 (2005) 296–299.
65. K. Arshaka , K.Twomey and D.Egan, " A Ceramic Thick Film Humidity Sensor Based on MnZn Ferrite", Sensors, 2(2002)50-61.
66. K. Bull, "Methods of Accurately Measuring Capacitive Rh Sensors",5th International Symposium on Humidity and Moisture – ISHM 2006 Brazil, May 02 – 05, 2006 – Rio de Janeiro, Brazil
67. Z. M.Rittersma, " Recent achievement in miniaturized humidity Sensor- A Review of transduction technique", Sensors and actuators A 96(2002) 196-210
68. Y. Köseo_glu, I. Aldemir, F. Bayansal, S. Kahraman and H. A. Çetinkara, "Synthesis, Characterization and Humidity Sensing Properties of $Mn_{0.2}Ni_{0.8}Fe_2O_4$ Nanoparticles", Materials Chemistry and Physics 139 (2013) 789-793.
69. H. Saha, "Porous Silicon Sensors- Elusive and Erudite"Intern.J.smart sensing and intelligent systems, 1 1(2008) 34-56.
70. Q. Q., Tong Zhang, Q. Yu, R.Wang, Y. Zeng, L. Liu, H. Yang, "Properties of Humidity Sensing ZnO Nanorods-Base Sensor Fabricated By Screen-Printing" Sensors and Actuators B 133 (2008) 638–643

71. J.M. Tulliani, C.Baroni, L.Zavattaro and C. Grignani, " Strontium-Doped Hematite as a Possible Humidity Sensing Material for Soil Water Content Determination", Sensors, 13(2013)12070–12092.
72. A. Lapina, P. Holtappels, and M. Mogensen, "Conductivity at Low Humidity of Materials Derived from Ferroxane Particles", International Journal of Electrochemistry, 2012 (2012) ID 930537, 7 .
73. S. N. Patil and B. P. Ladgaonkar, "Synthesis And Implementation Of Niznfe2o4 Ferrites To Design Embedded System For Humidity, Measurement", Intern. J. Adv. Res. in Electr., Electr. Instrum. Engg., 2 8 (2013) 3813-3821.
74. G. Gumano, G. Montesperelli, B. Morten, M. Prudenziati, A. Pumo and E. Traversa, " Thick films of MgFe2O4 for humidity sensors", J. Mater. Process. Technon., 56(1996)589-599.
75. G. Gumano, G. Montesperelli, P. Nunziante and E. Traversa, " Humidity sensitive electrical response of sintered MgFe2O4", J. Mater. Sci., 28(1993) 6171-6195.
76. T. Nittta, Z.Terada and S. Hayakawa, " Humidity sensitive electrical conduction of MgCr2O4-TiO2 porous ceramics", J. Am. Ceram. Soc., 63 5-6 (1980)295-300.
77. H.Nishikawa, R. Kurihara, and S.Sukemori, " Measurements of humidity and current distribution in a PEFC". J. Power Sources,155 (**2006)** 213-218
78. B. A. Aldar, R. K. Pinjari, N. M. Burange, " Electric and Dielectric behavior of Ni-Co-Cd Ferrite", IOSR Journal of Applied Physics, 6 4(2014) 23-26.
79. HIH-3605 humidity sensor data sheet, www.honeywell.com.
80. Humidity probes data sheets, www.vernier.com.
81. W. Qu, W. Wlodarski, "A thin-film sensing element for ozone, humidity and temperature", Sensors and Actuators B 64 (2000) 42–48.
82. R. L. Vander wal, G. W. Hunter, J. C. Xu, M. J. Kulis, G. M. Berger and T. M. Ticich, "metal oxide nanostructure and gas sensing performance", Sensors and Actuators B : Chemical, 138 (2009) 113-119.
83. L. Yang, X. Yong-an, Z. Heyuan, W. Xing-hiu and W. Yu-de, "preparation and gas sensing properties of $NiFe_2O_4$ semiconducting materials", J. Sol., Stat, Electr., 49 8(2005) 1029-1033.
84. I. A. Abdel-Latif, "Fabrication of Nano - Size Nickel Ferrites for Gas Sensors Applications", J. Phys., 1 2 (2012) 50 – 53.

85. G. Zhang, C. Li, F. Cheng and J. Chen, "$ZnFe_2O_4$ tubes: Synthesis and application to the gas sensor with high sensitivity and low energy consumption", Sensors and Actuators B Chemical, 120 (2007) 403-410.
86. N. Iftimie, E. Rezlescu, P.D. Popa and N. Rezlescu, "The Magnetic Oxide Semiconducting Ceramic As Gas Sensor", J. Opto. Electr. and Adv. Mater, 8 3 (2008) 1001-1003.
87. N. Iftimie, E. Rezlescu, P.D. Popa and N. Rezlescu, "Gas Sensitivity OfNanocrystalline Nickel Ferrite", J. Opto. Electr. and Adv. Mater, 8 3 (2008) 1016-1018.
88. N. Rezlescu, E. Rezlescu, A.F. Tudorachi and P.D. Popa, "Gas Sensing Properties Of Porous Cu,Cd and Zn Ferrites", Romanian Reports in Phys., 62 2 (2009) 233-234.
89. A. Chapelle, M. Yaacob, I. Pasquet, L. Presmanes, A. Barnable, P. Tailhodes, J.D.Plessis and K.K. Zadeh, "StructualAnd Gas Sensing Properties of CuO-$Cu_xFe_{3-20}O_4$ Nano-Structured Thin Films", Sensors and Actuators B: Chemical, 153 (2011) 117-124.
90. N.D. Hoa, N.V. Quy, H. Jung, D. Kim, H.Kim and S.K. Hong, "Synthesis Of PorousCuONanowires And Application To The Hydrogen Detection", Sensors and Actuators, B: Chemical, 146 (2010) 266-272.
91. N. Yamazoe, "Toward Innovations of Gas Sensor Technology", Sensors and Actuators B: Chemical, 108 (2005) 2-14.
92. L.B.Kong and Y.S.Shen, "Gas Sensing Properties and Mechanism Of$Ca_xL_{1-x}FeO_3$ Ceramics", Sensors and Actuators B: Chemical, 30 (1996) 217-221.
93. K. Wetchakun, T. Samerjai, N. Tamaekong, C. Liewhiran, C. Siriwang, V. Kruefu, A. wisitsoroat, A. Tuantranont and S. Phanichphant, "Semiconducting Metal Oxides As Sensors For Environmentally Hazardous Gases", Sensors and Actuators B: Chemical, 160 (2011) 580-591.
94. Y.L. Liu, Z. M. Liu, Y. Yang, H.F. Yang G. L. Shen and R.Q. Yu, "Simple Synthesis of $MgFe_2O_4$Nano-Particles As Gas Sensing Materials", Sensors and Actuator B:Chemical, 107 (2005) 600-604.
95. N. Xinsha, L.Yanli, X.Jiaiang, Chin Funct. Mater, 33(2002) 413.
96. C.V. Gopal Reddy, S.V. Manorama and V. J. Rao, "Semiconducting Gas Sensor For Chlorine Based On Inverse Spinal Nickel Ferrite", Sensor And Actuators B. 55(1999)90-95

97. N.Rezlesan. N. Iftimie, E. Rezfecu, C. Doroftei and P.D. Popa, "Semiconducting Gas Sensor For Acetone Based On The Fine Grained Nickel Ferrite", Sensors And Actuators B, 114(2006) 427-432
98. Z. Tiansha, P. Hing, Z. Jiancheng and K. Lingbing, "Ethanol Sensing Characteristics Of Cadmium Ferrites Prepared By Chemical Co-Precipitation", Mater. Chem. Phys, 61 3(1999)192-198.
99. R. B. Kamble and V. L. Mathe, "Nano Crystalline Nickel Ferrite Thick Film As An Efficient Gas Sensor At Room Temperature", Sensors And Actuators, B: Chem. 113, 1, 14(2008) 205-209
100. A. B. Gadkari, T. J. Shinde and P. N. Vasambekar, "Ferrite Gas Sensor", IEEE Sensor I, 11 4 (2011) 849-861
101. A. B. Gadkari, T. J. Shinde and P. N. Vasambekar, "Liquid PetroleumGas Sensor Based On Nano-Crystalline $Mg_{0.6}Cd_{0.4}Fe_2O_4$", Adv. Mat. Lett., 4 7 (2013) 573-576
102. S.A. Masti, A. K. Sharma and P. N. Vasambekar, "Liquefied Petroleum Gas Sensor Base On Cr^{3+} Substituted Mixed Mg. Cd. Spinel Ferrites", Arch Phys. Res., 6 1 (2015) 1-6.
103. A. Jain, R. K. Baranwal, A. Bharti, Z. Vakil and C. S. Prajapati, "Study of Zn-Cu Ferrite Nano-Particales for LPG Sensing", The Sci. World J., (2013) 1.
104. V. D. Kapse, F. C. Raghuwanshi and V. S. Sangawar, "Preparing And Ethanol Sensing Behavior Of Spinel-Type Nano-sized Mixed Ferrites Containing Zn", Int. J. Chem. and Phys. Sci. 4 1 (2015) 121-127.
105. V. D. Kapse, S. A. Ghosh, R.C. Raghuwanshi, S.D. Kapseand V.S. Khandekar, "Nano-Crystalline $NiO_6Zn_{0.4}Fe_2O_4$ A Novel Semiconducting Material for Ethanol Detection", Talanta, 78 (2009) 19-25.
106. U. B. Gawas, V. M. S. Verenkar and D.R. Patil, "Nano-StructedFerrite Based Electronic Nose Sensitive To Ammonia At Room Temperature", Sensors and Transducers J., 134 11 (2011) 45-55.
107. J. Wan-Li and Z. Lei, "Preparation and Gas Sensing Properties For Acetone Of Amorphous Ag Modified $NiFe_2O_4$Sensor", Trans. Nonferrous. Mater. Soc. China, 22 (2012) 1127-1132.
108. D. C. Bharati, K. Mukherjee and S. B. Majumdar, "Wet Chemical Synthesis And Gas Sensing Properties Of Magnesium Zinc Ferrit Nano-Particles", Mater., Chem. Phys., 120 (2010) 509-517.

109. Labidi, E. Gillet, R. Delamare, M. Maaref and K. Aguir, “Ethanol and ozone sensing characteristics of WO_3 based sensors activated by Au and Pd”, Sensors and ActuatorsB: Chem. 120 (2006) 338–345.
110. J. Herran, G.G. Mandaya and E. Castano, “Semiconducting BaTiO3–CuO mixed oxide thin films for CO2 detection”, Thin Solid Films 517 (2009) 6192–6197.
111. A.Z. Sadek, S. Choopun, W. Wlodarski, S.J. Ippolito and K. Kalantar-zadeh, Characterization of ZnO nanobelt-based gas sensor for H_2, NO_2, and hydrocarbon sensing”,J. IEEE Sensors, 7 (2007) 919–924.
112. C.M. Ghimbeu, M. Lumbreras, M. Siadat, J. Schoonman, “Detection of H_2S, SO_2, and NO_2 using electrostatic sprayed tungsten oxide films, Mater. Sci. Semiconduct. Proc. 13 (2010) 1–8
113. T. Zhang, L. Liu, Q. Qi, S. Li, G. Lu, Development of microstructure In/Pd-doped SnO2 sensor for low-level CO detection, Sens. Actuators B: Chem. 139 (2009) 287–291.
114. C.M. Ghimbeu, M. Lumbreras, J. Schoonman, M. Siadat, Electrosprayed metal oxide semiconductor films for sensitive and selective detection of hydrogen sulfide, Sensors 9 (2009) 9122–9132.
115. S. Das, S. Chakraborty, O. Parkash, D. Kumarb, S. Bandyopadhyay, S.K. Samudrala, Sena, H.S. Maiti, Vanadium doped tin dioxide as a novel sulfur dioxide sensor, Talanta 75 (2008) 385–389.
116. http://www.thermoscientific.com/content/tfs/en/product/midi-co-sub-2-sub incubators.html#sthash.Kvo6hkCO.dpuf
117. Ahmod Umar and Yoon-Bong Hahn, “Metal oxide Nanostructures and Applications”, American Scientific Publishers, 3(2010)31-52.
118. G. F. Fine, L. M. Cavanagh, A. Afonja and R. Binions, “Metal Oxide Semi-Conductor Gas Sensors in Environmental Monitoring”, Sensors 10(2010)5469-5502.
119. N. Barsan, M. Schweizer-Berberich and, W. M. Göpel, “Fundamental and practical aspects in the design of nanoscaled SnO_2 gas sensors”, A status report. Fresenius J. Anal. Chem. 1999, 365, 287–304.
120. N.Barsan and U. Weimar, “Understanding the Fundamental Principles of Metal Oxide Based Gas Sensors; the Example OfCO Sensing With Sno2 Sensors In The Presence Of Humidity”. J. Phys. Cond. Matt. 2003, 15, R813.

121. R. Binions, H.Davies, A. Afonja, S. Dungey, D. Lewis, D E Williams and I. P. Parkin, " Zeolite modified discriminating gas sensors", J. Electrochem. Soc. 156 (2009)J46–J51.
122. S. C. Naisbitt, K. F. E.Pratt, D E Williams and I. P. Parkin, "A microstructural model of semiconducting gas sensor response: The effects of sintering temperature on the response of chromium titanate (CTO) to carbon monoxide", Sens. Actuat. B-Chem. 114(2006)969–977.
123. X.Wang,N. Miura and N.Yamazoe, "Study of WO3-based sensing materials for NH3 and NO detection". Sens. Actuat. B-Chem. 66(2000)74–76.
124. B.Karunagaran, P.Uthirakumar, S. J. Chung, S.Velumani and E. K. Suh, "TiO2 thin film gas sensor for monitoring ammonia". Mater. Charact. 58(2007)680–684.
125. M. S. Wagh, G. H. Jain, D. R. Patil, S. A.Patil, and L. A. Patil, "Modified zinc oxide thick film resistors as NH3 gas sensor", Sens. Actuat. B-Chem. 115(2006)128–133.

*****

Topic 4

A Smart Sensor Module: An Embedded Design

4.A.(a) Introduction:

The rapid evolution of the electronic technologies, such as embedded technology, computer communication and network technology, microelectronics and sensor technologies, VLSI technologies etc enabled the vast proliferation of the field of electronic instrumentation. Due to this, the field of smart sensor module is emerging. The sensor technology is the core technology and producing the sensors based on physical transduction only. These sensors are rarely having analog as well as digital signal processing units. Depending upon physical properties of the transducer, the designer has to organize the further analog part of the circuit. In fact, the modern instrumentation depicts the need of plug-and-play modules of promising features. This leads to emergence of novel concept of Smart Transducer Interference Module (STIM) or Smart Sensor Module (SSM) [1]. The smart or intelligent module provides better solution to the problem of sensor interfacing to the devices. It also helps to simplify the software interfacing problems, normally occur in measurement and control instrumentation [2]. Many modular platforms have been developed to facilitate the design and implementation of smart sensing systems. Modular platforms can be of great benefit for system prototyping. In fact, smart and ubiquitous sensor systems are of increasing interest, which allows fast prototyping of new innovative sensor based systems. An implementation of smart sensor module also helps to enhance the features of the devices. Individual sensor based system can be designed and interfaced to the actual instrument. Each such system has its own data communication capabilities along with the signal conditioning stages. This can be done by providing a processor, protocol controller etc chips to each sensor path. This obviously causes to increase the cost of the system and complexity in hardware and software as well. The cost may be increased several dollars per sensor. Recently, the microcontroller from different families can be available. Also VLSI devices are available to design smart sensor module. Deploying

the configurability of the devices sensor module can be made smarter. Therefore, the design and development of Smart Sensor Module (SSM) is the need of the hour.

According the proposed architecture, the sensor module comprises a computing unit, analog signal conditioner, data acquisition and data converter, output protocols and display unit [Topic 1]. The IEEE 1451 standards also supports above architecture of the SSM. To maintain the portability of smart sensor module IEEE has drafted the standards and popularized as IEEE P1451 standards for smart transducer interface module.

During recent days, such sensor modules are available for typical sensors such as humidity (SY-HS-220, HSM20G), Temperature sensor module (KY-013, KY-015), carbon dioxide gas (B-530,MG-811), PIR sensor (HC-SR 501, SEN116A2B), alcohol gas(TW220), Hall effect sensor (SS441R) etc. However, these sensor modules consist of only analog signal processing circuit and therefore, these are not smart sensor module. Moreover, the cost of such sensor module is also high. Therefore, to provide cost effective solution, the smart sensor module is most suitable. It also provides following design requirements.

- Selection of only smart sensor module, which meet the design requirement. The physical properties of transducers are not necessary to consider.
- Use of same module for multiple devices.
- The data in required format can be obtained and hence bus protocol can be ensured.
- Significant reduction of installation cost by eliminating long and large number of analog wires.
- Acceleration of the design cycle, due to reduction in R & D work and calibration work as well.
- Dynamic configuration of measurement and control loop through software.
- Addition of intelligence by leveraging the advanced microcontrollers used for digital data processing.

Thus, the design and implementation of smart sensor module is novel area of the research. Therefore, to keep pace with the state of art of present electronic instrumentation, the smart sensor module is designed, wherein, embedded technology is realized. Moreover, the sensors are developed in the laboratory by using compositions

of polycrystalline nanoferrites as sensing materials and deployed in the present sensor module.

4.A (b) Review of the Literature:

During recent years, the technologists are focusing on the preciseness and reliability of the modern instruments. The significant attention is given on the introduction of themes of real-time operation. The efforts of the scientists are becoming milestones in the development process and a new area, wherein deployments of embedded technology are emphasized, is emerging [3]. During early days, the measurement instrumentation is based on direct interfacing of sensor. Moreover, these instruments rarely consist of any sophisticated computing unit. Therefore, these instruments are replacing with modern instruments, wherein a ubiquitous embedded technology is realized. Now days, the trend of designing and implementation of smart sensor module is emerging. Therefore, the researchers are showing interest in designing of sensor modules. Simic had designed microcontroller based system for monitoring of relative humidity and temperature [4]. This sensor system is developed about readily available sensors. Further, the system was also modified by incorporation of the GUI. The required GUI is developed about Labview and presented [5]. Due to addition of the GUI, the system became smarter. Opera et al had developed sensor module for temperature, humidity and gas on flexible substrates [6]. They developed sensing platforms for above parameters by using interdigitated electrodes. For humidity and gas sensing the dielectric properties of sensing materials are considered. Opera et al attempted to make the system smart. They deployed ΔΣ type of analog to digital converter, AD7746, and data is delivered on the I^2C bus of AD7746. They also made the provision of output data of USB standards. The system designed reveal good reliability and portability as well.

Employing CMOS based capacitive sensor, the system was reported by Kummer et al [7]. It is the realization of integrated technology. The sensors, for gas sensing are developed on Si substrate to ensure the concept of System-on-Chip. The wireless sensor network technology is the realization of the collaborative networking, wherein each sensor node depicts the deployment of embedded technology. The sensor nodes comprise an array of sensors and respective signal conditioning circuits. The microcontrollers satisfy the needs of computing unit. Moreover, the outputs provided by

the nodes are either by wireless node or wired communication. Therefore, it can be said that, the node of WSN is the realization of smart sensor module [8]. Based on advanced microcontrollers, such smart sensor nodes have been designed by many researchers and the results are interpreted [9-12]. The motes demonstrated by Wobscholl is R & D prototype ensuring automatic calibration [13]. However, the sensor modules (Motes) launched by Flyport and Wasp are commercial and revealing great portability [14,15]. However, the sensor modules are not calibrated and hence, it requires frequent calibration. This may suffer the preciseness. Emphasizing the reduction of power consumption an embedded system is designed for two gas sensor, wherein, the signal acquisition is ensured by the use of Wheatstone circuit [16]. The reduction in power consumption is achieved by pulse heating technique, wherein, the current through heating element is controlled by ON/OFF circuit [16]. This pulse heating method adversely affect on the stability in the operating temperature and hence the sensitivity of the sensor. The sensor modules of plug-and-play facilities depict good portability [14,15]. An intelligent humidity sensing module for agricultural applications was reported by Shinghal et al [17]. The standards for intelligent sensor module are laid down by the IEEE group numbered as 1451 [18]. Integration of various functions of the sensors on one board is concept of intelligent sensor unit [17]. General architecture of intelligent sensor module is the realization of embedded system [19,20,21].

To ensure sensor module, in addition to sensing element, the associated sections such as amplifiers, signal conditioners, data converters, memory and control circuitry etc causes to increase the intelligence in the sensor module [22-24]. To ensure biomedical applications, a smart sensor modules are designed and reported [25,26]. A smart sensor module for health monitoring was designed by Staszewski et al [25]. Moreover, for monitoring of the mechanical stress on various infrastructures the sensor module was designed and reported by Jovanov et al [26]. Feng and Jiangfeng [27] have designed sensor module for wireless gas sensor, wherein the smart device like Zigbee is installed to ensure wireless communication. Automatic gas circulation and threat as well as leakage monitoring electronic system was demonstrated by Ranwaka [28], wherein an embedded technology is deployed. Deploying VLSI techniques Reges et al had developed smart sensor network, wherein CAN technology is used [29]. Chaudhari and Dharavath have developed smart sensor module, wherein the standards of IEEE-P1451.2 are ensured [30]. They defined two sections for the sensor module as network independent section and network specific section and deployed the same for wireless

communication. Architecture for smart transducer interface was proposed by Schiefer and Lally [31], wherein the P1451 standards are considered. The network capable application processor is incorporated. Based on FR-4 as substrate Smart Wireless Integrated Module (SWIM) is designed by Palacios et al [32]. The module is designed for Wireless Sensor Network. It is the realization of System on Package (SOP), wherein two standards IEEE 802.15.4 and IEEE P1451.2 are implemented. It is also found that, the sensor modules such as SY-HS-220 are also available. However, these sensor modules do not include any computing unit. Therefore, these sensor modules are not intelligence. Therefore, it is proposed to design smart sensor module, wherein an embedded technology is ensured.

4.A (c) IEEE 1451 Standards for Smart Sensor Module:

The IEEE 1451 is the set of standards for Smart Transducer Interface Module (STIM) or Smart Sensor Module (SSM), developed by the Institute of Electrical and Electronics Engineers (IEEE), describing a set of parameters of SSM such as common analog and digital hardware, network-independent communication interfaces for connecting transducers (sensors or actuators) to microcontrollers, Networking protocols for wired and wireless communication etc.[33] The goal of the IEEE 1451 family of standards is to allow the access of transducer data through a common set of interfaces whether the transducers are connected to systems or networks via a wired or wireless means. IEEE 1451, designated as Standard Transducer Interface for Sensors and Actuators, consists of six document standards which are summarized in table 4.1.

TABLE 4.1 : IEEE Standards for Smart Transducer/ Sensor inteface module and their functionalites

Sr. No.	IEEE Standards	Functionality
1.	IEEE P 1451.0	Common Functions, Communication Protocols,
2.	IEEE 1451.1	Network Capable Application Processor (NCAP) Information Model for Smart Transducers
3.	IEEE 1451.2	Transducer to Microprocessor Communication Protocols
4.	IEEE 1451.3	Digital Communication and Distributed Multidrop Systems
5.	IEEE 1451.4	Mixed-mode Communication Protocols
6.	IEEE 1451.5	Wireless Communication

A key point in case of smart sensor module is information related to the sensor and its feature. According to IEEE 1451 standards, the sensor related information is

tabulated and presented in Transducer Electronic Data Sheet (TEDS). This TEDS format depends upon capabilities of the smart sensor module. As shown in table 4.1, the IEEE 1451.0 describes the set of common requirements of SSM and communication protocol. This is related to the network independent establishment of the electronic parts. Moreover, IEEE 1451.1 is devoted for Network Capable Application Processor (NCAP) and related TEDS. The IEEE 1541.2 described the interfacing of transducers to the microcontrollers of advanced feature. Present smart sensor module includes in this catagory. The IEEE 1541.3 & 4 emphasizes the wired communication technologies whereas the standard regarding wireless comunication are given by IEEE 1541.5 group of technical teams [34]. It is to be noted that, the signal conditioning part of the sensor module is not covered in these standards.

According to IEEE 1451 standards, an architecture of the smart sensor / transducer interface module is as depicted in the figure 4.1. As shown in the figure 4.1, the sensor module consists of transducer (sensors or actuators) followed by the signal conditioning

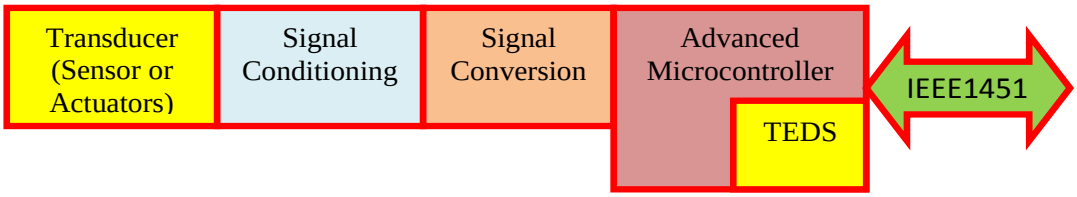

Figure 4.1: General architecture of Smart sensor module for four sensors (IEEE 1451 standards

stage. It is the design for four sensors. The physical properties of the sensing element is considered and signal conditioning circuit can be designed. While designing signal conditioner the cost of SSM should also be considered. Next block of SSM is the data converter. During early days, for data conversrion a separate devices (ADC or DAC) are employed. However, now days, the micrcocontrollers with on-chip ADC and DAC of smart features are available. Moreover, these microcontrollers also have sufficient on chip memory to store TEDS of the sensor module. These are the common designs. Now to establish the interface between STIM and NCAP, the standards IEEE 1451 offers the platform. This enabled the deployment of same transducer for many networks.

This is an overview of the technical aspects of the IEEE standards. According to IEEE 1451 standard the transducer functions for both as sesnor as well actualtors. Present investigation reveals the design for sensing mechanism only. Therefore, fudamentals of Smart Transducer Interface Module (STIM) and Smart Sensor Module

(SSM) are the same. However, practical consideration and implementation depends upon area of application and properties of the sesnor.

4.B The Design of Smart Sensor Module:

Sensors are used in many devices and systems to provide information of the parameters being measured or to identify the states of control. They are good candidates for increased built-in intelligence. In fact, use of microcontrollers would make sensors into smart sensor. With this added capability, it is possible for a smart sensor to directly communicate the data to an instrument or a system. In recent years, incorporation of the computer networking has gradually migrated into the sensor community. Networking of transducers (sensors or actuators) in a system and communicating transducer information via digital means versus analog cabling facilitates easy distributed measurements and control. In other words, intelligence and control, which were traditionally centralized, are gradually migrating to the sensor level. They can provide flexibility, improve system performance, and ease of system installation, upgrade, and maintenance. The rapid development and emergence of smart sensor and field network technologies have made the networking of smart transducers a very economical and attractive solution for a broad range of measurement and control applications. Deployment of embedded technology facilitates to keep pace with the modern instrumentation. Considering these facts into account, a smart sensor module is designed about AVR microcontroller, wherein the sensors designed in the laboratory by using polycrystalline spinel ferrites as sensing element, are employed. Present Sensor modules is designed for Temperature, relative humidity, carbon dioxide gas , ammonia and hydrogen sulfide gas. It is the realization of embedded technology. Therefore, both hardware as well as software is designed. Computing part of the hardware is designed about AVR AT mega8L microcontroller. Moreover, the firmware is developed by using Code Vision AVR , an Integrated Development Environment, in embedded C environment. Thus, the smart sensor module is designed and design issues are discussed in this topic through following points.

- Hardware of Smart Sensor Module
- Firmware of Smart Sensor Module

4.B.I) Organization of Smart Sensor Module:

A smart sensor module (SSM) is designed about AVR microcontroller and hardware of the same is described. The organization of SSM designed for present investigation is presented in figure 4.2. Moreover, the schematic of the same is depicted in figure 4.3. As indicated in figure 4.2, the SSM consist of microcontroller as a computing unit. This supports the definition of SSM and IEEE 1451.2 standards as well. The data output is available of different bus protocols, which may be applicable for establishment of sensor networking.

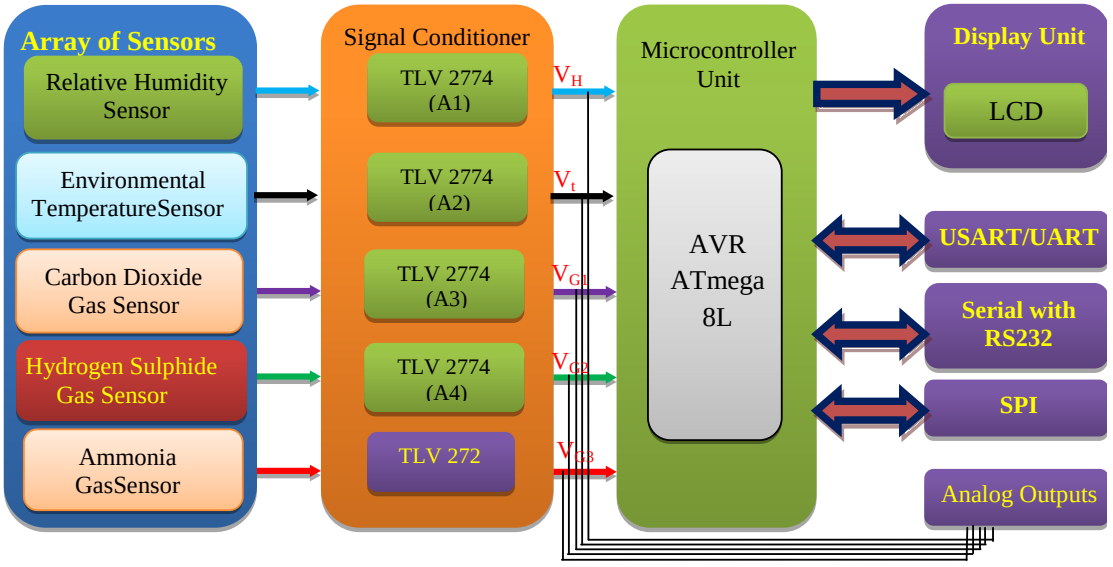

Figure 4.2: Block diagram of the Smart Sensor Module

4.B.II) The Circuit Description

The Smart Sensor Module (SSM), as presented in figure 4.3, consists of following sub-sections.

- An array of the sensors
- Signal conditioner
- Data Converter
- Microcontroller Unit
- Data Output unit
- Power Supply unit

All of these stages of the SSM are designed in the laboratory and will be discussed subsequently.

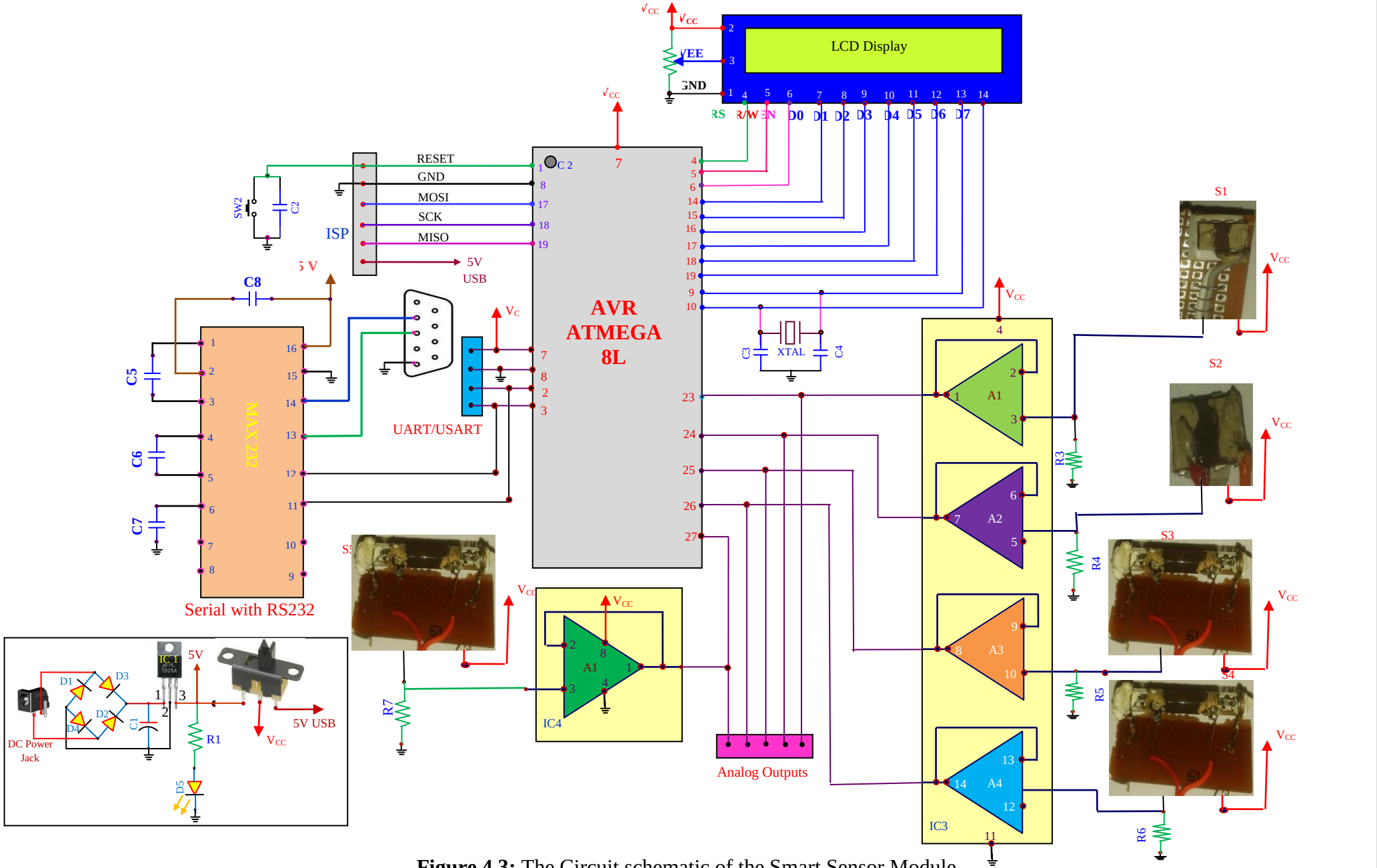

Figure 4.3: The Circuit schematic of the Smart Sensor Module

II. (a) An Array of the sensors :

The sensor is inherent part of the Smart Sensor Module (SSM). To enhance the reliability and preciseness of the SSM, the features of sensors play vital role. According to architecture of the SSM, given by the IEEE 1451 standards, the sensor is prime requirement. In fact, as discussed earlier, the physical properties are not considered by the IEEE technical committee. However, to increase adoptability, promisingly featured sensors are required.

Normally, the designers adopt readily available sensors, such MQ series, SH series, TGS series etc, vendored by different manufacturers [35, 36]. However, the reports on development of the sensors, wherein the sensing material is synthesized and deployed, are rare. As discussed in topic 2, the polycrystalline nanoferrites materials are successfully synthesized and studied for its suitability for sensor development [topic 3]. Employing these sensing materials, the sensors are designed and deployed for development of Sensing Unit of Smart Sensor Module (SSM). At present the SSM is designed for various environment parameters such as relative humidity, temperature, CO_2, H_2S, NH_3 etc. For each of the above parameters, a separate sensor is designed. Thus, five sensors are designed and implemented to facilitate the Sensing Unit of SSM. The sensing unit of SSM comprises following sensors.

- Relative Humidity Sensor
- Environmental Temperature sensor
- Carbon dioxide gas sensor
- Hydrogen sulfide gas senor
- Ammonia gas sensor.

The details regarding design and implementation of these sensors are discussed.

i) Relative Humidity Sensor:

Development of SSM for monitoring of relative humidity is one of objectives of present research. On investigation, it is proved that, the compositions of polycrystalline ferrite materials, $Mg_xZn_{1-x}Fe_2O_4$, $Ni_xZn_{1-x}Fe_2O_4$ and $Mn_xZn_{1-x}Fe_2O_4$, are most suitable as sensing element for relative humidity sensor. Employing this fact, humidity sensor is developed. It was attempted to design humidity sensor, by thick film technology, on various substrates [Topic 3]. However, the sensor developed on ceramic substrates reveals commendable features. In fact, the

compositions of above three series are investigated. However, on inspections of the results obtained, it decided to use $Ni_{0.4}Zn_{0.6}Fe_2O_4$ and $Mg_{0.4}Zn_{0.4}Fe_2O_4$ ferrite materials as sensing materials. Therefore, employing screen printing technique, a thick film of one of the above sensing materials is deposited on ceramic substrate. The technique of thick film deposition is already discussed. A thick film (4mm) of the sensor material is deposited on the rectangular substrate, of size 10mm x 5mm x 3mm, and slowly heated to the 300 ^{0}C [Figure 4.4]. The bands of silver paste are deposited on both ends of the film to establish the electrical contacts. A photograph of the sensor is presented in figure 4.5. This is resistive type of the sensor. The resistance of the sensing element varies with applied relative humidity. This sensor is interfaced to the circuit, figure 4. 3 and observed analog voltage is processed with signal conditioning circuit. The characteristics of the sensor depicted in table 4. 2. The calibration of the sensor module to relative humidity is %RH is carried out and the features of the SSM regarding monitoring of relative humidity are interpreted in next topic. As shown in figure 4.5, it is used in resistive divider combination, which is powered

1. Sensing Element
2. Silver Contacts
3. Ceramic Substrate

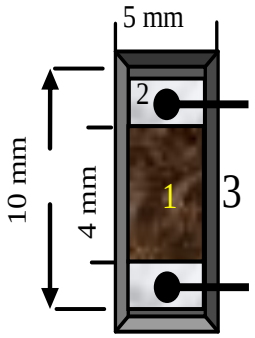

Figure 4.4: Polycrystalline ferrites Based Relative Humidity sensor.

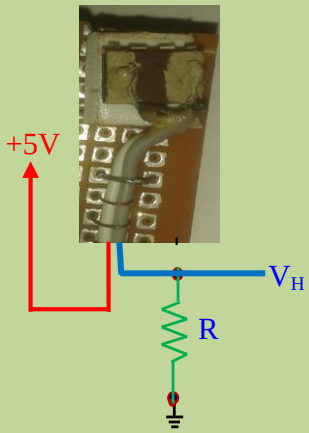

Figure 4.5: Photograph of Relative Humidity sensor designed for realization of SSM

TABLE 4.2: Characteristics of relative humidity sensor designed and used for present SSM

Sr. No.	Parameters	Typical Values
1.	Sensing Material	$Ni_xZn_{1-x}Fe_2O_4$
2.	Sensing Property	Resistive Type
3.	Current Consumption	25 μA Approx.
4.	Power supply	+5V
5.	Operating temperature	Room temperature
6.	Humidity range	30%-90% RH
7.	Storable Humidity range	Within 95%RH

by +5 Volt. Therefore, the humidity dependant voltage V_H is taken across resistor (R) of 1MΩ and connected to the signal conditioning stage.

ii) Environmental Temperature sensor:

Based on compositions of polycrystalline $Mg_{0.4}Zn_{0.6}Fe_2O_4$ and $Mg_{0.4}Zn_{0.4}Fe_2O_4$ ferrite materials as sensing materials, a temperature sensor is developed, wherein screen printing technique is employed to deposit thick film of above sensing materials. The photograph of temperature is depicted in figure 4.6. It is resistive sensor and revealing semiconducting behaviour with applied temperature. As per proposal, the sensor is designed for monitoring of environmental temperature. Therefore, it is calibrated for the range up to 100 ^{0}C. [Topic.5]. As shown in figure 4.6, it is used in resistive divider combination, which is powered by +5 Volt. Therefore, the temperature dependant voltage V_t is taken across resistor of 1MΩ and connected to the signal conditioning stage. The basic characteristics of this temperature sensor are tabulated and presented in table 4.3

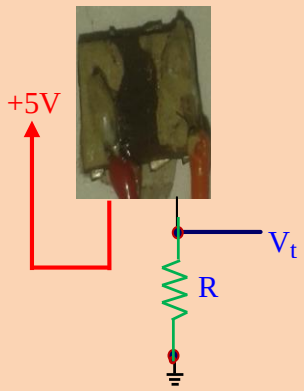

Figure 4.6: Photograph of temperature sensor designed for realization of SSM

TABLE 4.3: Characteristics of Temperature sensor designed and used for present SSM

Sr. No.	Parameters	Typical Values
1.	Sensing Material	$Ni_xZn_{1-x}Fe_2O_4$
2.	Sensing Property	Resistive Type
3.	Current Consumption	25 μA, Approx.
4.	Power supply	+5V
5.	Operating temperature range	RT – 100 ^{0}C

iii) Carbon dioxide gas sensor

The Smart Sensor Module is designed to monitor the carbon dioxide gas. It is known that, the carbon dioxide gas sensors such as MQ series and TGS series are available. By employing these sensors, a smart sensor module can be designed and the design can be extended to ensure wireless communication [35, 36]. However, these sensors are highly expensive. Therefore, it is proposed to synthesize the sensing material suitable for gas sensing applications. On

investigation, it is proved that, the compositions of polycrystalline ferrite materials reveal the phenomenon of chemisorptions at elevated operating temperature. This surface phenomenon causes to favour the gas sensing mechanism. Therefore, the compositions of $Mg_xZn_{1-x}Fe_2O_4$, $Ni_xZn_{1-x}Fe_2O_4$ and $Mn_xZn_{1-x}Fe_2O_4$, (x = 0.20 to o.80) ferrites are investigated. On investigation of the results regarding sensitivity, response timings, operating temperature etc, it is found that the compositions $Mg_xZn_{1-x}Fe_2O_4$, and $Ni_xZn_{1-x}Fe_2O_4$ are most suitable for carbon dioxide sensing. A thick film of sensing material is deposited on cylindrical glass tube as shown in figure 4.7. As shown in the figure 4.7, the heating element (HH) is along the axis of the cylindrical tube. The heating element is powered by separate supply. The current through heating element depends upon the operating temperature. Figure 4.8 shows, the photograph of the present sensor and schematic of the circuit used to interface the sensor to Smart Sensor Module under consideration. The basic characteristics of carbon dioxide gas sensor are presented in table 4.4. The properties in detail are discussed in topic 3. However, the SSM is calibrated and features of SSM are given in topic .

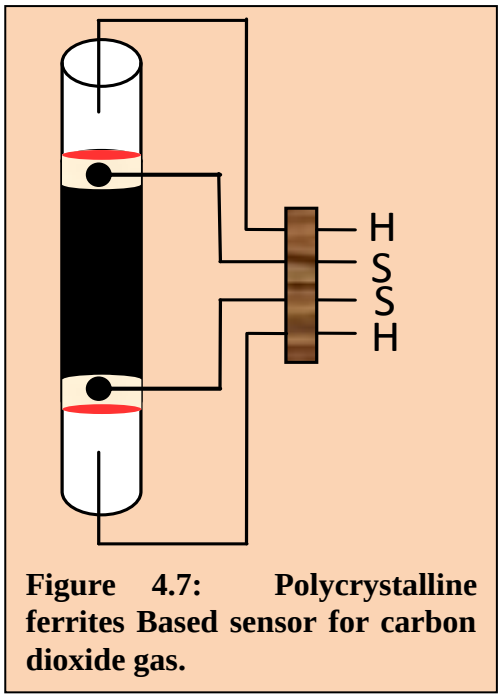

Figure 4.7: Polycrystalline ferrites Based sensor for carbon dioxide gas.

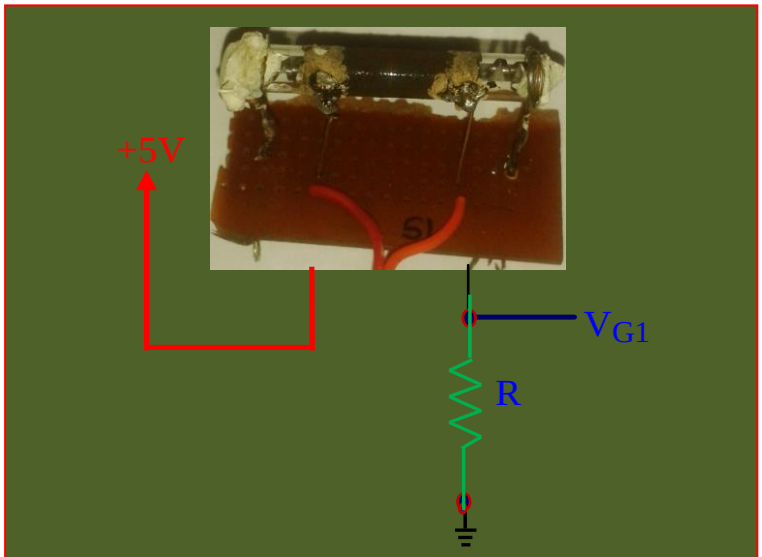

Figure 4.8: Photograph of carbon dioxide gas sensor and schematic of the circuit used to interface the sensor to SSM.

TABLE 4.4: Characteristics of Carbon dioxide gas sensor designed and used for present SSM

Sr. No.	Parameters	Typical Values
1.	Sensing Material	$Ni_xZn_{1-x}Fe_2O_4$
2.	Sensing Property	Resistive Type
3.	Current Consumption	25 µA, Approx.
4.	Power supply	+5V
5.	Operating temperature range	250 ^{0}C
6.	Heater Voltage	9 Volt
7.	Heater current	950mA

iv) Hydrogen sulfide gas senor:

With view to realize the design of Smart Sensor Module for multichannel sensor, it is designed to monitor the H_2S gas as well. It is known that, the H_2S gas is reducing gas and due to adsorption mechanism, at elevated temperature, it donates the electrons to the conduction band of the sensing materials [37,38]. Therefore, the sensing element, on exposure to this gas, shows decrease in the resistance. Ferrite materials are sensitive to H_2S gas and hence these materials are synthesized and used for present sensor. Out of the compositions studied, the $Ni_xZn_{1-x}Fe_2O_4$ is used to design hydrogen

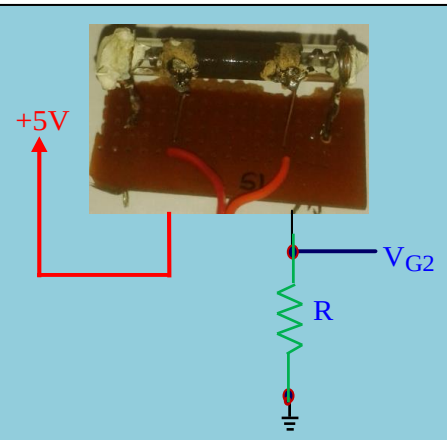

Figure 4.9: Photograph of H_2S gas sensor and schematic of the circuit used to interface the sensor to SSM.

TABLE 4.5: Characteristics of H_2S gas sensor designed and used for present SSM

Sr. No.	Parameters	Typical Values
8.	Sensing Material	$Ni_xZn_{1-x}Fe_2O_4$
9.	Sensing Property	Resistive Type
10.	Current Consumption	25 µA, Approx.
11.	Power supply	+5V
12.	Operating temperature range	160 ^{0}C
13.	Heater Voltage	9 Volt
14.	Heater current	600mA

sulfide gas sensor. The sensor is fabricated by depositing thick film of the sensing material on cylindrical tube. The sensor is as depicted in figure 4.9. The photograph and schematic of this sensor are shown in figure 4.8. The characteristics of the sensor are tabulated and presented in table 4.5.

v) Ammonia gas sensor:

The present Smart Sensor Module (SSM) is also facilitated with ammonia sensor to ensure the monitoring of ammonia gas within the environment of typical industries. The ammonia gas sensor is available from MQ as well as TGS series. However, deploying properties of the polycrystalline ferrites, the sensing material is synthesized and used to fabricate sensing element of the ammonia sensor. It is also known that, the NH_3 gas is reducing gas and due to adsorption mechanism, at elevated temperature, it donates the electrons to the conduction band of the sensing materials [39,40]. Therefore, the sensing element, on exposure to this gas, shows decrease in the resistance. The composition $Ni_xZn_{1-x}Fe_2O_4$ is used to design hydrogen sulfide gas sensor. The sensor is fabricated by depositing thick film of the sensing material on cylindrical tube. The sensor is as depicted in figure 4.7. The photograph and schematic of this sensor are shown in figure 4.10. The characteristics of the sensor are tabulated and presented in table 4.6.

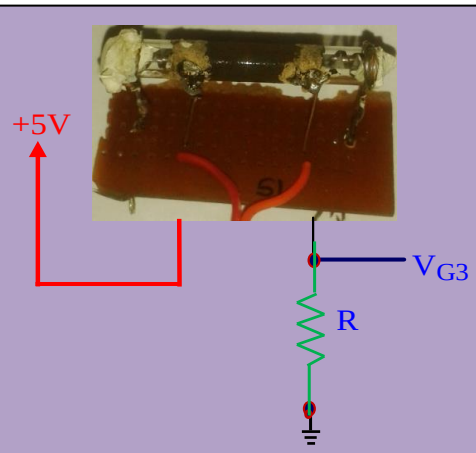

Figure 4.10: Photograph of ammonia gas sensor and schematic of the circuit used to interface the sensor to SSM.

TABLE 4.6: Characteristics of NH_3 gas sensor designed and used for present SSM

Sr. No.	Parameters	Typical Values
15.	Sensing Material	$Ni_xZn_{1-x}Fe_2O_4$
16.	Sensing Property	Resistive Type
17.	Current Consumption	25 μA, Approx.
18.	Power supply	+5V
19.	Operating temperature range	160 ^{0}C
20.	Heater Voltage	9 Volt
21.	Heater current	600mA

On investigation of ferrite compositions, as discussed in topic 3, it is found that these materials are also sensitive to LPG and other reducing and oxidizing gases. Moreover, the AVR ATmega 8L microcontroller used for present design has total six channels of analog inputs. Therefore, the design of SSM can be further extended to six parameters also.

II. (b) Signal conditioning Unit:

One of the major objectives of present research work is to design Smart Sensor Module to monitor five parameters, relative humidity, temperature, CO_2 gas concentration, H_2S gas concentration and NH_3 gas concentration. The Smart Sensor module is the realization of embedded technology, wherein along with digital design and configurability, an analog part is also equally important. For present SSM the sensors have been designed by using thick film of ferrite materials as sensing element. The signal extracted from sensing unit is analog in nature and it has to essentially make compatible with the requirement of further microcontroller based data acquisition system. To strengthen the signals, signal conditioning stage plays vital role in electronic instrumentation of measurement of control domain. Therefore, signal conditioning unit is designed for present Smart Sensor module and presented in this section.

The Smart Sensor Module under investigation has five analog channels designed for respective parameters. Therefore, the signal conditioner unit comprises five signal conditioning circuits. The five sensors are having different features. It is known that, use of one and single power supply to energize electronic parts of the circuits is always recommended to achieve reduction in the noise and stability in the operation. Moreover, it is proposed to design an embedded system which should operate on single battery. Therefore, all stages are designed to operate on +5 volt. The five signal conditioning stages are based with only one power supply. The designing issues of all of these signal conditioning stages are individually discussed.

i) Signal conditioner for relative humidity :

As discussed earlier, the humidity sensor, designed by depositing thick film of sensing element on ceramic substrate, is resistive type. Considering this fact, the signal conditioning stage is designed. The CMOS operational amplifier, TLV 2774, is

employed for this purpose. The schematic of the circuit designed for signal conditioning of humidity signal is shown in figure 4.11. As presented in figure 4.11, the operational amplifier, TLV 2774 plays vital role.

The CMOS operational amplifier TLV 2774 is the available in PDIP package with four operational amplifiers. It exhibits very high input impedance [41], which could really help to isolate the sensor from remaining analog part of the hardware. An important characteristic of TLV 2774 is that, it operates on single power supply from 2.5-V to 5.5-V and has rail to rail inputs as well as output. The TLV2774 CMOS operational amplifier family combines high slew rate and bandwidth. The rail-to-rail output swing and high output drive make these devices a good choice for driving the analog input or reference of analog-to-digital converters [42]. Out of four operational amplifiers, one is used for humidity signal conditioning. Use of one device for four channels helps to reduce the cost of designing and hence the cost of entire SSM.

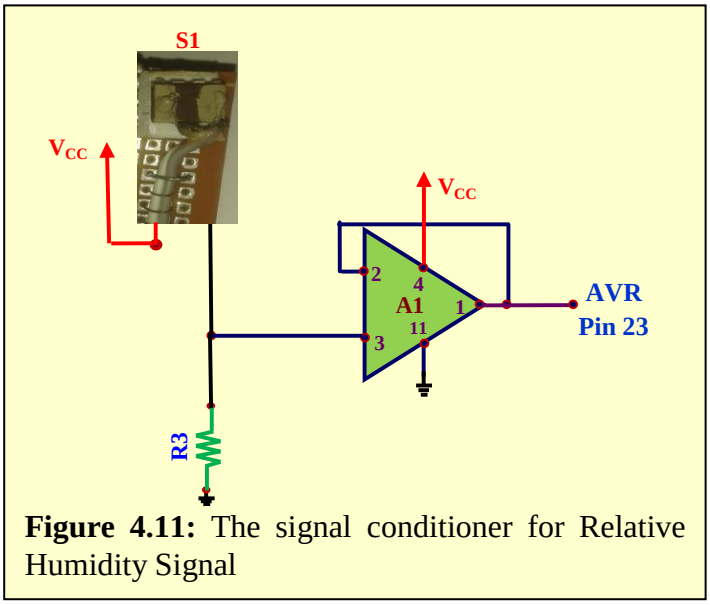

Figure 4.11: The signal conditioner for Relative Humidity Signal

As shown in the schematic the humidity dependent voltage from designed humidity sensor (V_H) is applied to this stage. The gain of this amplifier is configured to unity. This humidity dependent DC voltage (mV) is given to the analog channel 0 of AVR ATmega 8L microcontroller. The AVR ATmega 8L has provision to deploy internal source 2.56V as reference for on-chip ADC. Therefore, to ensure full range of operation the gain of the signal conditioning stage is limited to one. It provides better solution for buffering the signal. For digitization of the signal and further processing, on chip resources of AVR ATmega 8L are availed.

ii) **Signal conditioner for Temperature :**

It is known that, the temperature sensor is also resistive type. Employing second operational amplifier of TLV 2774, the signal conditioner stage for temperature sensor is designed. The schematic of the circuit designed for signal conditioning of temperature signal is shown in figure 4.12. The signal conditioning circuit is wired to

provide temperature dependent voltage (V_t). As discussed earlier, the TLV 2774 exhibits very high input impedance and hence, it is most suitable to read the signal without any loss. It is proposed to design the SSM for monitoring of environmental temperature. Therefore, the design is constrained for the range from 20°C to 100°C. However, the reference voltage selected for on-chip ADC is 2.56 volt. Therefore, to avoid the signal from its saturation for higher temperature, the gain of signal conditioner stage is limited to one. Otherwise, if this stage is configured for higher gain, then there is probability of the saturation. To avoid this problem, the amplifier is configured for Unit gain. This unit gain voltage amplifier helps to isolate the designed temperature sensor from further circuitry and protect the system from saturation as well. The conditioned analog signal is then given to microcontroller section for digitization and further processing.

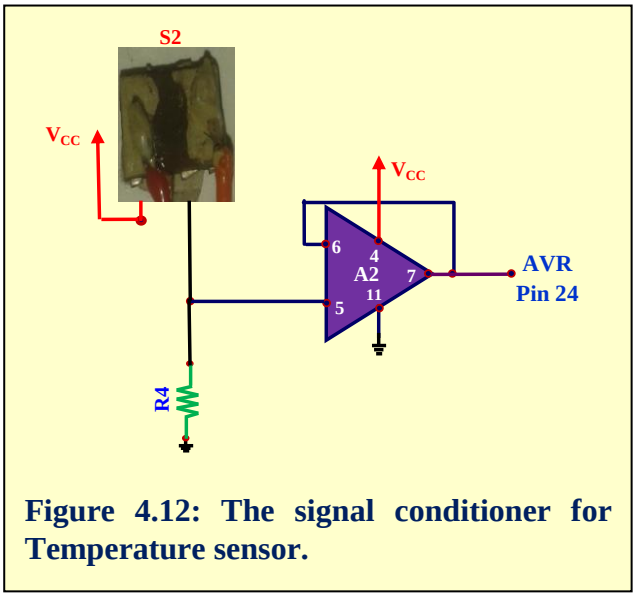

Figure 4.12: The signal conditioner for Temperature sensor.

iii) **Signal conditioner for CO_2 gas :**

The Smart Sensor Module is designed for sensing carbon dioxide gas. As discussed earlier, using fundamental properties of the ferrite materials, the carbon dioxide gas sesnor is designed and implemented. This is also resistive sensor. A change in resistance is reported due to existance of CO_2 gas. The sensor circuit is wired in resistive divider configuration and resulting emf V_{G1} (in mV) is used for further processing. This voltage is strenthened by specific signal condition circuit. Employing third operational amplifier of TLV 2774 the circuit is designed. The schematic of the circuit is depicted in figure

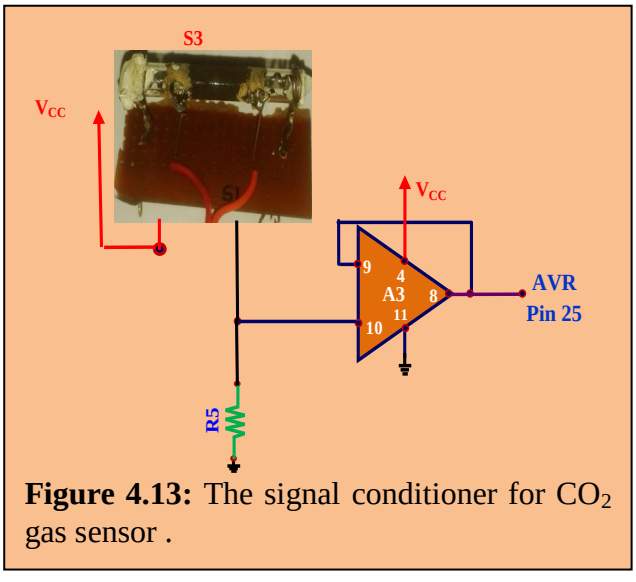

Figure 4.13: The signal conditioner for CO_2 gas sensor .

4.13. The circuit is wired to configure the gain as unity. Basically, the step size of ADC is very small about 2.56 mV. Therefore, an ADC can take small signal to ensure the preciseness. Hence, voltage amplification stage is not required. Moreover, on calibration, it is found that slight off set is present the data, which is compensated in the firmware. .

iv) **Signal conditioner for H_2S gas :**

It is known that, the Smart Sensor Modules for various environmental parameters are reported. However, the reports on development of Smart Sensor Module for H_2S gas are rare. Moreover, the ferrite compositions revealing good sensitivity for H_2S gas. Therefore, the present SSM is designed to monitor the H_2S gas. Such type of SSM are highly useful for chemical laboratories and industries. This is also useful for pollution control. Ferrite based H_2S sensor is designed and interfaced. The signal conditioner stage is wired about fourth operational amplifier of TLV2774. The sensor is resisitive sensor. The decrease in resistance is reported due to existance of H_2S gas. The sensor circuit is wired in resistive divider configuration and resulting emf V_{G2} (in mV) is used for further processing. This voltage is strenthened by specific signal condition circuit. The schematic of the circuit is depicted in figure 4.13. The features of SSM regarding detection of the gases are described in topic 5.

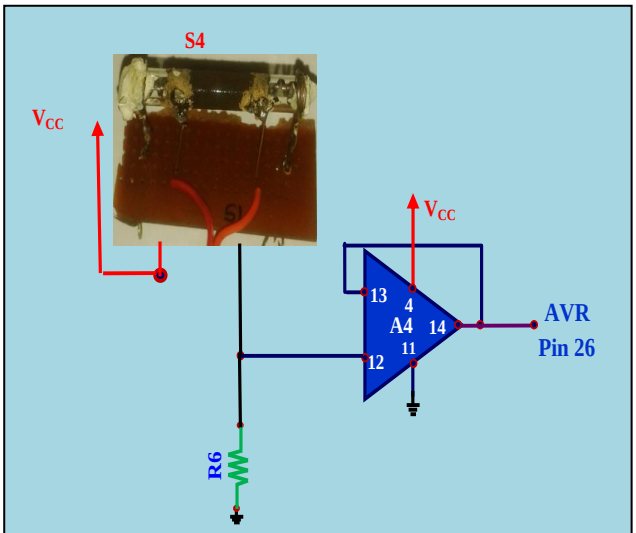

Figure 4.14: The signal conditioner for H_2S gas sensor.

v) **Signal conditioner for Ammonia gas :**

Ammonia gas has industrial importance. Therefore, to extend the applicability of the Smart Sensor Module, the design is extended for ammonia gas. Employnig ferrite as material, the ammonia gas sensor is developed in the laboratory and deployed for present SSM. Ammonia gas is the reducing gas. Due to process of adsorption, the ammonia gas favour the reduction reactioin and donate electrons to the materials. Due to this reduction in resistance takes place in the environment of ammonia gas. As discussed earlier, ammonia gas sesnor is designed and implemented. This is also

resisitive sensor. The sensor circuit is wired in resistive divider configuration and resulting emf V_{G3}(in mV) is used for further processing. This voltage is strenthened by specific signal condition circuit. The signal conditioing circuit is wired about TLV 272 [Figure 4.15]. For signal conditioner circuit of above four parameters the TLV2774 is used. It consist of 4 operational amplifiers. However, present design of SSM is for five parameters. Therefore, additional operatition amplifier of promising features is required. The Signal conditioning circuit for NH_3 gas concentration is designed about TLV 272, which is available in dual channel PDIP package. It exhibits very high input impedance. An important characteristic of TLV 272 is that, it also operates on single power supply from 2.5-V to 5.5-V and has rail to rail inputs as well as output [43,44]. The TLV272 CMOS operational amplifier family has high slew rate and bandwidth. The resulting emf, from NH_3 gas sensor is in mV, applied to the one of the channel of CMOS operational amplifier TLV272. The gain of the amplifier is programmed to unity. Therefore, it provides buffering of the signal. The output of this amplifier is applied to the on-chip ADC channel 5, of AVR ATmega 8L. Use of single power supply, shared by both digital and analog circuitry, ensures minimization of interference between the digital and analog circuitry [45]. Since, the microcontroller is operating at +5V the same supply is used to power the operational amplifier TLV 2774 and TLV 272. This causes to enhance stability in the operation.

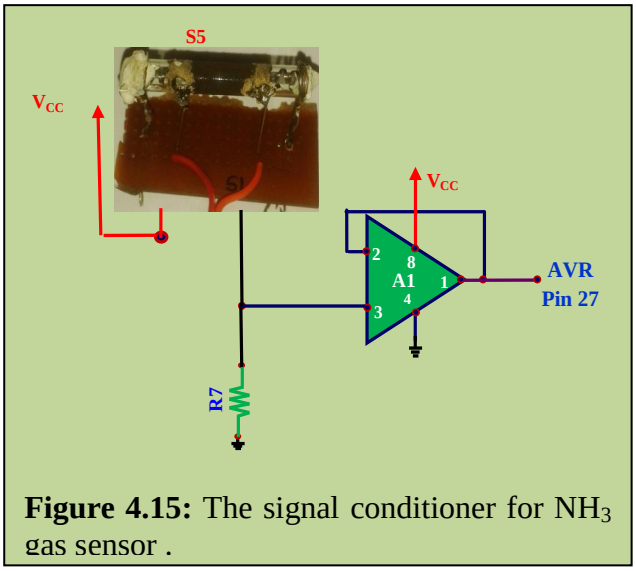

Figure 4.15: The signal conditioner for NH_3 gas sensor .

Thus, the signal conditioner stage is designed and implemented to realize the design of Smart Sensor Module. The output from the signal conditioning stages are given to the microcontroller

II. (c) Microcontroller Unit of an Embedded System:

According to the definition of the Smart Sensor Module, the configurable device such as microcontroller or FPGA is an inherent part. As Smart Sensor Module reveals embedded technology, the deployment of microcontroller plays significant role on the intelligence of the module. The salient features of microcontroller decide the reliability of the sensor module. Moreover, it also provides the solution to establish interface between STIM and NCAP by incorporation either wired or wireless platform for data communication [46, 47]. Major objective of SSM is establish the proper interface to the sensor and provides the data output in different domain. On literature survey, it is found that, the microcontrollers from various families such as AVR 128L [48, 49, 50], ARM [51], LPC [52, 53, 54], MSP [55, 56], PIC [57, 58] etc have been adopted for development of Wireless Smart Sensor modules. But, the microcontroller AVR ATmega 8L has promising characteristics with rather low cost. Therefore, deploying the microcontroller AVR ATmega 8L the computational part of the present Smart Sensor Module is developed. This microcontroller is small in size and exhibit low power consumption. It depicts, smart on chip resources, by availing which an embedded design can be realized. To design SSM, the microcontroller should be facilitated with on chip data converters. Otherwise, to ensure the data conversion, the designer has to rely on off chip devices. It increases the cost module and depicts increase in the complexity of synchronization. This impedes the design process. Therefore, it suggested to employ the microcontroller of advanced features. The microcontroller AVR ATmega 8L has promising features, which are summarized in table 4.7.

On investigation of table 4.7, it is found that, the present microcontroller is suitable for development of Smart Sensor Module under investigation. Basically, SSM is designed for five sensors such as temperature, humidity, carbon dioxide gas, H_2S, NH_3 etc gases. Moreover, the microcontroller under consideration has on chip 6 channels to ADC wherein the principle of successive approximation is realized. These ADC has 10 bit resolution, which causes to increase the preciseness of the SSM. Multiplexed power full IO lines satisfy the needs of interfacing by offering necessary sinking and sourcing currents.

As given in the table 4.7, the microcontroller is having sufficient on chip memory to store firmware and system related data as well. As discussed earlier, for realization SSM design, the microcontroller should be facilitated with communication

protocol. As presented in table 4.7, the AVR ATmega 8L has USART, UART, SPI communication facilities. Thus, employing AVR ATmega 8L microcontroller, the Smart Sensor Module is designed to realize the plug-and –play philosophy of modern measurement and control instrumentation.

TABLE 4.7: Salient Features of AVR ATmega 8L Microcontroller

Sr. No.	Features
1.	High-performance, Low-power AVR® 8-bit Microcontroller
2.	Advanced RISC Architecture
3.	130 Powerful Instructions – Most Single-clock Cycle Execution
4.	32 x 8 General Purpose Working Registers
5.	Up to 16 MIPS Throughput at 16 MHz
6.	**Nonvolatile Program and Data Memories**
	• 8K Bytes of In-System Self-Programmable Flash
	• 512 Bytes EEPROM
	• 1K Byte Internal SRAM
7.	**Peripheral Features:**
	• Two 8-bit Timer/Counters with Separate Prescaler, one Compare Mode.
	• One 16-bit Timer/Counter with Separate Prescaler, Compare Mode, and Capture Mode.
	• Real Time Counter with Separate Oscillator.
	• Three PWM Channels.
	• 6-channel ADC.
	• 10-bit resolution.
	• Byte-oriented Two-wire Serial Interface.
	• Programmable Serial USART.
	• Master/Slave SPI Serial Interface.
	• Programmable Watchdog Timer with Separate On-chip Oscillator.
	• On-chip Analog Comparator
8.	**Special Microcontroller Features:**
	• Power-on Reset and Programmable Brown-out Detection.
	• Internal Calibrated RC Oscillator.
	• External and Internal Interrupt Sources.
	• Five Sleep Modes: Idle, ADC Noise Reduction, Power-save, Power-down, and Standby.
9.	**I/O and Packages:**
	• 23 Programmable I/O Lines.
	• 28-lead PDIP, 32-lead TQFP, and 32-pad MLF.
10	**Operating Voltages:**
	• 2.7 - 5.5V (ATmega8L) • 4.5 - 5.5V (ATmega8)
11	**Speed Grades:**
	• 0 - 8 MHz (ATmega8L) • 0 - 16 MHz (ATmega8)

With view to deploy this microcontroller to SSM design, the architectural details of the AVR ATmega 8L are explored and details of its implementation are described briefly through following points.

i. Pin description of AVR ATmega 8L Microcontroller:

The pin description of AVR ATmega8L is depicted in figure 4.16. However, figure 4.17 represents internal architecture [59] of microcontroller AVR Atmega8L, wherein on chip resources of this microcontroller are shown.

The architectural details of this microcontroller have been explored. This microcontroller has promising on chip resources, out of which, the I/O ports, memory section, serial communication section, data conversion section etc are availed to ensure present embedded design. As per the need, these resources of the device are reconfigured.

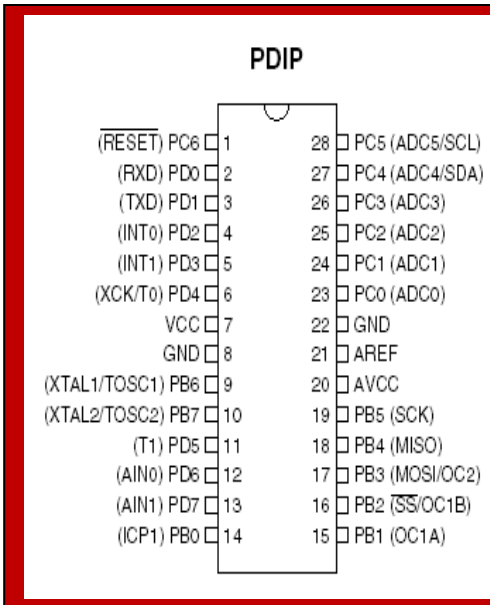

Figure 4.16: Pin description of AVR ATmega8L

The details regarding software required for reconfiguration of the devices are described in next section. This section discusses the hardware configuration of the resources.

To ensure embedded design, AVR Atmega 8L based Smart Sensor Module is wired and depicted in figure 4.3. Along with microcontroller, the figure 4.18 and Figure 4.19 show the design of clock circuit and reset circuit.

ii. Clock circuit:

The clock frequency of the processor determines the speed of execution. From datasheet, it is found that microcontroller AVR ATmega 8L can run with clock of frequency ranging from 32 kHz to 8 MHz [60]. The clock frequency for present design is fixed to 4 MHz.

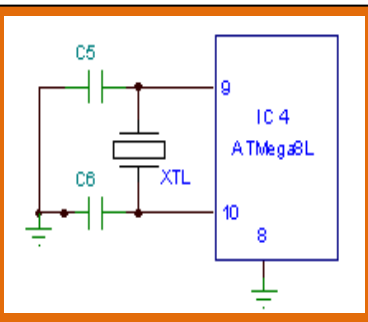

Figure 4.18: The Clock circuit

The controller has two clock sources one is the external clock, which is obtained by connecting desired quartz crystal between XTAL1 and XTAL2 and second clock is available with an internal RC oscillator. If any application does not demand the timing accuracies and also if the nominal clock frequency of 1 MHz at 5 V is sufficient for typical application, then the option of Internal RC Oscillator can be utilized [60]. However, this clock may have jitter, which could adversely affect the baud rate. For present circuit, the clock of frequency 4 MHz is configured. The circuit arrangement for clock circuit is presented in figure 4.18.

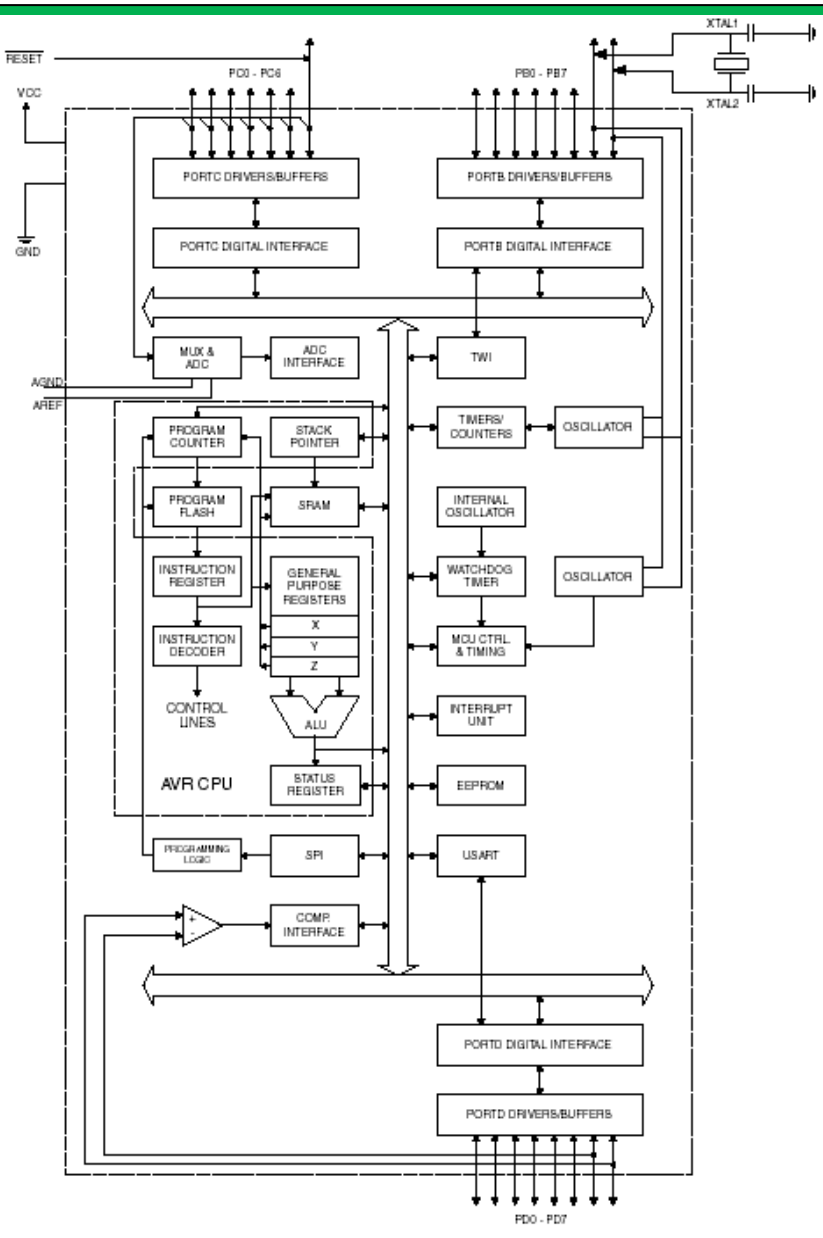

Figure 4.17: Block diagram of ATmega8L Microcontroller

iii. Reset circuit:

To ensure proper synchronization in hardware and software operation, the reset

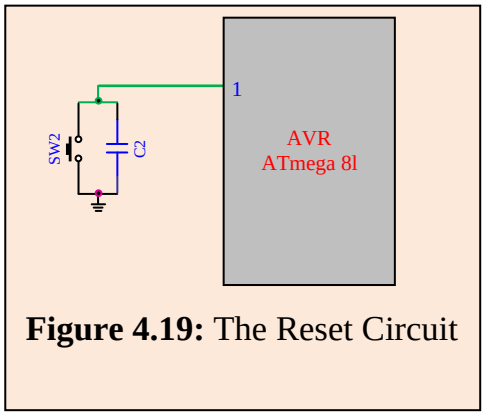

Figure 4.19: The Reset Circuit

circuit is needed. The present microcontroller has active low power on reset input, which when asserted then all on-chip resources reset and set to their default values. The reset circuit consists of a capacitor and switch for external reset as depicted in figure 4.19.

iv. I/O Ports:

The AVR microcontrollers have IO ports of true Read-Modify-Write functionality when used as general digital I/O ports [61]. This means that the direction of one port pin can be changed without unintentionally changing the direction of any other pin. Number of IO lines and hence the ports availability varies from device to device. However, the microcontroller AVR ATmega 8L consists of three ports spread over 23 IO lines. All port pins have individually selectable pull-up resistors with a supply-voltage invariant resistance. The structure of the typical port is presented in figure 4.20. The three SFRs, port register (PORTX), Data Direction Register (DDRX), and the Port Input Pins (PINX) are associated with three I/O ports, where X indicates port number.

The DDxn bits are accessed at the DDRx I/O address, the PORTxn bits at the

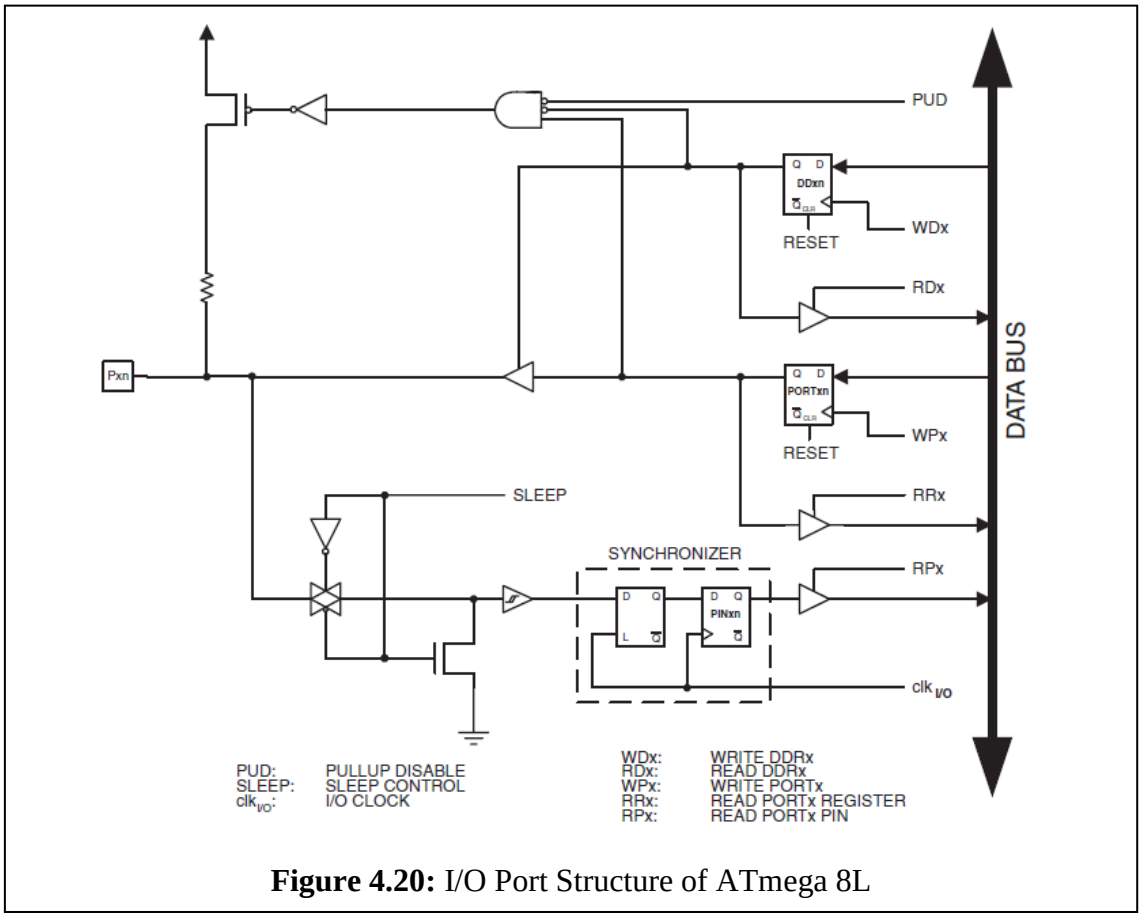

Figure 4.20: I/O Port Structure of ATmega 8L

PORTx I/O address, and the PINxn bits at the PINx I/O address. The DDxn bit in the DDRx Register selects the direction of this pin. If DDxn is written logic one, respective I/O line is configured as an output pin. If DDxn is written logic zero, then it is configured as an input pin. If PORTxn is written logic one when the pin is configured as an input pin, the pull-up resistor is activated. To switch the pull-up resistor off, PORTxn has to be written logic zero or the pin has to be configured as an output pin. The port pins are tri-stated when a reset condition becomes active, even if no clocks are running. If PORTxn is written logic one then the pin is configured as an output pin, the port pin is driven high (one). If PORTxn is written logic zero then the pin is configured as an output pin, the port pin is driven low (zero). Independent of the setting of Data Direction bit DDxn, the port pin can be read through the PINxn Register Bit.

Thus, the microcontroller AVR ATmega 8L is employed as computing device to ensure the design of Smart Sensor Module (SMM). As presented in the block diagram and given in the datasheet, it found that, this microcontroller is rich in the resources. However, out of all, necessary resources such as, IO Ports, Analog to digital converter, USART, SPI, SRAM, EPROM etc are availed for present design[61]. The table 4.8 describes the deployment of the microcontroller resources and associated pin for present design.

TABLE 4.8: List of resources used and associated pins of AVR ATmega 8L deployed for design of Smart Sensor Module

Sr. No.	Port Pin No.	Purpose for which it is deployed
1.	1	Reset/ ISP
2.	2	Rx for serial communication
3.	3	Tx for serial communication
4.	4	Control Signal for LCD
5.	5	Control Signal for LCD
6.	6	Control Signal for LCD
7.	7	Power supply
8.	8	Ground
9.	9	Clock circuit and Data line for LCD
10.	10	Clock circuit and Data line for LCD
11.	14	Data line for LCD
12.	15	Data line for LCD

13.	16	Data line for LCD
14.	17	Data line for LCD/ISP
15.	18	Data line for LCD/ISP
16.	19	Data line for LCD/ISP
17.	23	Input from Humidity Sensor channel
18.	24	Input from Temperature Sensor channel
19.	25	Input from Gas Sensor channel
20.	26	Input from Gas Sensor channel
21.	27	Input from Gas Sensor channel
22.	17	SPI communication
23.	18	SPI communication
24.	19	SPI communication
25.	2	RS232 port
26.	3	RS232 port

Present embedded design is dedicated to play with the analog signals extracted from respective sensor channels. As per architecture of Smart Sensor Module, the data conversion has significant importance. In fact, to ensure data conversion, present microcontroller is having smart on-chip analog to digital converter. Therefore, the details regarding this on-chip ADC facilities are discussed.

v. Analog-to-Digital Converter:

The present work emphasizes the designing of an embedded system, Smart Sensor Module (SSM) for monitoring

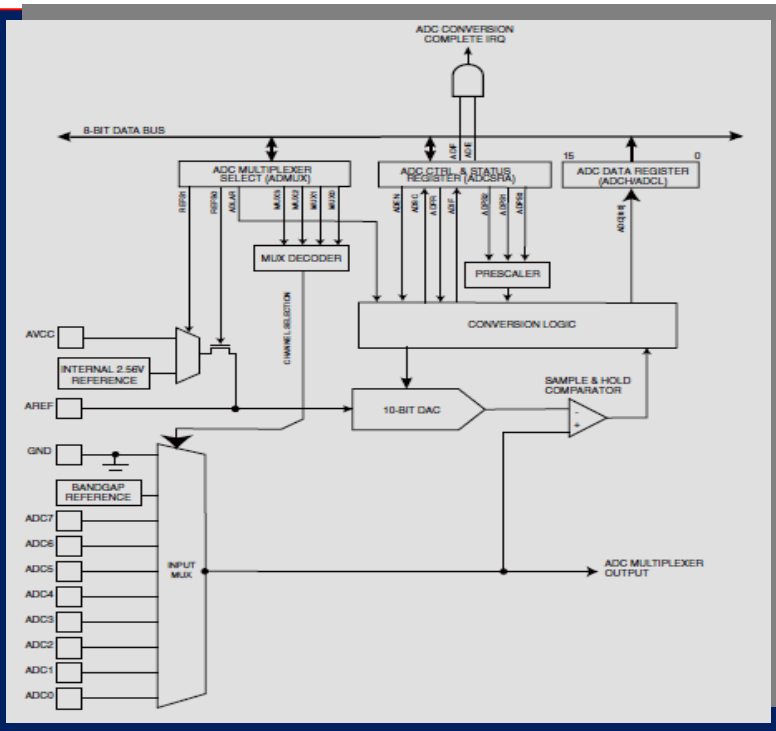

Figure 4.21: Architecture of on Chip ADC of AVR

of humidity, temperature and gas concentration. It ensures the fact of interfacing with real analog world. These signals should be digitized for which highly reliable analog to digital converter is essential. The microcontroller AVR ATmega 8L, has powerful on-chip analog to digital converter availing which the signals are digitized to 10 bit resolution. The details of these ADC resources are investigated and described below. The ADC of AVR ATmega 8L is featured promising salient features, which are presented in table 4.9. The architecture of on chip ADC of this microcontroller is also depicted in figure 4.21

TABLE 4.9: Salient featured of on-chip ADC of AVR ATmega 8L

Sr. No.	**Parameters**
1.	10-bit Resolution
2.	± 2 LSB Absolute Accuracy
3.	13 - 260 µs Conversion Time
4.	Up to 15 kSPS at Maximum Resolution
5.	6 Multiplexed Single Ended Input Channels
6.	0.5 LSB Integral Non-linearity
7.	2 Additional Multiplexed Single Ended Input Channels (TQFP and MLF Package only)
8.	Optional Left Adjustment for ADC Result Readout
9.	0 - VCC ADC Input Voltage Range
10.	Selectable 2.56V ADC Reference Voltage
11.	Free Running or Single Conversion Mode
12.	Interrupt on ADC Conversion Complete
13.	Sleep Mode and Noise Canceller

On inspection of figure 4.11 and table 4.4, it is found that, the on-chip analog to digital converter is very smart and reliable. It has six single ended inputs supported by 8-channel analog multiplexer and spread over the port C. It exhibit separate provision for analog supply (AVcc) and provides the analog ground separately. To overcome the noise, which may otherwise exist due to external reference voltage, the microcontroller comprises on chip source of reference voltage of 2.56 volt [62]. The present microcontroller provides three SFRs by availing which, one can synchronously control the operation of ADC. Thus, deploying these three SFRs into software, the ADC of this

microcontroller is configured dynamically and availed to digitize the signal coming from respective analog channels.

Analog channels ADC0 to ADC5 are given on Port C as a alternate function. Table 4.10 depicts the pin assignment of Port C.

TABLE 4.10: Analog channels and their use in present SSM

Sr. No.	Port C Pins	Alternate Functions	Analog Signal connected
1	PC0	ADC0	From Humidity Sensor channel
2	PC1	ADC1	From Temperature Sensor channel
3	PC2	ADC2	From Gas Sensor channel
4	PC3	ADC3	From Gas Sensor channel
5	PC4	ADC4	From Gas Sensor channel

Following three SFRs are used for configuration of the on chip ADC. These SFRs are modified during execution of the system.

- ADC Multiplexer Selection Register (ADMUX)
- ADC Control and Status Register A (ADCSRA)
- The ADC Data Register (ADCL and ADCH)

The techniques of deployment of these SFRs have been studied and discussed through following points.

a. ADC Multiplexer Selection Register (ADMUX):

As presented in the figure 4.22 the ADC has analog multiplexer and can be configured with the help of ADMUX register. This is read/write register and it could be used for configuration of both reference voltage levels and analog channels as well. Figure 4.12 shows the bit assignment of the SFR the ADMUX.

Definitions of bits of ADMUX register are given in table 4.6 and 4.7•

Bit	7	6	5	4	3	2	1	0
	REF1	REFS0	ADLAR	-	MUX3	MUX2	MUX1	MUX0
Read/Write	R/W	R/W	R/W	R	R/W	R/W	R/W	R/W
Initial Value	0	0	0	0	0	0	0	0

Figure 4.22: The SFR ADMUX of AVR ATmega 8L.

- **Reference Voltage Selection:** The two bits of ADMUX register (D7 and D6) are used for reference voltage selection. The table 4.11 gives the scheme of reference voltage selection. In fact, for present design the internal reference voltage of 2.56V is selected. Therefore these two bits are configured to 1.

TABLE 4.11: Voltage Reference Selections for ADC

REF1	REF0	Voltage Reference Selection
0	0	AREF, Internal Vref turned off
0	1	AVcc with external capacitor at AREF pin
1	0	Reserved
1	1	Internal 2.56V Voltage Reference with external capacitor at AREF pin

- **Justification of the result :** It is known that, an ADC of the microcontroller has 10 bit resolution [63]. Therefore, 8 bits of the results will be accommodated into ADCL and two bits into ADCH. It depends upon, whether it is right justified or left. The bit D5 is ADLAR bit used to configure the justification of the result. By default it is right justified, wherein two MSB bits are in ADRH register. Due to right justification the lower bits of the results are considered. Therefore, it helps in enhancing the preciseness in the result. Otherwise, the left justification neglects the LSB bits and hence causes to reduce the preciseness [64].
- **Analog Channel Selection**: As discussed earlier, the present Smart Sensor Modules realizes the monitoring of five parameters such as Humidity (H), Temperature (t), Gas Concentration (G1, G2 and G3). Thus, there are five analog signals, which are to be digitized. The digitization of these signals, the channels 0, 1, 2, 4 and 5 are dynamically selected by configuration bits D3 to D0. The table 4.12 presents the scheme of the channel selection.

TABLE 4.12: Channel selection for ADC

Sr. No.	Bits of ADMUX				Analog channel to be selected
	D3	D2	D1	D0	
1.	0	0	0	0	ADC 0
2.	0	0	0	1	ADC 1
3.	0	0	1	0	ADC 2
4.	0	0	1	1	ADC 3
5.	0	`1	0	1	ADC 4
6.	0	1	1	0	ADC 5

a) ADC Control and Status Register A (ADCSRA):

To control the operation of an analog to digital converter, the SFR ADCSRA, plays vital role. Definition of ADC control register ADCSRA is shown in Figure 4.23.

Bit	7	6	5	4	3	2	1	0
	ADEN	ADSC	ADFR	ADIF	ADIE	ADPS2	ADPS1	ADPS0
Read/Write	R/W	R/W	R/W	R/W	R/W	R/W	R/W	R/W
Initial Value	0	0	0	0	0	0	0	0

Figure 4.23: ADC Control and Status Register A (ADCSRA)

- **ADC Enable (D7) [ADEN]:**

  Writing this bit to one enables the ADC. By writing it to zero, the ADC is turned off. Turning the ADC off while a conversion is in progress will inhibit the conversion.

- **ADC Start Conversion (D6) [ADSC]:**

  In Single Conversion mode, write this bit to one to start each conversion. In Free Running mode, write this bit to one to start the first conversion.

- **ADC Free Running Select(D5) [ADFR]:**

  When this bit is set (one) the ADC operates in Free Running mode. In this mode, the ADC samples and updates the Data Registers continuously. Clearing this bit (zero) will terminate Free Running mode. For present case the ADC is configured in free running mode.

- **ADC Interrupt Flag (D4) [ADIF]:**

  This bit is set when an ADC conversion completes and the Data Registers are updated.

- **ADC Interrupt Enable:(D3)[ADIE]:**
- **ADC Prescaler Select Bits:(D2:D0)[ADPS2:0]:**

On configuration of above bits, the SFR **ADCSRA** becomes 0xE0H.

b) The ADC Data Register (ADCL and ADCH):

As discussed earlier, an ADC of AVR ATmega8L has 10 bit resolution. Therefore, two 8 bit registers, ADCH, and ADCL are made available to hold the result [65].

The converted digital data is stored in these data registers.

Bit	15	14	13	12	11	10	9	8
	-	-	-	-	-	-	ADC 9	ADC 8
	ADC 7	ADC 6	ADC 5	ADC 4	ADC 3	ADC 2	ADC 1	ADC 0
	7	6	5	4	3	2	1	0

Figure 4.24: The ADC Data Register

The figure 4.24 depicts the result register when right justified. While data processing these two registers must be packed. The process of packing of these registers is explained in next point.

vi. Interfacing of analog channels:

It is known that, the microcontroller AVR Atmega8L has six channels (ADC 0 to ADC 5) for Analog to Digital Conversion. However, the present embedded system is designed for monitoring of Humidity, Temperature and detection of the Gases. As discussed

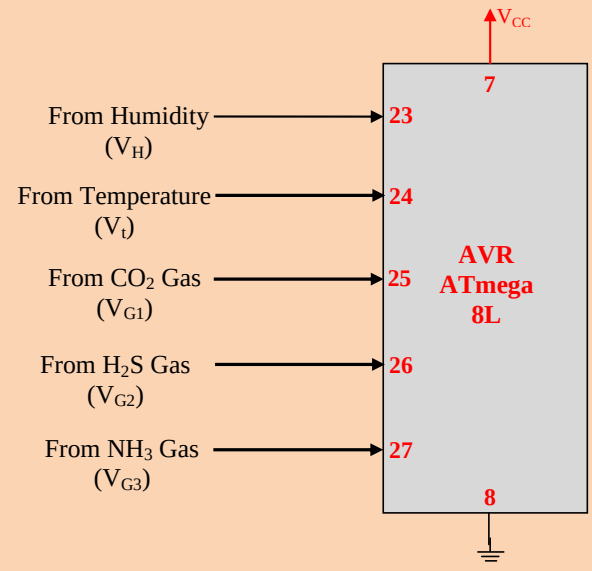

Figure 4.25: Circuit arrangement for interfacing analog signals

earlier, the system comprises five distinguish analog sections for these five parameters. Out of these five parameters, three are for the detection of the gases, one for temperature and one for relative humidity. Therefore, out of six, five channels, ADC 0, ADC1, ADC2, ADC3 and ADC4 of this ADC are deployed for digitization of respective analog signals. Figure 4.25 depict the interfacing of analog signals. Proper subroutines have been developed and sequentially called into main program to read analog signals. It is known that, deployment of such on chip facilities results in the reduction of not only in the hardware and software complexity, but also in the cost [66]. Moreover, it enhances the reliability of present Smart Sensor Module.

The SFR ADMUX (ADC multiplexer selection) is configured. It is known that AVR microcontroller has internal reference voltage facility [62]. Therefore, by selecting REFS1:0 bits to 11, the internal source of reference voltage of 2.56 Volt is enabled. By default, digital data is right justified, which gives preciseness in the result. The left justified data causes the reduction in the preciseness. The MUX bits of ADMUX register are configured as 000 for analog input ADC0. However, this bit is dynamically configured to play with all five signals continuously. The ADC normally requires three handshaking signals SC, EOC and OE. Particularly for off-chip ADC like 0808 etc [62]. However, present microcontroller is having on-chip ADC, which realizes on chip handling of such signal. The ADCSRA is employed for the handshaking of these signals, through the software routine [Section of firmware]. When an ADC conversion is completed, then the result is found in the two ADC data registers, ADCL and ADCH. Two successive read operations will read the lower byte and higher byte data. The ADCL consist lower byte and ADCH consist higher byte of converted digital data. These two unpacked byte can be packed by executing the expression [67]

$$\text{ADC\_Result} = (256 \times \text{ADCH}) + \text{ADCL} \qquad (1)$$

However, in the IDE (code vision AVR), the data register ADCW is available, wherein the packed 10-bit number is returned after completion of the analog to digital conversion. The process is repeated sequentially for five analog signals. For each analog channel, as per need, the SFRs are dynamically reconfigured. The five analog voltages V_H (Humidity), V_T (Temperature) and V_G (Gas Concentration) are digitized and digital data are stored in variables Humidity, Temperature and Gas respectively and

deployed for further processing. Entire operation of the analog to digital converter synchronized through the software. In addition to this, the microcontroller also plays vital role of providing data output in various domain [68].

II. (d) Output Section of the Smart Sensor Unit:

On investigation of an architecture of smart sensor module or smart transducer module, it is found that, as per the standards, the output section plays remarkable role to realize the features of plug-and-play philosophy of present day instrumentation [69]. In addition to analog output, the STIM or SSM emphasizes the digital outputs, wherein various bus protocols are ensured. To facilitate the interfacing with the devices, normally, the digital output in RS232 domain is required [70, 71]. Moreover, to satisfy the needs of NCAP, wireless protocols should be incorporated. For realization of Smart Sensor Module (SSM) the data output section is designed to provide the output in following domains.

- Digital Display unit
- Analog outputs
- Universal Synchronous /Asynchronous Receiver Transmitter (USART/UART)
- Serial with RS232
- Serial SPI mode

Figure 4.xx depicts the output section of the Smart Sensor Module under investigation. It also known that, along with above outputs, the values of the parameters should be directly displayed on the smart display. It is to be noted that, incorporation of display unit in the output section is not mandatory as per IEEE 1451 standards [72]. However, with view to enhance smartness of the module beyond the standard module, the display unit is designed about Smart LCD and incorporated in present Smart Sensor Module. Such inclusion of display unit in network capable smart sensor module is reported by some investigators [73, 74, 75, 76]. Thus the output section consists of five domains of data outputs. The designing issues of these outputs are discussed through subsequent points.

i) Display unit:

Present system (SSM) is developed for measurement of Humidity, Temperature and an detection of various gases. The system is designed as per the requirements of the embedded system. As discussed in the topic 5, the signal coming from various channels are calibrated in respective units by adopting standard calibration process. Therefore, present sensor provides the data in calibrated format. That means the sensor module is itself calibrated. To ensure digital readout the Display section is designed by employing smart LCD from Hitachi Corporation. The details regarding configuration of LCD and its interfacing are as follows.

Figure 4.16 show the schematic of the 16 x 2 line (Hitachi HD 44780) LCD [77]. The LCD used consists of required hardware along with proper controller, which controls entire operation of the LCD. As shown in figure 4.26, the LCD has 16 pin for interfacing out of which 8 pins are for data lines (DB0-DB7), three pins for power supply and contrast adjustment, three pins for control signals and two pins internal light source. The pin description is presented in table 4.14. These lines are interfaced to microcontroller as shown in figure 4.27.

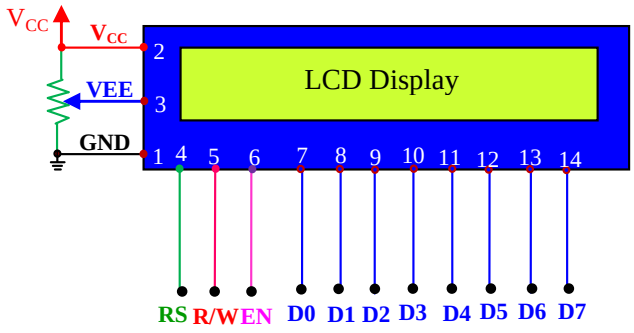

Figure 4.26: Schematic of this 16 x 2 line LCD.

TABLE 4.13: LCD commands

Code (Hex)	Command for initialization of LCD
01	Clear display screen
02	Return home
04	Decrement cursor (shift cursor to left)
06	Increment cursor (Shift cursor to right)
05	Shift display right
07	Shift display left
08	Display off, cursor off
0A	Display off, cursor on
0C	Display on, cursor off
0E	Display on, cursor on
0F	Display on, cursor blinking
10	Shift cursor position to left
14	Shift cursor position to right
18	Shift the entire display to the left
1C	Shift the entire display to the right
80	Force cursor to beginning of 1st line
C0	Force cursor to beginning of 2nd line
38	2 lines and 5X7 matrix

To display letter or number from A-Z or a-z and 0-9, we should send corresponding ASCII codes to LCD through data lines. To display character, it is essential to send the command for initialization of modes of the LCD. The

list of typical commands is given in the table 4.13. The LCD can be configured in two modes [78] Sending command & data with the time delay and Sending command and data with Busy Flag Checking.

In time delay mode, a delay of particular time is produced by the introduction of delay subroutine within two successive command or data fetch operation. The delay time produced should be proper otherwise interference of data may take place. For present SSM the LCD is configured in the time delay mode.

Moreover, the LCD can also be interfaced by using only four data lines. During this configuration the LCD must be configured accordingly. It adds complexity in the software. In the second mode, busy flag checking, the bit D7 of LCD is considered as a busy flag. During the character displaying the busy flag remains unaffected. The status of this flag is checked by polling mode, which means the microcontroller does not issue command or data till the LCD is ready. Thus, either of these modes can be considered for developing the software.

To adjust contrast a separate line called VEE is provided. The voltage across

TABLE 4.14: The pin description for LCD

Pin	Symbol	I/O	Description
1	V_{SS}	---	Ground
2	V_{CC}	---	+5V power supply
3	V_{EE}	---	Power supply to control contrast
4	RS	I	RS = 0 to select command register RS = 1 to select data register
5	R/W	I	R/W = 0 for write R/W = 1 for read
6	E	I/O	Enable
7	DB0	I/O	The data bus
8	DB1	I/O	The data bus
9	DB2	I/O	The data bus
10	DB3	I/O	The data bus
11	DB4	I/O	The data bus
12	DB5	I/O	The data bus
13	DB6	I/O	The data bus

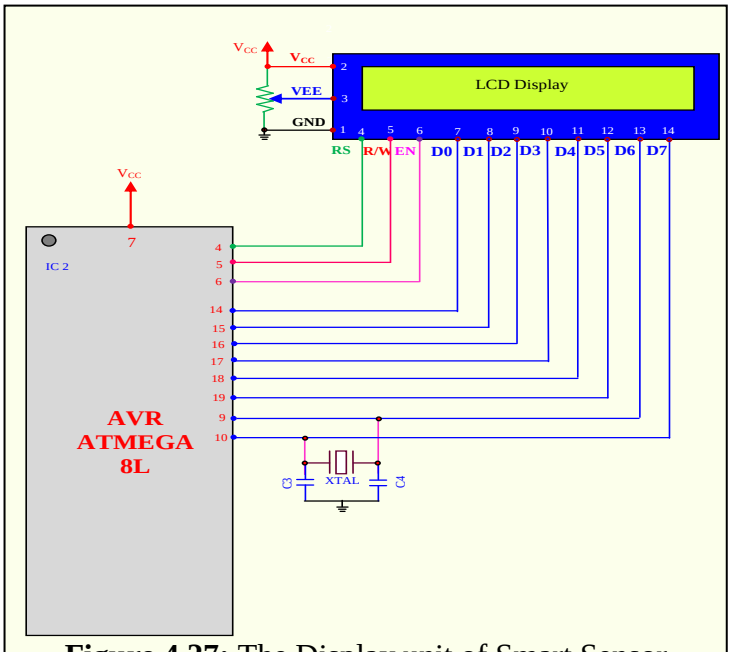

Figure 4.27: The Display unit of Smart Sensor Module

this pin must be properly controlled to achieve the better contrast in the display [78]. Interfacing of the LCD is depicted in figure 4.27.

As shown in figure 4.27, the LCD is interfaced to port B of microcontroller AVR ATmega 8L. The line D0-D7are connected to PB0-PB7. However, the three control signals RS, RW & EN are connected to three lines of Port D, i.e PD2, PD3 and PD4 of the microcontroller AVR ATmega8L.

The variable resister R is used to adjust the contrast voltage. The LCD is deployed to ensure digital read out of the values of respective parameters. This also helps to reduce the power consumption.

ii) Analog outputs Port:

The present sensor module is designed for temperature, relative humidity, carbon dioxide gas detection, detection of H_2S and HN_3. It is to be noted that, respective sensors are developed by employing polycrystalline nanoferrites as a sensing materials. The sensing materials reveal electrical properties sensitive to above parameters [79] The change in electrical resistance and dielectric properties take place due to exposure of these materials to the environmental conditions. Employing proper signal conditioning circuits, as discussed earlier, the change in the resistance is converted into change in the voltage (in mV). This is analog voltage. Each analog channel, dedicatedly designed for respective sensor, provides analog voltage, which proportionally varies with the values of the parameters. These analog signals can be used for development of the instrumentation. Therefore, five analog voltages are made

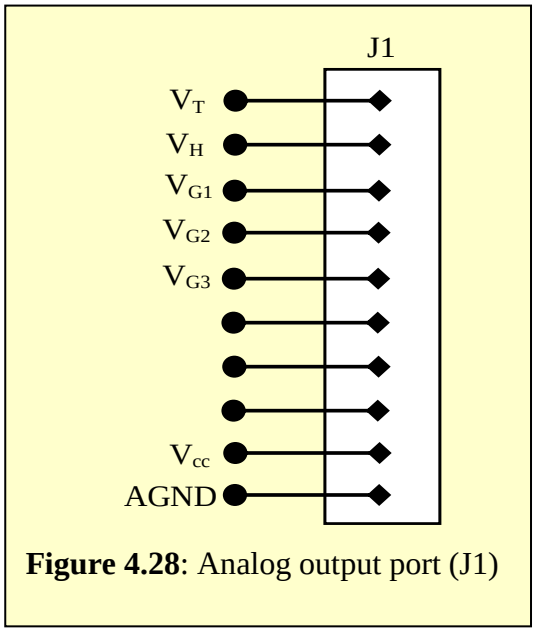

Figure 4.28: Analog output port (J1)

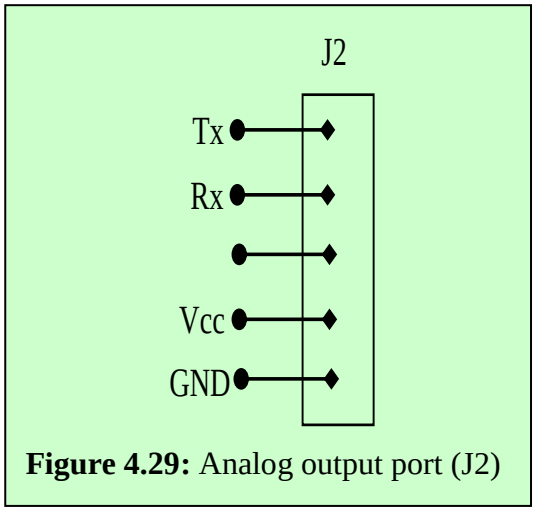

Figure 4.29: Analog output port (J2)

available as output from the present sensor module. The ranges of analog output voltages are given in topic 5. Figure 4.xx depicts analog output port (J1). As shown in figure 4. 28, the analog port J1 also includes the Vcc and ground pin to ensure the proper interface.

iii) Universal Synchronous /Asynchronous Receiver Transmitter (USART/UART) Port:

To ensure the deployment of present smart sensor module for network based capabilities, the availability UART or USART port is essential. Considering this fact into account and to ensure serial data communication, the serial Port is designed. A dedicated subroutine is also developed, described in next section, to put the data in asynchronous format on this port. However, to put data in USART mode a specific modification is essential in the firmware. This port is named as J2 and depicted in figure 4.29. Along with the Tx and Rx lines, the Vcc and Ground pins are also provided on this port to ensure the synchronization in the interfacing.

iv) Serial with RS232 Port :

The serial data with RS 232 standards is an inherent requirement of modern instrumentation. Keeping RS 232 standards in view, the port is designed to ensure compatibility in the logic level. The voltage levels of TTL and RS 232 are different. Computer can communicate with RS 232 standards, whereas the microcontroller based system normally plays with TTL level of voltages. To ensure this interface, the line driver Max 232 is sufficient. Therefore, using max 232 and availing RxD and TxD lines of the microcontroller this serial port (J3) is designed and presented in figure 4.30.

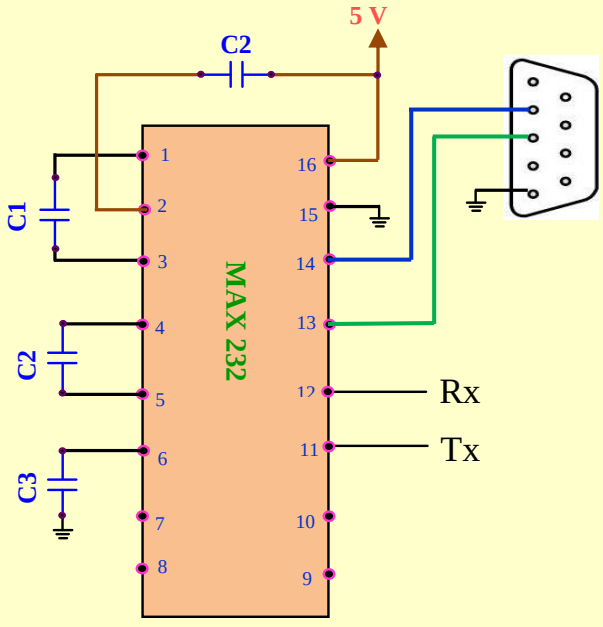

Figure 4.30: Serial Port with RS 232 compatibility.

v) Serial SPI Port:

The serial peripheral interface (SPI) on chip serial communication is available in AVR ATmega8L microcontroller. It is a synchronous serial communication bus, meaning that the transmitter & receiver involved in SPI communication must use the same clock [80]. The SPI bus was developed to provide relatively high- speed, short distance communication using a minimum number of microcontroller pins. SPI communication involves the philosophy of a master and a slave. Both the master and a slave send and receive data simultaneously. But the master is responsible for providing the clock signal for the data transfer. In this way, the master has control on the speed of data transfer[81].

TABLE 4.15: Microcontroller Interfacing Pin

Port Pin	**Alternate Functions**
PB7	SCK (SPI Bus Serial Clock)
PB6	MISO (SPI Bus Master Input/ Save Output)
PB5	MOSI (SPI Bus Master Output/ Save Input)

The master supplies the clock and eight bits of data, which are shifted out of the master-out-slave-in (MOSI) pin. Figure 4.31 presents the scheme of synchronous data transfer through SPI bus. The same eight bits are shifted into the slave unit, one bit per clock pulse, on its MOSI line. As the eight bits are shifted out of the master and into the slave, eight bits are also shifted out of the slave on its master-in-slave-out (MISO) line and into the master on its MISO pin. SPI communication, then, is essentially a circle in which eight bits flow from the master to the slave and a different set of eight bits flow from the slave to the master. In this way, the master and a slave can exchange data in a single communication. The port B of this microcontroller ensures SPI communication

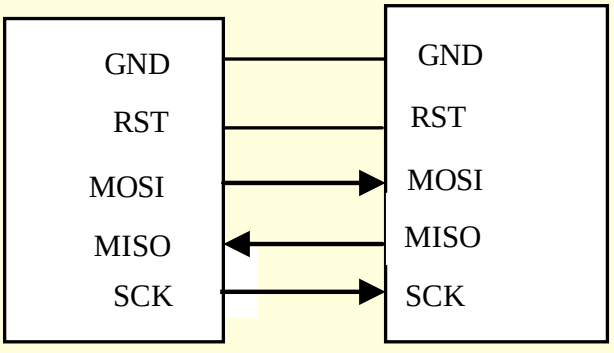

Figure 4.31: The Serial Peripheral Interface

[Table 4.15]. Therefore, using above pins of port B the SPI port is designed and made available in present SSM. The SPI port (J4) is depicted in figure 4. 32.

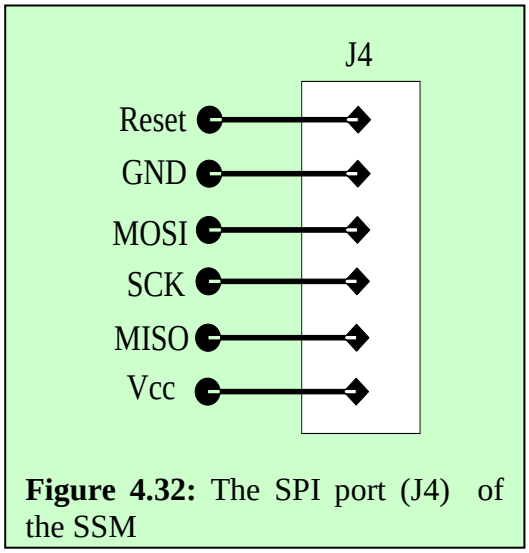

Figure 4.32: The SPI port (J4) of the SSM

II. (e) In System Programming [ISP] unit :

It is known that, the microcontroller AVR ATmega8L, from Atmel, has In System Programming [ISP] facility. Only because of this (ISP) feature the microcontroller ATmega8L is superior to some variants of from Intel or Atmel series. To ensure in system programming of the microcontroller, the same SPI port (J4) is deployed. The SPI port is designed for both purposes, to provide synchronous data output and second to carry out in system device programming. This facility may help to ensure dynamic configurability of various resources availed for present Smart Sensor Module.

II. (f) Power supply unit:

The present system operates only on +5V power supply. The preciseness of the result depends upon the stability of power supply used. Figure 4.33 represents the power supply unit of the present system. The microcontroller as well as other analog parts works with +5V power supply. Use of same power supply, for both analog as well as digital parts of the SSM, reveals compatibility for deployment.

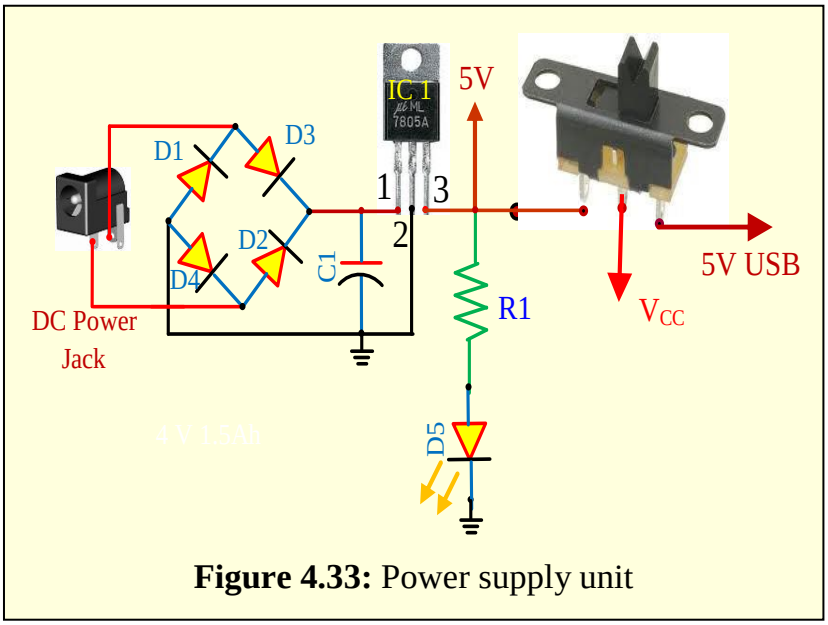

Figure 4.33: Power supply unit

Thus, the hardware of the Smart Sensor Module is designed for five sensors. It is attempted to incorporate the standards of IIII 1451. By providing different output buses

of different domains, the networking capabilities are also introduced. The PCB for the present Smart sensor Module is manufactured in the laboratory. The layouts and other details regarding PCB are given in the appendix-A. In fact, this SSM should be calibrated and standardized before implementation. Along with the implementation the process of calibration of the module is discussed in topic 5. However, the development of the firmware and programming of the device ensures the complete design of the Smart Sensor Module.

4.C Development of Firmware for Smart Sensor Module :

Present Smart Sensor Module (SSM) is the realization of an embedded system, wherein firmware is equally important. To ensure embedded technology, both hardware and software should be co-designed. In fact, present sensor module differs from traditional sensor only because of the intelligence provided by the embedded firmware. Along with the hardware, embedded firmware helps to introduce networking capabilities, due to which the SSM can be deployed in the IOT environment [82]. Therefore, such SSM is well suited for long term industrial environmental data acquisition for IOT representation [83]. With rapid development of IoT, major manufacturers are dedicated to develop multi-sensor acquisition interface equipment. There is a lot of data acquisition multiple interface equipments with mature technologies on the market. But these interface devices are very specialized in working style, so they are not individually adaptable to the changing IoT environment [84]. To perform this predefined task the microcontroller has to play with the real world. Meanwhile, these universal data acquisition interfaces are often restricted in physical properties of sensors. Now, microcontroller is used as the core controller in main stream data acquisition interface device. MCU has the advantage of low price and low power consumption, which makes it relatively easy to implement. It performs a task by way, which makes these multi-sensor acquisition interfaces adoptable. The design and construction of Smart Sensor Module is one of the important tasks of today`s electronic research. The enhancement in the intelligence by porting firmware into core to ensure configurability raises the smartness of the sensor system [85]. This intelligence is provided by the software that resides on the smart sensor interface. The software designed for the smart sensor module depicts layered architecture [71]. The bottom layer is of the device drivers, which directly interacts with the hardware interface and extracts digital data. The device manager interfaces with the device drivers and exposes a multiple data channel interface to the firmware layer. In the software framework, each sensor/actuator is composed of a combination of digital, analog or serial channels. Establishment of context to the extracted channel data is done at the firmware layer [86]. It also implements the application specific functionalities like real-time performance, data communication protocol with central control unit, smart sensor node management, etc.

Thus, the embedded firmware plays vital role in designing of Smart Sensor Module (SSM). The present Smart Sensor Module is designed about AVR microcontrollers for monitoring of five parameters such as relative humidity, temperature, CO_2 gas, ammonia gas and hydrogen sulfide gas. Therefore, the firmware required for present system is designed in embedded 'C' environment by using an IDE, Code Vision AVR.

In fact, an embedded system needs OS. However, on-chip memory of the microcontroller is sufficiently low and therefore, it is not possible to port the OS into target device. Therefore, the present firmware reveals the use of superloop to cater the need of operating system [87]. To develop the firmware, the development tool should consist of tools such as specialized editor, an assembler or compiler, debuggers, simulators, hardware emulators etc [88]. Therefore, it is recommended to deploy any smart Integrated Development Environment (IDE), the Code Vision AVR [89]. The designing issues of the hardware are intensively discussed in previous section. However, this section devotes the discussion on development of the software. Following are the major points of the discussion.

- An Integrated Development Environment (IDE), CodeVisionAVR .
- Programming tool
- Firmware designed for realization of SSM.

(a) An Integrated Development Environment CodeVisionAVR:

To satisfy the needs of firmware development, it is suggested to employ an Integrated Development Environment (IDE). The advantage of an IDE is that, all functions necessary to develop software for the microcontroller-based systems are incorporated within a single package. It consists of an editor for writing program code either in assembly language or in embedded C. A single keystroke can compile these codes. Moreover, the compiled program can be executed and simulated by enabling integrated simulator. An IDE after following procedure creates .hex file, which could be loaded directly into microcontroller flash memory. Depending upon family of microcontroller the variety of IDE are available. Present system is wired about AVR ATmega 8L microcontroller for which an IDE such as, AVR studio, Win AVR, Code vision AVR and Micro C OS-II etc are suitable. Therefore, the features of these IDEs are intensively studied.

However, it is found that, the CodeVision AVR, an IDE for AVR microcontrollers, has promising features and therefore, most of embedded developers are attracting towards this IDE [90]. Therefore, for present purpose, the CodeVision AVR is employed as an integrated development tool and required firmware is developed. The steps involved in the development of firmware for typical embedded application are highlighted. For programming the device, SinaProg 1.3.5.6 is employed.

1. Preparation:

Configuration of the Programmer types to ensure In system programming. To configure the programmer, start the CodeVisionAVR IDE and select the "Settings→Programmer" menu option. The dialog window shown in Figure 4.34 will open. Set the AVR Chip Programmer Type to "Atmel ATmega8L DEVELOPMENT BOARD/AVRISP", and the Communication Port used for In-System Programming of the system.

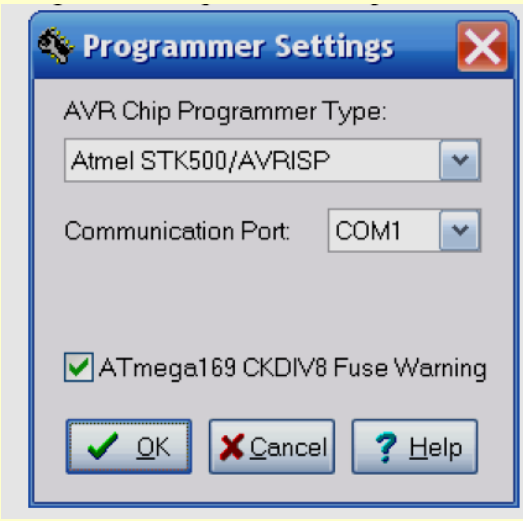

Figure 4.34: Configuration of the programmer to ensure In System Programming

After successfully completion of the preparation of this IDE suitable for development of firmware for AVR ATmega 8L microcontroller, the second stage is to start the creation of the new project. Following steps are involved to create and build either new project to realize the firmware developments.

2. Creating a New Project:

In order to create a new project, select the "File→New" menu option or press the toolbar button. The dialog window shown in Figure 4.35 will be displayed.

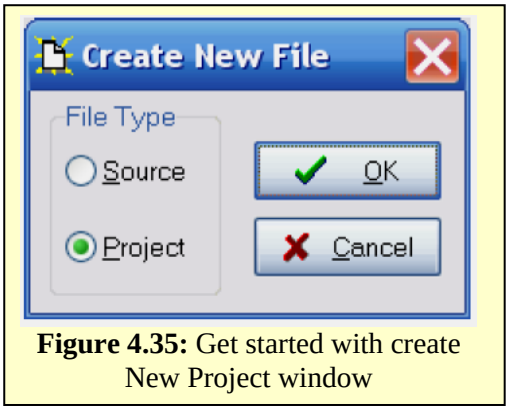

Figure 4.35: Get started with create New Project window

On selection of the Project option the development process begins. It is followed by the dialog box for its confirmation. On confirmation, the new window to called "CodeWizardAVR Automatic Program Generator" will be popped up. This step really helps the developer to design smart embedded firmware.

As discussed earlier, the CodeWizardAVR is a smart IDE only because of the fact that, it encompasses the tools like Automatic Program Generator (APG) [Figure 4.36]. This IDE is facilitated with such wizards. Therefore, the discussion on features of this IDE is given in this given in this report. It is known that, for development of the firmware for dedicated applications, a typical header files and the preprocessors should be included in the present project. However, the Code Vision AVR is facilitated with the self inclusion of primarily required files. Moreover, this APG help to configure the on-chip resources of the AVR Microcontroller. Otherwise, the embedded developer should create respective modules in the firmware. The process of creation of required modules for configuration of the on chip resources and synchronization of the same is tedious job. Therefore, the tool AGP is deployed and on chip resources are configured as per the need. Moreover, on inspection of the codes, it is found that, parameters of some on-chip resources are dynamically reconfigured.

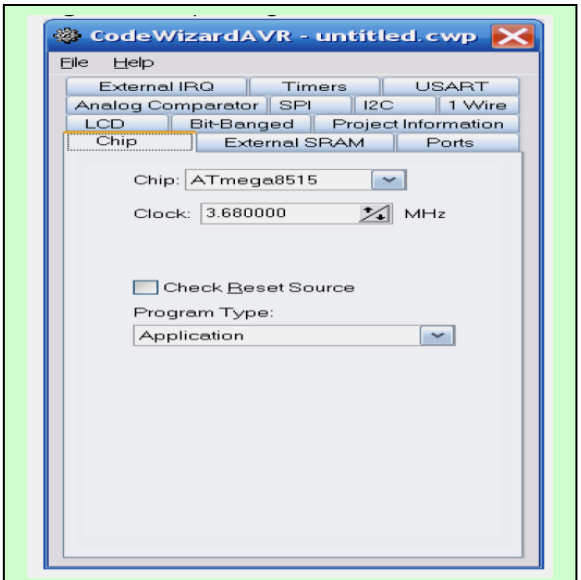

Figure 4.36: Automatic Program Generator of CodeWizardAVR

3) Device Selection and configuration of the Clock:

The devices AVR ATMega8L is selected for present embedded design. For the present system the clock is configured to 8 MHz. It depends upon the frequency of the crystal employed in the hardware. It also facilitates to select on chip clock source on configuration of internal RC oscillators. It has limited frequency and may exhibit jitter.

4) Configuration of Input / Output Ports:

As discussed in topic of hardware, all three ports are used for different purposes. The pin definition must be accordingly configured. This configuration can be done by using this AGP tool [Figure 4.36]. However, for preset embedded firmware, the pins are configured in the firmware.

5) Configuration of on chip Timer:

The AGP of Code Vision AVR supports the configuration of On Chip Timers. The Timer 1 is configured by developing respective module in the software.

6) Configuration of on chip ADC:

The AGP of Code Vision AVR supports the configuration of On Chip ADC. However, to ensure the dynamic configuration, the ADC modules is developed in the software.

7) Completion of the Project:

By selecting the "File→Generate, Save and Exit" menu option, the CodeWizardAVR will generate a skeleton C program, by following design rules, entire programme may be developed in C environment.

8) Viewing or Modifying the Project Configuration:

At any time, the project configuration may be changed using the "Project→Configure" menu option or by pressing the toolbar button. This will open the dialog window shown in Figure 4.37. This tool box can also be used for addition and deletion of the desired files. To change the target microcontroller, the clock rate etc, the "C Compiler" tab could be used.

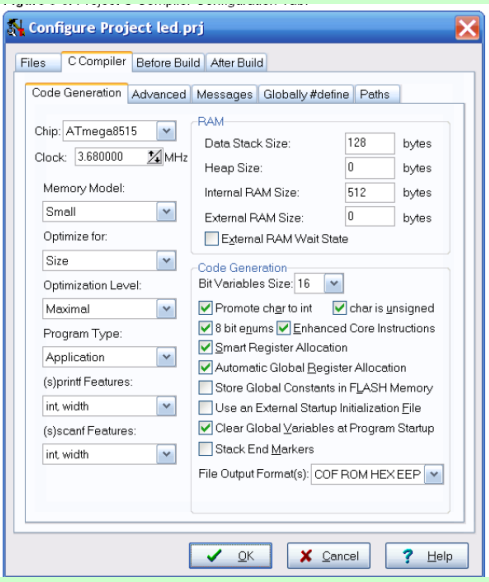

Figure 4.37: Project Configuration tool box

9. Writing Codes:

Writing of the source codes required to ensure present embedded design. The source codes are described in detail in next section. After writing of the codes, it is build by the process given by the Code Vision AVR IDE.

10. Building the Project:

Building of the project is an important stage, which compiles the program and converts the same in to .Hex file. The IDE code vision AVR has very powerful tool for building of the project. The window shows the RAM, EEPROM and FLASH memory usage as well. The successful building of the program realizes the bug free program. If it not built successfully, then there will be errors, which have to rectify. This stage should be iteratively attempted to produce bug free firmware.

(b) Programming of the Devices:

It is found that, the stage of building of the firmware is followed by simulation. Simulation ensures virtual instrumentation. The simulation can be performed by two ways. One in which, the IDE having simulator, by deploying, which the designer can validate the performance of the developed software. However, hardware simulation is the best tool.

To realize the operation of the embedded design, the program is ported into the target memory of the AVR ATmega 8L. The porting of the program into on chip memory of the AVR ATmega 8L microcontroller is called programming of the device. For programming of the device, a specific IDE recommended is called SinaProg 1.3.5.6. Deploying In System Programming (ISP) facility of the present microcontroller, as discussed in the section of hardware, the device is programmed, for which the programming tool SinaProg 1.3.5.6 is availed. In the beginning, the programming tool is configured for AVR ATmega8L device. The clock frequency, com port, etc are configured as per the hardware. Using tool the flash of the device is erased and made available for reprogramming. The typical USB supported programmer is availed for device programming. The flash of the microcontrollers are programmed by using SinaProg 1.3.5.6, which supports USB based programmer. When the device is programmed, Smart Sensor Module, under investigation is subjected for hardware emulation, wherein its physical performance validation is performed. If present system is successfully demonstrating its operation, as per the design specifications, then, it is subjected to monitoring of various environmental parameters.

c) The Firmware Development:

As discussed earlier, present Smart Sensor Module realizes the embedded technology, wherein entire hardware is designed about microcontroller AVR ATmega 8L. According to embedded philosophy, to process necessary information and to synchronize the operation of on-chip as well as off-chip resources, the firmware is required. Employing CodeVision AVR, an IDE, the firmware is developed in embedded C environment. The firmware developed for present Smart Sensor Module is described in this section.

Algorithm of the firmware, the flow of execution, is depicted in figure 4.38. Moreover, the source code of the same is presented in Appendix A.

On inspection of the Appendix A, it is found that software developed for monitoring parameters such as relative humidity, temperature, Concentration of CO_2, H_2S and NH_3 gases etc consists of various functions. All these functions are designed as per the functional requirement & perform the allotted task. The AVR Atmega8L microcontroller's architecture inherently supports the object oriented programming, that enables microcontroller to work in parallel with the other task having different threads of execution and can generate interrupts on the key event. However, present algorithm reveals sequential execution of the functions designed for dedicated task. Along with the main function, the firmware reveals following functions.

i) Analog to digital conversion [ADC (channel)]
ii) Measurement of Relative humidity [data_from_Channel_0]
iii) Measurement of Environmental temperature [data_from_Channel_1]
iv) Detection of CO_2 gas [data_from_Channel_2]
v) Detection of H_2S gas [data_from_Channel_3]
vi) Detection of NH_3 gas [data_from_Channel_4]
vii) Decimal to BCD and ASCII conversion [(dec-bcd)]
viii) Initialization of LCD [lcd_init( )]
ix) Character display [lcd_display]
x) Parameter value display [LCD( )]
xi) Configuration of LCD[LCD cmd ( )]
xii) Sending data to LCD[LCD data( )]
xiii) Sending data to Serial_port[Serial data( )]
xiv) Delay Function [Msdelay( )]

The title of the function reveals the task, which it has to perform. It is found that, these functions establish the thread with hardware resources. It also ensures the inter-function data transfer. These functions are sequentially called into main program as depicted in the flowchart in shown in figure 4.38. Synchronization of hardware and software is one of important characteristic of embedded system.

C (i) Main program:

It is known that, embedded software ensures the use of superloop that satisfies the need of operating system. However, as per structure of embedded C environment, the superloop is included in the main function. The details regarding algorithmic issues

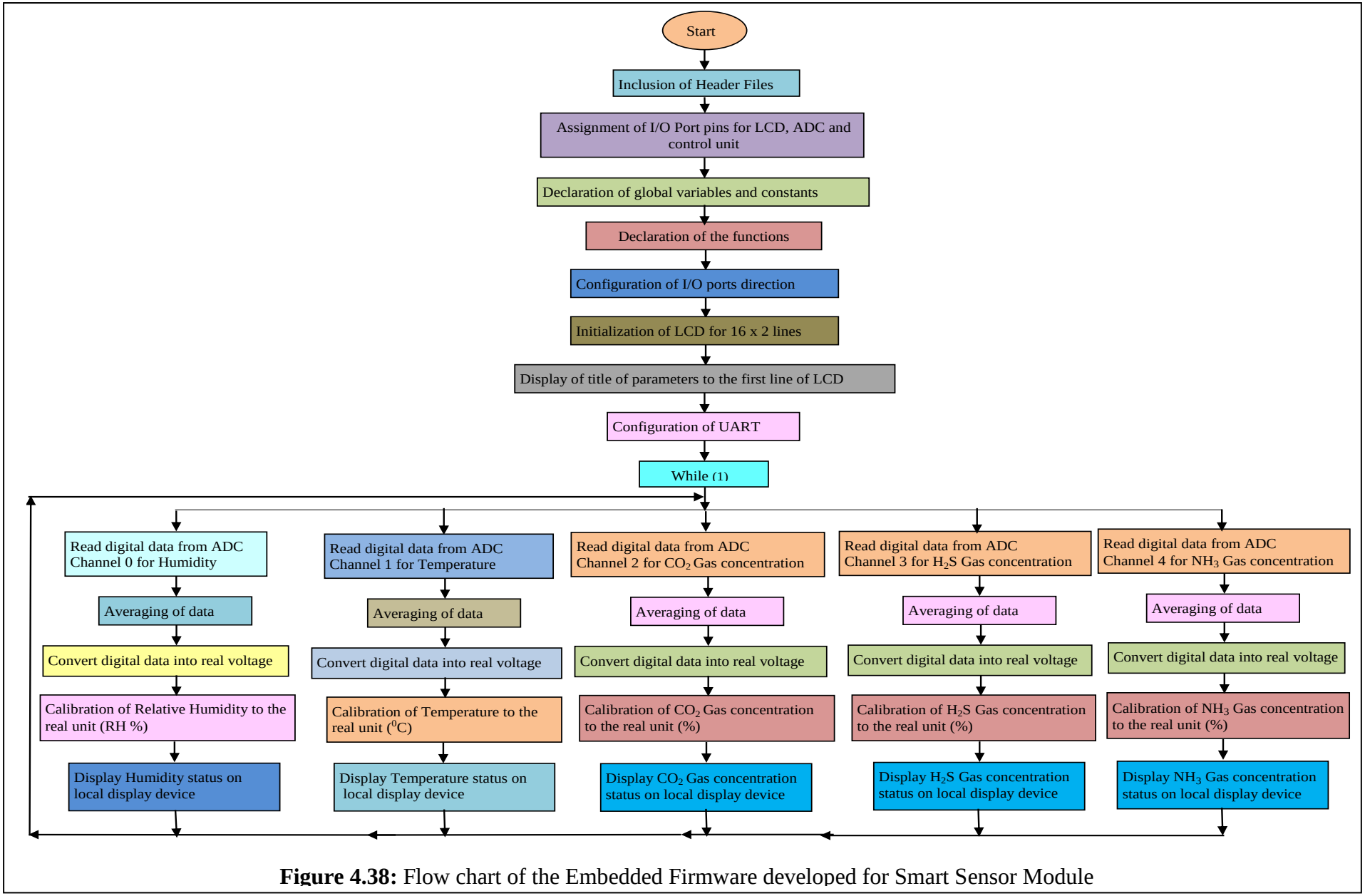

Figure 4.38: Flow chart of the Embedded Firmware developed for Smart Sensor Module

of main function are discussed. As presented in Appendix A, the source code, in the beginning, in order to enable the hardware resources of AVR Atmega8L, the header file mega8.h is included. To perform various tasks the functions are defined and declared globally. Variables, array, pointers etc. are also globally declared. Appendix A presents the range and type of variables and constants. The peripheral devices such as LCD, need typical I/O lines for data bus and control signals as well. Therefore, I/O lines required are globally assigned. Name of the variables self emits the purpose for which it has been declared.

When program control transfer into main function, as discussed previously, the data direction registers DDRD and DDRB are configured in output mode, because these ports are used to interface the LCD [Figure 4. 27]. On investigation of structural details of LCD, it is found that the, before use, the LCD must be configured in desired mode. However, this function is not portable for all types of hardware, but it is related to typical hardware configuration only. Therefore, the function (LCD_init) is developed and by calling the function (lcd_init), the LCD is configured. The names of the parameters, Humidity, Temperature and CO_2 gas are displayed on the first line of 16×2 LCD display. Then program transfers the control to the super loop constructed by using while (1) structure.

As discussed in the previous section, analog data of humidity is given to channel 0 of ADC (pin no.23) of Atmega8L, analog data of an temperature is given to channel 1 of ADC (pin no.24) and that of CO_2 gas, H_2S gas and NH_3 gas is given to channel 2, 3 and 4 of ADC . Therefore, in the beginning humidity data is processed. Then, the data of temperature and CO_2 data are processed [Appendix A]. The values of the parameters are displayed simultaneously on second line of 16×2 LCD display. The details regarding each function are given below.

ii) Measurement of Relative Humidity [data_from_Channel_0]:

This function is defined for conversion of data, which is read from ADC channel 0 (pin 23) into relative humidity scale (%RH). The function enters with the digital data obtained from channel 0 and returns with humidity reading. The data obtained from analog channel 0 is related to the relative humidity. However, it is simple decimal number with 10 bit resolution. It is converted into real voltage form and return into variable ‘H_Read’. Calibration equation is obtained from process of regression. The

process of calibration is described in next topic, whereas the source code (Appendix A) depicts the expression developed for calibration into humidity scale.

$$\left.\begin{aligned} \text{Relative Humidity 'H' (\% RH)} &= \frac{VRH-442.5}{29.75} \\ \text{Relative Humidity 'H' (\% RH)} &= \frac{VRH-1894.65}{5.873} \end{aligned}\right\} \quad (2)$$

Thus, this expression continuously executed by the firmware and humidity data is displayed on the LCD provided on the SSM. Moreover, this data also put on the serial bus to make it available to ensure networking.

iii) Measurement of Temperature [data_from_Channel_1]:

This function is defined for conversion of data, which is read from ADC channel 1 (pin 25) into temperature scale (^{0}C). The function enters with the digital data and returns with temperature reading. The data obtained from analog channel 1 is related to the temperature. It should be expressed in the unit of ^{0}C. However, the data obtained is simple decimal number. It is converted into real voltage form and return into variable 'T_Read'. Calibration equation is obtained from process of regression.

The process of calibration is described in next topic, whereas the software (Appendix A) represents the use of the desired expression.

$$\left.\begin{aligned} \text{Temperature (t) } ^{O}\text{C} &= ((V_T - 136.0)/9.335) \\ \text{Temperature (t) } ^{O}\text{C} &= ((V_T + 532.7)/20.83) \end{aligned}\right\} \quad (3)$$

The environmental temperature is allowed to display on the LCD. The position of the cursor is predefined. Moreover, this value is passed to the function serial data( ) to ensure either UART communication of RS232 communication.

iv) Detection of CO_2 gas [data_from_Channel_2]:

As discussed earlier, designing of SSM is one of objective of present research, for which hardware is already designed. This function is defined for detection of the carbon dioxide gas and presentation of the same in percentage unit. It is known that, CO_2 dependent analog voltage (V_{G1}) is available at channel 2 of ADC. It is then digitized

with 10 bit resolution. Equivalent digital data is read from this channel. It would be the input for this function. Using reference voltage of 2.56V and formula suggested, the digital data is converted into real voltage form[91]. On observation, it is found that the analog voltage appeared at this channel and that of converted by this function is almost same. This real voltage value is return into variable 'C_Read'. Calibration equation is obtained from process of regression. The process of calibration is described in next topic. The expression obtained from the process of two point calibration is given by

$$\text{Concentration of } CO_2 \text{ gas (\%)} = (1589.33 - V_{G1}) / 9.597 \quad \text{----- (4)}$$

v) Detection of H_2S gas [data_from_Channel_3]:

The present Smart sensor module is designed to monitor the concentration of the H_2S gas in % scale. Employing ferrite based sensor, a separate channel for H_2S gas is designed. Analog voltage (V_{G2}) related to the concentration of H_2S gas available at input of channel 3 of ADC is read. It is then digitized with 10 bit resolution. Equivalent digital data is read from this channel. It would be the input for this function. Using reference voltage of 2.56V and formula suggested, the digital data is converted into real voltage form [91]. This real voltage value is return into variable 'H2S_Read'. The expression obtained from the process of two point calibration is given by

$$\text{Concentration of } H_2S \text{ gas (\%)} = \frac{Vo}{VMax} \times 100\ \% \quad \text{-------- (5)}$$

vi) Detection of NH_3 gas [data_from_Channel_4]:

The monitoring of concentration of ammonia gas is essential for environmental study. Ammonia sensor is designed by using thick film technology and employed for present SSM design. Hardware section describes the designing issues of the same. A separate channel for NH_3 gas is designed. Analog voltage (V_{G3}) related to the concentration of ammonia gas available at input of channel 4 of ADC is read. It is then digitized with 10 bit resolution. This function is dedicatedly designed for detection of ammonia gas and presentation of the same in percentage scale. Using reference voltage of 2.56V, the digital data is converted into real voltage. This real voltage value is return into variable 'NH3_Read'. The expression obtained from the process of two point calibration is given by

$$\text{Concentration of } NH_3 \text{ gas (\%)} = \frac{Vo}{VMax} \times 100\ \% \qquad (6)$$

vii) Initialization of LCD [lcd_init( )]:

This function is defined to configure the operation of smart LCD. It calls the function LCD cmd(), which is declared to send command to the LCD and sequentially sends the command for configuration of LCD. The command required to initialize LCD are already discussed.

viii) Character display [lcd_display]:

This function is of void type and has two arguments; the row number at which the message is to be displayed and second the message to be displayed. The message is supported to be an array. It selects row and column number and displays the message to the desired location. By calling in main program, in the beginning at the first column the title 'Humid' is displayed. Then subsequently the title of four other parameters Temp, CO2, H2S and NH3 are displayed. The address of these can be varied.

ix) Analog to digital conversion [ADC (channel)]:

As discussed earlier, the availability of on-chip analog to digital converter (ADC), the AVR microcontroller not only reduces the complexity of DAS, but also helps to enhance the structure of software [92]. The microcontroller nicely plays the job of analog to digital conversion by exhibiting the reduction of handshaking signals, which otherwise required for off-chip ADC. Considering this fact into account, this function is defined, which reveals the access of on-chip ADC.

This function is of integer type and enters with the channel number, which it has to be selected for digitization. On chip ADC is enabled and configured. The registers ADMUX, ADCSRA and SREG are configured. The control words used are depicted in table 4.16. The ADCMUX register is dynamically configured.

Table 4.16: SFR and its Configuration

Sr.No.	Register	Control word	Configuration
1	ADCMUX	C0H	Internal reference voltage 2.56V, Right justified. Channel 0, 1, 2 [C0H, C1H, C2H]
2	ADCSRA	E0H	Free running mode, no prescaler
3	SREG	80H	Global interrupt enable.

The parameter values obtained on digitization are averaged typically over 500 samples and returns the averaged value. This function returns with the integer number bearing information of the parameter to be measured. This function is sequentially called for all above parameters.

x) Decimal to BCD and ASCII conversion [(dec_bcd)]:

This function is developed for conversion of decimal number into BCD forms and hence into ASCII form. This is because, for display the same on LCD, one must use ASCII format of data. Function represented in the appendix A self explain the technique employed for this conversion. The variables are always refreshing with values of respective parameters.

xi) Parameter value display [LCD( )]:

This function is of void type and designed to display the values of parameters on the second line at desired position. It enters with the column number and defines the address of the curser position where the parameters are to be displayed. Then the parameters in five digits are displayed on the LCD. Here LCD is configured in time delay mode, wherein 8 wires of data bus are used for data and command transfer.

xii) Configuration of LCD [LCD cmd( )]:

This function is of void type and it is defined to send command to the LCD. It enters with the LCD command. It also produces the handshaking signals, which must be issued prior to transfer other command.

xiii) Sending data to LCD [LCD data ( )]:

This function is void type and it is defined to send data to the LCD. It enters with ASCII code of data to be display. It also produces the handshaking signals, which must be issued prior to transfer of the data byte.

xiv) Sending data to Serial port:

This function is defined for UART / USART port of the SSM. It takes the data from various functions and put into serial port. The data could be available on TxD and RxD lines of microcontroller. Moreover, to this line the RS232 port is also interfaced. Using this function the data is also made available on this port to read into computer or other RS232 standard devices.

xv) Delay Function [Msdelay ( )]:

This function is defined to produce embedded delay of particular duration and called wherever necessary.

References:

1. IEEE Instrumentation And Measurement Society, IEEE Standard for a Smart Transducer Interface for Sensors and Actuators — Common Functions, Communication Protocols, and Transducer Electronic Data Sheet (TEDS) Formats. Institute of Electrical and Electronics Engineers, Inc. New York (2007), (ISBN 0-7381-5598-5).
2. IEEE 1451.2-1977 IEEE STANDARD for A SMART TRANSDUCER INTERFACE For SENSORS and ACTUATORS Transducer to Microprocessor Communication Protocols and Transducer Electronic Data Sheet (TEDS) Formats.
3. Mitar Simić, "Design of Monitoring and Data Acquisition System for Environmental Sensors", Proceeding of X International Symposium on Industrial Electronics INDEL 2014, Banja Luka, (2014) 146 -149.
4. M. Simić, "Microcontroller Based System for Measuring and Data Acquisition of Air Relative Humidity and Temperature", Presented at the 37th International Conference of IMAPS-CPMT Poland, (2013).
5. M. Simić, and M. Sireteanu, "Real Time Temperature and Relative Humidity Monitoring System using LabVIEW", In Proceedings of the International scientific conference of Metrology and Quality in Production Engineering and Environmental Protection – ETIKUM, (2014) 67-70.
6. Oprea, N. Bârsan, U. Weimar, J. Courbat, D. Briand and N.F. de Rooij, "Integrated Temperature, Humidity and Gas Sensors on Flexible Substrates for Low-Power Applications", IEEE SENSORS, (2007) 158-161.
7. M. Kummer, A. Hierlemann, and H. Baltes, "Tuning sensitivity and selectivity of complementary metal oxide semiconductor-based capacitive chemical microsensors", Analytical Chemistry, 76 (2004) 2470-2477.
8. A. Somov, A. Baranov and D. Spirjakin, "Wireless sensor–actuator system for hazardous gases detection and control", Sensors and Actuators, A 210 (2014) 157–164.
9. Y. Song, C. Gang, Y. Fang, J. Ma and X. Zhang, "Design Of Greenhouse Control System Based On Wireless Sensor Network And AVR Microcontroller", Journal Of Network 6, 12 (2011) 1668-1674.

10. C. Otto, A. Milenković, C. Sanders and E. Jovanov, “System Architecture Of A Wireless Body Area Sensor Network For Ubiquitous Health Monitoring”, Journal of Mobile Multimedia, 1 4 (2006) 307-326.
11. P. N. Kumar, N.S. M. Sharma, M.S. M. Mohan and D. Raj, “Design And Implementation Of ARM Intelligent Monitoring System Using Zigbee”, International Journal Research In Computer And Communication Team, 1, 7 (2012) 465-470.
12. V.Ramya, B. Palaniappan and A. Kumari, “Embedded Patient Monitoring System”, International Journal of Embedded Systems and Applications, 1 2 (2011) 51-63.
13. D. Wobscholl, “A wireless gas monitor with IEEE 1451 protocol”, in: Proceeding of Sensors Applications Symposium (SAS 2006) Houston, TX, USA,(2006) 162–164.
14. Flyport, “Sensing platform”, www.openpicus.com
15. Wasp, “Mote sensing platform”, www.libelium.com/products/waspmote
16. A. Somov, A. Baranov, A. Savkin, D. Spirjakin, A. Spirjakin and R. Passerone, “Development of wireless sensor network for combustible gas monitoring”, Sensors and Actuators A: Physical 171 (2011) 398–405.
17. K. Shinghal, A. Noor, N.Srivastava and R. Singh, “Intelligent humidity sensor for wireless sensor network agricultural application”, Intern. J. Wireless & Mobile Networks (IJWMN), 3 1 (2011) 118-128.
18. L.John S.Fernando Figueroa, J. Morris and M. Turowski, "Making Smart Sensors Intelligent: Building on the IEEE 1451.x Standards", 54th International Instrumentation Symposium, Pensacola, FL USA, (2008) 1-33
19. IEEE 1451.2 Standard, .A Smart Transducer Interface for Sensors and Actuators. Transducer to Microprocessor Communication Protocols and Transducer Electronic Data Sheet (TEDS) Formats,. Piscataway, NJ: IEEE Standards Department, (1998).
20. Sensor Device Data/Handbook, DL200/D Rev. 4, 1998, Motorola Semiconductor Products Sector, Austin, TX. Najafi, K., .Smart Sensors,. J. Micromechanics and Microengineering, 1, (1991)86-102.
21. Ina, O., .Recent Intelligent Sensor Technology in Japan,. Soc. Automotive Engineers, SAE891709, 1989.
22. NI Multisim user manual TM, “Analog Devices Edition: Getting Started with NI

Multisim Analog Devices Edition", available online. http://www.ni.com/pdf/manuals/372330a.pdf

23. Randy Frank, "Understanding smart sensors", Artech House sensors library, 2000.
24. Honeywell Datasheet, "HCH-1000 Series - Capacitive Humidity Sensor", available online, http:// sensing. honeywell.com /index.cfm /ci_id /146573/la_ id/1 /document/1/re_id/0.
25. W.J. Staszewski, C. Boller and G.R. Tomlinson, "Health monitoring of aerospace structures : smart sensor technologies and signal processing" , John Wiley & Sons Inc., 2004.
26. E. Jovanov, A O Lords, D. Raskovic, PG Cox, R. Adhami and F.Andrasik "Stress monitoring using a distributed wireless intelligent sensor system", IEEE Eng Med Biol Mag., 3 (2003) 49-55.
27. C. Feng and S. Jiangfeng, "Study on Wireless Gas Sensor, Proceedings of the Third International Symposium on Electronic Commerce and Security Workshops(ISECS '10)" Guangzhou, P. R. China, (2010) 380-382.
28. R.A.D.M.P.Ranwaka, "EMBEDDED LEAKAGE DETECTOR, SAITM Research Symposium on Engineering Advancements 2013 AUTOMATIC GAS CIRCULATION MONITORING SYSTEM THREAT AND AND LEAKAGE DETECTOR", SAITM Research Symposium on Engineering Advancements 2013 (SAITM – RSEA 2013)
29. J. E. O. Reges, and E.J.P. Santos "A VHDL CAN Module for Smart SensorsProgrammable Logic", IEEE 4th Southern Conference sensors (2008) 179 – 182
30. M. Chaudhari1 and S. Dharavath, "Study of Smart Sensors and their Applications", Intern. J. Adv. Res. Comp. and Comm. Engg., 3 1(2014)
31. M. Schiefer, and M Lally, "A Framework for Smart Transducer Interface Systems," SAE Technical Paper (1999)1858.
32. S. Palacios, A. Rida, S. Kim, S. Nikolaou, S. Elia and M. M. Tentzeris, "Towards a Smart Wireless Integrated Module (SWIM) on Flexible Organic Substrates Using Inkjet Printing Technology for Wireless Sensor Networks" (2012) IEEE (20-23).
33. K. Lee, "IEEE 1451: A Standard in Support of Smart Transducer Networking",

IEEE Instrumentation and Measurement Technology Conference Baltimore, MD USA, (2000)1-4.

34. K. B. Lee, J. D.Gilsinn, R. D. Schneeman and H. M. Huang, "First Workshop on Wireless Sensing"National Institute of Standards and Technology. NISTIR 02-6823, (2002).

35. S. R. Manihar, K. P. Dewagan and J. Rajpurohit, "Multiple gas Analyzer and Indicator", Intern. J. of Modern Engineering Research, 2 4 (2012)2753-2755.
36. K. Kishore, E. Narasimha and Y Shruthi, "SMART HELMET FOR COAL MINERS USING ZIGBEE TECHNOLOGY", Intern. J. for Res. in Sci. & Advanced Technol.2 2 (2013) 067-069.
37. C.M. Ghimbeu, M. Lumbreras, M. Siadat, J. Schoonman, "Detection of H_2S, SO_2, and NO_2 using electrostatic sprayed tungsten oxide films, Mater. Sci. Semiconduct. Proc. 13 (2010) 1–8
38. J. Wan-Li and Z. Lei, "Preparation and Gas Sensing Properties For Acetone Of Amorphous Ag Modified $NiFe_2O_4$Sensor", Trans. Nonferrous. Mater. Soc. China, 22 (2012) 1127-1132.
39. D. C. Bharati, K. Mukherjee and S. B. Majumdar, "Wet Chemical Synthesis And Gas Sensing Properties Of Magnesium Zinc Ferrit Nano-Particles", Mater., Chem. Phys., 120 (2010) 509-517. .
40. U. B. Gawas, V. M. S. Verenkar and D.R. Patil, "Nano-StructedFerrite Based Electronic Nose Sensitive To Ammonia At Room Temperature", Sensors and Transducers J., 134 11 (2011) 45-55.
41. Data sheet of TLV2774 , http://www.ti.com/product/TLV2774/technicaldocuments.
42. S. Liu, R. X. Gao, P. Freedson, " Design of a wearable multi-sensor system for physical activity assessment", Advanced Intelligent Mechatronics (AIM), IEEE/ASME International Conference on (2010) 254 – 259.
43. http://www.ti.com/product/tlv272
44. P. V. Mane-Deshmukh, B. P. Ladgaonkar, S. C. Pathan and S. S. Shaikh, " Microcontroller PIC 18F4550 based Wireless Sensor Node to monitor industrial environmental parameters", 3 10 (2013) 943-950.

45. S. Ye, F. Zhou, H. Chen and H. Yan, " Non-Invasive Method and Experimental Study for Measurement of Oxygen Saturation Rate in Wide Range", Bioinformatics and Biomedical Engineering, 2008. ICBBE 2008. The 2nd International Conference on (2008) 733 – 736.
46. B. B. Li and Z. F. Yuan, "Research on a Banknote Printing Wastewater Monitoring System based on Wireless Sensor Network", Journal of Physics: Conference Series 48 (2006) 1190–1194.
47. V.Ramya, B. Palaniappan and A. Kumari, "Embedded Patient Monitoring System", International Journal of Embedded Systems and Applications, 1 2 (2011) 51-63.
48. M. AL-Rousan, A. Rjoub and A. Baset, "A Low-Energy Security Algorithm for Exchanging Information in Wireless Sensor Networks", Journal of Information Assurance and Security, 4 (2009) 48-59.
49. U. Sharma and S.R.N. Reddy, "Design of Home/Office Automation using Wireless Sensor Network", International Journal of Computer Applications, 43 22 (2012) 53-60.
50. A. Francillon and C. Castelluccia, "Code Injection Attacks On Harvard-Architecture Devices", Proceedings of the 15th ACM Conference on Computer and Communications Security, 15-26.
51. P. N. Kumar, N.S. M. Sharma, M.S. M. Mohan and D. Raj, "Design And Implementation Of ARM Intelligent Monitoring System Using Zigbee", International Journal Research In Computer And Communication Team, 1, 7 (2012) 465-470.
52. Z. Yu-jie, S. Jiang-long and W. Rui, "Design of Equipment Room Environment Monitoring System Based on LPC2378", Journal of Jiangnan University, (2009-03).
53. B. Yan-min and X. Shu-gang, "Design of Programmable Industry Controller Based on ARM and CPLD", Journal of Equipment Manufacturing Technology, (2009-11).
54. L. Yuan and Z. Shan-an, "The Embedded Industry Controlling System Based On ARM9 and CPLD", Journal of Mechanical & Electrical Engineering Magazine, (2007-01).

55. S. K Jose, X. A. Mary and N. Mathew, “ARM 7 Based Accident Alert and Vehicle Tracking System”, International Journal of Innovative Technology and Exploring Engineering, 2 4 (2013) 93-96.
56. C. Otto, A. Milenković, C. Sanders and E. Jovanov, “System Architecture Of A Wireless Body Area Sensor Network For Ubiquitous Health Monitoring”, Journal of Mobile Multimedia, 1 4 (2006) 307-326.
57. A. Milenković, C. Otto and E. Jovanov, “Wireless Sensor Networks For Personal Health Monitoring: Issues and an Implementation”, Computer Communications, 29 13–14 (2006) 2521–2533.
58. C. Lynch, and F. O'Reilly, “PIC-based TinyOS implementation”, Proceedings of Second European Workshop on Wireless Sensor Networks, (2005) 378 – 385.
59. A. Pantelopoulos and N.G. Bourbakis, “A Survey on Wearable Sensor-Based Systems for Health Monitoring and Prognosis”, IEEE Transactions on Systems, Man, and Cybernetics, Part C: Applications and Reviews, 40 1 (2010) 1–12.
60. B.P. Ladgaonkar and S.N. Patil, “Designing Of Data Acquisition System For Susceptibility Measurement”, International Journal Of Electrical Engineering And Embedded Systems, 3 2 (2011) 87.
61. Datasheet of AVR Atmega 8L. http://www.atmel.in/Images/Atmel-2486-8-bit-AVR-microcontrollerATmega8L datasheet.pdf
62. M. A. Mazidi, S. Naimi and S. Naimi, “The AVR Microcontroller and Embedded Systems: Using Assembly and C”, Prentice Hall publication, (2011).
63. H. W. Huang, “The Atmel AVR Microcontroller: MEGA and XMEGA in Assembly and C”, USA.
64. http://en.wikibooks.org/wiki/Embedded_Systems/Atmel_AVR
65. S. F. Barrett and D. J. Pack, “Atmel AVR Microcontroller Primer: Programming and Interfacing”, Morgan and Claypool Publication.
66. D. Gadre, “Programming and Customizing the AVR Microcontroller”, McGraw-Hill Education publication, (2000).
67. Y. Song, C. Gang, Y. Fang, J. Ma and X. Zhang, “Design Of Greenhouse Control System Based On Wireless Sensor Network And AVR Microcontroller”, Journal Of Network 6, 12 (2011) 1668-1674.

68. D. Bhattacharjee and R.Bera, “Development of smart detachable wireless sensing system for environmental monitoring”, Intern. Journal on smart sensing and intelligent systems, 7 3 (2014) 1239-1253.
69. S. P. Wood, K. Lee and J. Bryzek, “ An overview of IEEE 1451.1 Smart Transducer Interface Module”, Analog integrated circuits and signal processing, 14(1997) 165-177.
70. A.Chu, F. Gen-Kuong and B.Swanson, “Smart Sensors and Network Sensor Systems”, http://www.eecs.wsu.edu/~holder/courses/cse6362/pubs/Chu.pdf
71. H. Ramamurthy, B. S. Prabhu, R. Gadh, and A. Madni, “Smart Sensor Platform for Industrial Monitoring & Control”, 4th IEEE Sensors, Irvine, California, (2005).
72. IEEE Standard for a Smart Transducer Interface for Sensors andActuators-IEEE 1451.3 edition, 2004.
73. S. Hwang and D. Yu, “Remote Monitoring And Controlling System Based On Zigbee Networks,” International Journal of Software Engineering and Its Applications, 6 3 (2012) 35–42.
74. C. Suh and Y. B. Ko, “Design and Implementation Of Intelligent Home Control Systems Based On Active Sensor Networks,” IEEE Transactions on Consumer Electronics, 54 3 (2008) 1177–1184.
75. A. Pawlowski, J. L. Guzman, F. Rodríguez, M. Berenguel, J. Sánchez, and S. Dormido, “Simulation of Greenhouse Climate Monitoring and Control with Wireless Sensor Network and Event-Based Control”, Sensors (Basel), 9 1 (2009) 232–252.
76. A.M. Pawar, S. N. Patil, A. S. Powar and B. P. Ladgaonkar, “Wireless Sensor Network To Monitor Spatio-Temporal Thermal Comfort Of Polyhouse Environment”, International Journal of Innovative Research in Science, Engineering and Technology, 2 10 (2013) 4866-4875.
77. Datasheet of Hitachi HD 44780 LCD
https://www.sparkfun.com/datasheets/LCD/HD44780.pdf
78. http://en.wikipedia.org/wiki/Hitachi_HD44780_LCD_controller
79. M.A. Ahmed, E. Ateia., L.M. Salah, A.A. El-Gamal, “Structural and electrical studies on La^{3+} substituted Ni–Zn ferrites”, Mater. Chem. and Phys., 92(2005)310–32.

80. J. Jeong and D. Culler, “Incremental Network Programming for Wireless Sensors”, International Journal Communications, Network and System Sciences, 5 (2009) 433-452.
81. http://www.cse.iitk.ac.in/users/amiteshm/reports/CS719_Wireless_System_ProjectReport.pdf
82. G. Tiwari and R. Kazi, “ Realization of the functions of automatic Smart Sensor Interface for Industrial in IOT environment”, Intern. J. Adv. Res. Comp. Sc. and Software Engg., 5 1 (2015) 878-883.
83. F. Salvadori et al., “Monitoring in industrial systems using wireless sensor network with dynamic power management,” IEEE Trans. Instrum. Meas., vol. 58, no. 9, pp. 3104–3111, Sep. 2009.
84. A. Goswami, T. Bezboruah, and K C. Sarma, “Design of an embedded system for monitoring and controlling temperature,” Porc. Of International conference on emerging technologies and applications in engineering, technology and science, 1(2008)105-110.
85. F. B. SPENCER, M.l RUIZ-SANDOVAL, N. KURATA, “SMART SENSING TECHNOLOGY FOR STRUCTURAL HEALTH MONITORING”, 13th World Conference on Earthquake Engineering, Vancouver, B.C., Canada Paper ID 1791, August 1-6, (2004) 1-13.
86. W. Heinzelman, A. P. Chandrakasan, and H. Balakrishnan, “An Application-Specific Protocol Architecture for Wireless Microsensor Networks,” IEEE Transactions on Wireless Communications, 1 (2002)660–670.
87. M . J. Pont, “Embedded C”, Addison-Wesley, (2002).
88. S. Dubey, D. S. Bais and A. Chouhan, “Real Time Operating System for Robotics using AVR Microcontrollers” , International Journal of Information & Computation Technology, 4 17 (2014) 1861-1868.
89. P. Kaur and S. Chatterji, “A novel framework based on AVR microcontroller for automated testing and analysis of DC motors” Recent Advances in Engineering and Computational Sciences (RAECS), (2014) 1–6.
90. Data sheet of CodeVisionAVR C Compiler http://www.atmel.com/images/doc2500.pdf

*****

Topic 5

Implementation of Smart Sensor Module

5.1 Introduction:

Recent trend in the field of electronic instrumentation is to develop intelligent sensor system of great portability. Classical sensors are adequately used for the traditional methodological operation such obtaining an electrical signal corresponding to the physical parameters. Now days, the industrial requirement of the sensor have changed tremendously in terms of cost, size, quality, reliability and deployment of modern technologies. Industrial measurement and control instrumentation is shifted from deployment of huge amount of distributed system to the smart systems with the features such as integrability, miniaturization, low power consumption, reliability, preciseness, configurability, great intelligence, additive capability of signal processing, etc. This modernization in the field of sensor based systems emerges new class called intelligent sensor module or Smart Sensor Module [1]. During early days, the designers were deploying sensor systems, which are dumb in context with the intelligence. The traditional sensor systems are not smart system. Therefore, the resulting systems were featured with less reliability and preciseness. Moreover, portability of the system to different environment is also limited. To overcome the limitations of early days` electronic systems, the term Smart Sensor System or Smart Sensor Module is evolving. The IEEE technical group have defined standards for intelligent sensor module with the title as IEEE 1451 standards [2]. Recently, the field of embedded system development is becoming more pervasive and it comprises microcontrollers of prominent features. Therefore, it finds wide spectrum of applications in the fields such as, Industrial automation, Agricultural Instrumentation, Biomedical Instrumentation, food processing, environmental parameter study, consumer electronics etc. In fact, an embedded system is the dedicated design[3]. Therefore, it plays significant role on the measurement and control instrumentation. Embedded devices are having on-chip storage capabilities. Therefore, intelligence can be ported in to on-chip memory of the microcontroller [4]. This results into enhancement in the smartness of system. According to IEEE 1451 standard, the intelligent system should be equipped with networking capabilities [5]. Incorporation of networking capabilities to the sensor module enhances the smartness

of the module. Therefore, the IEEE 1451 technical group assigns the two terms Smart Transducer/Sensor Interface Module (STIM or SSIM) and Network Capable Application Processor (NCAP). In addition to this, the term Transducer Electronic Datasheet (TED) is also playing vital role to represent the smartness of the sensor module. The availability of output on buses of different environment such as RS232, I2C, SPI, USART, UART etc ensures the deployment of Smart Sensor Module to establish the Smart Sensor Network [5, 6, 7]. The Smart Sensor Module should be designed to realize the plug and play philosophy [8]. Emphasizing embedded technology, the Smart Sensor Module, consisting of sensing unit, signal conditioning and data acquisition unit, data conversion unit, computing unit and output unit may be designed [9]. In short, deployment of smart sensor module with promising features, results into sophisticated measurement and control instrumentation.

The results of designing of Sensor Module for various parameters are available in the literature [10]. The reports on development Smart Sensor Modules, wherein embedded technology is realized, are also available in the literature [11]. In fact, the Smart Sensor Modules, for measurement of parameters such as relative humidity, environmental temperature, detection as well as monitoring of various gases etc have been designed and results are reported by the researchers [12-14]. However, these SSM are designed by employing readily available sensors. The reports on synthesis of the sensing materials of desired characteristics and deployment of the same to fabricate the sensors required for SSM are rare. Therefore, it is proposed to develop Smart Sensor Module, realizing typical IEEE 1451 standards, to measure the physical parameters such as temperature, humidity and gas concentration etc, wherein the sensing elements of polycrystalline spinel nanoferrites have been deployed.

As discussed in the previous topics, nanosized ferrite materials ($Mg_xZn_{1-x}Fe_2O_4$, $Ni_xZn_{1-x}Fe_2O_4$ and $Mn_xZn_{1-x}Fe_2O_4$) have been synthesized and characterized for their successful formation. Electrical properties sensitive to humidity, temperature, carbon dioxide H_2S and NH_3 gases are investigated. The results of investigation proved their suitability for sensor based applications. Employing typical sensing elements the sensors are developed and deployed for designing of Smart Sensor Module. Smart Sensor Module is good example of embedded design. Hardware and necessary firmware is developed for this dedicated application and issues regarding the same are discussed in previous topic 4. The present sensor module is designed about advanced microcontroller AVR ATMega8L. This topic is devoted to the implementation of Small

Sensor Module for which it has been developed. The results of implementation will be interpreted in this topic.

Present Smart Sensor Module is designed about sensors, wherein polycrystalline ferrites based sensing element is used. As discussed in topic 4, the signal conditioning circuits produces analog voltages proportional to the concentration of the parameters to be measured. Basically, the sensing elements depict change in the resistance due to the concentration of the parameters under test. However, to present the values of the parameters in respective, one has to calibrate the Sensor Module. Moreover, the present SSM provides output on various buses for further interfacing [15]. Moreover, as per IEEE 1451 standards, the table of specifications regarding Smart Sensor Module is essential to present with SSM. Therefore, it is essential to convert the data into respective scientific units [16]. Thus, before implementation, the Smart Sensor Module is calibrated for the parameters under investigation. Topic discusses following points.

- Calibration of Smart Sensor Module for respective parameters. Standardization of the SSM with standard instrument.
- Implementation of the SSM to monitor the parameters.

5.2 The Complete Smart Sensor Module:

Present work realizes the designing of Smart Sensor Module for monitoring of parameters such as relative humidity, temperature and gases such as CO_2, H_2S and NH_3. Emphasizing an architecture given by the IEEE 1451 standards, the Smart Sensor Module is designed, wherein embedded technology is realized to enhance the smartness of the module. Both hardware and firmware are equally important for featured Smart sensor module. As discussed in the topic 3, the hardware

TABLE 5.1: Set of the sensors and sensor Elements

Sr. No.	Name of the Sensor	Materials for Sensing Elements	
		SET -I	SET-II
1	Relative Humidity	$Ni_{0.40}Zn_{0.60}Fe_2O_4$	$Ni_{0.80}Zn_{0.20}Fe_2O_4$
2	Environmental Temperature	$Mg_{0.40}Zn_{0.60}Fe_2O_4$	$Mg_{0.60}Zn_{0.40}Fe_2O_4$
3	Carbon dioxide gas	$Ni_{0.40}Zn_{0.60}Fe_2O_4$	$Ni_{0.60}Zn_{0.40}Fe_2O_4$
4	H_2S gas	$Mn_{0.20}Zn_{0.80}Fe_2O_4$	$Mn_{0.60}Zn_{0.40}Fe_2O_4$
5	NH_3 gas	$Mn_{0.40}Zn_{0.60}Fe_2O_4$	$Mn_{0.60}Zn_{0.40}Fe_2O_4$

and firmware is successfully designed. The issues of development of both hardware and software are discussed in topic 4. After designing, the calibration plays vital role in electronics instrumentation. Present work ensures the monitoring of various parameters

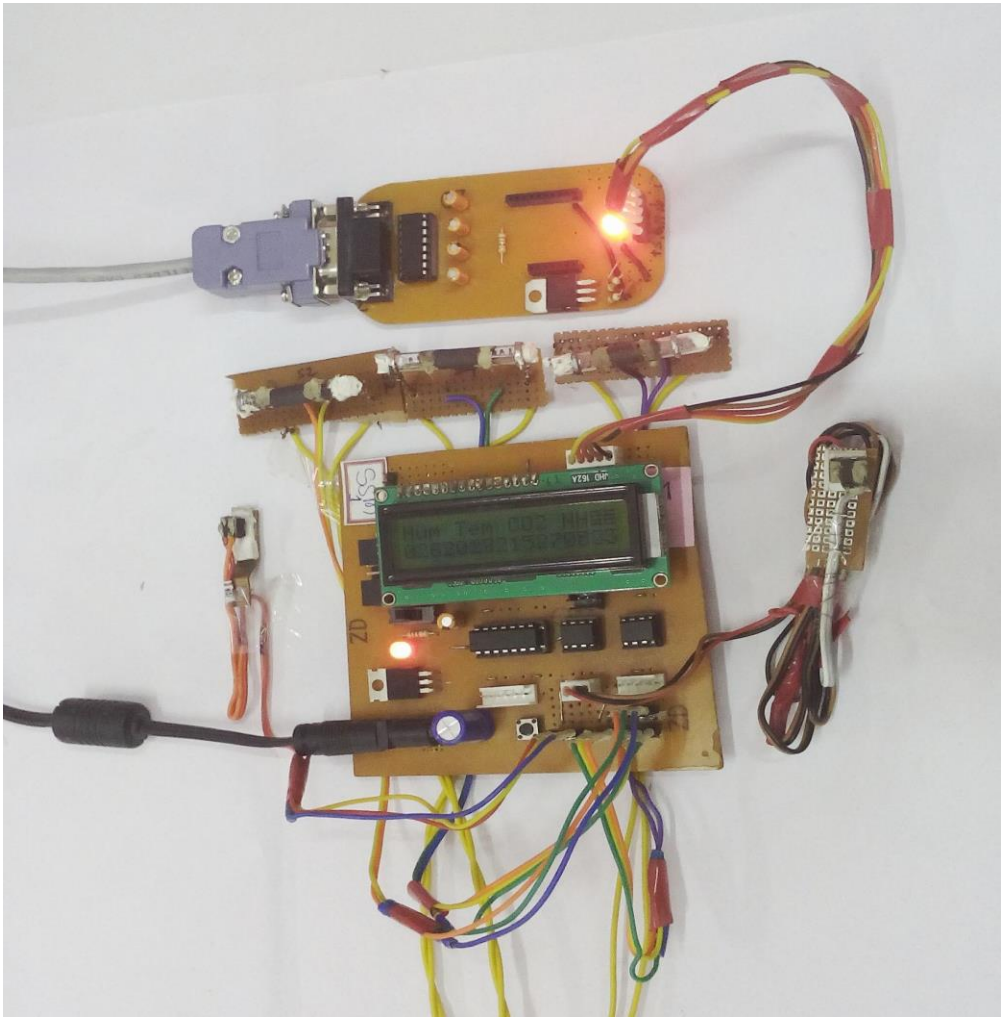

Figure 5.1 (a): Photographs of prototypes of the Smart sensor module designed by using Set –I of the sensors

of the environment. Therefore, the module is systematically calibrated typically for five parameters. Thus, after calibration the designing process is completed and module is ready for establishment in the modern measurement instruments.

As discussed earlier, implementing selection criteria on typical parameters, two sensing elements are selected for each parameter. Therefore, two sets of the sensors are developed. The sets of parameters and respective sensing elements are given in the table 5.1. For each set the Smart Sensor Module is designed. Thus, two SSM are developed and presented in Figure 5.1 (a & b).

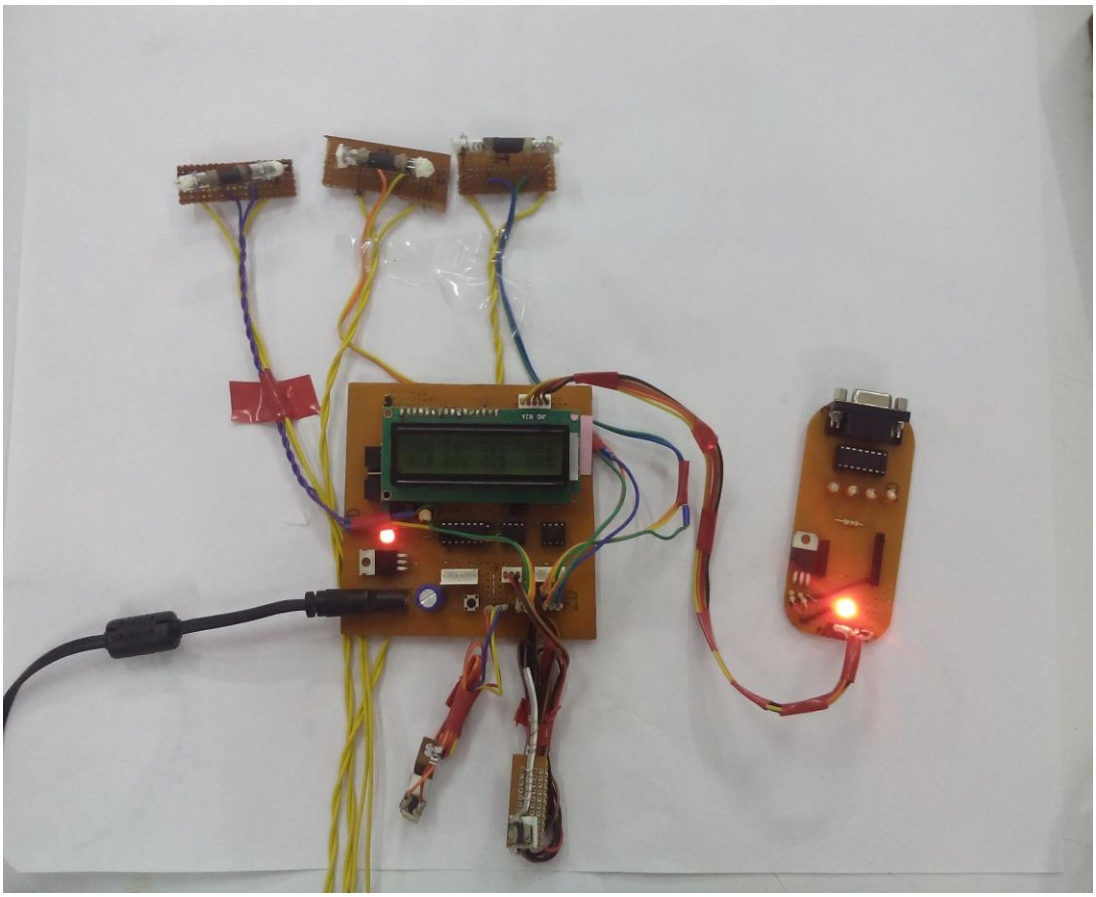

Figure 5.1 (b): Photographs of prototypes of the Smart sensor module designed by using Set –II of the sensors

5.3 Calibration of Smart Sensor Module:

Today`s measurement systems have been designed to accommodate large number of sensors. They have a variety of features and capabilities that have been developed over the years to satisfy the needs of the test and measurement community. Emphasizing the enhancement of the salient features of the Smart Sensor Module, it is calibrated to the scientific units. The present Smart Sensor Module is designed to monitor the parameters such as relative humidity, temperature, CO_2 gas, H_2S gas and NH_3 gas etc. Therefore, process of calibration is adopted for above parameters and details regarding the same are interpreted through following points.

a. Calibration of Smart Sensor Module to Relative Humidity in %RH.
b. Calibration of Smart Sensor Module to temperature in ^0C.
c. Calibration of Smart Sensor Module to Carbon dioxide (CO_2) gas in %.
d. Calibration of Smart Sensor Module to Hydrogen Sulfide (H_2S) gas (%).
e. Calibration of Smart Sensor Module to ammonia (NH_3) gas in %.

5.3.a Calibration of Smart Sensor Module to Relative Humidity in %RH.

The main aim of the proposed work is to design microcontroller based Smart Sensor Module (SSM) for measurement of relative humidity in %RH. As discussed earlier, the humidity sensor is developed by depositing thick film of polycrystalline ferrites as sensing element on highly standard ceramic substrate. Humidity dependent electrical properties of all compositions under study are investigated. On inspection of humidity dependent electric properties of the compositions, as given in topic 3, it is found that all compositions are showing humidity sensitive properties. However, out of these compositions, two sensing elements are selected for present SSM. While selecting the sensing elements the criteria such as ambient resistance of thick film, humidity dependent characteristics, ranges, timing responses etc are emphasized. Humidity sensor are developed about thick films of $Ni_{0.40}Zn_{0.60}Fe_2O_4$ and $Ni_{0.80}Zn_{0.20}Fe_2O_4$ ferrites, wherein use of ceramic substrate is ensured. Thus, the sensors are designed and deployed for present SSM design. The present humidity sensor is passive. As discussed in previous topic, on energize with +5V supply, the sensor produces analog output in proportion with humidity level. Thus, humidity dependant voltage V_H is observed at output of signal conditioning stage. By proper signal conditioning circuitry, the humidity dependent signal (V_{RH}) is produced. However, the demand is to design Smart Humidity Sensor Module, which could provide accurate data with great preciseness and the reliability in %RH. This analog signal is interfaced to the ADC of AVR microcontroller. The signal available is in form of mV. However, the output must be of humidity in %RH. Therefore, the SSM is calibrated in actual units.

Figure 5.2: Experimental set up to determine the range of variation of observed emf (V_{RH}) for humidity varying from normal room condition to the condensation of the water molecules.

For calibration, the humidity sensor under investigation is exposed to the variable relative humidity in %RH. The In the beginning, to get scope of variations,

the humidity dependent voltage is measured for entire range of air condition from normal environmental level, that is room temperature and normal humidity level, to the condensation of water. The condensation of water molecules reveals 100% saturation of air with water molecules. The DC voltage observed as output of the signal conditioner is measured by using digital multimeter model DM-97. Therefore, these data of analog voltage against applied humidity is used determine the range of output voltage in mV. At normal condition of temperature and humidity, the output voltage observed, after signal conditioning, is 1532 mV, whereas that of at saturation is 2507mV. However, the reference voltage used for digitization of the signal is 2.56 volt [26]. Therefore, the output of signal conditioning is not saturating even at condition of condensation of water molecules. Figure 5.2 depicts the photograph of the experimental arrangement to determine the limits of variation of observed emf (V_{RH}) for humidity varying from normal room condition to the condensation of the water molecules.

Further, the system is subjected for process of uniform calibration. For precise calibration, the humidity of different values are applied to the prepared sensor. For production of required environment, wherein humidity concentration is precisely controlled, a highly sophisticated humidity chamber, model Gayatri Scientific Ltd. Mumbai, is employed. This chamber is available in our laboratory. The humidity (H) from 25 RH% to 95 RH% with accuracy of 1 RH% is applied. Along with humidity, the chamber is facilitated with temperature controlling also. The temperature as well as humidity of the chamber is controlled by using PID techniques. The experimental arrangement for precise calibration is shown in figure 5.3. Keeping temperature constant, the humidity applied to sensor is varied between 30 RH% to 95 RH%. The observed voltage (V_{RH}) is plotted against applied humidity in %RH and shown in figure 5.4.

Figure 5.3: Experimental set up for calibration of SSM to relative humidity in %RH.

On inspection of figure 5.4, the calibration curve, it is found that, the observed emf follows the resistance variation with applied humidity within the range of investigation. From figure 5.4, it is found that, the curve of observed emf against applied relative humidity depicts two regions. First region of relative humidity is from 30 %RH to 60 %RH and second is from 60%RH to 95 %RH. Within these regions the trend of observed emf is almost linear with applied humidity. Therefore, the present SSM is calibrated for two regions. Such two region or piecewise calibration process is employed by researcher to calibrate the Smart Sensor module for typical parameters [17,18] Using

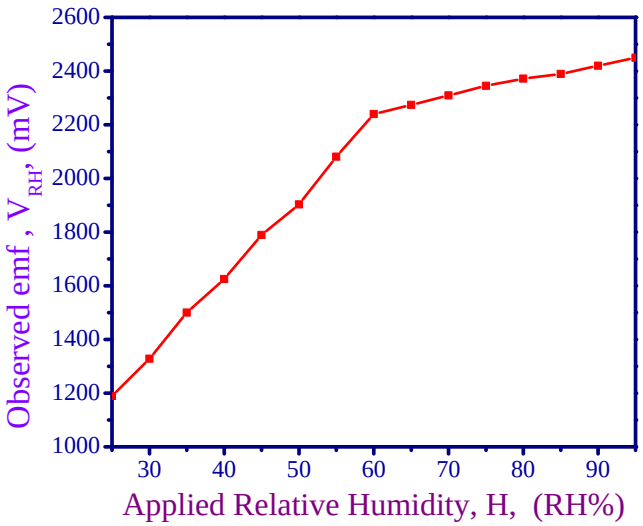

Figure 5.4: The graph of observed humidity dependent potential (V_{RH}) against applied relative humidity H in %RH

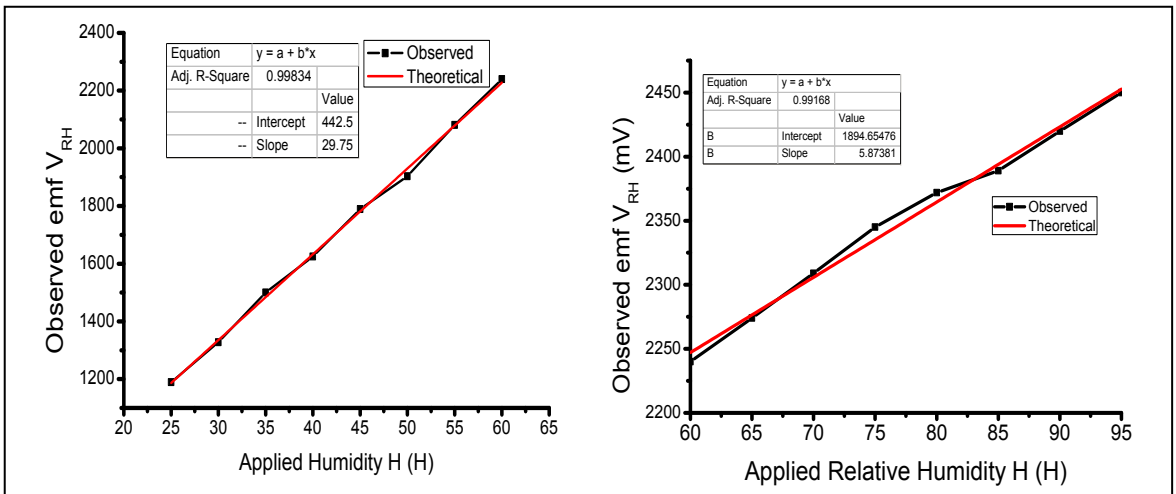

Figure 5.5: Realization Piecewise fitting process

least square fitting process, both regions are fitted to straight line [Figure 5.5]. The regression process results into two expressions. For the range of relative humidity from 30 %RH to 60 %RH the empirical relation obtained is

$$\text{Observed emf } (V_{RH}) = 29.75 \times H + 442.5 \quad (1)$$

Whereas for the region from 60 %RH to 95 %RH, the empirical relation obtained is given by

$$\text{Observed emf } (V_{RH}) = 5.873 \times H + 1894.65 \quad (2)$$

Where V_{RH} is the humidity dependent emf and H is applied humidity in %RH. Thus, from observed emf, obtained from signal conditioner, the humidity can be calculated by using expressions

$$\text{Relative Humidity 'H' (\% RH)} = \frac{VRH - 442.5}{29.75} \quad (3)$$

$$\text{Relative Humidity 'H' (\% RH)} = \frac{VRH - 1894.65}{5.873} \quad (4)$$

Expression 3 and 4 are employed in the firmware in respective function and executed continuously to provide output humidity in % RH. Thus, present SSM is calibrated to the relative humidity in %RH. As discussed earlier, the software depicts the compensation of offset voltage, this avoids additional hardware components otherewise required for offset compensation.

As discussed in topic 4, present SSM has provision of analog outputs also. A sepatrate port is provided for the analog outputs. The pin entitled as 'VH' is used to take analog voltage output if needed for further instrumentation. The analog voltage , V_{RH}, obtained from the Smart Sensor Module under investigation show close agreement with that of obtained from datasheet of standard humidity sensor module, SY-HS-220 for variable applied relative humidity [19]. This supports the process of standardization. Thus, present smart sensor module provides values of relative humidity in %RH directly on the display unit and respective analog voltage is also provided. This helps to satisfy the needs of SSM.

Standardization of the instrument is an inherent step of electronic instrumentaion. Therefore, to ensure standardiation, the Smart Sensor Module under investigation is exposed to the environment of variable relative humidity along with stanard relative humidity meter. The relative humidity shown by the system under invetsigation and that of obtained from standard humidity meters are

TABLE 5.2: Humidity data shown by system under investigation and that obtained from standard humidity meter

Humidity shown by the standard humidity chamber RH%	Humidity shown by the System under investigation in RH%
25	26
30	31
35	36
40	40
45	46
50	51
55	56
60	60
65	66
70	71
75	74
80	81
85	86
90	90
95	95

recorded and presented in table 5.2. On inspection of table 5.2, it can be said that, the values shown by present SSM and that of obtained from standard meters shows close match. From this it can be concluded that, the Smart Sensor Module is sucessfully designed and ready to implement in the smart instrumentation. The output data about relative humidity exhibit linearity, which is one of the features of Smart Sensor Module.

5.3.b Calibration of Smart Sensor Module to temperature in ^{0}C:

It is known that, temperature is one of the most significant environmental parameter. Therefore, it is essential to monitoring and control. Particularly, in the field of chemical industries, paper industries, precision agriculture, storage plants, home appliances, smart cars etc the monitoring of the temperature plays vital role. In fact, to realize the HVAC system the temperature should be essential controlled [20]. Therefore, it is need of hours to design cost effective a smart sensor module for this dedicated application. As discussed earlier, on investigation of temperature sensitive electric properties, it is proved that, polycrystalline spinel ferrites exhibiting semiconducting nature, are suitable for development of temperature sensor [21-23]. A thick films developed about ceramic substrate are revealing interesting features [24]. With the view to design sensors for Smart Sensor Module for monitoring of environmental temperature, the electrical properties of the compositions of MgZn, NiZn and MnZn ferrites are studied. From results of this intensive study, it is found that, the compositions are showing negative temperature coefficient of resistance and are suitable for designing the sensing element for temperature sensor. It is known that, this thermistor like nature support to design temperature sensor. As discussed in topic 3, all compositions are temperature sensitive. The sensors in bulk form, pellets, show good characteristics. However, the thick film sensors are exhibiting commendable features. Considering various parameters such as range of temperature, temperature coefficient, ambient resistance etc, the compositions of $Mg_{0.40}Zn_{0.60}Fe_2O_4$ and $Mg_{0.60}Zn_{0.40}Fe_2O_4$ ferrites are selected and sensing elements of the same are developed on ceramic substrates. It is known that, the present electronic system is designed for measurement for temperature in degree centigrade (^{0}C) unit. Therefore, it should be calibrated. Therefore, before further implementation the present sensor module is subjected to the process of calibration.

As discussed in topic 3, the exponential dependence of electrical conductivity of ferrites with temperature can be attributed to the semiconducting nature [25]. This property is utilized in this design. The sensor is excited by +5V supply. To achieve good stability in the output, it is recommended to employ highly stable and noise free power supply. The sensor is used in resistive divider combination. It provides DC voltage depending upon temperature of the surrounding in ^{0}C. The Temperature dependant voltage V_T is taken across resistor of 22MΩ and connected to the signal conditioning stage. The voltage observed is in millivolt range and it is as expected. The system generates an emf proportional to the variation in the temperature values.

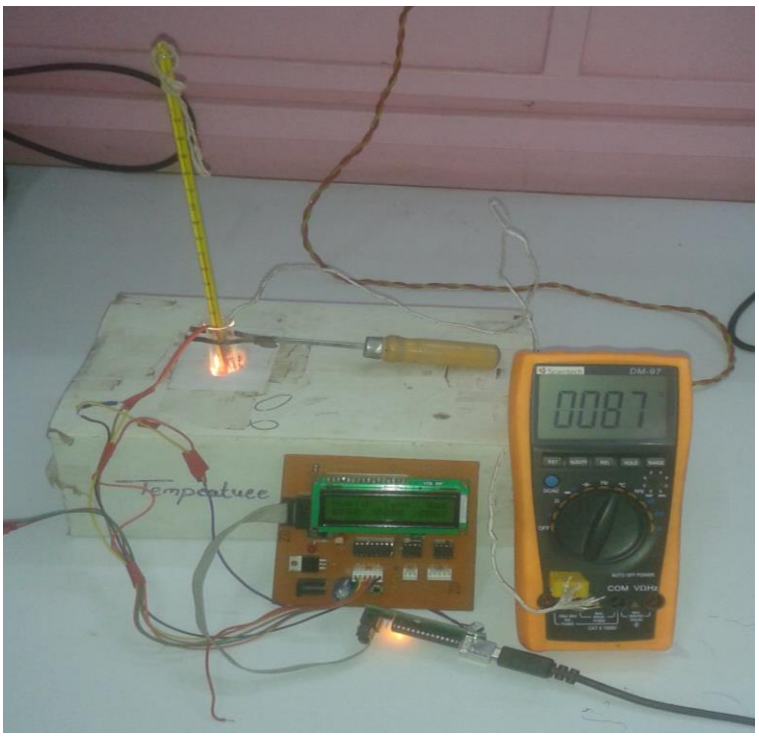

Figure 5.6: Experimental arrangement for calibration of the SSM for temperature in ^{o}C.

In the beginning, for calibration of the Smart Sensor Module to real unit, the degree celcius, the temperature dependent emf (V_T) is measured and plotted against

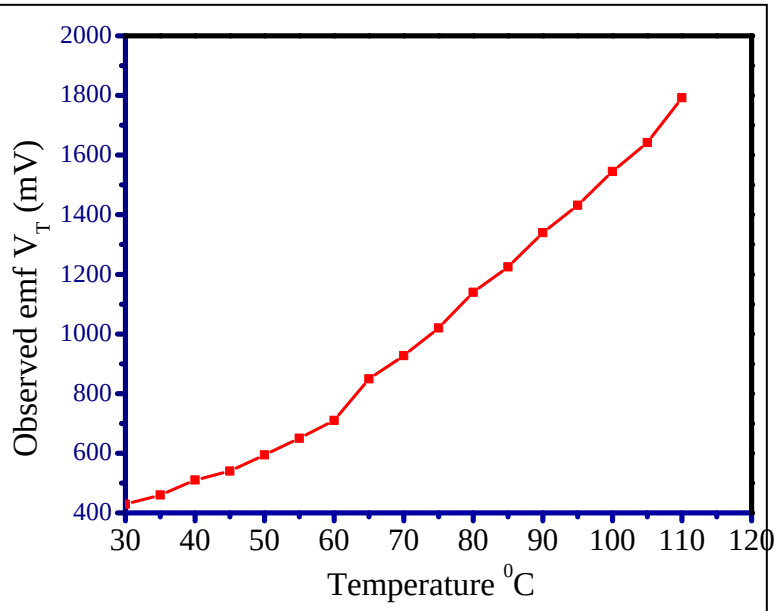

Figure 5.7: The Graph of Observed emf (V_T) in mV against applied Temperature in ^{o}C

temperature from 30°C to 100°C. An experimental set up used is shown in figure 5.6. Present SSM is designed for monitoring environmental parameters. Therefore, the range of calibration is from 25 ^{0}C to 100 ^{0}C. The temerature dependent emf is recorded at output of signal conditioing stage. As expected, the graph of V_T against t shown in figure 5.7 depicts deviation from linearity for range of investigation. To realize scientific calibration, it is essential to deploy process of regression to obtain standard empirical relation. On inspection of figure 5.7, it is found that, calibration can be ensured with the use of piecewise approximation[25, 26]. The graph of V_T against t can be divided into two regions. The regions are decided from slope of the graph. The first

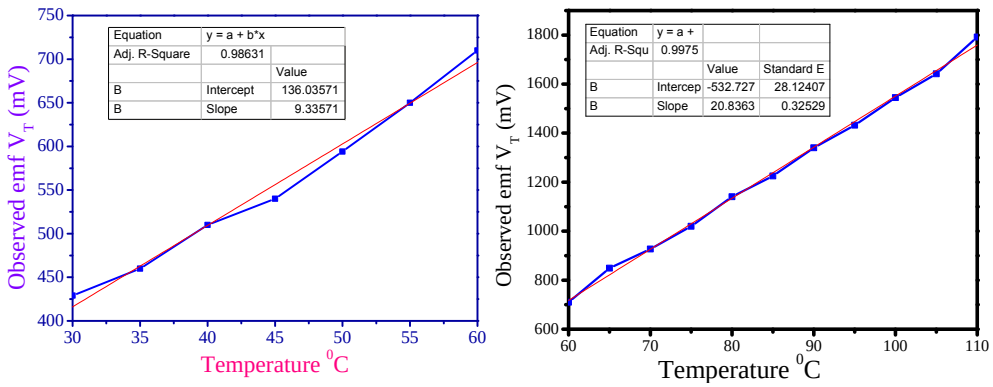

Figure 5.8: The Graph of Observed emf (V_T) in mV against applied Temperature in ^{o}C

region is from 30 ^{0}C to 60 ^{0}C and second regions is from temperature is from 60 to 100 ^{0}C. The graph is fitted by process of regression for both regions. The realization piecewise fitting to straight line is depicted in figure 5.8. The process of data fitting results into the relations

$$\text{Temperature (t) } ^O\text{C} = ((V_T - 136.0)/9.335) \quad (5)$$

$$\text{Temperature (t) } ^O\text{C} = ((V_T + 532.7)/20.83) \quad (6)$$

Where, V_T is temperature dependent emf.

These equations, eq. 5 and eq. 6, are employed in the firmware for calibration of the system. As discussed in previous topic, the function is continuously called into main programme. This system gives temperature reading continuously on the display unit. Thus, system is providing output temperature in the ^{0}C scale. The smart sensor module

under investigation is facilitated with the analog port also. Therefore, analog voltage V_T is made available for the designer for further instrumentation.

For validation of the calibration, the Smart Sensor Module is subjected to the process of standardization. To ensure standardization, the SSM is implemented to measure the temperature in degree centigrade. The temperature data shown by SSM under investigation and that of obtained from standard thermometer and Scientech digital temperature meter model DM-97 are presented in Table 5.3. From table 5.3, it is found that the temperature data obtained from the present SSM and that of shown by standard instruments are closely matched. Thus, SSM is calibrated to the temperature in ^{0}C. Now, the SSM is ready for further implementation to the monitoring of the parameters.

TABLE 5.3: Temperature data shown by system under investigation and that obtained from standard thermometer and digital meter.

Temperature shown by the standard thermometer in ^{0}C	Temperature shown by the standard digital meter DM-97 ^{0}C	Temperature shown by the System under investigation in ^{0}C
30	29	31
35	34	36
40	40	41
45	46	46
50	50	51
55	55	56
60	60	61
65	65	66
70	70	70
75	75	75
80	81	80
85	86	85
90	90	90
95	95	95
100	100	100
105	105	106
110	110	110

5.3.c Calibration of Smart Sensor Module to Carbon dioxide gas in % unit:

The Smart Sensor Module is designed for monitoring of carbon dioxide gas. Such type of module finds tremendous application in the high tech agriculture, wherein polyhouse system is ensured. Environmental carbon dioxide gas monitoring system helps to provide controlled environment to the crop [27]. To develop SSM for CO_2 monitoring, the sensors are developed in the laboratory by employing the thick films of the polycrystalline ferrites materials as a sensing element. As discussed earlier, the CO_2 sensor is developed on cylindrical glass tube. The physical dimensions are of these sensor are reported in topic 3. It is found that, the ferrite materials exhibit chemisorption properties at specific temperature, which ensure its application for gas sensing [29, 30]. As discussed in topic 3, majority of the compositions under investigations are sensitive to the carbon dioxide gas. However, implementing the selection criteria, such as

operating temperature, sensitivity, and ambient resistance etc, two compositions are selected as the sensing element. The selected compositions are $Ni_{0.40}Zn_{0.60}Fe_2O_4$ and $Ni_{0.60}Zn_{0.40}Fe_2O_4$. Thus, two CO_2 sensors are designed and deployed for development of present SSM. It is known that, these sensors are resistive sensors and resistance sensor increases with increase in the concentration of the carbon dioxide gas. As discussed in the topic 4, the signal conditioning circuit provides proportional analog voltage in mV. This analog voltage (V_{G1}) is read into the AVR microcontroller for digitization and further processing. In fact, as per IEEE 1451 standard, the output must be is digital domain and should in the form of scientific units. To achieve the output in scientific units, it has to be calibrated by employing standard means. For calibration, process of regression and fitting to the get empirical relation, is always recommended.

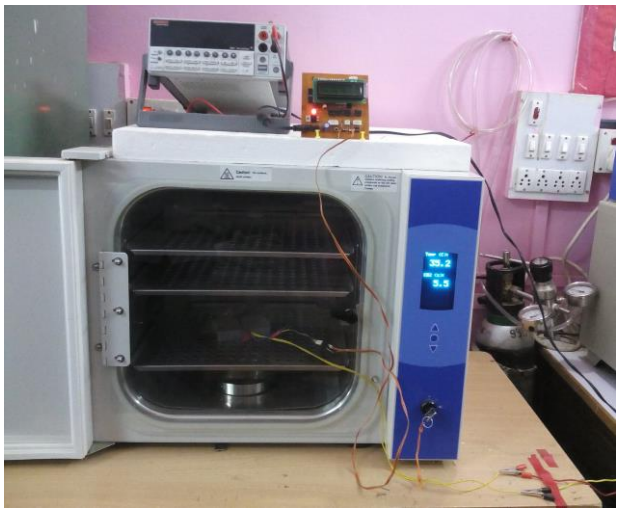

Figure 5.9: Experimental arrangement for calibration of the SSM for CO_2 in %.

For calibration of the Smart Sensor Module, the sensor under investigation is exposed to the carbon dioxide gas of variable concentration in % unit. The carbon dioxide gas, in controlled manner, is applied by employing sophisticated Carbon Dioxide gas Chamber from, Thermo Scientific, USA. An experimental set up used is shown in figure 5.9. The temperature of the sensing element is controlled to the operating temperature of 175 ^{0}C.

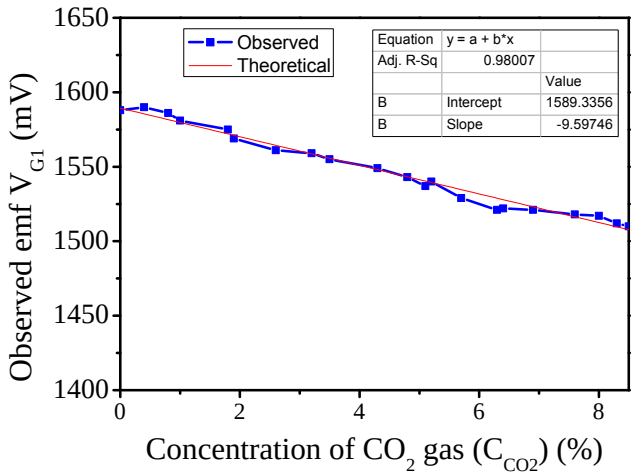

Figure 5.10: Graph of observed emf (V_{G1}) in mV against Concentration of carbon dioxide gas (C_{CO2}) in % unit.

The resulting emf (V_{G1}) in mV is recorded. The observed voltages V_{G1} (mV) are plotted against concentration of CO_2 gas in % unit and depicted in figure 5.10. On inspection of figure 5.10, it is found that, the observed emf decreases with increase in the CO_2 concentration. This can be attributed to the increase in the resistance of the sensing element with increase in the carbon dioxide gas [31]. The observed data is analyzed with regression process and fitted with the straight line. The empirical relation observed from fitting process is

$$V_{G1}\ (mV) = -\ 9.597 \times C_{CO2} + 1589.33 \qquad (7)$$

Where, V_{G1} is the carbon dioxide gas dependent emf and C_{CO2} is the concentration of carbon dioxide gas. This equation is reduced to

$$\text{Concentration of } CO_2 \text{ gas (\%)} = (1589.33 - V_{G1})/\ 9.597 \qquad (8)$$

This equation 8 is employed in the firmware for calibration of the system. As discussed in previous topic, the function is continuously called into main programme. This system gives observations regarding concentration of carbon dioxide gas continuously on the display unit. The smart sensor module under investigation is facilitated with the analog port also. Therefore, analog voltage V_{G1} is made available for the designer for further instrumentation. After calibration the SSM is subjected to the measurement of CO_2 gas. The data obtained from the system under investigation and that of given by standard instrument show match with acceptable deviations.

Thus, the Smart Sensor Module is ready for further deployment.

5.3.d Calibration of Smart Sensor Module to H_2S gas in % unit:

The smart Sensor module is also designed to monitor hydrogen sulfide gas. As discussed in topic 3, all compositions of the ferrites under investigation depict H_2S sensitivity for this reducing gas. However, implementing the selection criteria, such as operating temperature, sensitivity, and ambient resistance etc, two compositions are selected as the sensing element. The selected compositions are $Mn_{0.20}Zn_{0.80}Fe_2O_4$ and $Mn_{0.60}Zn_{0.40}Fe_2O_4$. Thus, two H_2S gas sensors are designed and deployed for development of present SSM. It is known that, these sensors are resistive sensors and resistance sensor decreases increase in the concentration of the H_2S gas. As discussed in the topic 4, the signal conditioning circuit provides proportional analog voltage in mV. This analog voltage (V_{G2}) is read into the AVR microcontroller for digitization and

further processing. To achieve the output in scientific units, it has to be calibrated by employing standard means. An experimental set up used is shown in figure 5.11. For calibration of the Smart Sensor Module to the concentration of H_2S gas in % unit, two point calibration process is ensured. The voltage given by the system is recorded for maximum concentration of H_2S. It is recorded as V_{Max} in mV. For present SSM the observed value of V_{Max} is 1025 mV. The temperature of the sensing element is controlled at operating temperature of 175 ^{0}C. The emf shown by the system for ambient condition is the offset voltage V_{offset} (in mV). In fact, this offset should be compensated. The compensation of the offset voltage can be done making suitable arrangement in the hardware. However, making provision for compensation of the offset voltage, in the hardware, changes from sensor to sensor. Therefore, the software compensation is always recommended. The offset voltage observed for this channel is 800 mV. After compensating the resulting emf would be Vo = (V_{G2} - V_{offset}). Thus, the concentration of hydrogen sulfide gas is calculated from expression

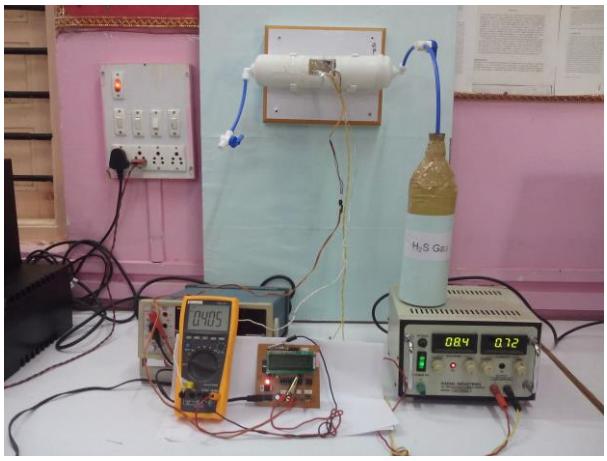

Figure 5.11: Experimental arrangement for calibration of the SSM for H_2S in %.

$$\text{Concentration of } H_2S \text{ gas (\%)} = \frac{Vo}{VMax} \text{ x } 100 \text{ \%} \qquad (9)$$

This equation 9 is employed in the firmware for calibration of the system. As discussed in previous topic, the function is continuously called into main programme. This system gives observations regarding concentration of hydrogen sulfide gas continuously on the display unit. The smart sensor module under investigation is facilitated with the analog port also. Therefore, analog voltage V_{G2} is made available for the designer for further instrumentation. After calibration the SSM is subjected to the measurement of H_2S gas. Thus, the Smart Sensor Module is ready for further deployment.

5.3.e Calibration of Smart Sensor Module to NH_3 gas in % unit:

As per the objectives, deploying sensing element of polycrystalline ferrite materials, Smart Sensor module, is designed to monitor concentration of ammonia gas. The system is designed to keep pace with the present industrial needs. The compositions of the ferrites under investigation depict ammonia gas sensitive electrical properties [32]. It is known that, ammonia gas is reducing gas and due to process of adsorption at elevated temperature causes reduction in the resistance. The reduction in the resistance of the sensing element is proportional to the concentration of ammonia gas. As discussed in topic 3, all compositions under investigation show significant sensitivity to the ammonia gas. However, implementing the selection criteria, such as operating temperature, sensitivity, and ambient resistance etc, two compositions are selected as the sensing element. The selected compositions are $Mn_{0.40}Zn_{0.60}Fe_2O_4$ and $Mn_{0.60}Zn_{0.40}Fe_2O_4$. Thus, two NH_3 gas sensors are designed and deployed for development of present SSM. It is known that, these sensors are resistive sensors and resistance sensor decreases increase in the concentration of the ammonia gas. As discussed in the topic 4, the signal conditioning circuit provides proportional analog voltage in mV. This analog voltage (V_{G3}) is read into the AVR microcontroller for digitization and further processing. An experimental set up used is shown in figure 5.12. For calibration of the Smart Sensor Module to the concentration of ammonia gas in % unit, two point calibration process is ensured. The voltage given by the system is recorded for maximum concentration of NH_3 gas. It is recorded as V_{Max} in mV. For present SSM the observed value of V_{Max} is 324 mV. The temperature of the sensing element is controlled at operating temperature of 175 ^{0}C. The emf shown by the system for ambient condition is the offset voltage V_{offset} (in mV). In fact, this offset should be compensated. The offset voltage observed for this channel is 299 mV. After

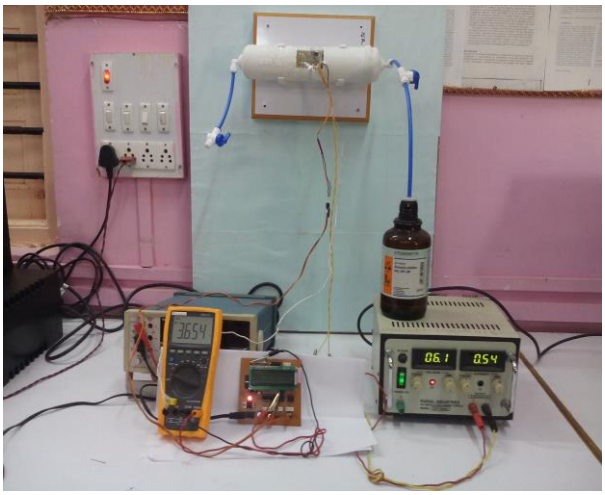

Figure 5.12: Experimental arrangement for calibration of the SSM for NH_3 in %.

compensating the resulting emf would be Vo = (V_{G3} - V_{offset}). Thus, the concentration of hydrogen sulfide gas is calculated from expression

$$\text{Concentration of } NH_3 \text{ gas (\%)} = \frac{Vo}{VMax} \text{ x } 100 \text{ \%} \qquad (10)$$

This equation 10 is employed in the firmware for calibration of the system. As discussed in previous topic, the function is continuously called into main programme. This system gives observations regarding concentration of ammonia gas continuously on the display unit. The smart sensor module under investigation is facilitated with the analog port as well. Therefore, analog voltage V_{G3} is made available for the designer for further instrumentation. After calibration the SSM is subjected to the measurement of ammonia gas. Thus, the Smart Sensor Module is ready for further deployment.

Thus, the smart module is designed for monitoring of physical parameters such as temperature, relative humidity, and concentration of CO_2, H_2S and NH_3 gas. It is calibrated to the respective scientific units. On implementation, it is found that, the module is depicting the values of the parameters very precisely.

According to IEEE 1451 standards the Smart Sensor Module should be intelligent and featured with various output data buses. Output data ports provided on this SSM are LCD Display, Serial and RS232 which realizes the plug and play philosophy.

To facilitate the smart sensor module, with digital outputs, a smart display unit is incorporated. As depicted in appendix-B, the firmware is designed to synchronize the LCD operation. The data is converted into ASCII format and send to the LCD port. Five parameters are displayed the LCD on second row. The LCD continuously refreshed to ensure data updating.

In addition to display unit the serial port comprising RxD and TxD lines, is provided. The data regarding five parameters and given to serial port by executing separate function called USART_Tx (void). These lines are also connected to RS232 port. The deployment of Max 232 facilitate, RS232 interfacing. Therefore, the Smart Sensor Network can be interfaced to the computer. Moreover, by the use of serial to USB connector, the Smart Sensor Module may be extended to ensure USB interfacing. As given in appendix B, the function USART_Tx (void) serially transmits the parameters values. The parameter values are associated with the codes. The codes GA,

GB, GC, GD and GE respectively assigned to the parameters Humidity, Temperature, CO_2 gas, Ammonia gas and H_2S gas.

Thus, present Smart Sensor Modules provides different digital data buses.

5.4 Conclusion

Ensuring an embedded technology a Smart Sensor Module is developed to monitor the physical parameters such as humidity, temperature and concentration of gases such as carbon dioxide, hydrogen sulfide and ammonia. Two sets of sensors, developed using polycrystalline ferrite based sensing elements, are deployed. Present sensor module is calibrated to the respective scientific unit by using standard process of regression. The empirical relations obtained are used in the firmware. This enhances the intelligence of the module. The module is also implemented to the monitor respective parameters. Results shown by the module under investigation show close agreement with that of obtained from sophisticated instrument. It can be concluded that, Smart Sensor Module, designed to monitor the physical parameters, is highly reliable and precise.

References

1. M. Bhuyan, “Intelligent Instrumentation: Principle and Applications”, CRC Press (2011) 87-110.
2. IEEE Instrumentation And Measurement Society, IEEE Standard for a Smart Transducer Interface for Sensors and Actuators — Common Functions, Communication Protocols, and Transducer Electronic Data Sheet (TEDS) Formats. Institute of Electrical and Electronics Engineers, Inc. New York (2007), (ISBN 0-7381-5598-5).
3. P.Ganesan, R.Venugopalan, P. Peddabachagari, A. Dean, F.Mueller and M. Sichitiu, “Analyzing And Modeling Encryption Overhead For Sensor Network Nodes”, Proceedings of the 2nd ACM International Conference On Wireless Sensor Networks And Applications, 151–159.
4. K. Aruna, A. S. Ramsagar and G.Venkateswarlu, “Mobile Operated Landrover Using DTMF Decoder”, International Journal of Modern Engineering Research, 3 2 (2013) 898-902.
5. IEEE 1451.2-1977 IEEE Standard for A Smart Transducer Interface For Sensors and Actuators Transducer to Microprocessor Communication Protocols and Transducer Electronic Data Sheet (TEDS) Formats.
6. Y. Song, C. Gang, Y. Fang, J. Ma and X. Zhang, “Design Of Greenhouse Control System Based On Wireless Sensor Network And AVR Microcontroller”, Journal Of Network 6, 12 (2011) 1668-1674.
7. V.Ramya, B. Palaniappan and A. Kumari, “Embedded Patient Monitoring System”, International Journal of Embedded Systems and Applications, 1 2 (2011) 51-63.
8. D. Wobscholl, “A wireless gas monitor with IEEE 1451 protocol”, in: Proceeding of Sensors Applications Symposium (SAS 2006) Houston, TX, USA,(2006) 162–164.
9. K. Konstantinos, X. Apostolos, K. Panagiotis and S. George, “Topology Optimization in Wireless Sensor Networks for Precision Agriculture Applications,” Sensor Communication, (2007) 526-530.
10. A. Baggio, “Wireless Sensor Networks in Precision Agriculture,” Delft University of Technology, Delft, (2009).

11. W. Zhang, G. Kantor and S. Singh, “Integrated Wireless Sensor/Actuator Networks in Agricultural Applications,” In 2nd ACM International Conference on Embedded Networked Sensor Systems, (2004) 317.
12. www.sensoplex.com Smart Sensor Module SP-M310 .
13. L.V. Shum, P. Rajalakshmi, A.Afonja, G. McPhillips, R. Binions, L.Cheng and S. Hailes, “On the Development of a Sensor Module for real-time Pollution Monitoring” IEEE Sensors (2011) 1-9.
14. B. Croxford and L Fairbrother, “Low cost accurate monitoring of indoor carbon monoxide concentrations”, Indoor and Built Environment, 14 (2005) 235-240.
15. A. Steed , S. Spinello , B. Croxford , C. Greenhalgh, “E-Science in the Streets: Urban Pollution Monitoring”, In Proceedings of 2nd UK e-Science All HandsMeeting, (2003).
16. Kavi K. Khedo, Rajiv Perseedoss and Avinash Mungur, “A Wireless Sensor Network Air Pollution Monitoring System”, International Journal of Wireless & Mobile Networks 2 2 (2010) 31-45
17. J.Yuan, N. H. Farhat and J.Van-der Spiegel,“Background Calibration With Piecewise Linearized Error Model for CMOS Pipeline A/D Converter”, IEEE Transactions on circuits and systems-I 55 1(2008)311-321.
18. Chen and C. Chen, “Evaluation of Piecewise Polynomial Equations for Two Types of Thermocouples”, Sensors 13(2013)17084-17097.
19. J. M. LIN, “Teaching and Design on Smart MEMS Pressure Sensor Module”, International Conference on Engineering Education and Research:Progress Through Partnership, (2004)273-281.
20. A.M. Pawar, S. N. Patil, A. S. Powar and B. P. Ladgaonkar, “Wireless Sensor Network To Monitor Spatio-Temporal Thermal Comfort Of Polyhouse Environment”, International Journal of Innovative Research in Science, Engineering and Technology, 2 10 (2013) 4866-4875.
21. A.Y Lipare’ ,P.N Vasambekar, A.S Vaingankar, “Dielectric behavior and a.c. resistivity study of humidity sensing ferrites”, Materials Chemistry and Physics, 81 1 (2003)108–115.
22. J. Wang , F. Wu, K.Shi, X.Wang and P. Sun, “Humidity sensitivity of composite material of lanthanum ferrite/polymer quaternary acrylic resin”, Sensors and Actuators B: Chemical, 99, 2–3, (2004)586–591.

23. N. Rezlescu', C. Doroftei, E. Rezlescu and P.D. Popa, "Structure and humidity sensitive electrical properties of the Sn^{4+} and/or Mo^{6+} substituted Mg ferrite", Sensors and Actuators B: Chemical, 115 2 (2006)589–595.
24. U. Sarma and P. K. Boruah, "Design and development of a high precision thermocouple based smart industrial thermometer with on line linearisation and data logging feature", Measurement 43(2010)1589–1594.
25. A.A. Ayman, and A.S.A .Ei-Lail, "A novel circuit for thermocouple signals linearization using AD converter". IJITCS, 3(2013)56–60.
26. Datasheet of AVR Atmega 8L Microcontroller.

*****

Topic 6

Summary and Conclusion

During recent days, the state-of-art is to develop smart instrumentation to cater present day needs and future requirements of various sectors, such as industrial parameters measurement and controlling, biomedical, agriculture, domestic appliances, R & D instrumentation etc. Modern instrumentation exhibits the deployment of an ubiquitous and most pervasive technologies to enhance the reliability and preciseness in the results. To achieve these goals, instead of traditional sensor system, the use of intelligent sensor system is recommended. The traditional sensor systems are based on early days` technologies. Therefore, the designers have to put rather more efforts in development of instrumentation. Moreover, the designer should have the knowledge of physical properties of the sensors. Therefore, the resulting product has less portability. To overcome these limitations and provide suitable solution for electronic instrumentation, a novel field called 'Smart Sensor Module' is emerging [1]. The word smart is related with the intelligence of the system. According to the definition, the sensor system, which consists of a computing unit, along with sensors and signal conditioning part and intelligence to ensure the configurability is called Smart Sensor Module [2]. Architecture of such smart sensor module is given by IEEE 1451 standards [3]. According to IEEE 1451 standards, Smart Sensor Module also consists of the resources to ensure networking capabilities [4]. Now days, an embedded technology is becoming more pervasive and has capabilities to provide the solution to the problems of modern instrumentation. Embedded system comprises computing device, such as advanced microcontroller, to realize the incorporation of the intelligence into system [5]. Moreover, recently the configurable devices such as FPGA, PSoC, CSoC etc can be used as computing unit [6]. By deploying configurability of mixed signal based PSoC devices, the smartness of the sensor system can be significantly increased. Moreover, networking capabilities such as wired or wireless networking can be added. Thus, deploying embedded technology, the Smart Sensor Module (SSM) of desired specifications can be developed. Industrial measurement and control instrumentation design paradigm is shifted to the use of the smart systems with the features such as integrability, miniaturization, low power consumption, reliability, preciseness,

configurability, great intelligence, additive capability of signal processing etc [7]. Therefore, to keep pace with the modern technologies, a Smart Sensor Module is developed for monitoring of typical parameters such as relative humidity, environmental temperature and concentration of various gases. Instead of deployment of the sensors, readily available in the market, it also proposed to develop the sensor in the laboratory and deploy the same to design Smart Sensor Module. Emphasizing the fact that, the polycrystalline nanoferrites reveals environmental parameters sensitive electrical properties, it is also proposed to synthesize the sensor material. It is proposed to undertake the research work entitled "Synthesis and Implementation of Electronic Materials for Smart Sensor Module". Present research work realizes the confluence of two technologies; an electronic technology, wherein ubiquitous embedded philosophy is used to ensure the development of smart sensor module and second synthesis of electronic materials suitable for development of sensors of promising features required to develop the sensor module of great portability. The major objectives of the research work are to synthesize polycrystalline ferrite materials suitable for development of sensors to measure typical parameters and to develop Smart Sensor Module for the same. The compositions of polycrystalline spinel ferrites are synthesized. Employing these materials the sensor and sensor module of promising features is developed. The results of implementation are interpreted through this report.

Present research is the realization of embedded technology. Therefore, the salient features of embedded technology are elaborated. Polycrystalline ferrites materials are used as sensing materials. Therefore, structural details of these materials are studied. The spinel ferrite materials are exhibiting remarkable electrical and magnetic properties revealing the 'magnetic semiconductor' nature [8]. The spinel ferrites having formula MFe_2O_4 depict two significant crystallographic sites such as tetrahedral (A) site and octahedral (B) site and it shows Fd3m (No. 227) [9] space group symmetry. Properties of theses materials are mostly sensitive to cation distribution among A and B sites. These materials, due to interesting electrical properties, found suitable for sensing element. Salient features of various sensors have been studied. Moreover, term Smart Sensor module is defined and suitable architecture was also proposed to the Smart Sensor Module. Advantages of the present research over the prior art include the ability to program the smart sensor module to interface with a variety of analog output sensors, signal processing and decision making capability,

improved sensor accuracy, increased dynamic range low cost and introduction of networking capabilities also.

As per the objectives, the compositions of polycrystalline, $Mg_xZn_{1-x}Fe_2O_4$, $Ni_xZn_{1-x}Fe_2O_4$ and $Mn_xZn_{1-x}Fe_2O_4$ (x = 0.2, 0.4, 0.6 and 0.8) spinel ferrites have been synthesized by using co-precipitation method, wherein hydroxides of the constituents are precipitated. On processing the precipitate, washing, drying, pre-sintering and sintering, the fine powder of above compositions are obtained. Based on thick film technology, the sensing element and hence the sensors are fabricated. Moreover, the sensor in pellet form is also fabricated. Different substrates have been attempted and their performances are comparatively studied.

Characterization of the compositions under investigation is inherent for materials investigations. To confirm the formation of the compositions the standard tools such as X-ray diffraction, FTIR absorption spectroscopy, Scanning Electron Microscopy etc are used. X-ray powder diffraction studies of the compositions under investigations reveals formation of single phase spinel ferrites. The diffractograms show well defined peaks of allowed reflections with 311 peak as predominant peak. On indexing, it is cleared that, the compositions are cubic FCC structure with Fd3m symmetry [10]. The lattice constant observed are compositional dependent and show close match with the earlier reports [11]. Using Scherrer relation the particle size is estimated. The average particle size is about 46 nm. This reveals the formation of nanocrystallite structure for the ferrites under investigation. The porosities are also within the allowed range. Further, the compositions are subjected to the characterization by FTIR absorption spectroscopy. Employing FT-IR Spectrometer, NICOLET 6700, USA, the compositions under investigations are investigated for FTIR within the range from 400 cm^{-1} to 4000 cm^{-1}. Absorption spectra for compositions depict significant absorption bands at various frequencies. The absorption bands observed at lower frequencies (ν_1, ν_2) are attributed to the cation-oxygen group complexes of tetrahedral and octahedral sites. The frequencies at which these absorption bands observed are compositional dependent and supports cation-oxygen bond distances observed for tetrahedral and octahedral sites. The values of frequencies of absorption bands show close agreement with earlier reports [12]. FTIR spectra for compositions under investigation show significant absorption bands at frequencies approximately equal to 1625 cm^{-1}, 2920cm^{-1} and 3435 cm^{-1}. These absorption band are attributed to the

vibration modes, symmetric stretching, asymmetric stretching and scissoring type stretching of the triatomic water molecule in vapour form [13, 14]. This support the conclusion that the, ferrites are hygroscopic in nature and can be used for development of humidity sensor. Microstructural details are investigated by exposing the compositions to the SEM studies. On inspection of micrographs, it is found that, compositions comprise well defined grains with uniform grain distribution. It is also depicted that, the agglomeration of the grains is rare. Average grain size varies from few nanometer to 2 micrometers. The micrographs also reveal that, the compositions are porous in nature with uniform inter granular pores. It is also found that the intra granular pores are absent. The size of pores is also adequate to favour the process of adsorption, which is required to ensure sensing mechanism.

These properties of ferrite materials, reveals their suitability for sensor based application. Emphasizing sensor based applications; the electrical properties of the compositions under investigation are investigated. The temperature Sensitive Electrical properties, Humidity Sensitive Electrical properties and Gas Sensitive Electrical properties of all compositions are investigated. To explore the temperature sensitivity, electrical properties of the compositions $Mg_xZn_{1-x}Fe_2O_4$, $Ni_xZn_{1-x}Fe_2O_4$ and $Mn_xZn_{1-x}Fe_2O_4$ (x= 0.20, 0.40, 0.60 and 0.80) of spinel ferrites are investigated within the temperature range from room temperature to 600 K using two probe method. The composition in pellet form is used. A silver paste is used to achieve Ohmic contacts. Highly precise digital meter, Tektronix Make model DMM4050, 6.5 Digit Resolution, Accuracy up to 0.0024%, 10 Ω to 1.2 GΩ Range, with 10 μΩ Resolution, is used for resistance measurement. The graph of logρ plotted against reciprocal temperature obeys Wilson relation. The decrease of resistivity with increase in the temperature depicts semiconducting behaviour of the composition. The conduction mechanism is attributed to the electron hopping mechanism, wherein conductivity due to thermally activated mobility of the charge carriers is ensured. The graphs also show the influence of magnetic ordering on electrical properties. The transition in the trend occurs at Curie temperature. From these graphs, the Curie temperatures are also estimated and interpreted in the topic 3. Increase in the Magnesium ion in MgZn ferrites, results into increase in the Curie temperature. This may attributed to cation distribution among tetrahedral and octahedral sites of the spinels. It can be concluded that, the Zinc ion

prefers to occupy A- sites, whereas magnesium preferentially distributes from A and B sites.

To ensure sensor based applications, a thick film of sensing element of the ferrites under investigation is deposited by adopting screen printing technology on various substrates. The sensor is developed on cylindrical glass tube of typical size. Temperature dependent electric properties of the compositions under investigation are investigated for temperature range from room temperature to 150 ^{0}C, the range of investigation. The results obtained are properly interpreted. The resistance of the compositions exponentially decreases with increase in the temperature. Moreover, the thick films of the sensing materials are deposited on ceramic substrate of ultra high resistivity. Temperature dependent electrical resistance of the sensing elements is measured. Relative deviation in the resistance and sensitivities are also measure with the temperature. The data recorded is used to decide the suitability of the material for sensor development.

The electrical resistance (R_H) of the compositions of the polycrystalline, $Mg_xZn_{1-x}Fe_2O_4$, $Ni_xZn_{1-x}Fe_2O_4$ and $Mn_xZn_{1-x}Fe_2O_4$ (x= 0.20, 0.40, 0.60 and 0.80) nanoferrites were measured with variable relative humidity in the range from 30%RH to 95%RH. For realization of humidity sensor, thick films of above compositions are prepared on the substrates, PCB (Epoxy resin with FR4 Standard), in interdigitated form and ceramic substrate. It is found that the resistance of the compositions under investigation exponentially decreases with increase in the relative humidity. On inspection of graph of R_H against H, it is found that, decrease of resistance R_H within lower level of humidity is more than that of for upper range. During 40 % RH to 70 %RH, the trend of variation in the R_H deviates from earlier range. Moreover, after 70%RH the resistance significantly decreases with applied RH. This behaviour can be attributed to the existence of protonic conduction mechanism [15]. For higher humidity level, the change in resistance is attributed to the existence of conductivity due to both protons hopping as well as capillary condensation of water molecules into the pores[16]. Humidity dependent sensitivities are measured for the entire range of investigation for all compositions. From the investigation of the results obtained, it can be concluded that, the compositions under investigations are suitable for development of humidity sensor and hence the sensor module. A sensor, once developed, should be studied for its timing parameters. Two parameters, response time (T_{RES}) and recovery time (T_{REC}) play significant role on features of the sensors [17]. A Pulse of relative

humidity 90%RH is applied for about 120 sec to the sensing element, deposited on ceramic substrate, and timing response are recorded in second. On inspection of the results, it can be concluded that the compositions are very fast in response to the humidity. The instantaneous values of these timing parameters are also measured within humidity 10 % RH and it is about 1 second. It can be concluded that, the humidity sensor developed by employing compositions of ferrite on ceramic substrate are very fast and hence, it can be implemented to develop Smart Sensor Module of Promising features.

Electrical properties of the compositions of polycrystalline $Mg_xZn_{1-x}Fe_2O_4$, $Ni_xZn_{1-x}Fe_2O_4$ and $Mn_xZn_{1-x}Fe_2O_4$ nanoferrites have been investigated for suitability of the same for gas sensing applications. Employing these materials, the sensing elements are developed on epoxy resin, cylindrical glass tube, ceramic etc substrates. The sensing elements are demonstrating the phenomenon of chemisorption at specific operating temperature [18]. The materials are n-type metal oxides and depict increase in the resistance due to presence of oxidizing gas and decrease in the resistance due to existence reducing gas [19]. Emphasizing this fact, sensing elements of the ferrite materials are exposed to the carbon dioxide gas, hydrogen sulfide gas and ammonia gas and results obtained are interpreted. The sensitivities are also estimated. From results obtained, it can be concluded, the compositions of NiZn ferrites are most suitable for development of carbon dioxide gas sensor. Moreover, the composition $Mg_{0.20}Zn_{0.80}Fe_2O_4$ is also suitable for fabrication of carbon dioxide gas sensor. Operating temperature determined for MgZn ferrites is 220 ^{0}C. Moreover, reduction in the operating temperature is observed for NiZn ferrite. Good sensitivity with low operating temperature, suggest implementation of NiZn ferrites for carbon dioxide gas sensor. The performances of the sensing elements are also tested for two reducing gases, the H_2S and NH_3. On application of these gases, the reduction is the resistance takes place, which is attributed to existence of n-type of conductivity at operating temperature [20]. The sensitivities of all sensing elements are estimated for various temperatures. The operating temperatures are obtained for all sensing element. The compositions under investigations are showing good sensitivities. However, the sensitivity observed for MnZn ferrites for both gases is remarkable. Therefore, it can be concluded that, the sensing elements MnZn ferrites are most suitable for fabrication of H_2S and NH_3 gas sensor. It is also found that, the operating temperature is significantly reduced. For H_2S gas sensing, for MnZn ferrites, the operating temperature is reduced

to 125 ^{0}C. On investigation of results obtained, it is confirmed that, the sensors developed on cylindrical glass tubes are most suitable for deployment of the same to design the Smart Sensor Module.

With the view to develop the sensors for typical parameters, the four compositions each series of MgZn, NiZn and MnZn ferrites have been investigated for structural and electrical properties. Out of these compositions, the two compositions are selected for development of sensors for relative humidity, temperature, CO_2 gas, H_2S gas and NH_3 gas. Thus, two sensors for each parameter are developed. This led to develop two Smart Sensor Modules.

Major objectives of the present research is to develop smart sensor module to monitor, the parameters such as temperature, relative humidity, concentration of gases such as CO_2, H_2S and NH_3. As per the objectives, the Smart Sensor Module is designed, wherein an embedded technology is realized. According IEEE 1451 standards, the Smart sensor module consist of a computing unit along with the other analog electronic parts[21]. Moreover, computing unit should be capable of providing intelligence required for SSM. To ensure portability and deployment in the smart instrumentation, the SSM should be capable of networking. Considering these facts into account and emphasizing the features of the embedded technology, the hardware and firmware of the Smart Sensor module is designed. The hardware is designed about advanced microcontroller AVR ATmega 8L. The hardware of the SSM comprises the sensors developed by technology discussed earlier, and the signal conditioning circuits. A separate signal path is designed for each channel. Along with this analog part smart display unit is also designed and established on the SSM to ensure the read out of the parameter values [22]. To keep pace with the IEEE 1451 standards the output data buses of different standards are also made available. Present SSM is facilitated with, RS232, Serial, SPI outputs. With use of these output buses the SSM can be installed into the distributed network [23]. Along with this data buses, analog interface is also made available on the SSM. As the SSM is good example of embedded development, the firmware is the inherent part of the SSM. The firmware, basically put intelligence in to the SSM. Deploying smart IDE, the Codevision AVR, the firmware is developed in embedded C environment. The firmware comprises various functions, defined for dedicated application and operating in synchronization with the hardware. On continuous execution of the firmware, the parameter values are available on the display unit as well as on the digital out data buses. The empirical relations obtained from

process of calibration are executed by the firmware in specific sequence. Thus, with design of hardware and development of the firmware, the design of Smart Sensor Module is successfully completed.

Emphasizing the enhancement of the salient features of the Smart Sensor Module, it is calibrated to the scientific units. The present Smart Sensor Module is designed to monitor the parameters such as relative humidity, temperature, CO_2 gas, H_2S gas and NH_3 gas etc. Therefore, process of calibration is adopted for these parameters. The sensing and signal conditioning path provides analog voltage in mV. However, it is essential to produce output in real unit. For calibration the scientific process of regression is adopted, wherein piece-wise linear analysis is ensured [24]. Entire range of investigation is divided into two regions. Each region is calibrated separately. Process of regression results into two empirical relations [topic 5]. Thus, the SSM provides output humidity in % RH. Further, it is also standardized with standard equipments. Similar to the humidity, the SSM also calibrated to temperature in degree centigrade. For this purpose again piecewise analysis method is employed. The two empirical relations are obtained from process of data fitting. Thus, it provides the more precise data of the temperature [25]. In addition to these parameters, the SSM is also calibrated to concentration of above mentioned gases as well. To calibrate the system for concentration of carbon dioxide gas, again process of regression is executed. This regression process gives an empirical relation. The SSM is calibrated for carbon dioxide gas in % unit. Moreover, for H_2S and NH_3 gas, the two point calibration method is adopted[26]. After calibration, the process of standardization is carried out.

It can be concluded that, as per the objectives, the composition of spinel ferrites have been synthesized and deployed as sensing element for sensors designed for the parameters. It is also concluded that, deploying these sensors Smart Sensor Network of prominent features is developed to monitor physical parameters such as relative humidity, temperature, concentration of carbon dioxide gas, hydrogen sulfide gas and ammonia gas. The Smart Sensor Modules works with great reliability and depict results with preciseness.

References :

1. Honeywell International Inc "Modular sensor assembly including removable sensing module" US Patent 8718981.
2. O. A. Postolache, J. M. D. Pereira, and P. M. B. S. Girao, "Smart sensors network for air quality monitoring applications," *IEEE Trans. Instrum.Meas.*, 58 9(2009) 3253-3262.
3. K. Lee, "IEEE 1451: A Standard in Support of Smart Transducer Networking", IEEE Instrumentation and Measurement Technology Conference Baltimore, MD USA, (2000)1-4.
4. IEEE Instrumentation And Measurement Society, IEEE Standard for a Smart Transducer Interface for Sensors and Actuators — Common Functions, Communication Protocols, and Transducer Electronic Data Sheet (TEDS) Formats. Institute of Electrical and Electronics Engineers, Inc. New York (2007), (ISBN 0-7381-5598-5).
5. D. Wobscholl, "A wireless gas monitor with IEEE 1451 protocol", in: Proceeding of Sensors Applications Symposium (SAS 2006) Houston, TX, USA,(2006) 162–164.
6. G. Tiwari and R. Kazi, " Realization of the functions of automatic Smart Sensor Interface for Industrial in IOT environment", Intern. J. Adv. Res. Comp. Sc. and Software Engg., 5 1 (2015) 878-883.
7. M. Simić, "Microcontroller Based System for Measuring and Data Acquisition of Air Relative Humidity and Temperature", Presented at the 37th International Conference of IMAPS-CPMT Poland, (2013).
8. Y. Qu, H. Yang, N. Yang, Y. Fan, H. Zhu and G. T. Zou, "The Effect of Reaction Temperature on the Particle Size, Structure and Magnetic Properties of Co-precipitated $CoFe_2O_4$ Nanoparticles",Mater. Lett., 60 29-30 (2006)3548-3552.
9. B. P.Ladgaonkar andA.S. Vaingankar, "X-ray Diffraction Investigation of Cation Distribution in $Cd_xCu_{1-x}Fe_2O_4$Ferrite System", Mater. Chem.Phys.,56(1998)280
10. N. M. Deraz and A. Alarifi, "Preparation and Characterization of Nano-Magnetic $Mn_{0.5}Zn_{0.5}Fe_2O_4$ System", Int. J. Electrochem. Sci., 7 (2012) 5828 – 5836.

11. S. V. Bangale, D. R. Patil and S. R. Bamane, "Preparation and Electrical Properties OfNanocrystallineMgFe_2O_4 Oxide By Combustion Route", Archives of Appl. Sci. Res., 3 5 (2011) 506-513.
12. Amarjeet and V. Kumar, "Synthesis, Thermal and FTIR Study of Zn-Fe Nano Ferrites", Intern. J. Latest Res.Sci.andTechn., 3 1 (2014) 61-63.
13. M.Mouallem-Bahout, ,S. Bertrand and O. Peña, "Synthesis and Characterization of $Zn_{1-x}Ni_xFe_2O_4$ Spinels Prepared By A Citrate Precursor", J. Solid State Chem., 178 4(2005)1080–1086.
14. S. Maensiri, M. Sangmanee and A. Wiengmoon, "Magnesium Ferrite ($MgFe_2O_4$) Nanostructures Fabricated by Electrospinning", Nanoscale Res Lett., 4 (2009) 221–228.
15. J. Wang , F. Wu, K.Shi, X.Wang and P. Sun, "Humidity sensitivity of composite material of lanthanum ferrite/polymer quaternary acrylic resin", Sensors and Actuators B: Chemical, 99, 2–3, (2004)586–591.
16. N. Rezlescu, , C. Doroftei, E. Rezlescu and P.D. Popa, "Structure and humidity sensitive electrical properties of the Sn^{4+} and/or Mo^{6+} substituted Mg ferrite", Sensors and Actuators B: Chemical, 115 2 (2006)589–595
17. A. Lapina, P. Holtappels, and M. Mogensen, "Conductivity at Low Humidity of Materials Derived from Ferroxane Particles", International Journal of Electrochemistry, (2012) 7.
18. C.M. Ghimbeu, M. Lumbreras, M. Siadat, J. Schoonman, "Detection of H_2S, SO_2, and NO_2 using electrostatic sprayed tungsten oxide films, Mater. Sci. Semiconduct. Proc. 13 (2010) 1–8
19. K. Wetchakun, T. Samerjai, N. Tamaekong, C. Liewhiran, C. Siriwang, V. Kruefu, A. wisitsoroat, A. Tuantranont and S. Phanichphant, "Semiconducting Metal Oxides As Sensors For Environmentally Hazardous Gases", Sensors and Actuators B: Chemical, 160 (2011) 580-591.
20. L.B.Kong and Y.S.Shen, "Gas Sensing Properties and Mechanism Of$Ca_xL_{1-x}FeO_3$ Ceramics", Sensors and Actuators B: Chemical, 30 (1996) 217-221.
21. Flyport, "Sensing Platform", www.openpicus.com

22. K. Shinghal, A. Noor, N.Srivastava and R. Singh, “Intelligent Humidity Sensor for Wireless Sensor Network Agricultural Application”, Intern. J. Wireless & Mobile Networks (IJWMN), 3 1 (2011) 118-128
23. Oprea, N. Bârsan, U. Weimar, J. Courbat, D. Briand and N.F. de Rooij, “Integrated Temperature, Humidity and Gas Sensors on Flexible Substrates for Low-Power Applications”, IEEE SENSORS, (2007) 158-161.
24. J.Yuan, N. H. Farhat and J.Van-der Spiegel,“Background Calibration With Piecewise Linearized Error Model for CMOS Pipeline A/D Converter”, IEEE Transactions on circuits and systems-I 55 1(2008)311-321.
25. Chen and C. Chen, “Evaluation of Piecewise Polynomial Equations for Two Types of Thermocouples”, Sensors 13(2013)17084-17097.
26. C.M. Ghimbeu, M. Lumbreras, M. Siadat, J. Schoonman, “Detection of H_2S, SO_2, and NO_2 Using Electrostatic Sprayed Tungsten Oxide Films, Mater. Sci. Semiconduct. Proc. 13 (2010) 1–8

*****

.

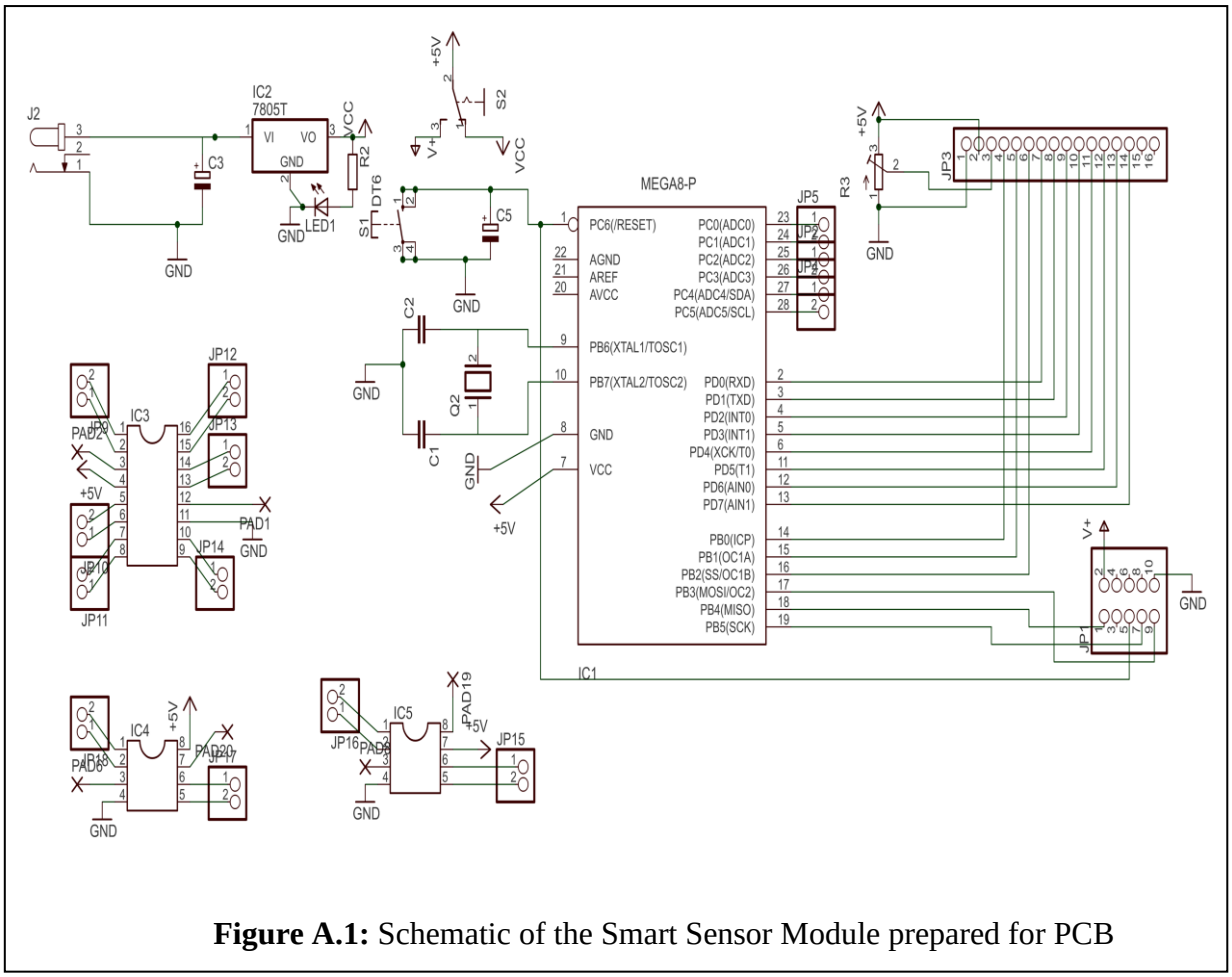

Figure A.1: Schematic of the Smart Sensor Module prepared for PCB

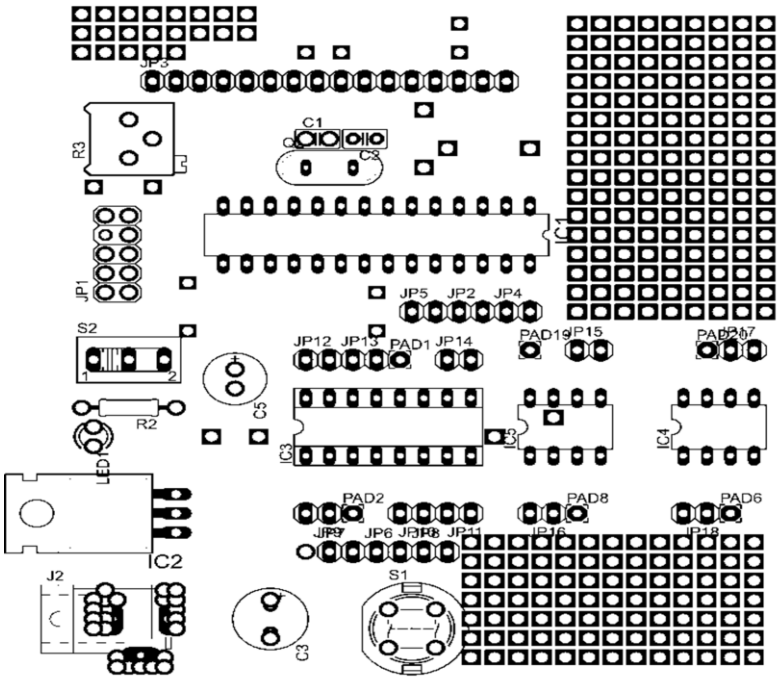

Figure A.2: Layout of the Smart Sensor Module Top View

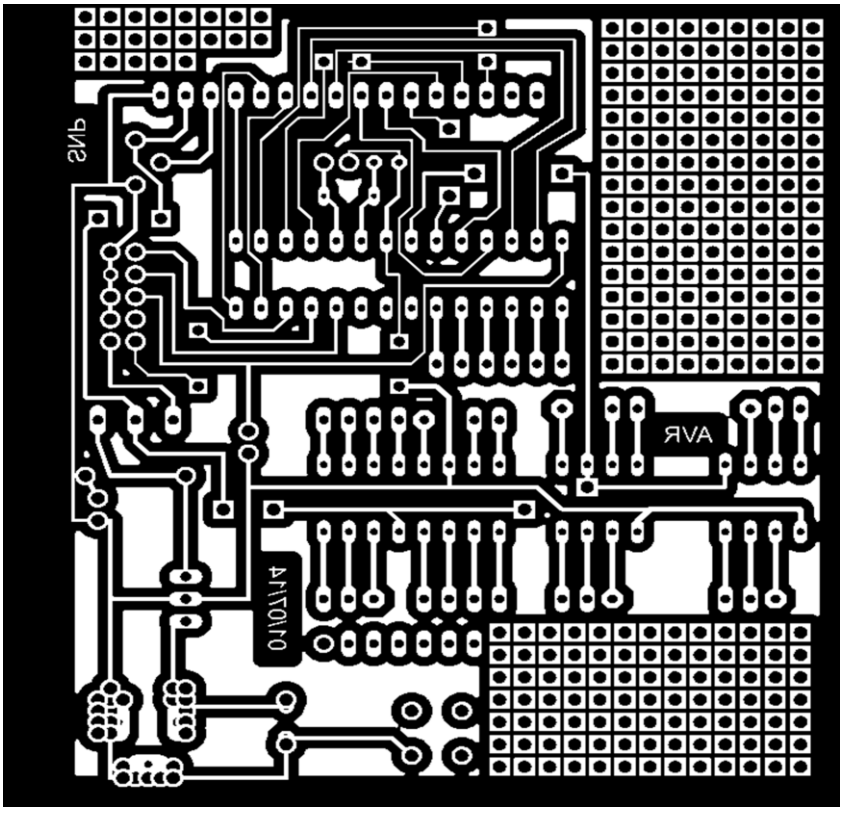

Figure A.3: Layout of the Smart Sensor Module Bottom View

Component List:

Sr. No.	Name of the components	Value	Qty
1.	IC1- LM 7805	-	1
2.	IC2-AVR ATmega 8L	-	1
3.	IC3-TLV 2774	-	1
4.	IC4-TLV 272	-	1
5.	IC5-Max 232	-	1
6.	IC6 – Smart LCD HD44780	-	1
7.	Diode D1-D4 – 1N4007	-	4
8.	Resisters R1	1 KΩ	1
9.	Trim Pot. R2	5 KΩ	1
10.	R3, R4	1 MΩ	2
11.	R5, R6	22 MΩ	2
12.	R7	10 MΩ	1
13.	Capacitors C1 (Electrolyte)	1000 µf	1
14.	C2, C5-C8 (Electrolyte)	10 µf	5
15.	C3, C4 (Disk)	0.01 µf	2
16.	Reset Switch	-	1
17.	Slide Switch	-	1
18.	DC Power Jack	-	1
19.	DB-9 Connector	-	1
20.	Crystal	4 MHz	1
21.	FRC Connector	-	1

The Programme Listing

```
#include<mega8.h>
#include<stdio.h>

void lcd (unsigned int col);
void lcd2(unsigned int col2);
void lcd_init (void);
void lcdcmd (unsigned char value);
void lcddata (unsigned char value);
void msdelay (unsigned int itime);
void USART_Tx(void);
void lcd_display (unsigned int row, flash unsigned char chardisp[ ]);

#define rs PB0
#define rw PB1
#define en PB2
#define ldata PORTD
#define lsignal PORTB
#define vref 2.56
#define fullscale 1023

unsigned int adc(unsigned int channel);
unsigned int bcd[5], bcd2[6];
unsigned int   Average_Data,data_from_Channel_0, data_from_Channel_1,
data_from_Channel_2,  data_from_Channel_3,data_from_Channel_4;
unsigned int calibration_for_Humidity (unsigned int data_from_Channel_0);
unsigned int calibration_for_CO2 (unsigned int data_from_Channel_2);
unsigned int calibration_for_Temperature (unsigned int  data_from_Channel_1);
unsigned int calibration_for_NH3 (unsigned int data_from_Channel_3);
unsigned int calibration_for_H2S (unsigned int data_from_Channel_4);
unsigned int dec_bcd (unsigned int dec);
unsigned int Humidity,Temperature,CO2,NH3,H2S;
float VCO2,VRH,VTH,VNH,VHS;
long int Raw_Data;
      void main(void)
                {
                    DDRD = DDRD| 0xFF;
                    DDRB = DDRB |0xFF;
                    PORTD = PORTD | 0xFF;
                    PORTC = PORTC | 0xFF;

                    lcd_init ();
                    msdelay(100);msdelay(100);
                    lcd_display (0x80,"Hum Te CO NH HS ");
```

```
            UCSRA = 0x22;
            UCSRB = 0x08;
            UCSRC = 0x86;
            UBRRL = 0x0C;
            UBRRH = 0x00;

        while(1)
        {
            data_from_Channel_0 = adc(0);
           Humidity=calibration_for_Humidity (data_from_Channel_0);
           dec_bcd (Humidity);
           lcd(0);

           data_from_Channel_1= adc(1);
           Temperature=calibration_for_Temperature (data_from_Channel_1);
           dec_bcd (Temperature);
           lcd(4);

           data_from_Channel_2= adc(2);
           CO2=calibration_for_CO2 (data_from_Channel_2);
           dec_bcd (CO2);
           lcd(7);

           data_from_Channel_3= adc(3);
           NH3=calibration_for_NH3 (data_from_Channel_3);
           dec_bcd (NH3);
           lcd(10);

           data_from_Channel_3= adc(4);
           H2S=calibration_for_H2S (data_from_Channel_3);
           dec_bcd (H2S);
           lcd(13);

           USART_Tx();
            }

       }
/*************************************************************/
   void USART_Tx(void)

           {

             printf("GA#%d#", Humidity) ;
               msdelay(50000);
               msdelay(50000);
               msdelay(50000);
             printf("GB#%d#", Temperature) ;
               msdelay(50000);
               msdelay(50000);
               msdelay(50000);
```

```
            printf("GC#%d#", CO2) ;
              msdelay(50000);
              msdelay(50000);
              msdelay(50000);
            printf("GD#%d#",NH3) ;
              msdelay(50000);
              msdelay(50000);
              msdelay(50000);
            printf("GE#%d#",H2S) ;
              msdelay(50000);
              msdelay(50000);
              msdelay(50000);
          }

/*****************************************************************
 * Function Name   :  lcd_display
 * Function Type   :   void
 * Description     : This function is defined for display the text on LCD
 * Argument        : Input row No ( 0 or 1) and String to be displayed
 * Return          : None
 *****************************************************************/
void lcd_display (unsigned int row, flash unsigned char chardisp[])
      {
       unsigned int i;
       lcdcmd(row);
       msdelay(10);
         i =0;
       while (i <= 16)
         {
            lcddata (chardisp[i]);
            msdelay(100);
            i=i+1;
         }
      }
/*****************************************************************
* Function Name   :  lcd_init
* Function Type   :   void
* Description     : This function is defined for initialization of LCD
* Argument        : None
* Return          : None
*****************************************************************/
void lcd_init (void)
      {
            lcdcmd(0x38);
            msdelay(10);
             lcdcmd(0x0C);
            msdelay(10);
            lcdcmd(0x06);
            msdelay(10);
       }
```

```
/*****************************************************************
    * Function Name   :  lcd
    * Function Type   :  void
    * Description     : This function is defined to numerical data of the
                      : respective parameters
    * Argument        : Cursor position
    * Return          : None
    *****************************************************************/
          void lcd(unsigned int col)
          {
            unsigned int i;
            unsigned int rowno,colno,cursor;
            PORTD = PORTD | 0xFF;
           rowno=0xc0;
           colno=0xc0|col;
           cursor=rowno|colno;
           lcdcmd(cursor);
           msdelay(10);
                 i=1;
           for(i=1;i<=4;i++)
                {
                  lcddata (bcd[i]);
                 /* if (i==2)
                     {
                        lcddata('.');
                     }
                  msdelay(500); */
                }
           msdelay(500);
           return;
          }
    /*****************************************************************
    * Function Name   :  lcdcmd
    * Function Type   :  void
    * Description     : This function is defined to send command for LCD
    * Argument        : command
    * Return          : None
    *****************************************************************/
          void lcdcmd (unsigned char value)
            {
               ldata = value;
               lsignal = 0x04;
               msdelay(10);
               lsignal = 0x00;
               msdelay(1);
               return;
          }
```

```
/*****************************************************************
    * Function Name   :  lcddata
    * Function Type   :  void
    * Description     : This function is defined to send data to LCD
    * Argument        : Data
    * Return          : None
    *****************************************************************/
    void lcddata (unsigned char value)
        {
            ldata = value;
            lsignal =0x05;
            msdelay(10);
            lsignal = 0x01;
            return;
        }
    /*****************************************************************
    * Function Name   :  adc
    * Function Type   :  unsigned int
    * Description     : This function is defined to select on chip ADC of
                        AVR ATmega8L for conversion of Analog signal to digital
    * Argument        : Channel No to which the analog signal given
    * Return          : Equivalent digital number
    *****************************************************************/
        unsigned int adc(unsigned int channel)
        {
          unsigned int ch,i;
          ch=channel;
            ADMUX = 0xC0;
            ADMUX = ADMUX|ch;
            ADCSRA=0xE0;
            SREG = 0x80;
             msdelay(100);
             Raw_Data=0;
             Average_Data=0;
             for(i=1;i<=500;i++)
                  {
                   Raw_Data= Raw_Data+ADCW;
                   //msdelay(10);
                   }
             Average_Data= Raw_Data/500;
             return(Average_Data);
        }

    /*****************************************************************
    * Function Name   :  calibration
    * Function Type   :  unsigned int
    * Description     : This function is defined to calibrate the data to Humidity
    * Argument        : signal from DAS
```

```
* Return          : Humidity data x
*******************************************************************/

unsigned int calibration_for_Humidity (unsigned int data_from_Channel_0)
       {
         unsigned int x;
         VRH=(data_from_Channel_0 *2.56/1024)*1000;

         if(VRH<2240)
           {
            x=((VRH-442.5)/29.75);
           }
        else
          {
            x=((VRH-1894.65)/5.873);
          }

        // x=(((VRH-0.0855)/0.0259)/1000);

        return (x);
       }

/*******************************************************************
* Function Name   :  calibration_1
* Function Type   :  unsigned int
* Description     : This function is defined to calibrate the data to temperature
* Argument        : signal from DAS
* Return          : Temperature  data
*******************************************************************/
unsigned int calibration_for_Temperature (unsigned int data_from_Channel_1)
       {
       unsigned int x;
       VTH= (data_from_Channel_1 *2.56/1024)*1000;
       if(VTH<700)
            {
               x=((VTH-136)/9.335)/1;
            }
         else
            {
               x=((VTH+532.7)/20.83)/1;
            }
         return(x);
       }

/*******************************************************************
* Function Name   :  calibration_2
* Function Type   :  unsigned int
* Description     : This function is defined to calibrate the data to CO2
* Argument        : signal from DAS
* Return          : CO2  data
```

```
*****************************************************************/

unsigned int calibration_for_CO2 (unsigned int data_from_Channel_2)
        {
         unsigned int x;
         VCO2= ((data_from_Channel_2) *2.56/1024)*1000;
         x=((1589-VCO2)/9.798);
         return(x);
        }

/*****************************************************************
* Function Name   :  calibration_3
* Function Type   :  unsigned int
* Description     : This function is defined to calibrate the data to NH3
* Argument        : signal from DAS
* Return          : NH3  data
*****************************************************************/
unsigned int calibration_for_NH3 (unsigned int data_from_Channel_3)
       {
        unsigned int x;
        VNH= ((data_from_Channel_3)*2.56/1024)*1000;
        x=((VNH-302)/305);
        return(x);
       }

 /*****************************************************************
* Function Name   :  calibration_4
* Function Type   :  unsigned int
* Description     : This function is defined to calibrate the data to H2S
* Argument        : signal from DAS
* Return          : H2S  data
*****************************************************************/
unsigned int calibration_for_H2S (unsigned int data_from_Channel_4)
         {
           unsigned int x;
           VHS= ((data_from_Channel_3)*2.56/1024)*1000;
           x=((VHS-800)/1025);
           return(x);
         }
/*****************************************************************
* Function Name   :  dec_bcd
* Function Type   :  unsigned int
* Description     : This function is defined to given decimal to BCD and then to
                    ASCII
* Argument        : Number in Decimal formn
* Return          : Data in ASCII format
*****************************************************************/


unsigned int dec_bcd (unsigned int dec)
```

```
{
int b1,b2,b3,b4,per;
per =dec;
      b1=per/1000;
      b2=(per-(b1*1000))/100;
      b3= (per -(b1*1000+b2*100))/10;
      b4= (per- (b1*1000+b2*100+b3*10))/1;
      bcd[1]=b1+0x30;
      bcd[2]=b2+0x30;
      bcd[3]=b3+0x30;
      bcd[4]=b4+0x30;
      return(0);
      }


/*****************************************************************************
   * Function Name   :  msdelay
   * Function Type   :  void
   * Description     : To create delay time
   * Argument        : count number
   * Return          : None
 *****************************************************************************/
      void msdelay(unsigned int itime)
      {
        while (itime)
          {
            itime--;
          }
       return;
      }
 /*****************************************************************************/
 void lcd2(unsigned int col2)
      {
      unsigned int i;
      unsigned int rowno,colno,cursor;
      PORTD = PORTD | 0xFF;
      rowno=0xc0;
      colno=0xc0|col2;
      cursor=rowno|colno;
      lcdcmd(cursor);
      msdelay(10);
            i=0;
      for(i=1;i<=5;i++)
            {
              lcddata (bcd2[i]);
            }
      msdelay(500);
      return;
       }
```

FIGURE CAPTIONS

TABLE CAPTIONS

The List of Research Publications

E.1 Research Papers Published in International Journals: 12

Sr. No.	Authors	Title of research paper	Name of Proceeding	Year	P. No.
1	S.K. Tilekar **S.N. Patil** S.S. Shaikh A.M. Pawar B.P. Ladgaonkar	Development and Implementation of An Embedded System to Measure Initial Permeability of Magnetic Materials	International Journal of Electronic Engineering Research ISSN 0975 - 6450 Research India Publications	3 (1) 2011	21–28
2	B.P. Ladgaonkar **S.N. Patil**	Designing Of Data Acquisition System For Susceptibility Measurement	International Journal Of Electrical Engineering And Embedded Systems (IJEEES)	3(2) 2011	87
3	R. H. Patil, **S.N. Patil** and B. P. Ladgaonkar	Electroluminescence, photoconductivity and optical absorption studies of (zn,cd)s:cu Mixed phosphors	International Journal of Energy Systems Computers and Control ISSN: 0976-6782	3 (2) 2012	93-101
4	**S.N. Patil** S.K. Tilekar B.P. Ladgaonkar	Development of LPC 2378 based an embedded system for precision measurement of displacement	International Journal of Industrial Engineering Practice ISSN: 0974-7745	4(2) 2012	59-61
5	Bhimrao P. Ladgaonkar and **Suhas N. Patil** and Shivprasad K. Tilekar	Development of Ni-Zn Ferrite based smart humidity sensor module by using mixed signal programmable System-on-chip	Applied Mechanics and Materials	310 2013	490-493
6	A. M. Pawar **S. N. Patil** and B. P. Ladgaonkar	Development of Microcontroller Based Embedded System to Detect and Alarm LPG Leakage	International Journal on Power System Optimization ISSN : 0975-458X	5 (2) 2013	13–14
7	R. H. Patil, **S.N. Patil**, S. V. Nikam and B. P. Ladgaonkar	Effect Of Rare-Earth Doping On Electroluminescence, Photoconductivity And Optical Absorption Properties Of (Zn, Cd) S Phosphors	International Journal of Advances in Engineering & Technology (IJAET) ISSN: 2231-1963	6 (2) 2013	688-695 **IF-1.56**
8	**S. N. Patil** and B. P. Ladgaonkar	Synthesis and implementation of $niznfe_2o_4$ ferrites to design embedded system for humidity measurement	International Journal of Advanced Research in Electrical, Electronics and Instrumentation Engineering ISSN (Online): 2278 – 8875 ISSN (Print) : 2320 – 3765	2 (8) 2013	3813-3821 **IF-1.686**
9	A. M. Pawar **S. N. Patil** A.S. Powar and B. P. Ladgaonkar	Wireless Sensor Network to Monitor Spatio-Temporal Thermal Comfort of Polyhouse Environment	International Journal of Innovative Research in Science, Engineering and Technology ISSN: 2319-8753	2 (10) 2013	4866-4875 **IF – 1.672**
10	A. M. Pawar **S. N. Patil** and B. P. Ladgaonkar	Design and Implementation of Wireless Sensor Node for WSN for Automatic Meter Reading	International Journal of Recent Research in Mathematics Computer Science and Information Technology	1 (1) 2014	28-31
11	S.K. Tilekar Abhay Tambe S.S. Shaikh **S.N. Patil** P.V. Mane-deshmukh B.P. Ladgaonkar	Analog Mixed Signal Based SoC for Measurement of AC Electrical Conductivity of Water	International Journal of Scientific & Engineering Research ISSN 2229-5518	5 (8) 2014	474-478 **IF-3.2**

12	Sachin. V. Chavan, Sumayaa. C. Pathan, Suha**S. N. Patil** and Bhimrao. P. Ladgaonkar	Design of LM4F120H5QR Based Node For Wireless Sensor Network To Monitor Environmental Parameters of Polyhouse	International Journal of Advances in Engineering & Technology ISSN: 22311963	8 (3) 2015	314-328

E.2 Research Papers Published in the International Conference, Seminars and Symposia: 03

Sr.	Authors	Title of research paper	Name of Proceeding	Year	P. No.
1	**S. N. Patil ,** A. M. Pawar, S. K. Tilekar and B. P. Ladgaonkar	Synthesis and Characterization of Nanocrystalline MnZn Ferrite for Humidity Sensor	International Conference on Advanced & Applied Material Science (ICAAMS-2014) Gopal krishan Gokhale College, Kolhapur.	15th & 16th January 2014	104-108
2	**S. N. Patil ,** A.M. Pawar, S. K. Tilekar and B.P.Ladgaonkar	An Implementation of Polycrystalline Ferrite to Design an Embedded System for Carbon Dioxide Gas Monitoring	International Conference on Functional Materials @ Nanoscale: Concerns and Challenges (ICFMNCC-2015) Karmaveer Bhaurao Patil Mahavidyala, Pandharpur, Dist.Solpaur (M.S.) India	9^{th} -11^{th} March 2015	18
3	S. K. Tilekar, S. C. Pathan, P. V. Mane-Deshmukh, **S. N. Patil**, S. V. Chavan, B. P. Ladgaonkar.	A New Paradigm of AMS-SoC Design for Monitoring of Physico-Chemical Parameters of the Water.	International Conference on Functional Materials @ Nanoscale: Concerns and Challenges (ICFMNCC-2015) KBP Pandharpur, Dist.Solpaur (M.S.) India	9^{th} -11^{th} March 2015	137

E.3 Research Papers Published in the Proceeding of the National Conference, Seminars and Symposia: 14

Sr. No.	Name of the Authors	Title of Research paper	Name of Proceeding	Year	P. No.
1	G. G. Mokashi, A. M. Pawar**, S. N. Patil** and B. P. Ladgaonkar	Design and Development of Wireless Sensor Network for Automatic Meter Reading	National Conference on Advances in Electronics and its interdisciplinary Applications [NCAEIA-2014] Sponsored by UGC, IEEE India SSCS & CAS Chapters Fergusson College, Depart. of Electronics, Pune	19^{th} - 20^{th} Sep. 2014	85
2	D. M. Adat, A. M. Pawar, **S. N. Patil** and B. P. Ladgaonkar	Design of Wireless Sensor Node for Measurement of Intensity of Light of Polyhouse Environment	**…..”……**	**..”……**	89
3	A.B. Ladgaonkar[1]**, S. N. Patil** and B.P. Ladgaonkar	Development of Mixed Signal Based System-on-Chip for Brushless DC Motor Controlling	**…..”……**	**…..”…**	141
4	**S. N. Patil** , A. M Pawar, S. k. Tilekar and B. P. Ladgaonkar	Implementation of Nanocrystalline NiZn Ferrite for Smart Humidity Sensor Module	**…..”……** Proceeding	…..”…	315
5	B. S. Jadhav, S. B. Shinde, **S. N. Patil** and B. P. Ladgaonkar	Development of an Embedded System for Measurement of Soil Moisture	National Conference on Modern Approach for Green Electronics and Computing (MAGEC-2014) Y. C. College, Satara. ISBN 978-81-928732-2-0	29^{th} 30^{th} Sep. 2014	8-10

6	V. R. Patil, J. K. Mulani, **S. N. Patil** and B. P. Ladgaonkar	Development of AVR Microcontroller Based an Embedded System for Susceptibility Measurement	**…..”……**	**…..”…**	20-23
7	S. S. Pise, N. Y. Wagh, **S. N. Patil** . and B. P. Ladgaonkar	An Embedded System for Monitoring of Carbon Dioxide Gas Concentration of Polyhouse Environment	**…..”……**	…..”…	188-193
8	G. G. Mokashi, A. M. Pawar, **S. N. Patil** and B. P. Ladgaonkar	Realization of Automatic Electric Meter Reading Through Wireless Sensor Network	National Conference on Advances in Wireless Sensor Network and Its Application (NCAWSNA-2014), Shankarrao Mohite ahavidyalaya, Akluj ISSN:2349-8226	12th and 13th Dec., 2014	2nd Prize Oral 47-50
9	**S. N. Patil** , A.M. Pawar, S. K. Tilekar and B.P.Ladgaonkar	Synthesis and Development of Nanosized Ferrite Sensors to Design an Embedded System for Carbon Dioxide Gas Monitoring	**…..”……**	**…..”…**	68-72
10	S.K. Tilekar, S.S.Jadhav, A.B. Dalvi, **S. N. Patil**, P. V. ManeDeshmukh and B. P. Ladgaonkar	Non-Invasive Cardiac Pulse Monitoring Using PIC Microcontroller	**…..”……**	**…..”…**	141-145
11	S. M. Pawar, P. B.Ekatpure, G.G.Mokashi, A.M.Pawar, **S.N.Patil** and B.P.Ladgaonkar	Wireless Sensor Network Based Automatic Meter Reading	**…..”……**	**…..”…**	199-201
12	B.D.Salvitthal, M.D.Bhais, A.M.Pawar, **S.N. Patil** and B.P.Ladgaonkar	ARM Microcontroller LPC 2148 Based An Embedded System Design For Temperature Monitoring For Industrial Applications	**…..”……**	**…..”…**	180-183
13	V.R.Patil, J.K.Mulani, **S.N.Patil**, B.P.Ladgaonkar	An Embedded Design to Ensure Magnetic Measurement	**…..”……**	**…..”…**	184-186
14	A.M.Pawar, J.K. Mulani, V.R. Patil, **S.N.Patil**, S.K.Tilekar and B. P. Ladgaonkar	Design of ARM Based Wireless Sensor Node For Warehouse Monitoring	**…..”……**	**…..”…**	36 161-166

E.4 Research Papers Published in the National Conference, Seminars and Symposia: 50

Sr. No.	Name of the Authors	Title of Research paper	Name of Proceeding	Year	P. No.
1	A.M. Kadam, P. A. Pote, **S. N. Patil ,** S.K. Tilekar B.P. Ladgaonkar	Development of Humidity & Temperature Controlling System For High-Tech Polyhouse Application.	National Conference on Emerging Trends in Electronics and Computer Science	08th to 10th Feb.,2010	CD
2	**S.N.Patil** S.K.Tilekar A.M.Kadam B.P.Ladgaonkar	Data acquisition system for susceptibility measurement	National Conference on Emerging Trends in Electronics and Computer Science, Padmashree Dr. D. Y. Patil Arts, Commerce & Science College, Pimpri, Pune-18	08th to 10th Feb.,2010	CD

3	P. A. Pote A.M.Kadam S.K.Tilekar **S. N. Patil** B.P. Ladgaonkar	ARM LPC 2378 Microcontroller based embedded design for temperature controllings	National Conference on Emerging Trends in Electronics and Computer Science, Padmashree Dr. D. Y. Patil Arts, Commerce & Science College, Pimpri, Pune-18	8th to 10th Feb.,2010	CD
4	**S.N.Patil** S.K.Tilekar S.S.Shaikh A.M.Pawar B.P.Ladgaonkar	Data acquisition system for susceptibility measurement	National Conference on Advanced Nanomaterials, sensor & Instrumentation(NCANSI-2011) DBF Dayanand College Solapur	21st to 22nd Jan, 2011	98
5	A. M. Pawar **S. N. Patil** S. K. Tilekar B.P.Ladgaonkar	Development of Zigbee Technology Based Wireless Sensor Network System for Greenhouse Applications	National Conference on Advanced Nanomaterials, sensor & Instrumentation(NCANSI-2011) DBF Dayanand College Solapur	21st to 22nd Jan, 2011	116
6	Pote P.A Tilekar S.K **Patil S.N** Nikam S.V Pise A.G Ladgaonkar B.P	ARM LPC 2378 Based Embedded System Designing For Controlling of Agricultural Parameters	National Conference on Advanced Nanomaterials, sensor & Instrumentation(NCANSI-2011) DBF Dayanand College Solapur	21st to 22nd Jan, 2011	112
7	A.M.Kadam A. G. Pise **S. N . Patil** B. P. Ladgaonkar	Development of PIC 16f877 Based Distance Measuring System	National Conference on Advanced Nanomaterials, sensor & Instrumentation(NCANSI-2011) DBF Dayanand College Solapur	21st to 22nd Jan, 2011	117
8	P.V. Mane-Deshmukh G.S. Phule S.K. Tilekar **S. N. Patil** B.P. Ladgaonkar	Design & Development of Zigbee Module for Wireless Humidity Sensor Node	UGC sponsored National Conference on Advanced Nanomaterials, Sensors & Instrumentation (NCANSI 2010-11), Organized by Dept. of Electronics, DBF dayanand College of Arts & Science, Solapur MS 413002	21-22 January 2011	114
9	A. G. Pise, **S. N. Patil ,** B. P. Ladgaonkar	Design and Implementation of PSoC Based Home Security System	National Seminar On Advances In Vlsi Design And Technology (NSAVDT-2011) Shankarrao Mohite ahavidyalaya, Akluj	19th to20th Dec, 2011	17
10	**S.N.Patil** S.K.Tilekar B.P.Ladgaonkar	Study of Humidity Sensitive Properties of the $ZnNiFe_2O_4$	National Seminar On Advances In VLSI Design And Technology (NSAVDT-2011) Shankarrao Mohite ahavidyalaya, Akluj	19th to20th Dec, 2011	24
11	**S. N. Patil,** S. K. Tilekar B. P. Ladgaonkar	Design wireless Humidity sensor	------”-----	19th to20th Dec, 2011	31

12	R. K. Pawar, **S. N. Patil** B. P. Ladgaonkar	Microcontroller PIC 16F 877A Based An Embedded System For Distance Measurement	------"-----	19th to20th Dec, 2011	21
13	S. A. mane, V. B. Yadav, **S.N. Patil,** A. G. Pise B. P. Ladgaonkar	Development of an embedded system to detect and alarm LPG lekage	------"-----	19th to20th Dec, 2011	25
14	S. V. Patil, Y. D. Bhosale, **S. N. Patil** B. P. Ladgaonkar	Development of LPC 2378 Based an Embedded system for precision measurement of displacement	------"-----	19th to20th Dec, 2011	25
15	M. M. Kolapkar, **S. N. Patil ,** A. G. Pise B.P.Ladgaonkar	Design of an embedded system for Online Measurement of climatic parameters of Greenhouse Environment	------"-----	19th to20th Dec, 2011	27
16	A.M. Pawar, S.K. Tilekar, **S.N. Patil** B.P. Ladgaonkar	Development of Wireless Sensor Node for Wireless Sensor Network for High-tech Agriculture	------"-----	19th to20th Dec, 2011	29
17	**S.N. Patil,** A.M. Pawar and B. P. Ladgaonkar	Development of polycrystalline ferrite based smart humidity sensor module by using advanced microcontroller	State Level Seminar on Recent Developments In Embedded Technology (SS-RDET-2012) KBP, Pandharpur, Dist Solapur	21st to 22nd Dec, 2012	40
18	M. B. Pawar, C. B. Damal **S.N.Patil**	Development of lpc 2378 based an embedded system for precision measurement of displacement	------"-----	21st to 22nd Dec, 2012	50
19	**S. N. Patil ,** A.S. Powar, S.K.Tilekar B. P. Ladgaonkar	Development of polycrystalline ferrite based smart humidity sensor module by using mixed signal programmable system on chip	A national conference On Emerging technologies for Sustainable developments Dept. of Technology, Shivaji University, Kolhapur,	27th to 28th Dec, 2012	109
20	A.M. Pawar, **S.N. Patil** B.P. Ladgaonkar	Design of sensor node for wireless sensor network to monitor light intensity of greenhouse environment	------"-----	27th to 28th Dec,2012	101-102
21	Y. B. Khot, **S. N. Patil** and B.P.Ladgaonkar	An Implementation of Polycrystalline Ferrite Based Sensor to Design Humidity Meter	National Conference On Recent Initiatives towards Green Electronics, Brijlal Biyani Science College Amrawati.	8th -9th Feb,2013	74
22	**S.N.Patil,** S.A.Jadhav and Dr.B.P.Ladgaonkar	Implementation of Polycrystalline Ferrites to Design CO_2 Gas Sensor Module	------"-----	8th -9th Feb,2013	75
23	A.M. Pawar, **S.N. Patil** and B.P. Ladgaonkar	Design Of Sensor Node For Wireless Sensor Network To Monitor Humidity And Light Intensity Of Green House Environment	National Conference On Recent Initiatives towards Green Electronics, Brijlal Biyani Science College Amrawati.	8th -9th Feb,2013	80
24	**S. N. Patil** , P. P. Ghule And B. P. Ladgaonkar	Embedded System for Monitoring Carbon Dioxide Gas Concentration of Polyhouse	UGC--SAP Sponsored & Technically Sponsored by IEEE Bombay Section National Conference on Latest	February 14 - 15, 2014	75

			Advances, Trends in Electronic Science and Technology, Shivaji University, Kolhapur,		
25	A.M. Pawar, **S. N. Patil ,** A. S. Powar and B. P. Ladgaonkar	Design and Implementation Wireless Sensor Node for WSN to Monitor Polyhouse Environment In Spatio-Temporal Domain	------”-----	February 14 - 15, 2014	142
26	A.M. Pawar, **S. N. Patil** and B. P. Ladgaonkar	Realization of Precision Agriculture By Deployment of Wireless Sensor Network	National Conference on Advances in Electronics and its interdisciplinary Applications [NCAEIA-2014] Sponsored by UGC, IEEE India SSCS & CAS Chapters Fergusson College, Department of Electronics, Pune	19th -20th Septemb er 2014	81
27	A.M. Pawar, **S. N. Patil** and B. P. Ladgaonkar	Designing of Computer Simulator for Base Station of Wireless Sensor Network	National Conference on Modern Approach for Green Electronics and Computing (MAGEC-2014) Y. C. College, Satara.	29th 30th Septemb er 2014	
28	R. A. Mahadik, S. B. Shinde, A. M. Pawar, **S. N. Patil** and B. P. Ladgaonkar	Development of an Embedded System for Monitoring of Alcohol Gas for Sugar Industry	------”-----	**…..”…**	
29	S. S. Pise, **S. N. Patil** , S. K. Tilekar and B. P. Ladgaonkar	Development of P89V51RD2 based an Embedded System for 3D LED Matrix Interfacing	------”-----	**…..”…**	
30	B. S. Jadhav, N. Y. Wagh, **S.N.Patil**, A.M.Pawar and B. P. Ladgaonkar	Development of Wireless Sensor Node for Measurement of Soil Moisture	National Conference on Advances in Wireless Sensor Network and Its Application (NCAWSNA-2014) Shankarrao Mohite ahavidyalaya, Akluj	**…..”…**	14
31	S. S. Pise, P. N. Badhe, M.B. Pawar, C.B. Dhamal, **S. N. Patil**, S. K. Tilekar and B. P. Ladgaonkar	Development of AVR ATmega 16 based an Embedded System for LED Matrix Interfacing	**…..”……**	**…..”…**	1st Prize Oral 19
32	A. M. Pawar, D. M. Adat, V. M. Deokate, **S. N. Patil**, G. G. Mokashi and B. P. Ladgaonkar	Wireless Sensor Network: The Solution for Precision Agriculture	**…..”……**	**…..”…**	21
33	R. A. Mahadik, S. B. Shinde, A. M. Pawar, **S. N. Patil** and B. P. Ladgaonkar	Development of an Embedded System for Wireless Sensor Network For Sugar Industry	**…..”……**	**…..”…**	2nd Prize oral 22
34	G. C.Yeshamala, S.S.Kulkarni, **S. N. Patil**, P.V.Mane Deshmukh, A.	Development of Matlab Based Interface for Electronic Instrumentation	**…..”……**	**…..”…**	33

	M. Pawar and B. P. Ladgaonkar				
35	K. V. Adat, V. Y. Inamdar, P. V. Mane Deshmukh, **S. N. Patil**, S. V. Chavan, B. P. Ladgaonkar	An Embedded System to Monitor Speed of the Vehicle	**…..”……**	**…..”…**	37
36	G. R. Arde, M. M. Mulik, **S. N. Patil**, S.K. Tilekar, P. V. Mane-Deshmukh, and B.P.Ladgaonkar	Development of an Embedded System for Smart Home	**…..”……**	**…..”…**	42
37	**S. N. Patil**, A. M. Pawar and B. P. Ladgaonkar	Deployment of Wireless Sensor Network to Ensure Site Specific Variability	**…..”……**	**…..”…**	43
38	A.M. Pawar, **S.N. Patil**, and B. P. Ladgaonkar	Design of Standing Wave Ratio Meter	**…..”……**	**…..”…**	39
39	S. K. Tilekar, M. B. Bagale, C.B. Pise, S.C.Pathan, **S. N. Patil** and B. P. Ladgaonkar	Synthesis of AMS Based Wireless Sensor Node For Measurement Of Temperature Compensated Ac Electrical Conductivity	**…..”……**	**…..”…**	2nd Prize Oral 32
40	S. K. Tilekar, M. B. Bagale, C. B. Pise, S. C. Pathan, **S. N. Patil** and B. P. Ladgaonkar	Synthesis Of Ams Based Wireless Sensor Node For Measurement Of Temperature Compensated Ac Electrical Conductivity	UGS Sponsored National Conference on Recent Advances In Embedded Technology (NCRAET-2015) Organized by Department of Electronics Ramkrishna Paramhansa Mahavidyalaya, Osmanabad	29th - 30th January 2015	1
41	G. G. Mokashi, A. M. Pawar, **S. N. Patil** and B. P. Ladgaonkar	Design and implementation of Wireless Sensor Network for Electric Power Distribution	**…..”……**	**…..”…**	8
42	G. R. Arde, M. M. Mulik, **S. N. Patil**, S. K. Tilekar, P. V. Mane-Deshmukh, and B.P.Ladgaonkar	Development of an Embedded System for Smart Home	**…..”……**	**…..”…**	15
43	**S. N. Patil**, A. M. Pawar, S. K. Tilekar and B.P.Ladgaonkar	Synthesis and Development of Nanosized Ferrite Sensors to Design an Embedded System for Carbon Dioxide Gas Monitoring	**…..”……**	**…..”…**	17
44	S. S. Pise, P. N. Badhe, M.B. Pawar, **S. N. Patil**, S. K. Tilekar and B. P. Ladgaonkar	Development of AVR ATmega 16 based an Embedded System for LED Matrix Interfacing	**…..”……**	**…..”…**	31

45	V.R.Patil, J.K.Mulani, **S. N. Patil**, B.P.Ladgaonkar	An Embedded Design to Ensure Magnetic Measurement	**…..”……**	**…..”…**	35 Ist Prize
46	A. M. Pawar, **S. N. Patil**, S. K. Tilekar and B. P. Ladgaonkar	ARM LPC2148 Based Wireless Sensor Network for Site Specific Data Management for Agriculture Application	UGC, IEEE India SSCS & CAS Chapters Sponsored National Conference on Emerging Trends in Electronics and Computer Science (ETECS-2015) Dept. of Electronics, Shivaji University, Kolhapur,	**1**3th -14th February 2015	OP-5
47	S. K. Tilekar, **S. N. Patil** , S. C. Pathan, P. V. Mane-Deshmukh, G. G. Mokhashi and B.P.Ladgaonkar	Mixed Signal Based System-On-Chip for Monitoring of Physical Parameters of the Water	**…..”……**	**…..”…**	OP-19
48	S. S. Pise, V. Y. Inamdar, A. M. Pawar, **S. N. Patil** , S. K. Tilekar and B. P. Ladgaonkar	Development of AVR ATmega 16 based an Embedded System for LED Matrix Interfacing	**…..”……**	**…..”…**	OP-22
49	G. G. Mokashi, A. M. Pawar, **S. N. Patil** , and B. P. Ladgaonkar	Wireless Sensor Network for monitoring Electrical Power Distribution	**…..”……**	**…..”…**	OP-75
50	**S. N. Patil**, A. M. Pawar and B. P. Ladgaonkar	Wireless Sensor Network to Ensure Site Specific Variability	**…..”……**	**…..”…**	OP-76

E.5 Research Papers Presented at the University and State level Avishkar

Sr. No.	Name of the Authors	Title of Research paper	Name of Proceeding	Year
1.	A. M. Pawar **S. N. Patil** S. K. Tilekar B. P. Ladgaonkar	Development of Zigbee Technology Based Wireless Sensor Network System for Greenhouse Applications	Avishkar, (University Level) A. G. Patil Institute of tech. solapur	2009
2.	A.M.Pawar, **S.N.Patil,** S.K.Tilekar B.P.Ladgaonkar	Development of Zigbee Technology Based Wireless Sensor Network System for Greenhouse Applications	Avishkar, (State Level) Maharashtra University of Health Sciences	2010
3.	**S.N.Patil** A.M.Pawar S.K.Tilekar B.P.Ladgaonkar	Synthesis of polycrystalline ferrite based Humidity Sensor	Avishkar, (University Level) Sangola college, Sangola	2012
4.	**S.N.Patil** A.M.Pawar S.K.Tilekar B.P.Ladgaonkar	Synthesis of polycrystalline ferrite based Humidity Sensor	Avishkar, (State Level) Balasaheb Savant Krishi Vidyapith, Dapoli	2013
5.	S. K. Tilekar, **S. N. Patil** and B. P. Ladgaonkar	Development of Mixed Signal Based Programmable System- on-Chip for Measurement of TDS of Water	Avishkar – 2013 (University Level) Orchid Engineering college, Solapur	1st-2nd Jan, 2014
6.	**S. N. Patil ,** S. K. Tilekar and B. P. Ladgaonkar	Development of Mixed Signal Based Programmable System- on-Chip for Measurement of TDS of Water	Avishkar, (State Level) North Maharashtra University Jalgaon	16th -18th Jan, 2014

E.6 Prize/Awards received

Sr. No.	Name of the Award / Prize	Conferring Body	Year
1.	Vijay Pratap Gauav Puraskar	Vijay Gramin Bigar sheti Sahkari Patsanstha, Akluj	2008
2.	First Prize as a Best Research Paper Presentation	National Conference on Emerging Trends in Electronics and Computer Science, Padmashree Dr. D. Y. Patil Arts, Commerce & Science College, Pimpri, Pune-18	2010
3.	First Prize as a Best Research Project Under Pure Science Faculty	Avishkar – 2010:A.G. Patil Institute of Engineering, Solapur	2010
4.	First Prize as a Best Research Project Under Pure Science Faculty	Avishkar – 2012 Sangola college, Sangola	2012-13
5.	First Prize as a Best Research Project Under Pure Science Faculty	Avishkar – 2013 Orchid Engineering college, Solapur	2013-14
6.	First Prize as a Best Research Paper Presentation	National Conference on Advances in Wireless Sensor Network and Its Application (NCAWSNA-2014), Shankarrao Mohite ahavidyalaya, Akluj	2014-15